TECHNICAL UNIVERSITY OF LIBEREC
Faculty of Mechatronics, Informatics
and Interdisciplinary Studies

UNIVERSITÉ TOULOUSE III PAUL SABATIER
Université de Toulouse

Power Quality in DC Supplied Grids: Application to Lighting Networks

Dissertation

Study programme: P2612 – Electrical Engineering and Informatics
Study branch: 2612V045 – Technical Cybernetics

Author: **Ing. Leoš Kukačka**
Supervisors: doc. Ing. Milan Kolář, CSc., prof. Georges Zissis
Consultants: Ing. Jan Kraus, Ph.D., Dr. Ir. Pascal Dupuis

Liberec, Toulouse 2017

Declaration

I hereby certify that I have been informed that Act 121/2000, the Copyright Act of the Czech Republic, namely Section 60, School-work, applies to my dissertation in full scope. I acknowledge that the Technical University of Liberec (TUL) and Université Toulouse III—Paul Sabatier (UPS) do not infringe my copyrights by using my dissertation for their internal purposes.

I am aware of my obligation to inform TUL and UPS on having used or licensed to use my dissertation in which event they may require compensation of costs incurred in creating the work at up to their actual amount.

I have written my dissertation myself using literature listed therein and consulted it with my supervisors and my consultants.

I also hereby declare that the hard copy of my dissertation is identical with its electronic form as saved in the IS STAG portal.

Date:

Signature:

Abstract

This dissertation thesis is concerned with temporal fluctuations of the luminous flux of LED lamps, a phenomenon referred to as *flicker*. Flicker is usually regarded as a disturbance due to its negative impact on human health. For lighting systems based on light emitting diodes (LED), its definition has recently been formalised in norm IEEE 1789:2015 and has been documented on devices supplied with AC voltage.

AC flicker results from interactions between network impedance, voltage and current harmonics, and the AC to DC converter. DC supplies are generally obtained by switching converters. Consequently, the same perturbing factors are present on DC networks. The thesis summarises the differences between the characteristic properties of flicker under AC and DC supplies.

It has been shown in the literature and also in this thesis that the key factor affecting flicker with LEDs is the design of the LED driver—a necessary part of the LED lighting systems. This thesis describes a methodology for the evaluation of the flicker sensitivity of DC supplied LED lamps and analyses how the sensitivity changes when the LED drivers are simplified and accustomed to DC supply.

The thesis presents a set of measurement experiments aimed to determine the typical flicker response of LED lamps both under AC and DC supply. Further experiments were performed to reveal the impact of accustomising the driver to the DC supply (removing the diode rectifier). It was found that some lamps show better flicker immunity while other lamps show worse flicker immunity. These experiments are accompanied by LED driver simulations aiming to reproduce and explain the measurement results.

The thesis further describes a measurement experiment aimed to show the typical severity of the voltage fluctuation in a low voltage DC network coupled to AC mains and its impact on the flicker. It is concluded that such a system is robust enough to filter out any perturbations coming from the AC supply, but an undesired interaction between the lamp and the supply may occur.

Key words: DC grid, DC supply, flicker, LED driver, LED lamp, Power Quality

Abstrakt

Předkládaná dizertace se zabývá nežádoucím kolísáním světelného toku LED žárovek[1], běžně označovaným jako *flikr* (z angl. flicker). U systémů založených na principu svítivých diod (LED) byl tento jev podchycen v normě IEEE 1789:2015 a patřičně zdokumentován u žárovek napájených střídavým napětím.

Při střídavém napájecím napětí může flikr vznikat interakcí mezi vlastnostmi sítě (impedance, harmonické zkreslení napětí, proudu) a AC-DC měničem. Prvky v DC sítích jsou obvykle tvořeny DC-DC měniči, proto v nich mohou vzniknout obdobné podmínky. Tato práce popisuje typické rozdíly mezi flikrem v DC a AC sítích.

V dostupné odborné literatuře (a také v této práci) bylo již ukázáno, že klíčovým prvkem, který ovlivňuje flikr u LED žárovek je elektronický předřadník. Předřadník je nezbytnou součástí každého LED svítidla. V této práci je zdokumentováno měření citlivosti na flikr u LED žárovek napájených stejnosměrným napětím, a dále je zjišťováno, jakým způsobem bude tato citlivost ovlivněna, bude-li elektronický předřadník přizpůsoben stejnosměrnému napájení.

Dizertační práce popisuje několik experimentů, jejichž cílem je určit typickou odezvu (ve smyslu flikru) LED žárovek při střídavém a stejnosměrném napájení. Další experimenty mají za cíl určit, jakým způsobem bude ovlivněna citlivost LED žárovek na flikr, bude-li z elektronického předřadníku vyňat diodový usměrňovač. Z těchto experimentů vyplývá, že u některých žárovek ze zkoumaného vzorku se citlivost zlepší, u jiných žárovek se naopak zhorší. Proto jsou tyto experimenty doplněny simulacemi, které si kladou za cíl naměřené chování napodobit a následně vysvětlit.

Dále tato práce popisuje experiment, jenž má napodobit kolísání napětí v malé stejnosměrné síti s vazbou na střídavou síť a dopad tohoto kolísání na flikr. Výsledky ukazují, že taková soustava je poměrně odolná vůči rušení pocházejícímu ze střídavé sítě. Může však dojít k nežádoucí interakci mezi zdrojem a LED žárovkou.

Klíčová slova: DC napájení, DC síť, flikr, Kvalita elektrické energie, LED předřadník, LED žárovka

[1]Autor má za to, že – ač jde v technických souvislostech o jistý protimluv – lze v české terminologii užívat sousloví *LED žárovka* namísto dle jeho názoru poněkud neobratného *LED svítidlo* především proto, že je tento termín dosti intuitivní a zažitý rovněž u laické veřejnosti.

Résumé

Cette thèse de doctorat porte sur les fluctuations temporelles du flux lumineux des lampes LED, ce phénomène portant le nom de papillotement (flicker). Le papillotement est habituellement considéré comme une perturbation en raison de son impact négatif sur la santé. Pour les systèmes d'éclairage à base de diodes électroluminescentes (LED), sa définition vient d'être formalisée dans la norme IEEE 1789:2015 et a été décrite pour les appareils alimentés en courant alternatif (CA).

Ce papillotement alternatif résulte des interactions entre l'impédance du réseau, l'onde de tension, les courants harmoniques et le convertisseur de courant alternatif en courant continu (CA – CC). L'alimentation en courant continu est généralement obtenue via des convertisseurs à découpage. Par conséquent, les mêmes facteurs perturbateurs sont également présents sur les réseaux à courant continu. Cette thèse résume les différences entre les propriétés caractéristiques du papillotement sous alimentation en CA et en CC.

Il a été montré dans la littérature et aussi dans cette thèse qu'avec les LED, le facteur clé qui affecte le papillotement réside dans la conception du driver de LED – une partie indispensable des systèmes d'éclairage à LED. Cette thèse décrit une méthodologie d'évaluation de la sensibilité au papillotement des lampes LED sous alimentation en CC et analyse la façon dont cette sensibilité se modifie lorsque les drivers de LED sont simplifiés et adaptés à des alimentations CC.

La thèse présente un ensemble d'expériences de mesure visant à déterminer la réaction typique du papillotement des lampes LED à la fois sous alimentation CA et CC. D'autres expériences ont été effectuées pour révéler l'impact de l'adaptation du driver à l'alimentation CC (en enlevant le pont redresseur à diodes). On constate que certaines lampes présentent une meilleure résistance au papillotement, tandis que d'autres lampes présentent une moindre résistance. Ces expériences sont accompagnées de simulations de drivers pour les lampes LED visant à reproduire et à expliquer les résultats des mesures.

La thèse décrit en outre une expérience de mesure visant à montrer la sévérité typique de la variation de tension dans un réseau CC à basse tension couplé au CA domestique et son impact sur le papillotement. On conclut qu'un tel système est suffisamment robuste pour filtrer les perturbations provenant du CA, mais une interaction indésirable entre la lampe et l'alimentation peut se produire.

Mots clés: alimentation CC, driver LED, lampe LED, Power Quality, réseau CC, scintillement (flicker)

Acknowledgements

In this place, I would like to express my greatest thanks to my family who have supported me in my studies. It has always been important for me to know that they value my work. I would like to thank my girlfriend Nadiia for psyche support especially during the final stage of my writing and for tolerating my internships abroad, albeit it was sometimes difficult.

I would like to thank my Czech supervisor Milan Kolář for giving me his unlimited support at my domestic university and to my consultant Jan Kraus for his friendship, motivation and helpful ideas. I would like to thank my French supervisor Georges Zissis for giving me an unexpected and once-in-a-lifetime opportunity to study a double degree programme under his partial supervision in Toulouse and also for sending me to an internship in Japan which proved to be another once-in-a-lifetime experience.

I would like to express my deep gratitude to Pascal Dupuis whose personality is very inspiring and from whom I gained a lot of professional experience. His aid with my studies and with this thesis was very important. Similarly I would like to thank to Jiří Drápela for significant help with my thesis and for several very fruitful and inspiring discussions. I consider myself honoured (and lucky) to have worked together with these two gentlemen.

My thanks also belong to Míra Novák and Richard Schreiber for help with some of the experiments. I would like to acknowledge some minor help from some of my students, namely David Crha and Lukáš Vele. My further thanks go to all my friends and colleagues at TUL, UPS and outside the academic circles; the list would be too long and never complete.

It is great to know that I am surrounded by people who wish me good luck.

Contents

List of Figures

List of Tables

List of Source Codes

List of Abbreviations

AC	Alternating Current
AFV	Abrupt Failure Value
ASM	Averaged Switch Modelling
CCM	Continuous Conduction Mode
CFL	Compact Fluorescent Lamp
CMC	Current Mode Control
CPC	Current Physical Components
CRIEPI	Central Research Institute for Electric Power Industry
DB	Diode Bridge
DC	Direct Current
DCM	Discontinuous Conduction Mode
DER	Distributed Energy Resource
DFT	Discrete Fourier Transform
ELV	Extra Low Voltage
EMC	Electromagnetic Compatibility
EMI	Electromagnetic Interference
EN	European Standard
ESR	Equivalent Series Resistance
ESS	Energy Storage System
EUT	Equipment Under Test
FM	Flicker Meter
FT	Fourier Transform
IC	Integrated Circuit
IEC	International Electrotechnical Commission
IEEE	Institute of Electrical and Electronics Engineers
IES	Illuminating Engineering Society
IET	Institution of Engineering and Technology
INL	Integral Nonlinearity
LAPLACE	Laboratoire Plasma et Conversion de l'Energie
LED	Light Emitting Diode
LFM	Light Flicker Meter
LV	Low Voltage
MG	Microgrid
N.A.	Not Available
OLED	Organic Light Emitting Diode

PD	Photodiode
PELV	Protected Extra Low Voltage
PFC	Power Factor Correction
PI	Proportional – Integral Controller
PQ	Power Quality
PV	Photovoltaics
PWM	Pulse Width Modulation
RHP	Right Half Plane
RM	Rectangular Modulation
RMS	Root Mean Square
RVC	Ripple Voltage Control
SELV	Separated (or Safe) Extra Low Voltage
SEPIC	Single Ended Primary Inductor Converter
SAM	Sinusoidal Amplitude Modulation
SM	Sinusoidal Modulation
SPICE	Simulation Programme with Integrated Circuit Emphasis
SSL	Solid State Lighting
TAČR	Technological Agency of the Czech Republic
TB	Talbot–Plateau Law
T&D	Transmission and Distribution
TF	Transfer Function
TR	Technical Report
TUL	Technical University of Liberec
UPS	Université Toulouse III Paul Sabatier
VFM	Voltage Flicker Meter
VMC	Voltage Mode Control
VQ	Voltage Quality

List of Symbols

Symbol	Unit	Description
a	—	modulation depth multiplier
a_i	—	sensitivity coefficient for ΔV_{10}
Acc	V	measurement accuracy
AFV	%	abrupt failure value
b	—	model parameter multiplier
c	$\mathrm{m\,s^{-1}}$	speed of light; in air $c \doteq 2.997\,00 \cdot 10^8\,\mathrm{m\,s^{-1}}$
C	F	capacity
C_{DC}	F	smoothing capacitor, its capacitance
C_{o}	F	converter output port capacitor, its capacitance
CCT	K	correlated colour temperature
CFF	Hz	critical fusion frequency
CMR	dB	common mode rejection
CMRR	—	common mode rejection ratio
d_{DC}	%	relative ripple depth, relative modulation depth of the DC voltage
d_{ih}	%	relative modulation depth of the interharmonic component
$d_{\mathrm{RM,SM}}$	%	relative modulation depth of the RM or SM
D	%	duty ratio
$\widetilde{D}$	%	equivalent duty ratio
D_{LFSD}	—	low frequency sinusoidal disturbances index
$D_{V,I,\mathrm{H}}$	var	voltage, current, harmonic distortion power
E	$\mathrm{lm\,W^{-1}}$	luminous efficacy, wall–plug efficiency
E_{photon}	J	photon energy
EQE	—	external quantum efficiency
f	Hz	frequency (generally)
f_1	Hz	fundamental frequency, in Europe $f_1 = 50\,\mathrm{Hz}$
f_{GF}	Hz	frequency for evaluating the *GF*
$f_{\mathrm{h,ih}}$	Hz	harmonic, interharmonic frequency
f_{m}	Hz	modulation frequency
f_{sw}	Hz	switching frequency
$F_{\mathrm{A,B}}$	—	active driver relative parameters
F_{s}	Hz	sampling frequency

Symbol	Unit	Description
FI	—	flicker index
FP	%	percent flicker
G	—	amplifier gain
G_{cm}	—	common mode amplifier gain
$G(s)$, $G'(s)$	—	converter transfer function
GainErr	ppm	gain error
GainTempCo	ppm/°C	gain temperature coefficient
$\boldsymbol{GF}_{\Phi}$	—	gain factor evaluated from flux
$\boldsymbol{GF}_{V}$	—	gain factor evaluated from voltage
h	J s	Planck constant, $h \doteq 6.626\,069\,9 \cdot 10^{-34}\,\mathrm{J\,s}$
i	—	generic index
$i(t)$	A	current waveform
$i_{\sim}(t)$	A	current ripple
i_{D}	A	diode current
i_{L}	A	inductor current
i_{LED}	A	LED current
i_{T}	A	transistor current
I	A	current (generally, the RMS value)
I_0	A	reverse saturation current
I_1	A	current—fundamental frequency component
I_{d}	A	diode current
I_{dark}	A	photodiode dark current
I_{DC}	A	current DC component
I_{H}	A	RMS of harmonic components of current
I_{light}	A	photodiode light induced current
I_{out}	A	output port current
I_{PD}	A	photodiode current
I_{PI}	s^{-1}	PI controller integral component
INL	ppm	INL error
IQE	—	internal quantum efficiency
j	—	harmonic order
k	$\mathrm{J\,K}^{-1}$	Boltzmann constant, $k \doteq 1.380\,648 \cdot 10^{-23}\,\mathrm{J\,K}^{-1}$
$k_{1,2}$	—	LED model coefficients
k_i	—	DFT i-th coefficient, absolute value
$k(f)$	—	FT coefficient for frequency f, absolute value
K	—	controller gain
K_{L}	—	lamp model sensitivity constant
l	—	generic index
L	H	inductance
L_{b}	H	converter inductor or its inductance
$\underline{L}_{\mathrm{b}}$	H	effective inductance
L_{L}	$\mathrm{lm\,W}^{-1}$	lamp model—conversion efficiency constant
$L70$	h	median useful time

Symbol	Unit	Description
m_1	%	m_{DC} evaluated with clean supply
m_2	%	m_{DC} evaluated with distorted supply
m_{ih}	%	relative interharmonic magnitude of the AC voltage
m_{DC}	%	relative modulation magnitude of the DC voltage
m_{RM}	%	relative modulation magnitude of the RM
m_{SM}	%	relative modulation magnitude of the SM
m_{W}	%	relative modulation magnitude of DC perturbed by waveform $W(t)$
n	—	diode emission coefficient (ideality factor)
n_{elect}	—	number of electrons
n_{photon}	—	number of photons
N	—	number of elements in a set
$\widetilde{N}$	var	nonactive power
NoiseUnc	V	uncertainty caused by noise
OffsetErr	ppm	offset error
OffsetTempCo	ppm/°C	offset temperature coefficient
p	—	FM and LFM gain constant
p_{inst}	—	instantaneous flicker
$p(t)$	W	instantaneous power
P	W	electric power (generally, or active)
P_1	W	fundamental active power
P_{DB}	W	DB power losses
P_{DC}	W	DC component active power
P_{H}	W	harmonic active power
P_{LED}	W	LED power consumption
P_{lt}	—	long term flicker severity index
P_{PI}	—	PI controller proportional component
P_{st}	—	flicker severity index evaluated from voltage
$P_{\mathrm{st}}^{\mathrm{LM}}$	—	flicker severity index evaluated from luminous flux
$P_{\mathrm{st1}}^{\mathrm{LM}}$	—	$P_{\mathrm{st}}^{\mathrm{LM}}$ evaluated in connection with the DB
$P_{\mathrm{st2}}^{\mathrm{LM}}$	—	$P_{\mathrm{st}}^{\mathrm{LM}}$ evaluated in connection without the DB
q_{e}	C	elementary charge, $q_{\mathrm{e}} \doteq 1.602\,176\,62 \cdot 10^{-19}$ C
Q	C	charge
Q_1	var	fundamental reactive power
Q_{e}	J	radiant energy
R	Ω	resistance
$R(s)$	—	controller transfer function
R_{b}	Ω	inductor series resistance
R_{DC}	Ω	smoothing capacitor ESR
R_{eq}	Ω	equivalent resistance
R_{o}	Ω	converter output port capacitor ESR
R_{s}	Ω	series resistor, its resistance
R_{sens}	Ω	sensing resistor, its resistance

Symbol	Unit	Description
Range	V	set measuring range of a measurement device
Reading	V	value of a measurand read from the measurement device
RefTempCo	ppm/°C	reference temperature coefficient
ResGainErr	ppm	residual gain error
ResOffsetErr	ppm	residual offset error
RndNoise	V	noise level of a measurement device at given *Range*
s	—	Laplace transform operator
S	VA	apparent power
$S_{1,\mathrm{H,N}}$	VA	fundamental, harmonic, nonfundamental apparent power
t	s	time
T	s	period (generally, fundamental)
T_{sw}	s	switching period
T_{s}	s	sampling period
T_{sim}	s	simulation time
$THD_{I,V}$	%	current, voltage total harmonic distortion
$u_{\mathrm{A,B}}(X)$	V	uncertainty of a measurand X, type A or B
$u_{\mathrm{AB}}(X)$	V	combined uncertainty of a measurand X
$u_{\mathrm{C}}(X)$	V	combined standard uncertainty of a measurand X
$U(X)$	V	expanded uncertainty of a measurand X
$v(t)$	V	voltage waveform
$v_{\sim}(t)$	V	voltage ripple
v_{D}	V	diode voltage
v_{DC}	V	DC link voltage (at the DB output)
v_{LED}	V	LED head voltage
v_{T}	V	transistor voltage
V	V	voltage (generally, RMS value)
V_{DC}	V	voltage DC component
V_{fw}	V	diode forward voltage
V_{g}	V	bandgap voltage
V_{H}	V	RMS of harmonic components of voltage
V_{in}, $v_{\mathrm{in}}(t)$	V	voltage at the input port
V_{m}	V	SAM modulating magnitude
V_{out}	V	voltage at the output port
V_{pp}	V	ripple PQ index
V_{ramp}	V	ramp signal peak value
V_{sens}	V	sensed voltage
V_{T}	V	thermal voltage
V_1	V	voltage—RMS of fundamental frequency component
$V(f)$	V	voltage—frequency component f
$V(\lambda)$	—	luminosity function
X_i	V	measurand, i-th observation
$\bar{X}$	V	measurand, mean value of the observations

Symbol	Unit	Description
X_{Lb}	Ω	inductor switching frequency reactance
z	—	z transform operator
Γ	—	subset of $(0;T)$ used for calculating *FI*
Δf	Hz	frequency difference
Δm	%	relative change of the relative modulation magnitude
$\Delta P_{\mathrm{st}}^{\mathrm{LM}}$	%	relative change of $P_{\mathrm{st}}^{\mathrm{LM}}$
ΔV	V	ripple depth, modulation depth
ΔV_{10}	—	equivalent $10\,\mathrm{Hz}$ voltage fluctuations flicker index
$\Delta\tau_{\mathrm{ext}}$	°C	temperature change from last external calibration
$\Delta\tau_{\mathrm{int}}$	°C	temperature change from last internal calibration
ε	—	machine epsilon, the smallest number addable to one; on the PC where the simulations were run $\varepsilon \doteq 2.220\,45 \cdot 10^{-16}$
ζ_i	—	transfer function nominator coefficients
η	%	efficiency
θ_1	rad	angle difference between voltage and current phasors at f_1
Θ_{j}	K	p-n junction thermodynamic temperature
κ	$\mathrm{lm\,W^{-1}}$	luminous efficacy of the source of the radiation
λ	m	wavelength
$\lambda_{1,\mathrm{D}}$	—	displacement, distortion power factor
λ_{FM}	—	FM filter constant
λ_{PF}	—	power factor
$\Lambda_{1,2}$	lm s	integrals used for calculating the *FI*,
μ	—	mean value
π	—	ratio of the circle's circumference and diameter, $\pi \doteq 3.141\,592\,6$
ρ	—	measurement uncertainty coverage factor
σ	—	standard deviation
τ	s	time constant
$\tau_{C,Cdc,Co}$	s	capacitor time constant
τ_{L}	s	incandescent lamp—filament thermal time constant
τ_{Lb}	s	DC-DC converter inductor time constant
τ_{PI}	s	PI regulator—integral time constant
$\varphi(f)$	rad	frequency component f phase angle
φ_{m}	rad	modulation frequency phase angle
Φ	lm	luminous flux
Φ_{e}	W	radiant flux
$\bar{\Phi}$	lm	luminous flux mean value
$\Phi(f)$	lm	luminous flux—frequency component f
ψ_i	—	transfer function denominator coefficients
ω	$\mathrm{rad\,s^{-1}}$	angular frequency (generally)
ω_{ESR}	$\mathrm{rad\,s^{-1}}$	angular frequency, transfer function ESR pole

Symbol	Unit	Description
ω_{RHP}	$\mathrm{rad\,s^{-1}}$	angular frequency, transfer function right half-plane zero
ω_0, ω_z	$\mathrm{rad\,s^{-1}}$	angular frequency, transfer function zero
ω_{1-4}	$\mathrm{rad\,s^{-1}}$	FM filter constants
ω_p	$\mathrm{rad\,s^{-1}}$	angular frequency, transfer function pole

Preface

This thesis came into being under dual supervision at two universities, the Technical University of Liberec, Czechia, and Université Toulouse III Paul Sabatier, France. During the time of my studies I spent some time in the laboratories of both. Furthermore, some of the experiments were performed in the laboratories of the Brno University of Technology, Czechia, and Ehime University, Japan. This is why various laboratory equipment was used throughout the thesis and sometimes the tested lamps were brought from one laboratory to another.

The thesis is written in English. This is why, contrary to conventions used in France and Czechia where a decimal comma is commonly used, a decimal point is used in this thesis for typing numbers with decimal cyphers. In compliance with the SI/ISO 31-0 standard, a space is used as a "thousands separator".

In some drawings and diagrams it is necessary to indicate the direction of voltage and current flow. According to a convention used in Czechia, the current is marked by a "full–point" arrow:

pointing in the opposite direction to the actual flow of the electrons. In a resistor, the current arrow would point from a higher potential node towards a lower potential node. Voltage is marked by a "hollow–point" arrow:

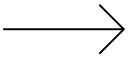

pointing from a higher potential node towards lower potential node and thus it is aligned with the current arrow when placed upon a resistor where the electric power is consumed:

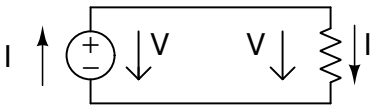

This way, the electric power dissipated by the resistor is positive.

Part I

Theoretical Background

1 Introduction

In the last decade, DC grids are an ever expanding field due to the advances of the related (mostly semiconductor based) technology, renewable power resources and LED lighting technology. DC grids are a promising concept in the field of electric power distribution for many reasons. Compared to AC grids they offer higher efficacy and reliability and they can reduce the complexity of the necessary technology.

AC grids have been used ever since the end of the 19$^{\text{th}}$ century. The reason behind that was related to the technology available in that period. AC voltage is easily generated using alternators, it can be transformed to various voltage levels with very high efficiency and it can be easily used to power synchronous and asynchronous induction motors. Incandescent lamps can operate on AC with a small risk of causing flicker.

For AC power transmission and distribution there has been enough time for the concept of *power quality* (PQ) to become very well established, defined and limited by standards, ensuring that the impact on human health is minimised.

During the course of the 20$^{\text{th}}$ century, the possibility to transmit and distribute power via DC was not given much attention. The use of DC was mostly restricted to special cases. Since then, the character of both the loads and energy sources has dramatically changed. Some distributed energy resources (DERs) such as photovoltaics (PVs) and energy storage systems (ESSs) such as batteries are naturally DC devices. When these are connected to AC supply the voltage needs to be converted to AC first; in the case of batteries, the conversion must be bi-directional.

In recent years, even natural AC loads (induction motors) are supplied through power semiconductor electronics (frequency converters, etc.) which can be supplied both by AC or DC. Most modern low–power appliances (household electronics power supplies, lighting applications) are supplied via switched supply where AC is rectified first. Particularly in lighting systems (according to [1], around 20 % of the total electricity consumption is on lighting), incandescent lamps were first replaced by fluorescent tubes and compact fluorescent lamps (CFLs), which in turn are to become obsolete due to LED lighting technology. As is explained further on in the thesis, LED is a DC–friendly technology.

In an environment where these energy sources and appliances are used, DC grids allow one to reduce the number of lossy AC-DC and DC-AC conversion stages in the grid either at the power sources, ESSs or at the load side. It is natural to expect that DC grids will be utilised even more frequently in new installations. Because it is a relatively young field, for the DC, the PQ concept is not established and

the corresponding standards are either insufficient or missing.

As it has already been mentioned earlier, light emitting diodes represent a breakout technology promising to replace older and less energy efficient artificial light sources. LEDs have been available since the 60s of the 20$^{\text{th}}$ century. In the beginning they were not suited for high power applications and, moreover, only monochromatic LEDs existed for several decades. With intensive research in this area more colours at higher brightness are becoming available.

With the invention of the high power blue LED in 1994 [2] it also became possible to construct an LED emitting white light, either by a combination of blue, red and green LEDs, or by using a blue LED in combination with a suitable phosphor layer. Further research is being made on increasing the power and brightness, this key invention has opened door to using LEDs in general lighting applications. For inventing blue LEDs, a Nobel prize for physics was awarded in 2014.

According to [3], LED penetration increased from $0.3\,\%$ worldwide in 2010 to $26\,\%$ in 2016 and is still expected to grow. By 2014, the LED penetration in lighting applications reached $3\,\%$ in the US and it was estimated that a complete replacement of all light sources for LED might save up to $1\,400\,\text{GWh}$ a year in the US only [4]. The same source states that the average efficacy of LED light sources ranged from $58\,\text{lm}\,\text{W}^{-1}$ to $108\,\text{lm}\,\text{W}^{-1}$ and the maximum efficacy reached up to $158\,\text{lm}\,\text{W}^{-1}$.

Intensive research is still going on in the area of LED lighting. It is to be expected that the penetration of LED technology throughout the world would increase together with the efficacy, making it an even more attractive alternative to traditional light sources.

It is to be expected that LEDs would be used in modern supply (possibly smart) grids very soon. These, in turn, can be expected to operate with low voltage DC. Indeed such networks already exist at least in the scale of units of buildings ([5], the EDISON project [6, 7] or the ABCDE project [8]).

LEDs are a specific technology and as such they represent a specific type of electric load when connected to the supply grid. Their reaction to various voltage variations is also difficult to predict. Only very recently the emitted standards begin to reflect the specificities and requirements of LED lighting systems.

One of these specifics is flicker. The term *flicker* can refer to any disturbing temporal variations of artificial (or even natural) light. All artificial light sources can flicker, though the cause and severity may vary. Flicker represents a risk for human health and safety. The flicker phenomenon is sufficiently described and documented for traditional lighting technologies, such as incandescent lamps and fluorescent tubes. With traditional light sources, the cause of flicker is usually poor supply voltage quality (along with ageing). This is why flicker has become an inseparable part of power quality considerations and standards. LED lamps have been shown to produce significant amount of flicker if measures are not taken to minimise it [LK1][STD1][9, 10, 11].

Enough attention has been paid to the efficiency, feasibility and reliability of DC grids and microgrids in recent research and dedicated literature (in addition to previously cited works, also see for example [12, 13, 14]). As both the DC networks and LEDs are relatively recent technologies, research on power quality in DC networks

is scarce though, and the discussions do not cover the topic of LEDs and flicker. (The author was surprised to see how little literature he could find on the topic of *power quality* in DC (see sec. 3.3)). This thesis aims to expand the work on this topic by analysing the flicker of LED lamps rated for extra low voltage. It aims to analyse how flicker properties of LED lamps would change if the lamps were adapted from an AC to DC supply.

Part I: Theoretical Background of the thesis summarises all the relevant information about LEDs, power quality and flicker and its evaluation. Chapter 2 DC Grids is dedicated to some aspects and devices typical for DC grids and for working with DC voltage. Chapter 3 Power Quality, Flicker, contains definitions and references relevant to power quality in both AC and DC, and importantly also on flicker. Chapter 4 Solid State Lighting Technology is dedicated to LED lighting technology and describes the current state of the art as far as the flicker is concerned.

Part II: Practical Part is split into three chapters. After setting the Thesis Objectives, Chapter 6 Experimental Part describes all performed experiments that are relevant to the topic of the thesis and their results. The evaluated experiments all relate to flicker of LED lamps. Most importantly, flicker immunity of ELV LED lamps under DC supply is tested with the original driver and afterwards with a simplified driver accustomed to a DC supply. Part of this set of experiments is meant to illustrate the current state of the art.

Chapter 7 Simulations describes all of the performed and relevant simulations and models thereof. A model of an LED lamp and a driver is created to mimic the situation of performed experiments. The aim is to explain the observed behaviour of the tested lamps. The thesis concludes with Chapter 8 Conclusion where all the results are summarised.

2 DC Grids

This thesis is not concerned with DC grids into deep detail. Instead it focuses on the behaviour of LED lamps under DC supply. To accomplish this and to give a reference frame for further considerations, this chapter is dedicated to some typical aspects of DC grids and devices working with DC voltage. Section 2.3 is dedicated to DC-DC converters, a topic which is related both to DC grids and to lighting technology.

The utilization of DC networks is very attractive for many reasons; mainly:

- with modern appliances fewer AC-DC conversions will be necessary; AC-DC conversions are lossy and add complexity to the system;
- no power factor correction (PFC) is needed in DC circuits; PFC is lossy and adds complexity to the system;
- no synchronisation of the network elements to the system frequency is needed;
- higher efficiency than AC;
- higher reliability than AC;
- no skin effect with DC transmission—thinner wires may be used;
- no parasitic inductance or capacitance in the wires;
- fewer lines; two or three wires with DC in comparison to two or four wires with AC;
- the number of "DC friendly" loads is increasing.

The reason for slow penetration of DC grids into our daily lives is that there are yet some engineering and research problems that need to be addressed. These are:

- voltage level conversion more complicated than with AC; in recent years advances in semiconductor technology have allowed the construction of minimal loss DC-DC converters; still these are more complicated devices than regular transformers used for AC voltage level conversion;
- DC-AC conversion is necessary with motors; high power motors may be expected to be supplied through control electronics which may be supplied with DC, but small household appliances like fans or mixers use AC designed motors;
- lack of standards for voltage levels;
- lack of standards for DC PQ (both indices and limits); for EMC there are existing standards which may be applied;
- switching represents a problem; the lack of natural zero crossing of the current may result in the risk of arcing in switches and circuit breakers, thus safety may be compromised [15].

2.1 DC Grid Types

The utilisation of DC networks can fall into one of these categories:

- transmission,
- distribution,
- microgrids.

The transmission networks are used to transmit electric power from large power plants to the region of utilisation, usually at very high voltage levels. The electric power distribution networks are responsible for supplying individual consumers. Both in transmission and distribution (T&D) grids the direction of power flow is given by definition. DC has been used for T&D for some time [16, 17]. Microgrids are a specific class of networks, see Sec. 2.1.1.

In DC transmission and distribution systems, the scheme can either be two–wired or three–wired (called *unipolar* and *bipolar*, respectively). In the first case, one of the wires is positive voltage and the other carries the ground potential. In the latter case, two wires are a positive voltage and a ground potential (neutral); the third wire is a negative voltage. Such a scenario helps to enhance the transmission grid capacity. The neutral line can be designed to conduct smaller currents.

2.1.1 Microgrids

A microgrid (MG) is a grid covering a small area (a single building or a neighbourhood). A microgrid can be connected to the main grid but it is usually capable of island operation. A MG contains appliances as well as distributed energy resources (DER), energy storage systems (ESS) and autonomous control systems. This means that the direction of power flow in a microgrid is not constant. MGs can either utilise AC, DC, or both. Hybrid MGs can benefit from either approach. Some reviews of DC MG topologies are available in [15, 17, 18, 19].

2.1.2 DC Grids with a Coupling to AC Grids

In most applications the DC network is connected to the AC distribution grid via a converter. In these cases the VQ will be influenced by the AC fundamental component and ripple, at twice the fundamental frequency, can be expected. The DC network can be coupled to the AC one either by a uni-directional or bi-directional converter; the latter one allows for energy flow in both directions. Coupling can be expected in residential areas, industrial supply networks, data centres, etc. [20]

2.1.3 Standalone DC Systems

DC systems have been extensively used in special applications, such as cars, ships [17], aircrafts [21] or remote stations in island operation. These standalone systems

lack coupling to the AC grid. For the PQ, it is important that there will be lack of ripple caused by the AC-DC conversion.

2.2 Voltage Levels

The standard IEC 60038 ed.7:2009 [STD2] defines the voltage levels both for AC and DC grids (Tab. 2.1). Several voltage levels are defined by the standard for each class. There are many standardised voltage levels with no assigned preference of purpose for DC.

Suitable voltage levels for DC grids are also discussed in [22]. The paper compares 24 V, 48 V and 120 V levels (ELV levels according to 2.1). It is found that 24 V level is too low; a high current level forces costly cabling in order to avoid conduction losses. This level can be used for extra low power appliances only, possibly LED lighting.

Table 2.1: Voltage level classes according to IEC 60038 ed.7:2009 [STD2]

class	AC (V_{RMS})	DC (V)	risk
high voltage	> 1 000	> 1 500	risk of arcing
low voltage	50–1 000	120–1 500	risk of shock
extra low voltage	< 50	< 120	low risk

2.3 DC-DC Converters

While for AC, the voltage level can be changed by a transformer, a more complicated approach is necessary for DC. Two–port circuits allowing one to transform the DC voltage level are called *DC-DC converters*. As they are one of the key subjects of study in this thesis, this section is dedicated to a summary about DC-DC converters.

Many converter topologies exist, each having its own uses, advantages and drawbacks. They can be sorted according to several aspects.

- **Direction of power flow**: uni-directional, bi-directional
- **Galvanic isolation**: isolated, non-isolated

As they are commonly used in electronic ballasts for lighting equipment, this thesis is primarily concerned with uni-directional converters. As a uni-directional AC-DC converter is basically a DC-DC converter equipped with a diode bridge, the reader can refer to [23] for more details or more topologies. An overview is also available in [24].

DC-DC converters are switched circuits. This means that the key part is a field effect transistor switched at high frequency (tens or hundreds of kHz) and a given duty ratio, changing the topology of the circuit. When the transistor is conducting current, the inductor is charging to a certain current level. When the transistor is

switched off, the inductor discharges into the load. If the inductor current reaches zero during the switching cycle, the converter is operated in the *discontinuous conduction mode* (DCM). If the current never reaches zero, we talk about the *continuous conduction mode* (CCM).

Converters usually utilise a feedback control loop to manipulate the switching duty ratio and, thus, to stabilise their output voltage. The converters can either be operated in *voltage mode control* (VMC) or *current mode control* (CMC). In the first mode, the only feedback quantity is the output voltage; in the latter mode, the inductor current is used for an additional feedback.

DC-DC converters are not completely lossless. The largest part of the losses occurs on the parasitic resistances of the switching transistor and the flywheel diode. Even so, the converters can be very efficient (with over $90\,\%$ efficiency).

Step–up (Boost) Converter Boost converters are uni-directional non-isolated converters used to raise the voltage level. Diagram is shown in Fig. 2.1a. Boost converters are used in electronic ballasts for fluorescent tubes to raise the rectified voltage up to approx. $400\,\mathrm{V}$.

The output voltage can be expressed as [25]:

$$V_{\text{out}} = V_{\text{in}} \frac{1}{1-D}\,, \tag{2.1}$$

$$V_{\text{out}} = V_{\text{in}} \frac{1}{2}\left(1 + \sqrt{1 + 2D^2 R_{\text{load}} \frac{1}{L_{\text{b}} f_{\text{sw}}}}\right) \tag{2.2}$$

for CCM and DCM, respectively; D is the duty ratio, R_{load} is the load resistance, L_{b} is the converter inductor and f_{sw} is the switching frequency. V_{in} and V_{out} is the voltage at the input and output ports, respectively. The plant transfer function (control to output, i.e., from the switch duty ratio to the output voltage) of the boost converter in the VMC [26] is:

$$G_{\text{boost,VMC}}(s) = \frac{V_{\text{in}}}{V_{\text{ramp}}\,(1-D)^2} \frac{\left(\frac{s}{\omega_{\text{ESR}}} + 1\right)\left(1 - \frac{s}{\omega_{\text{RHP}}}\right)}{\left(\frac{s}{\omega_0}\right)^2 + 1}\,, \tag{2.3}$$

where

$$\begin{aligned}
\omega_{\text{ESR}} &= \frac{1}{R_{\text{o,ESR}}\, C_{\text{o}}}\,,\\
\omega_{\text{RHP}} &= \frac{R}{\underline{L}_{\text{b}}}\,,\\
\omega_0 &= \frac{1}{\sqrt{\underline{L}_{\text{b}} C_{\text{o}}}}\,,\\
\underline{L}_{\text{b}} &= \frac{L_{\text{b}}}{(1-D)^2}\,,
\end{aligned}$$

$R_{\text{o,ESR}}$ is the equivalent series resistance of the capacitor C_{o}, ω_{RHP} is the right half plane zero and ω_0 is the double pole. $\underline{L}_{\text{b}}$ is the effective inductance. The PWM is

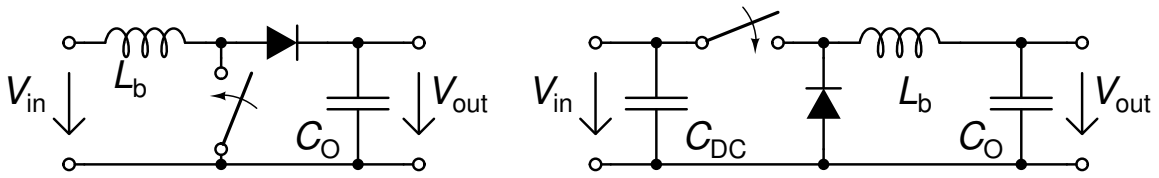

(a) step–up (boost) converter

(b) step–down (buck) converter; the capacitors can sometimes be excluded

Figure 2.1: Two of the most common DC-DC converter topologies

usually obtained from a comparator where one of the inputs is the error and the other input is a sawtooth signal. V_{ramp} is the peak of the sawtooth. RHP zero is typical for boost converters; it usually occurs at relatively high frequency compared to other modes.

Under CMC, the transfer function is more simple. Most notably, the double pole ω_0 is simplified to a single pole.

Step–down (Buck) Converter Buck converters are used to lower the voltage level. They are commonly utilised in LED lamp drivers. Diagram is shown in Fig. 2.1b.

The output voltage can be expressed as [27]:

$$V_{\text{out}} = V_{\text{in}} D\,, \tag{2.4}$$

$$V_{\text{out}} = V_{\text{in}} \frac{2}{1 + \sqrt{1 + 8 L_{\text{b}} f_{\text{sw}} \frac{1}{D^2 R_{\text{load}}}}} \tag{2.5}$$

for CCM and DCM, respectively. The plant transfer function of the buck converter in the VMC [26]:

$$G_{\text{buck,VMC}}(s) = \frac{V_{\text{in}}}{V_{\text{ramp}}} \frac{\frac{s}{\omega_{\text{ESR}}} + 1}{\left(\frac{s}{\omega_0}\right)^2 + 1}\,, \tag{2.6}$$

where

$$\omega_{\text{ESR}} = \frac{1}{R_{\text{ESR}} C_{\text{o}}}\,,$$
$$\omega_0 = \frac{1}{\sqrt{L_{\text{b}} C_{\text{o}}}}\,.$$

The quantities are the same as in the boost transfer function.

Other Converter Topologies include

- non-isolated: SEPIC, Ćuk, buck–boost;
- isolated: flyback.

Their detailed analysis is beyond the scope of this thesis.

2.3.1 Converter Compensation

There are several compensation designs used in converter design [26, 28]. In a majority of cases standard feedback loop with a controller is used. The feedback quantity is usually the output voltage (VMC—*voltage mode control*). In some cases an additional feedback loop from the inductor current is used (CMC—*current mode control*). The manipulated variable is usually the switch PWM duty ratio.

It is necessary that all the controllers are first order astatic. This means that one of the poles is placed in the origin. First order astatic systems are able to provide nonzero manipulated variable even if the error is zero and the setpoint has been reached. All the controllers may be easily implemented using an operational amplifier.

Type I Controller is basically an integrator; the transfer function of a Type I controller:

$$R_{\mathrm{I}}(s) = K\,\frac{1}{s} \tag{2.7}$$

This controller topology is the simplest one to use, but is not widely used for its limited dynamic properties.

Type II Controller contains two poles and a zero; one of the poles is placed at the origin:

$$R_{\mathrm{II}}(s) = K\,\frac{1}{s}\,\frac{\frac{s}{\omega_{\mathrm{z}}}+1}{\frac{s}{\omega_{\mathrm{p}}}+1} \tag{2.8}$$

Usually the modes are placed like this [28]:

$$\begin{aligned}\omega_{\mathrm{z}} &= \omega_0\,,\\ \omega_{\mathrm{p}} &= \omega_{\mathrm{ESR}}\,,\\ \text{or}\quad \omega_{\mathrm{p}} &= \frac{f_{\mathrm{sw}}}{2}\,.\end{aligned}$$

According to [26], the type II controller is commonly used in buck converters or boost converters under CMC.

Type III Controller contains three poles and two zeros, one pole is placed at the origin:

$$R_{\mathrm{III}}(s) = K\,\frac{1}{s}\,\frac{\left(\frac{s}{\omega_{\mathrm{z1}}}+1\right)\left(\frac{s}{\omega_{\mathrm{z2}}}+1\right)}{\left(\frac{s}{\omega_{\mathrm{p1}}}+1\right)\left(\frac{s}{\omega_{\mathrm{p2}}}+1\right)} \tag{2.9}$$

Usually the modes are placed like this [28]:

$$\begin{aligned}\omega_{\mathrm{z1}} &= \omega_{\mathrm{z2}} = \omega_0\,,\\ \omega_{\mathrm{p1}} &= \omega_{\mathrm{ESR}}\,,\\ \omega_{\mathrm{p2}} &= \frac{f_{\mathrm{sw}}}{2}\,.\end{aligned}$$

The type III controller has to be used in boost converters operated in the VMC and CCM [26].

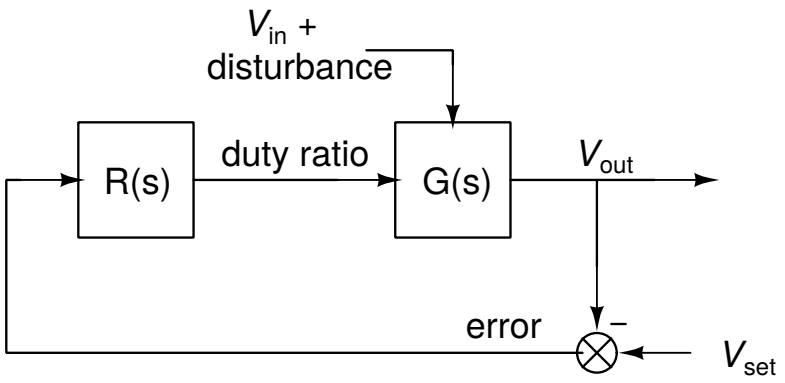

Figure 2.2: DC-DC converter feedback control loop; $R(s)$ is the regulator TF, $G(s)$ is the converter (boost, buck or any other topology) plant TF

PI Controller is one of the most commonly used feedback control structures containing a proportional and integral part:

$$R_{\mathrm{PI}}(s) = K\,\frac{\tau_{\mathrm{PI}}s + 1}{\tau_{\mathrm{PI}}s} = P_{\mathrm{PI}} + I_{\mathrm{PI}}\frac{1}{s}\,. \tag{2.10}$$

Hysteretic Control is an alternative approach to standard feedback controllers [26]. In this case there is no compensator used in the design. Instead the feedback variable is required to be within a predefined range. When its value reaches beyond the allowed limits an action is performed (switch on if the previous state was off and the variable is too low, or vice versa). The controlled variable is usually an inductor current.

With a hysteretic control, the switching can be performed either synchronously (switch is performed after the nearest clock pulse) or asynchronously (switch is performed instantaneously). The former requires an oscillator to generate clock signal and a D-latch; the latter is much simpler to implement, requiring only a comparator with hysteresis. With an asynchronous hysteretic control, the switching frequency is not fixed, but is dependent on the inductor size and load.

2.3.2 Converter Feedback Control with Disturbance

This thesis is primarily concerned with voltage variations. This section describes the reaction of a feedback controlled DC-DC converter to supply voltage disturbances. The DC input voltage disturbances can be described in the time domain as

$$v_{\mathrm{in}}(t) = V_{\mathrm{DC}} + v_{\sim}(t)\,. \tag{2.11}$$

Applying the Laplace transform will yield

$$V_{\mathrm{in}}(s) = \frac{V_{\mathrm{DC}}}{s} + V_{\sim}(s)\,. \tag{2.12}$$

Figure 2.2 shows the feedback loop used for stabilising the DC-DC converter output. From control theory, it is known that this circuit can be described by a closed loop transfer function in the form

$$F(s) = \frac{R(s)\,G(s)}{1 + R(s)\,G(s)}\,, \tag{2.13}$$

which is the TF from the V_{out} setpoint to the real output. Assuming the V_{out} setpoint is constant, this expression directly represents the description of the output voltage.

Equations (2.3) and (2.6) show that the TF can be split to the input voltage and the rest of the TF:

$$G(s) = V_{\text{in}}(s)\,G'(s)\,. \tag{2.14}$$

Substituting this into (2.13) we obtain

$$F(s) = \frac{V_{\text{in}}(s)\,R(s)\,G'(s)}{1 + V_{\text{in}}(s)\,R(s)\,G'(s)}$$

and further

$$F(s) = \frac{\left[\frac{V_{\text{DC}}(s)}{s} + V_{\sim}\right] R(s)\,G'(s)}{1 + \left[\frac{V_{\text{DC}}(s)}{s} + V_{\sim}\right] R(s)\,G'(s)}\,,$$

which can be expanded into

$$F(s) = \frac{V_{\text{DC}}(s)\,R(s)\,G'(s) + s\,V_{\sim}(s)\,R(s)\,G'(s)}{V_{\text{DC}}(s)\,R(s)\,G'(s) + s\left[1 + V_{\sim}(s)\,R(s)\,G'(s)\right]}\,. \tag{2.15}$$

After plugging in the buck TF (2.6) for $G'(s)$ and the PI controller TF (2.10) for $R(s)$, one can arrive to:

$$F(s) = \frac{\zeta_1 s^3 + \zeta_2 s^2 + \zeta_3 s + \zeta_4}{\psi_1 s^4 + \psi_2 s^3 + \psi_3 s^2 + \psi_4 s + \psi_5}\,, \tag{2.16}$$

where

$$\begin{aligned}
\zeta_1 &= \frac{V_{\sim}\tau_{\text{I}}}{\omega_{\text{ESR}}}\,,\\
\zeta_2 &= \frac{V_{\text{DC}}\tau_{\text{I}}}{\omega_{\text{ESR}}} + \frac{V_{\sim}}{\omega_{\text{ESR}}} + V_{\sim}\tau_{\text{I}}\,,\\
\zeta_3 &= V_{\sim} + \frac{V_{\text{DC}}}{\omega_{\text{ESR}}} + V_{\text{DC}}\tau_{\text{I}}\,,\\
\zeta_4 &= V_{\text{DC}}\,,\\
\psi_1 &= \frac{V_{\text{ramp}}\tau_{\text{I}}}{K\omega_0}\,,\\
\psi_2 &= \frac{V_{\sim}\tau_{\text{I}}}{\omega_{\text{ESR}}}\,,\\
\psi_3 &= \frac{V_{\text{DC}}\tau_{\text{I}}}{\omega_{\text{ESR}}} + \frac{V_{\sim}}{\omega_{\text{ESR}}} + V_{\sim}\tau_{\text{I}} + \frac{V_{\text{ramp}}\tau_{\text{I}}}{K}\,,\\
\psi_4 &= V_{\sim} + \frac{V_{\text{DC}}}{\omega_{\text{ESR}}} + V_{\text{DC}}\tau_{\text{I}}\,,\\
\psi_5 &= V_{\text{DC}}\,.
\end{aligned}$$

The presence of the $V_{\sim}$ in the $F(s)$ numerator and denominator suggests that expressing the direct effect of the input voltage disturbances is not straightforward and that the ripple affects not only the output voltage but also the system dynamics. Thus, the system can no longer be assumed to be time invariant as far as the setpoint to output TF is concerned.

3 Power Quality, Flicker

In order to ensure perfect function of all the appliances connected to the grid, the grid must satisfy many criteria. Power quality (PQ) is a term referring to a set of quantities and standardised limits, ways to monitor these quantities and to evaluate the reliability of the grid. Generally, the PQ problematics can be sorted in these groups:

1. Voltage quality (VQ),
2. Transfer efficiency, and
3. Reliability.

This thesis is primarily concerned with the VQ issues.

3.1 Relevant Standards

The voltage quality issues and electromagnetic compatibility (EMC) is treated in several standards.

Electromagnetic compatibility is generally treated by the IEC 61000 family of standards. The family is split into several parts. This section lists those relevant to flicker and devices with a current rating smaller than 16 A. This work is not concerned with devices with a higher rated current.

From part 2 of the family—the environment—the standard IEC 61000-2-2:2002 [STD3] gives us compatibility levels for low frequency disturbances (below 9 kHz) in low voltage AC grids. The P_{st} (see Sec. 3.4.2) is required to be below 1; P_{lt} is required to be lower than 0.8. Limits are also given for particular harmonic frequencies, see Tab. 3.1. The relevant voltage *THD* for the limits in the table is 11 %. Similar limits to the standard IEC 61000-2-2:2002 can be found in the standard IEEE 519:2014 [STD4].

From part 3 of the family—the limits—the standard IEC 61000-3-2 ed.4:2015 [STD5] gives us the limits for the harmonic current emission of appliances connected to an AC grid. The current distortion limits are important for two main reasons. Firstly, high THD_I lowers the *PF* in AC grids (as shown later in Sec. 3.2.1); secondly, due to grid impedance, it causes voltage distortion. This standard is also relevant for light sources. Light sources with (active) power consumption above 25 W are required to fulfil limits given in the standard. In practice this implicates the utilisation of an active PFC. For light sources below 25 W (the standard particularly names

Table 3.1: Compatibility levels for harmonic frequencies according to IEC 61000-2-2:2002 [STD3]; j denotes the harmonic order, m_h the allowable harmonic voltage in % of fundamental voltage.

Odd j, non-multiple of 3		Odd j, multiple of 3		Even j	
j	m_h (%)	j	m_h (%)	j	m_h (%)
5	6	3	5	2	2
7	5	9	1.5	4	1
11	3.5	15	0.4	6	0.5
13	3	21	0.3	8	0.5
17–49	$2.27(17/j) - 0.27$	27–45	0.2	10–50	$0.25(10/j) + 0.25$

discharge lamps), different specifications for the shape of the current waveform may be used. LED lamps should be named in this standard along with discharge lamps to make the standard more versatile.

From part 3 of the family, another standard, IEC 61000-3-3 ed.3:2014 [STD6], gives us the limits for voltage flicker emission by devices connected to an AC grid. The P_st is required to be lower than 1; P_lt must be below 0.65. To the author's knowledge, there is no similar standard for emissions in DC grids.

Part 4 of the family—testing and measurement techniques—standardises the means to test the immunity of grid connected devices to the VQ events: dips, interruptions and distortion. Let us name particularly:

- IEC 61000-4-11 ed.2:2004 [STD7] standardises tests to determine immunity to voltage dips and voltage interruptions in AC grids
- IEC 61000-4-13:2003 [STD8] standardises tests to determine immunity to harmonics and interharmonics below 2 kHz in AC grids
- IEC 61000-4-14:2000 [STD9] standardises tests to determine immunity voltage fluctuations in AC grids
- IEC 61000-4-15 ed.2:2010 [STD10] defines *voltage flickermeter* (FM), for details, see Sec. 3.4.2 and App. A; this standard was adopted into the IEEE system of standards as IEEE Standard 1453-2015 [STD11]
- IEC 61000-4-17:1999 [STD12] standardises tests to determine immunity to voltage ripple in DC grids
- IEC 61000-4-19:2014 [STD13] standardises tests to determine immunity to supraharmonics up to 150 kHz in AC grids
- IEC 61000-4-29:2000 [STD14] standardises tests to determine immunity to voltage dips and interruptions in DC grids

General normative definitions and references about EMC emission and immunity are given in part 6 of the family—generic standards. Let us mention standard

IEC 61000-6-1 ed.2:2005 [STD15], touching the immunity of household and light industry devices.

Outside of the IEC 61000 family of standards, the immunity requirements for lighting equipment are given in standard IEC 61547 ed.2:2009 [STD16]. This standard works with the overall luminous flux produced by the tested lamp. Lamps with active drivers are required to pass relevant tests from the IEC 61000-4 family of standards. Lamps with passive drivers are not required to pass any tests whatsoever. This standard does not work with flicker as the observed quantity.

The technical report IEC TR 61547-1:2015 [STD17] defines a *light flickermeter* (LFM) as a simplification of the FM defined in IEC 61000-4-15 ed.2:2010. For further details see Section 3.4.3 and Appendix B.

3.2 Power Quality in AC Grids

This thesis is primarily concerned with DC grids, but it is essential to examine the PQ in AC grids also. The PQ requirements for the public AC grid in the European Union has been standardised in EN Standard 50160 [STD18]. According to the standard, the following quantities should be measured and monitored:

- voltage RMS value
- voltage asymmetry
- voltage events—dips, interruptions, swells, rapid voltage changes, transients
- fundamental frequency
- harmonic components up to 2 kHz
- IEC flicker (see Sec. 3.4.2)

The standard gives us limitations for each of these quantities and events. Parallel to EN Standard 50160 there is also IEEE Standard 1159-2009 [STD19], dealing with power quality in general.

Alien frequencies in the mains voltage can be sorted into these groups:

- subharmonics—below 50 Hz
- harmonics—integer multiples of the fundamental 50 Hz component up to 2 kHz
- interharmonics—non-integer multiples of the fundamental component between 50 Hz and 2 kHz

PQ measurement devices are called *PQ analysers* and should comply with standards [STD3, STD20].

In recent years, with the utilisation of modern semiconductor switching technology, the scientific community has become aware of a significant rise of harmonic distortion above 2 kHz (and commonly below 150 kHz). These frequency

components are commonly referred to as ***supraharmonics*** even though the term has not been standardised yet [29]. The components are not sorted between harmonics and interharmonics any more in this frequency band. Large quantities of data are necessarily generated when analysing supraharmonics. To decrease the amount of such data on storage devices, some grouping algorithm is required. Standard IEC 61000-4-7 ed.2:2002 [STD21] and [LK2] refer to this topic.

With the presence of an alien frequency component, the voltage waveform can be described as

$$v(t) = V_1\sqrt{2}\,\sin(2\pi f_1 t) + V(f_{\text{ih}})\sqrt{2}\,\sin(2\pi f_{\text{ih}} t + \varphi_{\text{ih}})\,, \tag{3.1}$$

where V_1 is the fundamental voltage RMS value, f_1 is the fundamental frequency, f_{ih} is the alien frequency (not necessarily harmonic) and φ_{ih} its angle; $V(f_{\text{ih}})$ denotes the interharmonic RMS value. The relative interharmonic component magnitude is defined as the ratio of the interharmonic RMS value and V_1 expressed in a %:

$$m_{\text{ih}} = \frac{V(f_{\text{ih}})}{V_1} \cdot 100\,. \tag{3.2}$$

Frequency f_{ih} may also sometimes be denoted as f_{h} if it refers to the integer harmonic component, and similarly m_{ih} may be denoted as m_{h}.

With the ***sinusoidal amplitude modulation*** (SAM, or SM), the voltage waveform can be described as

$$v(t) = V_1\sqrt{2}\,\sin(2\pi f_1 t)\Big(1 + \frac{m_{\text{SM}}}{100}\sin(2\pi f_{\text{m}} t + \varphi_{\text{m}})\Big)\,, \tag{3.3}$$

where, in this case, f_{m} is the modulation frequency and φ_{m} is the angle of the modulating function, m_{SM} is now the modulation magnitude expressed in a % of the nominal voltage:

$$m_{\text{SM}} = \frac{V_{\text{m}}}{V_1} \cdot 100\,, \tag{3.4}$$

V_{m} being the modulating sine magnitude. The modulation depth would be obtained as $d_{\text{SM}} = 2m_{\text{SM}}$. The modulating sine function can be substituted by some other function (often rectangular; in such case Eq. (3.3) describes the ***rectangular amplitude modulation*** and the corresponding quantities would be denoted as m_{RM} and d_{RM}).

3.2.1 Calculating Power Quantities in AC

Calculating the transmitted electric power in AC grids is not straightforward due to all the VQ issues. The definitions are standardised in standard IEEE 1459:2010 [STD22]. First of all, the ***active power*** is defined as

$$P = \frac{1}{T}\int_0^T p(t)\,\mathrm{d}t = \frac{1}{T}\int_0^T u(t)i(t)\,\mathrm{d}t\,, \tag{3.5}$$

where $p(t)$ is the ***instantaneous power*** gained as the voltage waveform times the current waveform $u(t)i(t)$ and T is a time interval over which the power is evaluated. It

should be a multiple of the fundamental period (in $50\,\mathrm{Hz}$ systems, $T = 20\,\mathrm{ms}$). The active power shows how much electric power has been transmitted to the end customer and effectively used for supplying loads.

The thermal effect of the AC voltage and current on a resistive load can be expressed using an RMS value:

$$V = \sqrt{\frac{1}{T}\int_0^T v^2(t)\,\mathrm{d}t}\,, \tag{3.6}$$

$$I = \sqrt{\frac{1}{T}\int_0^T i^2(t)\,\mathrm{d}t}\,. \tag{3.7}$$

Using the voltage and current RMS values, the *apparent power* can be defined:

$$S = VI\,. \tag{3.8}$$

The definition of the apparent power for a single–phase system is straightforward; the situation is much more complicated for three–phase systems. Although the power calculations have been standardised in [STD22] they are still subject to debate [30, 31, 32][LK3].

Because of the Definitions (3.5), (3.6) and (3.7), from the Cauchy–Schwartz inequality, it is clear that $S \geq P$. Their ratio is called the *power factor*:

$$\lambda_{\mathrm{PF}} = \frac{P}{S}\,. \tag{3.9}$$

Its values are between 0 and 1, with 1 being the ideal value. A low λ_{PF} means non-ideal power flow in the grid and unnecessarily high line losses. The λ_{PF} is an important quantity showing how much of the power flowing in the grid can be turned into useful work. This is why attention is paid to it in this work.

Assuming the voltage and current are perfect sine waveforms the λ_{PF} can be decreased when the current and voltage waveforms are not in phase with each other. This is called the *displacement power factor*:

$$\lambda_1 = \cos\theta_1 = \frac{P_1}{S_1}\,, \tag{3.10}$$

where φ is the phase shift between the voltage and current waveforms and 1 denotes the fundamental harmonic component. The λ_1 is usually compensated using an additional capacitor or inductor connected to the load.

For single phase scenarios, where harmonic distortion is present, the voltage and current waveforms may be written down as

$$v(t) = v_1(t) + v_{\mathrm{H}}(t)\,, \tag{3.11}$$

$$i(t) = i_1(t) + i_{\mathrm{H}}(t)\,. \tag{3.12}$$

For RMS values, one can obtain

$$V^2 = V_1^2 + V_\mathrm{H}^2\,, \tag{3.13}$$
$$I^2 = I_1^2 + I_\mathrm{H}^2\,. \tag{3.14}$$

Standard [STD22] defines the fundamental active, reactive and apparent powers:

$$P_1 = V_1 I_1 \cos\theta_1\,, \tag{3.15}$$
$$Q_1 = V_1 I_1 \sin\theta_1\,, \tag{3.16}$$
$$S_1 = V_1 I_1 = \sqrt{P_1^2 + Q_1^2}\,, \tag{3.17}$$

non-fundamental (harmonic) active power, apparent power and non-active power:

$$P_H = P - P_1\,, \tag{3.18}$$
$$S_N = \sqrt{S^2 - S_1^2}\,, \tag{3.19}$$
$$\widetilde{N} = \sqrt{S^2 - P^2}\,, \tag{3.20}$$

and finally the current distortion power, voltage distortion power, harmonic apparent power and harmonic distortion power:

$$D_I = V_1 I_\mathrm{H}\,, \tag{3.21}$$
$$D_V = V_\mathrm{H} I_1\,, \tag{3.22}$$
$$S_\mathrm{H} = V_\mathrm{H} I_\mathrm{H}\,, \tag{3.23}$$
$$D_\mathrm{H} = \sqrt{S_\mathrm{H}^2 - P_\mathrm{H}^2}\,. \tag{3.24}$$

The physical meaning of at least some of these quantities is questionable.

The power factor λ_PF can, thus, also be decreased by the harmonic distortion. The harmonic distortion of the voltage or current is usually expressed by a quantity called *total harmonic distortion* (*THD*):

$$\mathit{THD}_V = \frac{V_\mathrm{H}}{V_1}\,, \tag{3.25}$$
$$\mathit{THD}_I = \frac{I_\mathrm{H}}{I_1}\,. \tag{3.26}$$

In this case, the λ_PF can be expressed as:

$$\begin{aligned}\lambda_\mathrm{PF} &= \frac{P}{S_1\sqrt{1+\mathit{THD}_V^2}\sqrt{1+\mathit{THD}_I^2}} = \\ &= \lambda_1 \frac{\frac{P_\mathrm{H}}{P_1}+1}{\sqrt{1+\mathit{THD}_V^2}\sqrt{1+\mathit{THD}_I^2}} = \lambda_1\lambda_\mathrm{D}\,,\end{aligned} \tag{3.27}$$

where the new fraction is called the *distortion power factor*. The λ_D is more problematic to compensate. Usually it is compensated using passive filters or active power factor correction circuits (active PFC) whose aim is to decrease the *THD*.

3.3 Power Quality in DC Grids

Power quality (and voltage quality) in DC grids is neither standardised nor monitored. For the purpose of PQ monitoring, it is possible to transfer some AC definitions to DC. DC grids will experience voltage dips, notches, short interruptions, etc. The instantaneous power definition is still valid.

However, the evaluation of some AC quantities (harmonic distortion, apparent power) will be problematic in DC because they need to be evaluated over a prespecified time interval T. It is questionable how long this time interval should be in DC grids. In AC-coupled grids, the evaluation period may be equal to the fundamental period of the AC grid; in this way, all AC PQ indices and power components may be evaluated, substituting V_{DC} for the AC fundamental components V_1, as is shown later in this section. An unsuitable choice of T will result in spectral leakage of the voltage and current frequency components and possibly the wrong value of V_{DC}.

The methods for measuring and evaluating power quality in DC grids should reflect the nature of the possible sources of disturbances or distortion as well as appliances. Periodic voltage disturbances may be expected as well as transients, voltage dips and interruptions, periodic current distortion and current inrush peaks [19, 33].

A discussion over VQ in DC grids was opened in [33]. Assuming the DC voltage is composed of its mean value and *ripple*:

$$v(t) = V_{\mathrm{DC}} + v_{\sim}(t)\,, \tag{3.28}$$

the ripple is practically any signal which remains after removing the DC voltage:

$$V_{\mathrm{DC}} = \frac{1}{T}\int_0^T v(t)\,\mathrm{d}t\,, \tag{3.29}$$

where T denotes an interval over which the quantity is evaluated. This means that the mean value of the ripple is zero. The *ripple depth* is given by:

$$\Delta V = \max_T v(t) - \min_T v(t) = \max_T v_{\sim}(t) - \min_T v_{\sim}(t)\,. \tag{3.30}$$

The *relative ripple depth* can be then defined by

$$d_{\mathrm{DC}} = \frac{\Delta V}{V_{\mathrm{DC}}} \cdot 100\,, \tag{3.31}$$

and the *relative ripple magnitude* is then given by

$$m_{\mathrm{DC}} = \frac{\Delta V}{2V_{\mathrm{DC}}} \cdot 100 = \frac{d_{\mathrm{DC}}}{2}\,. \tag{3.32}$$

If the ripple is caused by a single frequency (or a particular known waveform; for example, an artificially imposed ripple as a part of an experiment), these quantities

can be referred to as the *(relative) modulation depth* and the *(relative) modulation magnitude* instead. There is no need to make a difference between amplitude modulation and adding an extra frequency component in DC. [33] states similarly to [STD12] that the main source of ripple are rectifiers.

Further, [33] defines *low frequency sinusoidal disturbances* as a DC alternative to harmonics. Based on these, a D_{LFSD} index is proposed, similar to *THD*:

$$D_{\mathrm{LFSD}} = \sqrt{\frac{1}{V_{\mathrm{DC}}^2} \sum_{f=1}^{N} V(f)^2} \,, \tag{3.33}$$

where $V(f)$ are the N evaluated frequency components of the voltage spectrum. Similarly, the D_{LFSD} may be defined for the current. [33] further defines the ***ripple PQ index*** as

$$V_{\mathrm{pp}} = \max_{i,l} \left(V[i] - V[i + l + l_T] \right) \,, \tag{3.34}$$

where $V[i]$ is the i-th sample of the evaluated signal and l_T the minimum length of the evaluation window in the samples. Its existence is aimed at filtering out high frequency noise. The V_{pp} index does not need T for the evaluation.

A recent advance in defining PQ indices is given in [34] and [35]. In a general case of lack of predefined T, these works suggest using a first order low pass filter for determining V_{DC} (the filter TF in the z domain):

$$H_{\mathrm{LP}}(z) = \frac{1 + z^{-1}}{(1 + 2\tau F_{\mathrm{s}}) + (1 - 2\tau F_{\mathrm{s}}) z^{-1}} \,, \tag{3.35}$$

F_{s} being the sampling frequency and τ the time constant of the filter. This approach removes the need to define T. Instead, the filter time constant τ must be chosen. If τ is chosen conservatively (large enough), the V_{DC} calculation will be tolerant towards frequency variations of the ripple.

3.3.1 Calculating Power Quantities in DC Grids

It is not clear how to calculate electric power in DC systems. Electric power components like active power, reactive power, apparent power are commonly used to evaluate the utilisation of an AC electric system. In DC systems, their definitions will be problematic. This is due to lack of a natural evaluation period T. In DC systems, a certain part of the loads will be resistive (heaters, boilers), while the rest of the loads will be DC-DC converters. The simulation in Sec. 7.4.2 (Fig. 7.13) shows the current consumption of a loaded low power DC-DC converter. The current consumption reflects the switching frequency of the converter, unless an EMI filter is used.

As already mentioned earlier, in case the evaluation period T is given (AC-coupled networks), the voltage DC component may be identified easily (see Eq. (3.29)) and, thus, the voltage (and also current) waveform may be written down

as already shown in Eq. (3.28). Now, the active power P may be defined in the usual way also; the fundamental active power will be

$$P_{\mathrm{DC}} = V_{\mathrm{DC}} I_{\mathrm{DC}} \,. \tag{3.36}$$

Because of Eqs. (3.29), (3.28) and (3.6) and because the mean value of $v_{\sim}(t) = 0$, for the RMS value of the ripple, one may write:

$$\begin{aligned} V_{\mathrm{H}}^2 &= \frac{1}{T}\int_0^T \big(v(t) - V_{\mathrm{DC}}\big)^2 \mathrm{d}t = \frac{1}{T}\int_0^T \big(v^2(t) - 2v(t)V_{\mathrm{DC}} + V_{\mathrm{DC}}^2\big)\mathrm{d}t = \\ &= \frac{1}{T}\int_0^T v^2(t)\mathrm{d}t - \frac{2V_{\mathrm{DC}}}{T}\int_0^T v(t)\mathrm{d}t + \frac{1}{T}\int_0^T V_{\mathrm{DC}}^2\mathrm{d}t = V^2 - V_{\mathrm{DC}}^2 \,, \end{aligned} \tag{3.37}$$

and similarly for the current.

For the active power, one may write:

$$\begin{aligned} P &= \frac{1}{T}\int_0^T \big(V_{\mathrm{DC}} + v_{\sim}(t)\big)\big(I_{\mathrm{DC}} + i_{\sim}(t)\big)\mathrm{d}t = \\ &= \frac{1}{T}\int_0^T \big(V_{\mathrm{DC}} I_{\mathrm{DC}} + V_{\mathrm{DC}} i_{\sim}(t) + v_{\sim}(t) I_{\mathrm{DC}} + v_{\sim}(t) i_{\sim}(t)\big)\mathrm{d}t = \\ &= V_{\mathrm{DC}} I_{\mathrm{DC}} + \frac{1}{T}\int_0^T v_{\sim}(t) i_{\sim}(t)\mathrm{d}t = P_{\mathrm{DC}} + P_{\mathrm{H}} \,, \end{aligned} \tag{3.38}$$

Further, all of the power components defined in Sec. 3.2.1 may be defined for DC also:

$$S_{\mathrm{DC}} = V_{\mathrm{DC}} I_{\mathrm{DC}} \,, \tag{3.39}$$

$$D_I = V_{\mathrm{DC}} I_{\mathrm{H}} \,, \tag{3.40}$$

$$D_V = V_{\mathrm{H}} I_{\mathrm{DC}} \,. \tag{3.41}$$

The remaining quantities (S_{H}, S_{N}, $\widetilde{N}$, D_{H}, *THD*) will even follow the same equations. It is apparent that $S_{\mathrm{DC}} = P_{\mathrm{DC}} = V_{\mathrm{DC}} I_{\mathrm{DC}}$. There is no need to define the fundamental reactive power Q_{DC} in DC systems.

The hereby proposed system of power components is based on the IEEE Std. 1459-2010 [STD22] where each of the standardised power components for AC has its own parallel for DC.

3.4 Flicker

Flicker (both a noun and verb) is a term used for describing annoying rapid changes in the quality or quantity of artificial light (photometric flicker, Sec. 3.4.1). Because

one of the main causes of flicker is poor voltage quality, it is very often considered as a specific part of VQ problems. In a more narrow sense, it is a VQ quantity used for evaluating the impact of poor VQ on a human exposed to artificial light, Sec. 3.4.2.

3.4.1 Photometric Flicker

In order to differentiate from the VQ quantity, I prefer to use the term *photometric flicker* for actual rapid changes in light produced by artificial light sources even though this term is not commonly used in literature.

The human retina has been shown to transfer frequencies as high as 165 Hz [36]. However, this does not mean that conscious flicker perception can be induced at such frequency. The term *critical fusion frequency* (*CFF*) refers to a frequency at which the human observer fails to perceive (sense, consciously observe and possibly report) flickering light and experiences steady perception. The *CFF* varies under different conditions (modulation depth, chromaticity, ambient light, etc.) but generally it is in the range from 50 Hz to 90 Hz [STD1].

CFF estimates do not take eye motion into account. A fast pulsing light (above *CFF*) may result in a series of repetitive visual patterns on the observer's retina during rapid eye movement (saccade) [37, 38]. This phenomenon is called *intrasaccadic flicker perception* and is the reason behind some common visual phenomena such as *rainbow effect* or *phantom array effect.* If the eye is steady and the light source is moving, the phenomenon is called *stroboscopic effect.* According to [37], the intrasaccadic perception can occur with light pulsing at up to 2 kHz. Thus, the flicker can be sorted in three categories [STD1][9, 36, 37, 39] according to the frequency:

Visible flicker below the *CFF*; visible flicker is sensed by the eye via direct observation, perceived by the brain, consciously recognised and can be reported;

Invisible flicker above the *CFF*, but below approx. 165 Hz to 200 Hz; invisible flicker is not consciously perceived by direct observation but is sensed by the eye retina and, thus, can also cause headaches and have other biological impact; interference with other flickering light sources may possibly result in visible flicker.

High frequency flicker up to 2 kHz can cause intrasaccadic flicker perception, stroboscopic effect or phantom array effect; interference with other flickering light sources may possibly result in visible flicker.

The causes of flicker are explained later in Sec. 4.3. Flicker at various frequencies can cause various problems in lighting applications. These can be sorted into two groups.

Health problems include tiredness, work inefficiency, headache, migraine (mostly in sub-clinical variants—not reported to a doctor) and epileptic seizures in the most extreme situations. A summary of the health impact of flicker is given in [40].

Safety issues include stroboscopic effect (moving parts of rotary equipment appear stationary) or phantom array effect (multiple perception of a single source). These effects pose a problem for workers in factories or late night drivers.

A very detailed summary of health risks and other flicker related issues is given in [STD1]. It is the author's impression that despite all the cited research and evidence, the flicker is not a recognised problem among the uninformed public.

Luminance Flicker

Luminance flicker refers to time–based fluctuations of the luminous flux. Naturally it can be evaluated using two quantities, the flicker index (*FI*) and percent flicker (*FP*) [STD1]:

$$FP = \frac{\max_{t\in(0;T)}\left(\Phi(t)\right) - \min_{t\in(0;T)}\left(\Phi(t)\right)}{\max_{t\in(0;T)}\left(\Phi(t)\right) + \min_{t\in(0;T)}\left(\Phi(t)\right)} \cdot 100\,, \tag{3.42}$$

$$FI = \frac{\Lambda_1}{\Lambda_2}\,, \tag{3.43}$$

where

$$\Lambda_1 = \int_\Gamma \left(\Phi(t) - \bar{\Phi}\right) \mathrm{d}t\,,\ \Gamma = \left\{t \in (0;T) : \Phi(t) > \bar{\Phi}\right\},$$

$$\Lambda_2 = \int_0^T \Phi(t)\,\mathrm{d}t\,,$$

$\Phi(t)$ denotes the observed luminous flux and T is the length of the time interval over which the quantities are evaluated; preferably it will be a fundamental period of the fluctuations, if there is any. Evaluating the *FI* and *FP* has been standardised in [STD1]. *FP* is a value between 0 and $100\,\%$, where $100\,\%$ indicates the highest possible modulation depth; for even a very short period of time, the light goes completely dark during the flicker cycle. *FP* does not take the period length into account.

FP might seem similar to the modulation depth d. However, one has to bear in mind that the *FP* cannot be higher than $100\,\%$, while d can be any positive number. Differences will be significant, especially if the waveform reaches zero. These two quantities will be equivalent if the mean value is equal to half of the sum of minimum and maximum.

FI is an unbounded non-negative value. It takes into account the waveform shape. This is why the correlation between *FP* and *FI* is not guaranteed. *FI* and *FP* do not take frequency of the flickering into account and do not evaluate the severity of the flicker impact on a human observer.

Standard IEEE 1789-2015 [STD1] assesses the risk of high frequency flicker and intrasaccadic flicker perception in relation to *FP* and frequency. Practice recommendations are given, stating how large the *FP* can be for given frequency up to $3\,\mathrm{kHz}$. A graphical representation of the recommendation for minimising high frequency flicker perception is shown in Fig. 3.2. The standard offers three recommended practices:

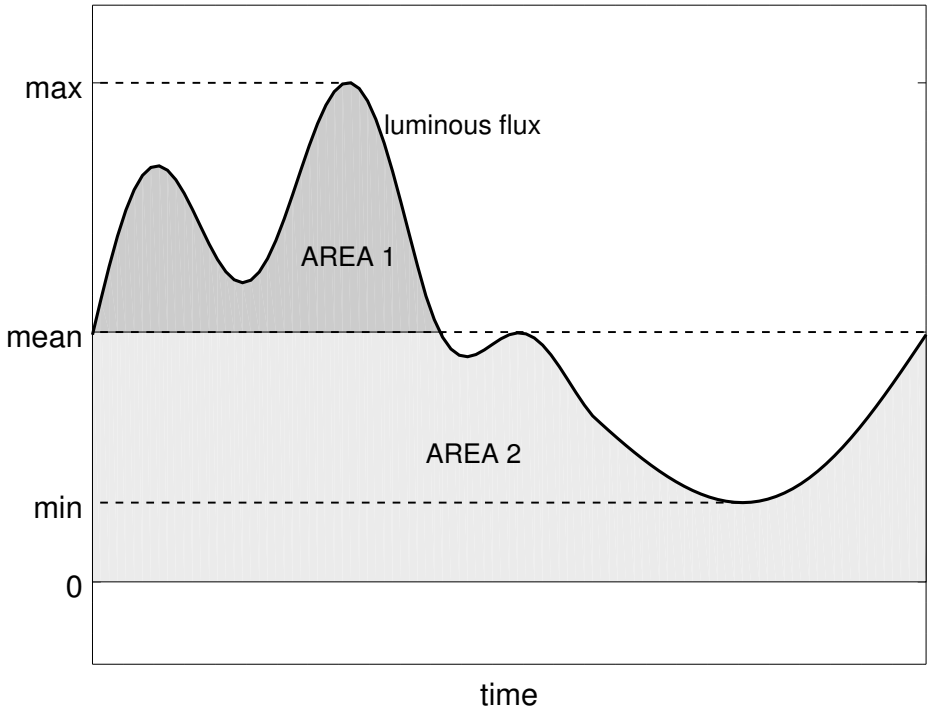

Figure 3.1: Graphically depicted calculation of *FI* and *FP*, Eqs. (3.42) and (3.43); area S_1 corresponds to AREA 1 in the figure; area S_2 corresponds to AREA 1 + AREA 2 in the figure.

1. to minimise any "*adverse biological effects of flicker*" (in Fig. 3.2, it is shown as a yellow line):
   - below 90 Hz, the *FP* should be smaller than $0.025 \times$ frequency (result in %),
   - between 90 and 1 250 Hz, the *FP* should be smaller than $0.08 \times$ frequency (result in %),
   - above 1 250 Hz, no limitations apply;
2. to stay at no observable effect level (NOEL, in Fig. 3.2, it is shown as a green line):
   - below 90 Hz, the *FP* should be smaller than $0.01 \times$ frequency (result in %),
   - between 90 and 3 000 Hz, the *FP* should be smaller than $0.033\,3 \times$ frequency (result in %),
   - above 3 000 Hz, no limitations apply;
3. to prevent seizures, below 90 Hz, the *FP* should be smaller than 5 % (in Fig. 3.2, it is shown as a red line).

In case there are several frequencies present in the flux waveform, the limits applied should correspond to the lowest frequency component. Because higher fre-

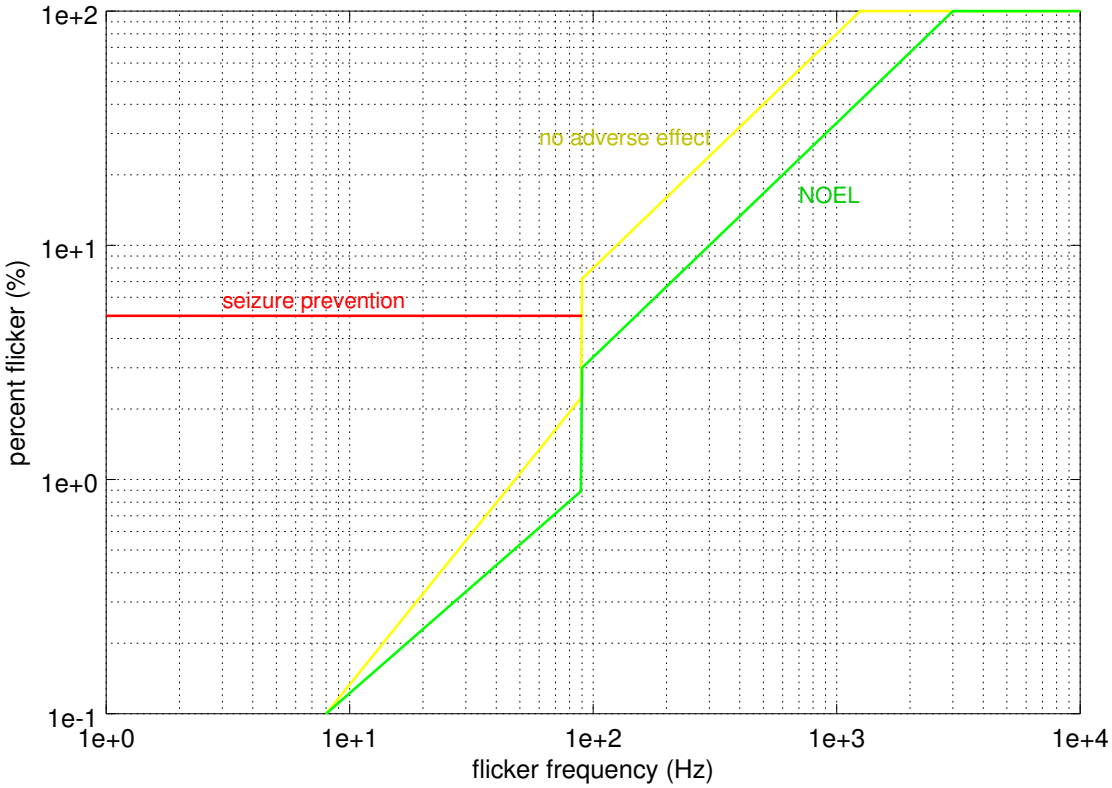

Figure 3.2: *FP* limits for minimising flicker perception according to IEEE Standard 1789-2015 [STD1]

quencies might be beyond the relevant bandwidth, they may be excluded from the evaluation.

Heterochromatic Flicker

The term *heterochromatic flicker* refers to rapid changes of the spectral distribution of the analysed light, while the intensity stays constant. There are no standards nor established measurement techniques for analysing heterochromatic flicker. It is known that the *CFF* for chromatic flicker is generally lower than for luminance flicker (approx. 25 Hz [39]). Heterochromatic flicker is not discussed further in this thesis.

Spatial Flicker

The term *spatial flicker* refers to disturbing or annoying spatial patterns in the visible field of an observer. Analogically to luminous or heterochromatic flicker, a spatial frequency can be defined as a number of repetitive visual (dark / light) patterns per degree of the visual angle [41]. In the terms of spatial frequency, the *critical spatial frequency* as an analogy to the *CFF* can be defined also.

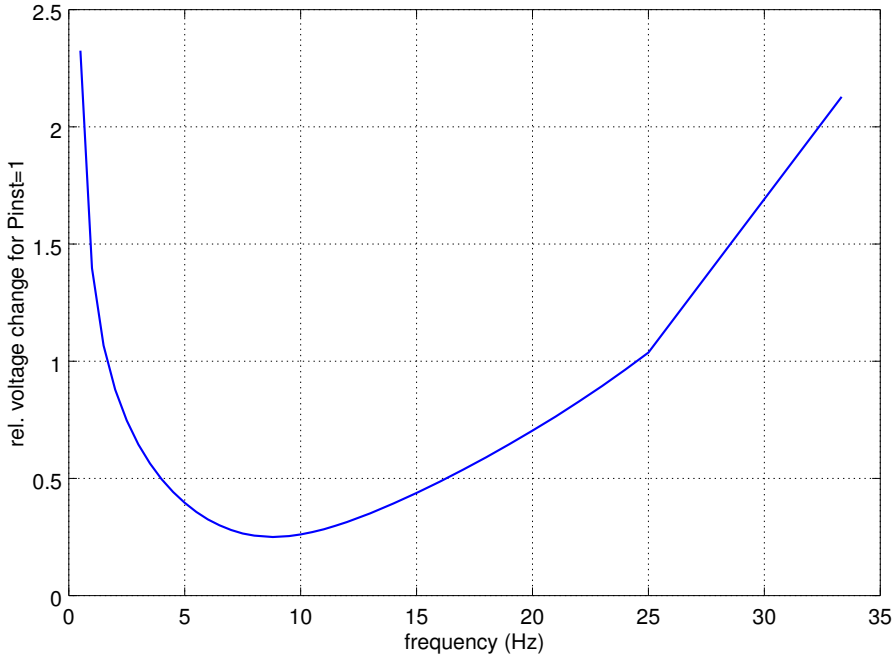

Figure 3.3: Eye immunity to luminous flux modulations caused by a relative sinusoidal voltage change supplying a 60 W incandescent bulb, according to IEC 61000-4-15 [STD10]

3.4.2 Voltage Related Flicker Quantities

IEC Flicker and Flicker Meter

The IEC Standard 61000-4-15 [STD10] defines a way of estimating the annoyance of flicker produced by 60 W incandescent lamp supplied by a distorted 230 V AC voltage from the voltage measurement without actually analysing the light output of the lamp.

In the standard, there are several indices defined; firstly the instantaneous flicker p_{inst}, the short–term flicker P_{st}, evaluated from 10–minute intervals and long–term flicker P_{lt}, evaluated from 2–hour intervals. Evaluation from an interval of arbitrary length (more than one minute) is allowed; in such a case, the flicker index is denoted by P_T, where T is given time interval. Thus, $P_{1\text{min}}$ denotes flicker evaluated from a 1 min long measurement.

The IEC flicker meter is a device capable of calculating P_{lt} and P_{st} from the AC voltage measurements.

Part of the IEC FM is a model of a 60 W two–filament incandescent lamp. This is why the IEC flicker corresponds to the actual photometric flicker only when such lamp is used. Other lighting technologies may behave in a completely different way. Furthermore, only visible flicker perception is taken into account. Invisible and high frequency flicker is disregarded with IEC FM.

Details about the included filters and their transfer functions are included in Appendix A. Several improvements of IEC FM were proposed [42, 43, 44, 45, 46, 47].

Equivalent Ten Hertz Voltage Fluctuations Flicker Index

In some countries in eastern Asia a distinct quantity is used to evaluate flicker from voltage measurements. The so called *equivalent* 10 Hz *voltage fluctuations flicker* (denoted as ΔV_{10}) was proposed by the Central Research Institute for Electric Power Industry, Japan (CRIEPI). It is much simpler to evaluate than the IEC P_{st} and P_{lt} quantities [48, 49]:

$$\Delta V_{10} = \sqrt{\sum_{i=1}^{N} (a_i V_i)^2}\,, \tag{3.44}$$

where a_i are given sensitivity coefficients for the i-th voltage harmonic, $a_{10} = 1$. A more detailed link between the voltage variations and flickering of a particular lamp is missing, however. ΔV_{10} is required to be below 0.45. A single and straightforward way to convert between ΔV_{10} and P_{st} values cannot be determined [50]. ΔV_{10} is not used further in this thesis.

3.4.3 Objective Flicker Meters

Since IEC FM evaluates P_{st} from public grid voltage measurements only, there have been efforts to evaluate the same quantity directly from light intensity measurements. Such devices are called *objective flicker meters* [51, 52, 53] or *light flicker meters* (LFM) [STD17]. A LFM implemented according to [51] was used in this work. Details about LFM are given in Appendix B. The output quantity of LFM is $P_{\mathrm{st}}^{\mathrm{LM}}$.

The technical report IEC TR 61457-1:2015 [STD17] adopts the testing voltage signals from [STD10]. These signals are originally used for FM calibration purposes. The technical report suggests one to use these signals as immunity tests for lighting devices. As for P_{st}, the commonly recognised limit is 1, one can presume that the same limit will apply to $P_{\mathrm{st}}^{\mathrm{LM}}$, even though such information is missing in the TR.

3.4.4 Flicker Evaluation Summary

From the previous sections it is clear that there are many ways to measure and evaluate the flicker level, each of them having its own advantages and disadvantages. A summary is presented at this point (Tab. 3.2).

Voltage–based metrics are problematic to be used with kinds of lamps other than incandescent. Therefore, flux–based metrics are preferred to be used. These can also be applied to DC supplied devices, because the supply voltage is not relevant for them any more.

Standard IEEE 1789-2015 [STD1] does not specify the voltage conditions under which flicker requirements should be fulfilled. This way, the *FP* and *FI* may be evaluated at any time, but a conservative approach must be taken when judging compliance with the standard under non-nominal conditions.

The testing signals (modulated AC voltage) in IEC 61000-4-15 [STD10] are only meant for testing FM implementation. The testing signals are adopted for immunity tests in IEC TR 61547-1 [STD17] but still these are only applicable to AC supplies.

In this thesis, $P_{\mathrm{st}}^{\mathrm{LM}}$ and *FP* are used to evaluate flicker from luminous flux. P_{st} is used in Sec. 6.2 only to be compared with $P_{\mathrm{st}}^{\mathrm{LM}}$.

3.4.5 Flicker in AC Grids

The problem of flicker in AC grids is well studied. VQ issues connected with flicker in AC are mainly [54]:

- Amplitude modulation—simplified cases that are usually regarded in literature are sine modulation (SM) and rectangular modulation (RM)
- Phase modulation
- Phase jumps
- Subharmonic or interharmonic pollution

Fundamental sinusoidal voltage with added sub- or interharmonic component can be written as (see Eq. (3.1) also)

$$v(t) = V\left[\sin(2\pi f_1 t) + \frac{m_{\mathrm{ih}}}{100}\sin(2\pi f_{\mathrm{ih}} t)\right]. \tag{3.45}$$

An example of such a waveform is shown on Fig. 7.4 in Sec. 7.2. It is apparent that adding an interharmonic component is very similar to an amplitude modulation at a relatively low frequency f_{m}. Assuming that $f_{\mathrm{ih}} = f_1 + \Delta f < 2f_1$, the voltage waveform (3.45) can be rewritten as [55]:

$$\begin{aligned} v(t) = V\left[\sin(2\pi f_1 t) + \frac{m_{\mathrm{ih}}}{100}\cos(2\pi \Delta f t)\right]\sin(2\pi h f_1 t) + \\ + V\frac{m_{\mathrm{ih}}}{100}\sin(2\pi \Delta f t)\cos(2\pi f_1 t)\,. \end{aligned} \tag{3.46}$$

Table 3.2: Summary of the available standardised flicker metrics and their properties

standard	IEC 61000-4-15 [STD10]	IEC TR 61547-1 [STD17]	IEEE 1789-2015 [STD1]	CRIEPI
metric	P_{st}	$P_{\mathrm{st}}^{\mathrm{LM}}$	*FP*, *FI*	ΔV_{10}
metric applicable to DC devices	no	yes	yes	no
evaluated quantity	voltage	flux	flux	voltage
limits exist	yes	no	for *FP*	yes
invisible and HF flicker	no	no	yes	no
evaluates health impact	yes	yes	no	yes
EUT immunity tests	no	yes	no	no
tests applicable to DC devices	NA	no	NA	NA

The last term shows that there is a harmonic term with a fundamental frequency f_1 amplitude modulated at frequency Δf which is the sought after modulation frequency f_m. This reasoning can be expanded to higher interharmonic frequencies; the modulation frequency will be equal to

$$f_\mathrm{m} = |j f_1 - f_\mathrm{ih}| \,, \tag{3.47}$$

j being the order of the harmonic component closest to f_ih.

This has an important impact. It shows that even at a high frequency ($> 100\,\mathrm{Hz}$) interharmonics can cause voltage fluctuations at frequency below CFF and, thus, cause visible flicker perception.

In DC grids, the situation will be different as there is no fundamental frequency and, thus, no intermodulation occurs. Visible flicker can be caused by frequencies below *CFF* only, etc. This situation is demonstrated via a simulation in Sec. 7.2.

3.4.6 Flicker Around Us

Practically all artificial light sources flicker. Incandescent lamps supplied by clean $50\,\mathrm{Hz}$ voltage flicker at $100\,\mathrm{Hz}$ with $FP = 8\,\%$. Due to thermal inertia of the filament, the lamp does not go off when the supply voltage drops to zero, but cools down and thus emits less light at a different dominant wavelength (Planck's law). Therefore, incandescent lamps produce temporal as well as chromatic flicker at an unobservable level. Flicker may be observable if the supply voltage is distorted with sub- and interharmonic frequencies.

In fluorescent tubes, light is produced by electric discharge. When supplied by AC voltage at low frequency, the discharge goes off. Due to this, fluorescent tubes flicker considerably too. Compact fluorescent tubes (CFLs) with electronic driver usually mitigate this problem as a driver is necessary for supplying the discharge by high frequency voltage. Even CFLs are not completely flicker immune though [56].

The light in fluorescent tubes is usually produced at an invisible wavelength and is transformed to a visible wavelength using a phosphor. Depending on the particular type of the phosphor, it usually has some inertia as well (time constant in the order of units to tens of ms) and, thus, the produced FP is not always $100\,\%$.

Flickering is particularly problematic with LED lamps. This is because LED drivers may follow various topologies with different flicker sensitivity. Flicker is no longer only a VQ or ageing issue.

Generally, with any kind of lighting technology, flicker can be caused by supply voltage variations. These are mostly unintentional and caused by appliances connected to the grid. However, ripple voltage control (RVC) can also cause visible flicker. In Czechia, RVC telegrams are transmitted mostly at $216.6\,\mathrm{Hz}$ (other interharmonic frequencies are also used, sometimes up to $3\,\mathrm{kHz}$); due to resonances, the ripple magnitude may rise up to $9\,\%$ [STD8].

3.4.7 Pulsing Light and Human Perception

In the 19th century, it was shown [57] that light pulsing continuously above the *CFF* at a photopic intensity level is perceived at the same effective (subjective) brightness as the steady light of the average objective level. This is known as the *Talbot–Plateau* (TB) law.

As contrary to the Talbot–Plateau law, at the beginning of the 20th century, it was discovered [58] that a single light pulse at a scotopic intensity level is perceived brighter than it would have been if it were steady. This is known as the Broca–Sulzer effect. Discovery of the Broca–Sulzer effect led to efforts to revise the Talbot–Plateau law below the *CFF*. It has been shown by several experiments [59, 60, 61] that a continuously pulsing light also appears brighter than it would if the TB held. Thus, the TB does not hold below the *CFF*. This is known as the *brightness enhancement effect*. The brightness enhancement effect is strongest at about 10 Hz.

The TB was formulated based on experiments performed with technology available in 19th century, i.e., a steady light source and a shutter. These did not allow for the very steep rising and falling slopes of the pulses. SSL technology allows for that, which has led to attempts to revise the TB above the *CFF* also for bright (photopic) continuously pulsing light using SSL allowing for very steep rising and falling slopes [LK4, LK5][62, 63, 64, 65, 66, 67, 68]. However, the results published in these works are inconsistent and, moreover, it has been shown [LK6] that some of them are systematically over- or under-estimated due to an incorrect evaluation.

4 Solid State Lighting Technology

Solid state lighting technology (SSL) is a term referring to lighting technologies based on semiconductors (LED and OLED) contrary to incandescent lamps and fluorescent tubes. While OLEDs find their usage in display technology, inorganic compound based LEDs are used in general lighting applications and therefore are more of concern for this thesis. An overview of solid state lighting technology, its features, advantages and drawbacks is available in [69, 70] and [71].

This chapter describes the light emitting diodes, their operating principle and the properties of the light they produce. LED drivers as a necessary part of any LED lighting system are described in detail. The specifics of flicker produced by LEDs are also mentioned.

4.1 Characteristics of LEDs

LEDs are different from other artificial light sources. They allow for very fast switching (order of µs) and can endure many more switching cycles. The lifetime of LEDs is much longer than that of incandescent lamps or fluorescent tubes (tens of kilohours). The luminous efficacy of LEDs reaches beyond $100\,\mathrm{lm\,W^{-1}}$.

4.1.1 Diodes—p-n Junctions

From an electrical point of view, LEDs are diodes. The ideal relationship between the applied voltage V_d and the diode current I_d can be modelled by Shockley's law [72]:

$$I_\mathrm{d} = I_0 \left(e^{\frac{V_\mathrm{d}}{nV_\mathrm{T}}} - 1 \right), \tag{4.1}$$

where $V_\mathrm{T} = \frac{k\Theta_\mathrm{j}}{q_\mathrm{e}}$ is the *thermal voltage* given by the junction temperature Θ_j, the Boltzmann constant k and elementary charge q_e, I_0 is the reverse saturation current. The parameter n is the *emission coefficient* or *ideality factor*, usually varying from 1 to 4. Shockley's law does not account for diode series resistance, which is an important element especially at higher diode currents at which high power LEDs are usually operated.

In Eq. (4.1) there is explicit dependency on the junction temperature. The reverse saturation current I_0, the series resistance and the emission coefficient n are also dependant on the junction temperature [73]. Similarly, as with regular diodes, there are no parameter values typical for LEDs. The parameters can vary rapidly. A V-I

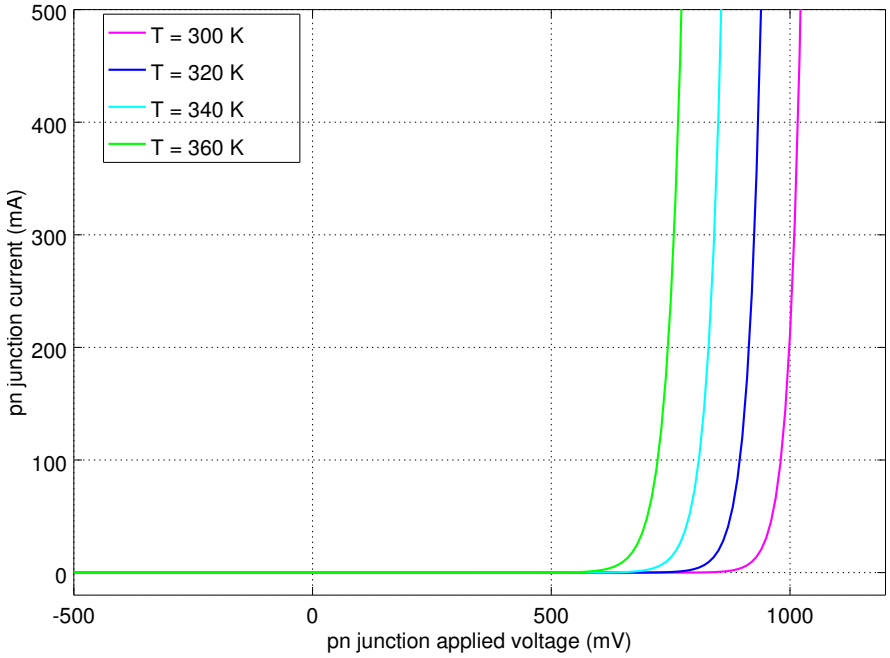

Figure 4.1: A V-I characteristic (Shockley's law) for an ideal diode; temperature dependence is shown, $n = 1$.

characteristic derived from Eq. (4.1) is shown on Fig. 4.1. It can be observed that at higher junction temperatures with constant current, the voltage decreases; thus, the power consumption decreases also.

4.1.2 Light Emission in LEDs

The light in LEDs is emitted when the p-n junction is forward biased. As the electrons recombine with holes in close vicinity of the depletion layer, a quantum of energy is released. This energy may be wasted as heat or emitted in the form of a photon, an effect called *electroluminescence*. The ratio of heat recombinations and radiative recombinations is called the *internal quantum efficiency* (*IQE*). The ratio of electrons flowing into the p-n junction and radiated photons is called the *external quantum efficiency* (*EQE*) [74]. The frequency of the radiated photon is given by the bandgap energy of the junction. Thus, it is a constant property of the junction material. Normally, LEDs produce monochromatic light. Various semiconductive compounds are used to produce various wavelengths.

The luminous flux produced by an LED is a function of the LED current and temperature [75]. Let us examine how. For the following considerations, let us assume a monochromatic green LED radiating at wavelength $\lambda = 555\,\mathrm{nm}$.

The current flowing through the p-n junction represents charge Q moving in a given direction. For constant current, we can express the diode current I_d as

$$I_\mathrm{d} = \frac{Q}{t} \tag{4.2}$$

where t is time. Knowing the elementary charge of an electron q_e, we can calculate the total number of transferred electrons $n_\mathrm{elect} = \frac{Q}{q_\mathrm{e}}$ and so

$$I_\mathrm{d} = \frac{n_\mathrm{elect} q_\mathrm{e}}{t}\,. \tag{4.3}$$

As already mentioned above, the quantity ***EQE*** represents the ratio of electrons flowing into the junction and the emitted photons, and thus

$$I_\mathrm{d} = \frac{n_\mathrm{photon}}{\boldsymbol{EQE}} \frac{q_\mathrm{e}}{t}\,. \tag{4.4}$$

The energy of a single photon E_photon at a given wavelength is equal to the bandgap energy which is known to be

$$E_\mathrm{photon} = \frac{hc}{\lambda} \tag{4.5}$$

(h is Planck's constant, c the speed of light) and so we also know the total energy radiated by the LED $Q_\mathrm{e} = n_\mathrm{photon} E_\mathrm{photon}$. Radiant flux Φ_e can be expressed from the energy as

$$\Phi_\mathrm{e} = \frac{Q_\mathrm{e}}{t} = \frac{n_\mathrm{photon} E_\mathrm{photon}}{t} = \frac{n_\mathrm{photon} hc}{t\lambda}\,, \tag{4.6}$$

which will give the luminous flux (at $555\,\mathrm{nm}$ the $V(\lambda) = 1$)

$$\Phi = 683.002 \Phi_\mathrm{e}\,. \tag{4.7}$$

Plugging (4.4) into (4.7) will yield the relationship between the luminous flux and diode current:

$$\Phi = 683.002\, \boldsymbol{EQE}\, \frac{hc}{q_\mathrm{e}\lambda} I_\mathrm{d}\,. \tag{4.8}$$

The term $\frac{hc}{q_\mathrm{e}\lambda}$ is in volts and, therefore, it is also sometimes referred to as the ***bandgap voltage*** V_g [73]. The product $V_\mathrm{g} I_\mathrm{d}$ is why the radiant power comes in watts even though it is neither linked to LED electric power consumption nor diode voltage.

EQE is dependant on the diode current and the junction temperature Θ_j, and, thus, $\boldsymbol{EQE} = \boldsymbol{EQE}(I_\mathrm{d}, \Theta_\mathrm{j})$ [74]. The same is true for $\lambda = \lambda(I_\mathrm{d}, \Theta_\mathrm{j})$ [73, 76]. These dependencies need to be evaluated experimentally as they vary among diodes. ***EQE*** can range from $8\,\%$ to $70\,\%$ [74].

In reality, Eq. (4.8) will be more complicated as LEDs are rarely strictly monochromatic and the wavelength of the emitted photons is subject to a certain spread. Moreover, white LEDs incorporating a phosphor layer (see Sec. 4.1.3) emit light through the entire visible spectrum ($380\,\mathrm{nm}$ to $780\,\mathrm{nm}$) and the overall efficacy is decreased by the phosphor layer. According to [73], it is possible to model the light output of a phosphor based white LED using the ***luminous efficacy of the source of radiation***:

$$\kappa = \frac{\Phi}{\Phi_\mathrm{e}} \tag{4.9}$$

which exhibits only a slight linear dependency on the forward current and junction temperature. This way, for white LEDs, the Eq. (4.8) may be rewritten as

$$\Phi = \kappa \boldsymbol{EQE}\, V_\mathrm{g} I_\mathrm{d}\,. \tag{4.10}$$

When the diode power consumption P_{LED} is known, luminous efficacy can be defined as ([77])

$$E = \frac{\Phi}{P_{\mathrm{LED}}}\,, \tag{4.11}$$

where E is the luminous efficacy in $\mathrm{lm\,W^{-1}}$. E is also sometimes called the *wall–plug efficiency*, albeit this term invokes the (wrong) impression that the efficiency of the LED driver has been taken into account. The highest possible value is $E = 683.002\,\mathrm{lm\,W^{-1}}$ which will be achieved for an ideal green ($\lambda = 555\,\mathrm{nm}$) LED with $EQE = 1$.

For the purpose of this thesis, it is necessary to estimate the amount of produced light from the simulated electrical quantities. There are several approaches for modelling the light output [73, 77, 78]. Each of them necessarily incorporates thermal properties of the lamp and its heat sink. It is clear that the thermal effect is always important and non-negligible when the operating point is moving significantly.

When such a thermal model is not available, it may seem reasonable to assume isothermal conditions (constant junction temperature). Particularly for the purpose of this thesis, the objective is to estimate flicker, i.e. luminous flux fluctuations around a constant operating point. In LED lamps, the diodes are usually mounted on a heat sink serving as a low–pass filter for the temperature. If unknown, according to [73], it is advisable to assume the junction temperature $\Theta_{\mathrm{j}} = 85\,^{\circ}\mathrm{C}$.

Under *isothermal* conditions estimating the flux as a linear function of the LED, the current seems reasonable as the true relationship is close to linear [73, Figs. 6, 18 and 22][79, Fig. 15][80, Figs. 4a and 4b]. However it is necessary to bear in mind that such an estimation is limited to small variations of the operating point and only valid if thermal equilibrium has been reached.

4.1.3 White Light Output Characteristics

Using the LEDs white light can be produced either by a combination of blue, green and red LEDs (RGB solution) or by using a monochromatic blue (or ultra-violet) LED in combination with a phosphor in order to transform the produced light into other wavelength bands [81].

The RGB approach suffers from several drawbacks; particularly the supply electronics need to be relatively complex and, therefore, this solution is used only when there is need to dynamically adjust the produced wavelength spectrum.

The latter (phosphor based) solution is commonly used in lighting applications. An example of a spectrum produced by a phosphor based white LED is in Fig. 4.2. The figure shows a spectrum of a cool white LED; the exact position of the primary emission peak (blue region, approx. 460 nm) may vary in dependence on the type of LED used and for a single LED it usually varies with the junction temperature [73]. Secondary (phosphor) emission is apparent in the figure within the range from 500 nm to 700 nm. The primary emission peak shifts towards shorter wavelengths with a rising junction temperature and, thus, with the diode current level also; the *CCT* changes from 6 400 K to 7 500 K.

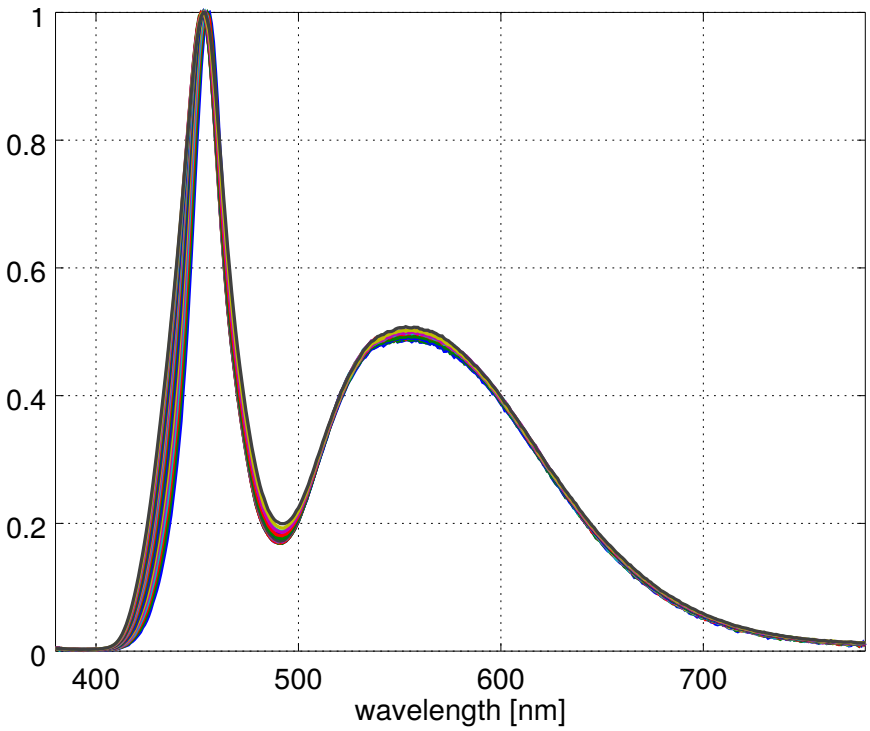

Figure 4.2: A typical (normalised) wavelength spectrum of a phosphor based cool white LED; 22 measurements with varying supply current.

The secondary emission may vary due to the specific type and amount of the phosphor. The more phosphor used, the more energy is transferred into the green and red region of the spectrum and a warmer colour is produced for the cost of luminous efficacy. Lengthening the photon's wavelength decreases its energy according to Eq. (4.5) and, thus, the radiant power is decreased also (not so the luminous flux).

For a complete picture, the standard photopic luminosity function $V(\lambda)$ is shown also (see Fig. 4.3). The human eye is most sensitive roughly between 400 and $700\,\mathrm{nm}$.

4.1.4 LED Ageing

Even though the lifespan of a typical LED is given in tens of kilohours, they are not immune to ageing effects. The degradation of the diodes causes decrease of the light output and change in the wavelength spectrum [82]. The ageing is caused mainly by thermal stress of the junction. Thus a properly designed heat sink is important for LED lamps.

The lifespan for LEDs is often given as the mean time when the LED reaches $70\,\%$ of its nominal output (*Median Useful Life* denoted as *L70*, [11]). Both primary and secondary emission is subject to ageing [82]. An accelerated ageing process for research purposes can be made via thermal stress [83]. Other ageing parameter is the *Abrupt Failure Value* (*AFV*) [11]. It is the percentage of lamps which completely fail at *L70*. Ageing is not known to affect flicker.

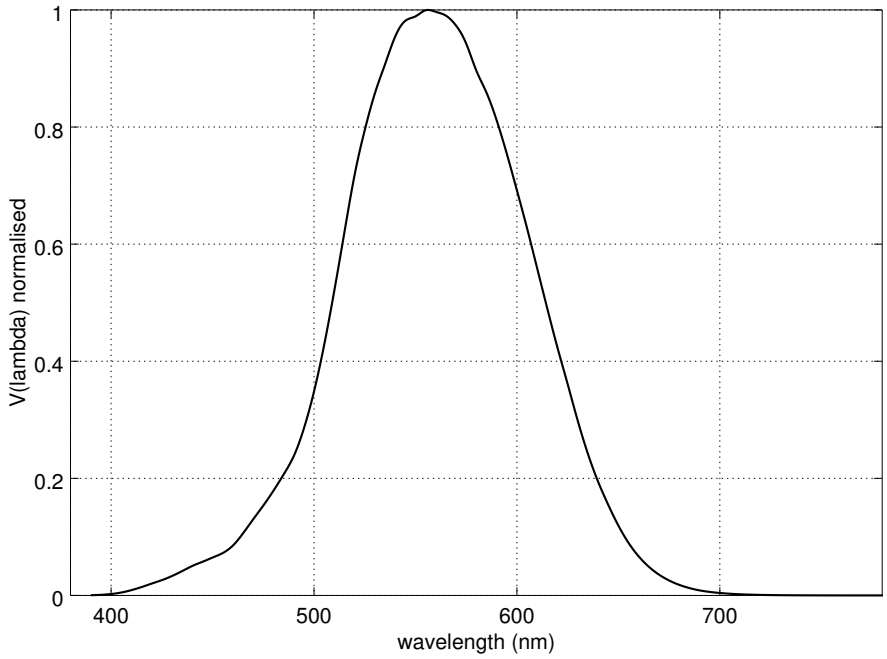

Figure 4.3: Photopic luminosity function $V(\lambda)$—eye sensitivity to light at a given wavelength

4.2 LED Lamps—Drivers

In order to ensure LEDs operate at a constant operating point, it is necessary that LEDs are supplied from a customised LED driver [LK7, LK1][STD1][9, 11, 84]. The primary function of the driver is to ensure constant operating point for the LED matrix via a constant voltage or constant current control. If it is desired, the driver can also implement a dimming feature. A compact combination of LEDs (in the vast majority of cases there is more than one diode, connected in a series chain or series–parallel matrix) and a driver to form an LED lamp. The driver can be separated from the LED head in special applications [11]. Each lamp manufacturer uses their own driver design and, thus, there are many various driver topologies used [LK7, LK1][84].

The following text describes the parts of two stage LED drivers in more detail. Single stage drivers may be encountered where the PFC circuit is combined with a DC-DC converter.

Electromagnetic Interference Filter Under AC supply, the driver can produce a significant amount of harmonic current emission. Except for poor quality drivers where EMC is ignored, the high frequency part of the emission is removed by a simple EMI filter at the input of the driver. The filter can be implemented using an inductor, a pair of magnetically coupled inductors, a resistor, or a combination of either.

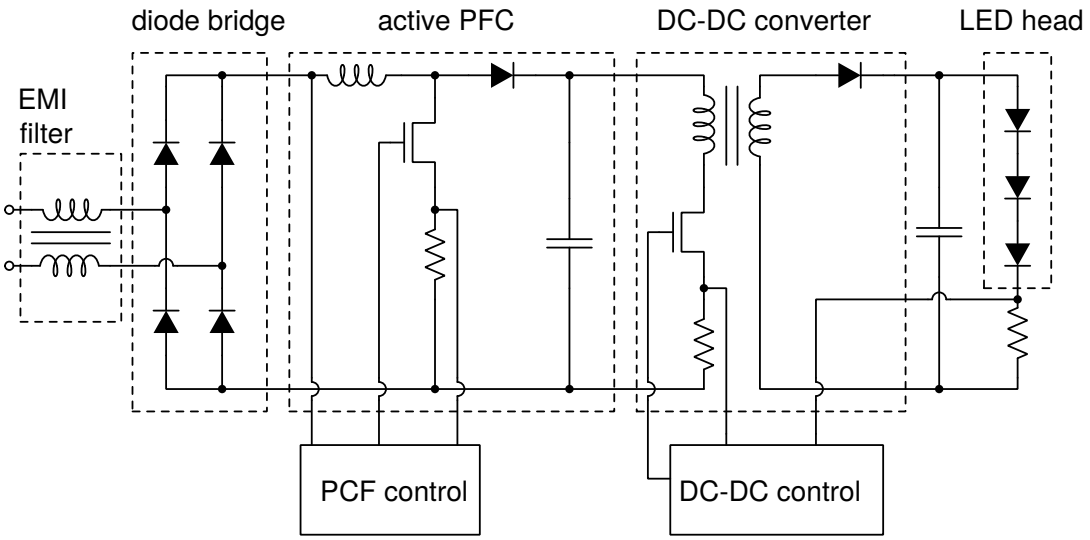

Figure 4.4: A diagram of a two stage LED driver for AC supply; the drawing shows an EMI filter realised by a pair of magnetically coupled inductors, a diode bridge, an active PFC circuit, a DC-DC conversion stage and an LED head

Diode Bridge In AC applications the voltage needs to be rectified and converted to DC in the driver. This is why any driver declared for AC supply can be safely used with DC supply without the risk of harming the driver or the lamp. The rectification is done via a *diode bridge* (DB, also referred to as *diode rectifier* or *Graetz bridge*). The DB is a key subject of research in this thesis, so it is worthy to pay some attention to its properties.

The DB (shown in Fig. 4.4) is a two–port circuit consisting of four diodes in such a way that regardless on the voltage polarity at the input port, the voltage polarity at the output is always the same. When AC voltage is applied at the input, during each half-period, two of the diodes are in conduction mode and two are in blocking mode.

The price of the DB is negligible[1] and is not likely to be the reason for excluding the DB in DC applications. The DB represents a drawback mainly due to power losses. When a DB is employed in a circuit there are two diodes connected in series with the rest of the circuit at all times. The forward voltage of the DBs is usually above 1 V (0.5 V per diode). In LV and ELV applications, where the current consumption is higher, this voltage drop can cause non-negligible power losses. Schottky diodes are sometimes used to reduce the losses as they offer significantly smaller forward voltage, but they usually are more expensive than regular diodes by an order of magnitude. Therefore, excluding the DB in LV and ELV DC applications can be desirable and expected.

Power Factor Correction Circuit In high quality lamps or in drivers with power consumption above 25 W, where the limits for harmonic emission are more strict

[1]During the work on this thesis the prices of DBs were below €0.5, minimum price being €0.1

[STD6], the low frequency EMI is removed using an active power factor correction (PFC) circuit. The PFC circuit is a DC-DC converter (boost) controlled in such a way that the current consumption is roughly sinusoidal in phase with the supply voltage. In common household LED lamps, however, the power consumption is smaller than 25 W and usually smaller than 10 W. Thus, the active PFC is usually missing [LK7]. The PFC circuit becomes excessive with a DC supply.

DC-DC Converter The DC-DC converter part is usually based on one of several typical topologies. According to a detailed overview [84], these can be

- **active**—containing a controller and probably a feedback loop; these topologies are able to eliminate voltage ripple up to certain level and have low losses (as low as units of % of lamp power consumption),
- **passive**—only passive parts are used (resistors, capacitors); these solutions are usually lossy (up to 35 % of the lamp power consumption) and unable to eliminate voltage ripple, thus flicker can be expected from these drivers.

Active solutions basically employ a variety of DC-DC converters, refer to Sec. 2.3. Other sorting is possible depending on the inclusion of a transformer:

- **isolated**—containing a transformer operated at high frequency provided that the connection assures galvanic isolation from the power source; this is useful if the driver serves to supply multiple lamps in which case the driver creates an enclosed SELV or PELV system ([7]). In isolated topologies, feedback for the controller is usually taken from a tertiary transformer winding,
- **non-isolated**—transformer-less topologies or with transformers, but without galvanic isolation.

More LED specific DC-DC converters exist employing various regulation techniques (for example, a high frequency peak current control via pulse density modulation (PDM) combined with low frequency dimming via pulse width modulation (PWM), [85]). It is beyond the scope of this thesis to make an exhausting list of the possible LED driver topologies.

Passive drivers may be implemented using either a resistor based voltage divider (a relatively lossy solution) or a capacitor based voltage divider. Such solution reduces losses, but because it contains a capacitor connected in series with the rest of the circuit, it is intended solely for AC supply.

LED Head The output voltage of the driver is dependant upon the arrangement of the LED head and can range from units up to tens of volts. The current is more important for driving the LEDs. The nominal current is usually in the order of hundreds of mA for high power LEDs used in lighting applications. Power consumption is in units of watts. There is usually more than one LED in the LED head, especially in higher power lamps. They are arranged in a single or several series branches or to form a matrix.

Intensive research is going on on how to implement a good quality driver [86, 87, 88, 89, 90, 91, 92, 93]. Most often, the aim is to minimise cost and maximise the efficiency and lifetime, sometimes dimming is featured. Flicker immunity is only sometimes taken into account. DC supply is very scarcely assumed [7, 94].

An LED lamp equipped with a standard driver connected to DC supply may work in a different way than with AC supply. This is because the rectified voltage with 12 V AC supply reaches $12 \cdot \sqrt{2} = 17\,\mathrm{V}$ and the mean value is usually only slightly smaller than that. On the other hand, the "rectified" voltage with 12 V DC supply will be 12 V. A smaller voltage level at the DC-DC converter input will force a larger duty ratio.

4.2.1 LED Dimming

Dimming is a feature often desired from lamps used in lighting applications. With incandescent lamps and also with CFLs, dimming was achieved using a special dimming circuit to supply the lamp. These dimming circuits comprise a thyristor or a triac which allows one to phase-cut the sinusoidal voltage in order to decrease the RMS value. Usage of these devices is, thus, restricted to AC. Depending on the principle, phase-cut dimmers may either be leading edge or trailing edge dimmers [11].

Phase-cut dimmers are known to cause a large amount of flicker and other problems (audible noise, flashing) when used with regular LED drivers. Their usage is discouraged unless a special dimmable LED driver is used. These dimmable drivers are more complicated as it is necessary to decode the desired dimming level from the mains voltage and set appropriate LED head voltage (current) at the output.

Alternatives to phase-cut dimmers exist. Utilisation of power line communication or usage of a third wire (low voltage control) are both possible for telling the LED driver what the desired dimmed level is. Usually these are part of a complete solution together with the LED drivers. Such approaches are usable in DC networks also.

Within the driver, actual LED dimming may be performed using either of two approaches [95]:

- decrease the DC component of the LED current, or
- supply the LED with the PWM at a given duty ratio.

The first approach may result in a chromaticity change of the produced light, which is discussed in the Sec. 4.1.2 already. The latter approach keeps the chromaticity because the current level is kept constant. The problem is that the PWM frequency is usually chosen in the order of hundreds of hertz, which may result in any high frequency flicker related phenomena.

4.3 LEDs and Flicker

Photobiological safety of LED produced light (where flicker is only one of the discussed aspects) is discussed in [10]. Until the recently released standard [STD1],

there had been no normative definition of LED driver flicker properties.

Depending on the driver properties, the flicker with LEDs can be induced by several causes:

Clean AC supply voltage can cause flicker with poor quality drivers. This kind of flicker is not detectable by IEC FM or any other voltage measurement based method; it needs to be detected by optical means. Flicker caused this way is constant and lasts for the entire lifetime of the device.

Distorted (AC or DC) supply voltage caused flicker can be detected from voltage measurements provided that the proper lamp model is known and used. Flicker caused this way lasts only for the duration of the disturbance.

Standard switched supply driver can cause high frequency flicker if a switched supply is used. This is rarely an issue as the frequencies are usually high enough (tens of kHz). Naturally, such flicker can only be detected using optical measurements. Flicker caused this way lasts for the entire lifetime of the device.

Dimmable PWM controlled driver can cause flicker in dependence on the PWM frequency and duty ratio. This kind of flicker usually lasts only when the dimming level smaller than $100\,\%$ is requested.

Phosphors used in white LEDs can have various time constants ranging from the order of nanoseconds up to tens of milliseconds. Slower time constants attenuate higher frequencies.

Driver properties are a key factor affecting the flicker of LED lamps. The flicker response is influenced by the parts dimensioning and the feedback regulator settings. The *gain factor* (*GF*, [96]) is a quantity evaluating the frequency response of a driver. It can be defined either for produced luminous flux:

$$GF_{\Phi}(f) = \frac{\dfrac{\Phi(f)}{\bar{\Phi}}}{\dfrac{V(f)}{V_1}}, \tag{4.12}$$

where Φ is the produced luminous flux, $\bar{\Phi}$ its mean value, V the output voltage and V_1 its fundamental component; or for the driver output voltage:

$$GF_{V}(f) = \frac{\dfrac{V_{\text{out}}(f)}{\bar{V}_{\text{out}}}}{\dfrac{V(f)}{V_1}}, \tag{4.13}$$

where V_{out} is the output voltage and $\bar{V}_{\text{out}}$ its mean value. For DC supplied devices, V_1 is replaced by the mean value of the supply voltage V_{DC}. The drawback of this quantity is that it ignores the non-linear behaviour of the driver. A single frequency component in the supply voltage can result in several frequency components of the output

quantity which are not reflected in the *GF*. Also, it cannot be said whether the value of $\Phi(f)$ is a result of the influence of $V(f)$ (and to what extent) or it would be the same even under a distortion free supply.

To demonstrate this, let us assume that the "natural waveform" of a lamp output (i.e., with an ideal voltage supply) has a single frequency component at $10\,\mathrm{Hz}$ and that

$$\frac{\Phi(10)}{\bar{\Phi}} = 10\,\%\,.$$

When the sinusoidal distortion is applied to the supply voltage at the same frequency and $m_{\mathrm{AC}} = \frac{V(10)}{V_1} = 2\,\%$, the non-linear driver reacts by creating more components at $10\,\mathrm{Hz}$, $20\,\mathrm{Hz}$ and $30\,\mathrm{Hz}$, so we will now have

$$\begin{aligned}\frac{\Phi(10)}{\bar{\Phi}} &= 12\,\%\,,\\ \frac{\Phi(20)}{\bar{\Phi}} &= 1\,\%\,,\\ \frac{\Phi(30)}{\bar{\Phi}} &= 1\,\%\,.\end{aligned}$$

This way we will obtain $GF_{\Phi}(10) = \frac{\Phi(10)}{\bar{\Phi}} : \frac{V(10)}{V_1} = \frac{12}{2} = 6$. This value by no means shows that a) the output fluctuation was present before applying the perturbation, and b) that new frequency components appeared.

Part II

Practical Part

5 Thesis Objectives

This thesis is concerned with luminance flicker of LED lighting systems supplied with low or extra low DC voltage. The thesis looks at the problem of flicker in LED systems generally and aims to analyse the risk of flicker when DC supply is used instead of AC. It frames several experiments with flicker properties of LED lamps, whose results were published in [LK1, LK7, LK8, LK9]. The work is expanded by more experiments and simulations in this thesis.

One of the advantages of DC grids over AC ones is the reduction of the number of AC-DC and DC-AC conversions. AC-DC conversion causes VQ problems both on the AC and DC side (current harmonics, ripple). These problems need to be compensated for using more advanced circuitry (PFC, converters with feedback control). Replacing AC supply with DC seems to be a natural way to decrease the complexity of the network and the appliances connected to it.

Most of the LED drivers may be operated without change in the DC network. However, the diode rectifier will become excessive, and, thus it may be removed in order to increase the efficiency of the LED drivers. It can be expected that, as more and more devices become adapted to DC supply, their design will omit the lossy and excessive AC-DC conversion stage. While the power loss savings of such an adaptation are indisputable, especially in low voltage and extra low voltage scenarios, its impact on flicker immunity of the LED lamps has never been studied.

The primary aim of this thesis is to *analyse the effect of the diode bridge upon the flicker immunity of LED drivers.* The means to achieve this goal are:

1. determining the flicker level and perturbations immunity of several LED lamps by measurements of $P_{\mathrm{st}}^{\mathrm{LM}}$ and *FP*,

2. determining the change of flicker level and perturbations immunity of LED lamps when the diode bridge is bypassed (observing the relative change of $P_{\mathrm{st}}^{\mathrm{LM}}$),

3. explaining the observed behaviour using a suitable model of an LED driver; this means

    - creating a suitable model according to the known information about the analysed LED drivers,
    - successfully predicting the flicker level and its frequency dependency compared to the measurements,

4. analysing the conditions under which the removal of the diode bridge will not increase the flicker level of the LED lamps, i.e.

    - identifying the possible means of ripple amplification,
    - varying the identified circuit properties,
    - observing the impact of the variations on the flicker level ($P_{\mathrm{st}}^{\mathrm{LM}}$),
    - observing the impact of the variations upon the relative change of $P_{\mathrm{st}}^{\mathrm{LM}}$.

Another partial aim is the analysis of the immunity of the chain *supply—lamp* to AC side perturbations. For that reason, the thesis is accompanied by an EMC immunity test of several AC-LVDC supplies powering LED lamps (Experiment 1). The work is further accompanied by an experiment (Experiment 2) and several simulations (Simulations 1 and 3) which are relevant to the topic and serve for demonstrative purposes.

The thesis, in general, aims to contribute to an ongoing discussion over power quality in DC grids. To the author's knowledge, it is for the first time that flicker and LED technology would enter this discussion. Furthermore, the author hopes the knowledge accumulated in this thesis might be useful for upcoming standards about LED lighting technology and flicker.

6 Experimental Part

This chapter describes all the experiments performed in the scope of the thesis. The experiments are meant to give a picture about the flicker sensitivity of the available LED lamps and about the driver design also. Some of the experiments also represent a model validation basis for the simulations performed further on. Most notably, the experiment described in Sec. 6.4.4 aims to show the impact of removing the diode bridge upon the flicker response of a DC supplied lamp.

Experiment 1 Firstly (see Sec. 6.2) a set of AC-DC converters (24 V DC supplies) was analysed in terms of immunity to supply voltage distortion and voltage dips. The immunity was evaluated both with a resistive load (DC link voltage distortion was observed, Experiment 1a) and LED lamps (photometric flicker was observed, Experiment 1b). The aim of this experiment is to show if flicker in a DC network is likely to be caused by VQ issues on the AC side.

Experiment 2 Secondly (see Sec. 6.3), a set of 230 V LED lamps in terms of flicker, when the lamps are supplied by clean AC voltage. This experiment is meant to show that even the AC supply itself can cause flicker depending on the LED driver design.

Experiment 3 Thirdly (see Sec. 6.4), a set of 12 V LED lamps was analysed. The lamps were supplied by clean AC and distorted DC. This part of the experiment was performed in the LAPLACE laboratory (Experiment 3a). The frequency resolution of the DC distortion was limited to seven distinct frequencies. The second part of the experiment was performed in the laboratories of the Brno University of Technology (Experiment 3b). In this part of experiment, the lamps were supplied by distorted AC and distorted DC with 1 Hz resolution. The produced $P_{\mathrm{st}}^{\mathrm{LM}}$ was acquired both in dependence on the frequency and modulation magnitude. The lamps were disassembled and the key elements of the drivers were noted. In the following part of the experiment, the measurements were repeated with the diode bridge electrically bypassed. The relative change of $P_{\mathrm{st}}^{\mathrm{LM}}$ was evaluated.

6.1 Luminance Flicker Acquisition Techniques

This section describes techniques and equipment suitable for measuring luminance flicker. The described equipment was used in the experiments in the following sections (Secs. 6.2, 6.3 and 6.4).

The experimental conditions for performing measurements with LED lamps are described in standard [STD23]. Most notably the lamp must be placed in its design position (socket-up for retrofit lamps) and the ambient temperature must be kept within $(25.0 \pm 0.5)\,°\mathrm{C}$.

Ulbricht sphere

An *Ulbricht sphere* is a device constructed for calibrated measurements of luminous flux, produced by a light source. It is a hollow sphere with the inside surface covered with special coating of baryum sulfide. The coating is designed to reflect and evenly diffuse the incident light for all wavelengths. The sphere diameter can vary from tens of cm up to $2.5\,\mathrm{m}$; in dependence on the diameter, the sphere is more proper for smaller lamps or larger and more powerful light sources.

Because of the spherical design, the surface illuminance is constant and is proportional to the total luminous flux produced by the light source enclosed within the sphere at the centre point. The ratio of the surface illuminance and the light source luminous flux is the sphere's calibration constant and is known prior to measurements. The Ulbricht sphere is, thus, a device suitable for measuring the luminous flux, wavelength spectrum and also flicker. Several experiments in this chapter were performed with the lamp placed in an Ulbricht sphere.

Black Box and White Box

For measuring flicker, only the relative change of the lamp luminous flux are relevant and calibrated flux measurements are not necessary. Thus, a more simple alternative to the Ulbricht sphere is a black box or white box. These can be basically of any shape, the only important requirement is to have a uniform spectral reflectance; hence the inside surface can either be black or white.

A white box was constructed in order to perform some of the experiments in this chapter. The spectral reflectance of the white surface is shown in Fig. 6.2.

Photodiodes

In order to measure rapid changes in the luminous flux produced by the EUT it is necessary to use a photodiode (PD). A photodiode is essentially a diode with its p-n junction uncovered so that electromagnetic radiation can reach the junction. An incident photon in the p-n junction creates an electron–hole pair. If the electron–hole pair is created outside of the depletion layer, they will diffusively move until they annihilate each other. However if the electron–hole pair is created within the depletion layer where there is electric field, they start to drift according to the direction of the electric field, thus creating measurable electric current. One incident photon will, thus, cause a current impulse with an area equal to q_e.

PDs usually have a large chip area (units of mm^2) in order to achieve a higher sensitivity for the cost of a higher junction capacitance. The sensitivity is usually in the order of hundreds of $\mathrm{mA\,W}^{-1}$.

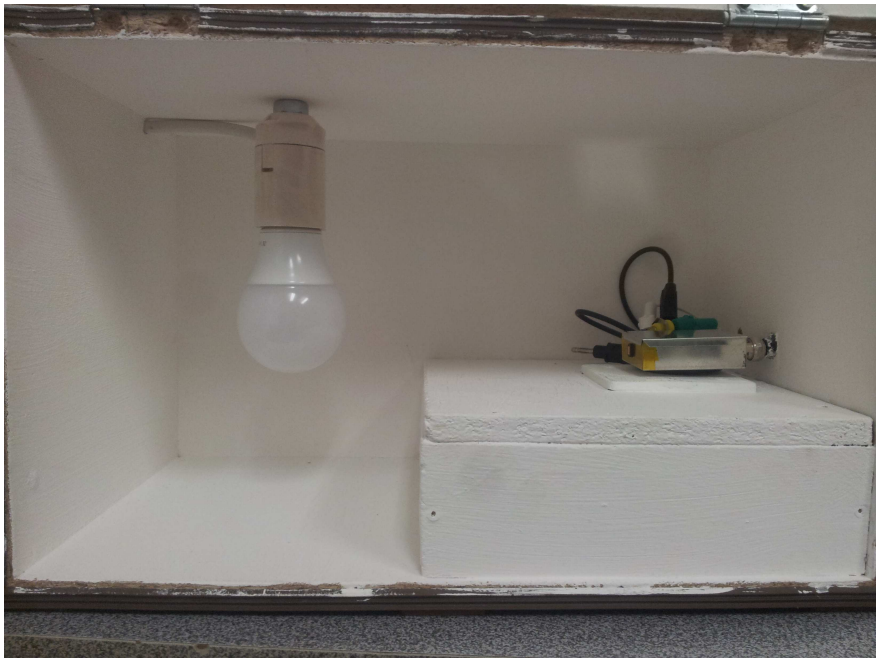

Figure 6.1: White box used for a part of the experiments, photodiode and linear amplifier in the right

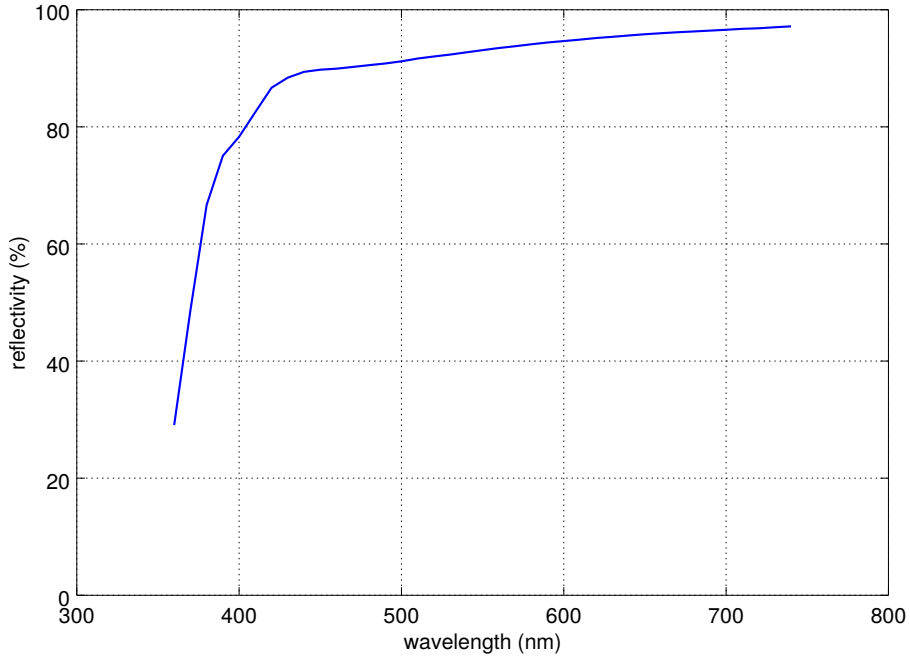

Figure 6.2: The spectral reflectance of the white box surface; the reflectance drops in the ultra-violet area of the spectrum (below 400 nm) which is invisible for humans

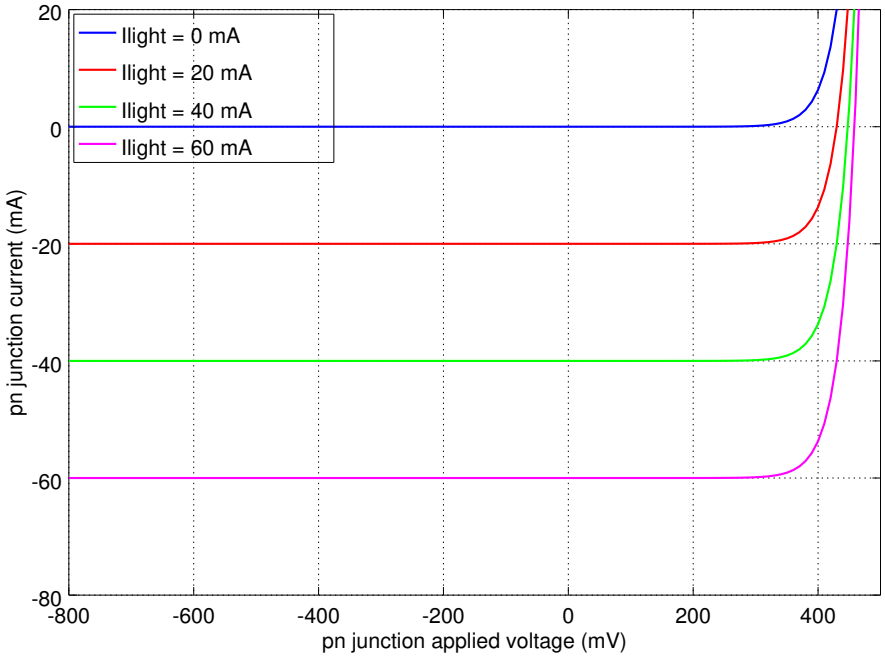

Figure 6.3: A photodiode V-I characteristic under various illumination levels

The PD can either be connected forward biased (photovoltaic—PV—mode) or reverse biased (photoconductive mode). In the PV mode, the PD output quantity is voltage. In photoconductive mode, the output quantity is current. This mode is usually used in the discussed field of interest as it offers more linearity and broader bandwidth for the cost of smaller output signal. The output of a PD in photoconductive mode needs to be amplified using a *transimpedance amplifier*, creating a low impedance current sink for the diode and converting the signal to voltage.

The photodiode current is obtained as [97]:

$$I_{\mathrm{PD}} = I_0 \left(e^{\frac{V}{n V_{\mathrm{T}}}} - 1 \right) - I_{\mathrm{light}} - I_{R\mathrm{shunt}} \,, \tag{6.1}$$

where I_0, V, n, and V_{T} are the same quantities as used in (4.1). I_{light} is the current produced by the incident light and $I_{R\mathrm{shunt}}$ is the shunt resistor current. A V-I characteristic of a photodiode is shown in Fig. 6.3.

The PD photocurrent is linearly dependent on the illuminance of the chip [98]. As the *FI* and *FP* (Eqs. (3.42) and (3.43)) are rational, they can be evaluated directly from the PD photocurrent instead of the luminous flux.

As has already been mentioned, for flicker evaluation, it is not necessary to convert the signal to photometric quantities using a calibrated Ulbricht sphere. Even so, an Ulbricht sphere is a convenient device for performing flicker experiments because of its reflective surface. It is required that the surface does not change the wavelength spectrum (colour) of the measured light for the following reason; in some analysed lamps (incandescent lamps), heterochromatic flicker occurs together with luminance flicker. While the chromatic changes are minimal, if the colour of the analysed light were changed towards either end of the spectrum, the PD signal would not corres-

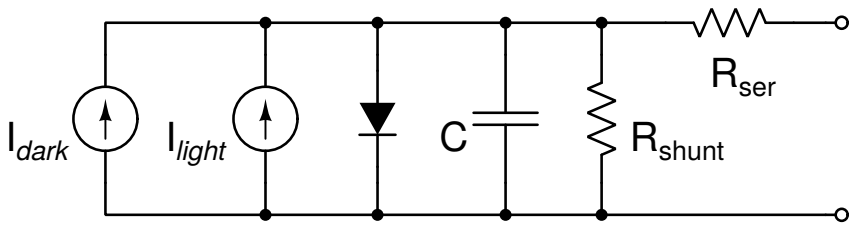

Figure 6.4: A simple electric photodiode model [97]

pond precisely with what human eye would see. This is why flicker experiments are usually performed in an integrating sphere, a white box or a black box. For this reason, it is also required that a filter is used in the PD to mimic the wavelength sensitivity (the $V(\lambda)$ function) of a human eye ($400\,\text{nm}$ to $700\,\text{nm}$).

The photodiode model includes a regular diode and two current sources. The dark current source is assumed constant in most applications, but in reality it is dependent on the applied voltage to a small extent. The light current is linearly dependent on the irradiance of the photodiode chip. As mentioned earlier, PDs usually have large capacitance; this fact is reflected in the model. The capacitance is also dependent on the applied voltage.

Logarithmic Transimpedance Amplifier

Logarithmic amplifiers are used when it is required to cover a large or unknown range of the input signal. There is a wide variety of designs. Some of the experiments described in this section were performed using a logarithmic amplifier. A diagram is shown in Fig. 6.5.

The reverse TF is important for determining the PD photo current. The analytic reverse transfer function of the amplifier is:

$$I_{\text{light}} = I_3 \,\exp\left\{\frac{1}{V_{\text{T}}(R_1+R_2+R_6)}\left[\frac{(R_1R_6)V_{\text{out}}}{R_{\text{out}}} - (R_2+R_6)(1.22-V_{\text{D1}})\right]\right\} - I_{\text{dark}}\,, \tag{6.2}$$

I_{dark} is the photodiode dark current, V_{T} is the thermal voltage (Sec. 4.1.1), other indices refer to the parts marked in Diagram 6.5.

From the calibration measurements of the amplifier, a different transfer function was inferred:

$$\begin{aligned} V_{\text{out}} = 1.471\,666 + 0.043\,57 \ln\left(\frac{I_{\text{light}}+I_{\text{dark}}}{I_3}\right) + 6.414\,395\, I_{\text{light}} + \\ + 0.026\,331\,5\, V_{\text{out}}^2 - 0.067\,112\,1\, V_{\text{out}} - 0.687\,414\,. \end{aligned} \tag{6.3}$$

This is a transcendental equation and expressing I_{light} must be done using an iterative approach. Appendix C contains a source code of Newton's iterative method used for evaluating I_{light} from the measurements of V_{out}.

The photodiode used together with this amplifier was a Silonex SLD-70BG2 [99]. The amplifier bandwidth was experimentally verified to be $1\,\text{MHz}$.

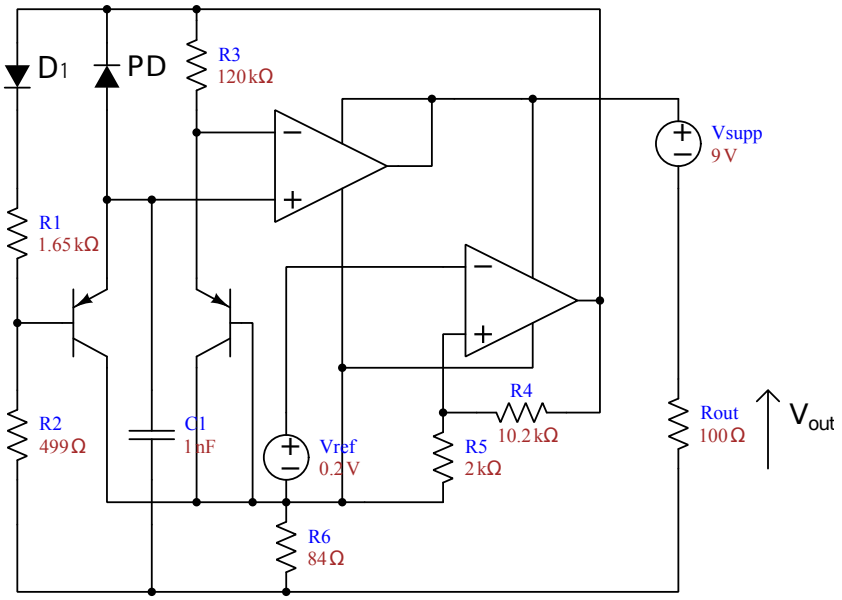

Figure 6.5: A logarithmic transimpedance amplifier; diode D1 is used to provide logarithmic dependency

Linear Transimpedance Amplifier

Linear amplifiers are used when the range of the acquired signal strength is small and known. They can be very accurate.

A linear amplifier was constructed for use in some of the described experiments. The bandwidth of the amplifier was experimentally determined to be approx. 120 kHz. The bandwidth is further reduced by a first order filter placed at the output (cut-off frequency approx. 4 kHz) which serves as a simple anti-aliasing filter. The transfer function was verified by simulation in SPICE. It is linear within the specified bandwidth. Therefore, the output signal of the linear amplifier can be used for the direct calculation of *FP* and *FI* or even P_{st}.

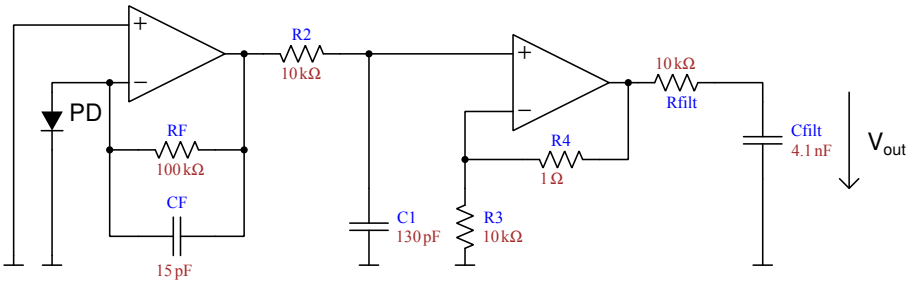

Figure 6.6: A linear transimpedance amplifier diagram; the amplifier transimpedance is given by the resistor RF

The photodiode used together with this amplifier was a Hamamatsu S7686 [98].

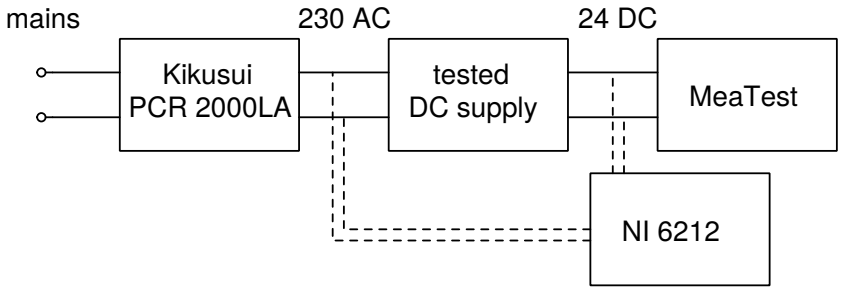

Figure 6.7: Laboratory setup of the DC supply immunity test

6.2 Immunity Test of *DC Supply—LED Lamp* Chain

This experiment is meant to analyse the conditions in small ELV DC networks used for lighting. ELV DC networks are used in industry for lighting and for supplying control systems and devices with relatively low power consumption; their advantage is safety and the possibility to use batteries for backup. For this reason, a commonly used, 24 V voltage level was chosen.

In the first part of the experiment, a set of commercially available 24 V DC supplies was analysed in terms of immunity to VQ issues (voltage drops, sags, interruptions, harmonic distortion) while loaded with the resistive load. In the second part of the experiment, the supplies were supplying a 24 V LED lamp whose produced light was observed in a white box.

The aim of this experiment was to identify the flicker related EMC immunity of a small hypothetical DC network used for lighting in industry conditions.

6.2.1 DC Power Supply Immunity

This part of the experiment analyses the power supplies loaded by a programmable resistive load. It is intended merely as a preliminary test which would allow one to pick the most suitable supplies for testing with LEDs (the following section) as well as provide a reference measurement for comparison of the two distinct types of loads (resistive vs. LED).

A Kikusui PCR 2000LA programmable power source was used for generating the AC voltage with the desired properties. The DC output of the tested supplies was connected to a programmable load MeaTest. The voltage was sampled by an NI USB 6212. A connection diagram is shown in Fig. 6.7. Table 6.1 lists all the tested supplies. The sampling frequency was $F_s = 12\,804$ Hz. This value results from the inner properties of the NI 6212 sampling device and it caused minor difficulties with the frequency domain evaluation of the results.

The distortions applied to the AC voltage covered:

- various RMS voltage levels from 90 V to 250 V (a static characteristic),
- subharmonic sinusoidal amplitude modulation, f_m being 1, 2, 5, 10, 20, 25 and 40 Hz, m_{SM} being 1 %, 2 %, 5 % and 10 %,

Table 6.1: Used power supplies and their nominal rating

EUT label	Power (W)	Max. DC current (A)	DC voltage (V)
SUP1	84	3.5	24
SUP2	48	2	24
SUP3	72	3	24
SUP4	42	1.75	24
SUP5	30	1.25	24
SUP6	40	1.5	27.6
SUP7	70	2.5	27.6
SUP8	12	0.5	24
SUP9	100	4.2	24
SUP10	15	0.65	24
SUP11	50	2.2	24
SUP12	25	1.04	24
SUP13	100	4.17	24
SUP14	15	0.625	24

- subharmonic frequency component, f_{ih} being 1 Hz, 2 Hz, 5 Hz and 10 Hz, m_{ih} being 1 %, 2 %, 5 % and 10 %,
- harmonic and interharmonic component, chosen frequencies up to 1 000 Hz, m_{ih} same as in the previous part,
- voltage dips and interruptions according to IEC 61000-4-11 [STD7, Sec. 5.1, Tabs. 1, 2 and 3].

For each measurement the loading resistance was determined such as to load the EUT at 100 % of its nominal power. For more powerful EUTs (SUP1, SUP9 and SUP13), the 100 % load was out of the capabilities of the MeaTest devices (even though two identical ones were connected in parallel to further decrease the resistance). In these cases, the resistance was chosen to the minimum possible value ($R_{\text{load}} = 7.5\,\Omega$) and, thus, the EUT load might not reach 100 % of the EUT nominal power.

The DC voltage was first sampled with a clean AC voltage supply and then the distortions were added. All of this was performed for comparison. From the sampled DC voltage the relative modulation magnitude m_{DC} was evaluated firstly with a clean AC voltage (m_1) and secondly with a distorted AC voltage (m_2). The relative change of the rel. modulation depth was observed:

$$\Delta m = \frac{m_2 - m_1}{m_1} \cdot 100\,\%\,. \tag{6.4}$$

The gain factor for a given frequency was also observed:

$$GF_V = \frac{\dfrac{V(f_{GF})}{\bar{v}_{\text{DC}}}}{m_{\text{SM/ih}}}\,. \tag{6.5}$$

Table 6.2: Relative modulation magnitude of the DC voltage for the distorted AC supply, $f_{\mathrm{m/ih}} = 10\,\mathrm{Hz}$, $m_{\mathrm{SM/ih}} = 10\,\%$ at full load. First column: AC SAM, second column: AC + subharmonic injection

supply	SAM, m_{DC} (%)	subharm., m_{DC} (%)
SUP1	0.40 ± 0.24	0.37 ± 0.24
SUP2	0.37 ± 0.24	0.34 ± 0.23
SUP3	0.37 ± 0.23	0.43 ± 0.24
SUP4	0.34 ± 0.24	0.34 ± 0.23
SUP5	0.40 ± 0.22	0.46 ± 0.23
SUP6	0.57 ± 0.23	0.67 ± 0.21
SUP7	0.32 ± 0.21	0.32 ± 0.21
SUP8	0.37 ± 0.21	0.37 ± 0.23
SUP9	0.34 ± 0.23	0.34 ± 0.24
SUP10	0.37 ± 0.23	0.37 ± 0.23
SUP11	0.37 ± 0.23	0.40 ± 0.23
SUP12	0.37 ± 0.23	0.40 ± 0.23
SUP13	0.37 ± 0.23	0.37 ± 0.23
SUP14	0.40 ± 0.23	0.40 ± 0.23

$V(f_{GF})$ is a magnitude of frequency component f_{GF} in the DC voltage. The choice of f_{GF} is not straightforward; for tests where a subharmonic SAM was applied on the AC supply voltage the f_{GF} should be identical to the modulating frequency, and so $f_{GF} = f_{\mathrm{m}}$. However, for tests where the AC voltage contained a single subharmonic or interharmonic frequency, the f_{GF} should be the frequency of an intermodulation component between 0 and 50 Hz, and so $f_{GF} = 50 - f_{\mathrm{ih}}$. Other quantities evaluate the signal regardless of output modulation frequency. For each of the evaluated quantities its uncertainty was estimated also. See App. D for the approach of uncertainty estimation.

Results

Table 6.2 shows the relative modulation magnitude of the DC output of the supplies. For various reasons, the uncertainty of Δm and GF_V was very high and, thus, the results were not suitable for further processing. Particularly, because of a bad choice of measurement range for the DC voltage channel in NI 6212. The relative modulation magnitude values are shown in Tab. 6.2. The table shows the results for the disturbance frequency $f_{\mathrm{m/ih}} = 10\,\mathrm{Hz}$ and modulating magnitude $m_{\mathrm{SM/ih}} = 10\,\%$.

Large uncertainties do not allow one to draw important conclusions, but the aim of the experiment was to pick several DC supplies to continue the experiment further with LED lamps. To limit the amount of lengthy measurements, only five supplies with the worst performance were to be picked for further experiments. After excluding SUP8 which was not able to supply the tested LED lamps and after taking the supply response to voltage dips and interruptions into consideration, these supplies were picked for further experiment: SUP5, SUP6, SUP7, SUP11 and SUP12.

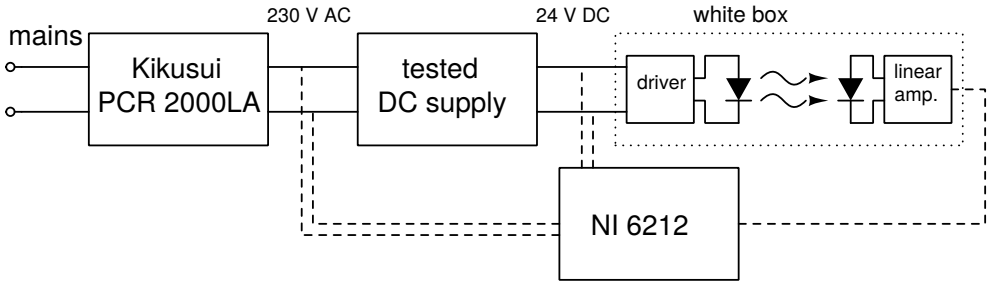

Figure 6.8: Laboratory setup of the *DC supply—lamp* immunity test

6.2.2 *DC Supply—LED Lamp* Chain Immunity

In this part, the light output of a DC supplied LED lamp was observed. The experiment diagram is shown in Fig. 6.8. The tested LED lamp was placed in a white box and its output was observed with a photodiode connected to a linear transimpedance amplifier. The sampling frequency of the NI USB 6212 was $F_s = 80\,\text{kHz}$. A simple first order RC filter was placed in each channel to perform basic anti-aliasing. The cut-off frequency of the filter was approx. $4\,\text{kHz}$, providing a $20\,\text{dB}$ attenuation at the Nyquist frequency of $40\,\text{kHz}$. The rest of the laboratory setup was the same as in the previous section.

The tested lamps and details are listed in Tab. 6.3. As mentioned in the previous section, not all available supplies were used in this part of test. Five of the tested supplies exhibiting the worst behaviour were chosen; these were: SUP5, SUP6, SUP7, SUP11 and SUP12.

The set of the performed tests was smaller than in the previous case:

- various RMS voltage levels from $90\,\text{V}$ to $250\,\text{V}$ (a static characteristic),
- subharmonic sinusoidal amplitude modulation, f_m being 1, 2, 5, 10, 20, 25 and $40\,\text{Hz}$, m_{SM} being $1\,\%$, $2\,\%$, $5\,\%$ and $10\,\%$,
- subharmonic frequency component, f_{ih} being $1\,\text{Hz}$, $2\,\text{Hz}$, $5\,\text{Hz}$ and $10\,\text{Hz}$, m_{ih} being $1\,\%$, $2\,\%$, $5\,\%$ and $10\,\%$.

During the tests, each lamp was powered for 20 minutes prior to running the measurements in order to reach thermal equilibrium. From the sampled photodiode output, the flicker quantities were evaluated, namely the P_{st}^{LM} and

Table 6.3: Used LED lamps

Lamp symbol	Nominal power (W)	*CCT* (K)	lifetime (h)	flux (lm)	socket
LED1	10	4 000	—	800	E27
LED2	9	3 500	25 000	700	E27
LED3	12	4 000	—	900	E27
LED4	—	—	—	—	GU5.3

FP. The $P_{\mathrm{st}}^{\mathrm{LM}}$ was calculated using an LFM implementation described in App. B. The overall *GF* of the chain was evaluated. For comparison, the P_{st} was also evaluated from the AC voltage supplied from a Kikusui source using a commercial class A flickermeter ARTIQ. The P_{st} was evaluated from $10\,\mathrm{s}$ long measurements. Uncertainties for *FP* were evaluated following the same approach as in the previous section (App. D).

Results

Tables 6.4c and 6.4a show the *FP* and $P_{\mathrm{st}}^{\mathrm{LM}}$ of the worst-case test, SAM with $f_{\mathrm{m}} = 10\,\mathrm{Hz}$, $m_{\mathrm{SM}} = 10\,\%$. The results show that the $P_{\mathrm{st}}^{\mathrm{LM}}$ is very low in all cases; however for the combination SUP7+LED1 the $P_{\mathrm{st}}^{\mathrm{LM}}$ is notably higher than for the rest of the combinations. Importantly, the $P_{\mathrm{st}}^{\mathrm{LM}}$ stays below 1 in all cases.

The *FP* metric reflects flux fluctuations at any frequency and, thus, may reveal very high frequency flicker, even above the relevant band. Table 6.4c shows that the *FP* varies mainly with the lamp, but is independent on the supply. The worst flicker was with lamp LED_4 (approx. $\mathit{FP} = 3\,\%$). A more detailed analysis revealed that the fluctuations occur in the order of tens of kHz and, thus, are irrelevant to flicker sensation. This further means that the actual *FP* might have been higher than the acquired values, as these are subject to the attenuation of the RC filter placed at the photodiode amplifier output. The flux fluctuation of these properties (high frequency, independent on the supply) is caused by the switching operation of the LED driver.

Tables 6.4b and 6.4d show the same results for the injected subharmonic frequency component, $f_{\mathrm{m}} = 10\,\mathrm{Hz}$, $m_{\mathrm{ih}} = 10\,\%$. The results are very similar as with SAM. Again, Tab. 6.4b shows that the $P_{\mathrm{st}}^{\mathrm{LM}}$ was the worst with the combination SUP7+LED1.

Figure 6.9 shows P_{st} and $P_{\mathrm{st}}^{\mathrm{LM}}$ measured with one of the tested supplies (subharmonic SAM). It is apparent that the P_{st} evaluated from the AC voltage grossly overestimates the actual flicker level. Also, it is seen that the AC voltage distortion does not affect the light output in any way. The results with other tested supplies are very similar.

With several combinations of a supply and a lamp, there were observable fluctuations of the DC link voltage. An example is documented in Fig. 6.10. These fluctuations occur at $50\,\mathrm{Hz}$. They were not observed when the DC supply was loaded with a MeaTest and, thus, they must be caused by the interaction of the supply with the LED lamp. The fluctuations do not affect the light output.

6.2.3 Experiment Summary

During the measurements in this section, several conclusions were drawn. Firstly it is concluded that the chain *DC supply—LED lamp* is, in most cases, robust enough to filter out even severe AC voltage distortion. Secondly, fluctuations caused by LED drivers are present and measurable, but not relevant to flicker due to very high frequencies they occur at (order of tens kHz).

Table 6.4: *FP* and P_{st}^{LM} produced by LED supplied by ELV DC power supply with perturbations coming from the AC side

(a) P_{st}^{LM}; AC SAM $f_m = 10\,\text{Hz}$, $m_{SM} = 10\,\%$

supply \ LED lamp	LED1	LED2	LED3	LED4
SUP5	0.020	0.032	0.015	0.022
SUP6	0.018	0.056	0.008	0.041
SUP7	0.270	0.025	0.008	0.018
SUP11	0.025	0.040	0.011	0.025
SUP12	0.016	0.036	0.059	0.020

(b) P_{st}^{LM}; AC with injected subharmonic $f_{ih} = 10\,\text{Hz}$, $m_{ih} = 10\,\%$

supply \ LED lamp	LED1	LED2	LED3	LED4
SUP5	0.012	0.037	0.044	0.028
SUP6	0.011	0.034	0.008	0.018
SUP7	0.263	0.034	0.012	0.016
SUP11	0.019	0.036	0.008	0.024
SUP12	0.014	0.039	0.011	0.020

(c) *FP*; AC SAM $f_m = 10\,\text{Hz}$, $m_{SM} = 10\,\%$

supply \ LED lamp	LED1	LED2	LED3	LED4
SUP5	0.90 ± 0.07	1.05 ± 0.09	0.70 ± 0.06	3.23 ± 0.09
SUP6	0.86 ± 0.07	0.95 ± 0.08	0.74 ± 0.05	2.99 ± 0.09
SUP7	1.06 ± 0.12	1.11 ± 0.08	0.74 ± 0.05	3.08 ± 0.09
SUP11	0.85 ± 0.06	0.92 ± 0.08	0.72 ± 0.05	3.16 ± 0.09
SUP12	0.88 ± 0.07	1.00 ± 0.09	0.73 ± 0.05	3.28 ± 0.09

(d) *FP*; AC with injected subharmonic $f_{ih} = 10\,\text{Hz}$, $m_{ih} = 10\,\%$

supply \ LED lamp	LED1	LED2	LED3	LED4
SUP5	0.89 ± 0.07	1.12 ± 0.09	0.71 ± 0.06	3.20 ± 0.09
SUP6	0.89 ± 0.07	1.00 ± 0.08	0.76 ± 0.05	3.04 ± 0.09
SUP7	1.08 ± 0.12	1.15 ± 0.08	0.70 ± 0.05	3.05 ± 0.09
SUP11	0.88 ± 0.06	1.03 ± 0.08	0.70 ± 0.05	3.19 ± 0.09
SUP12	0.88 ± 0.06	1.03 ± 0.09	0.81 ± 0.05	3.23 ± 0.09

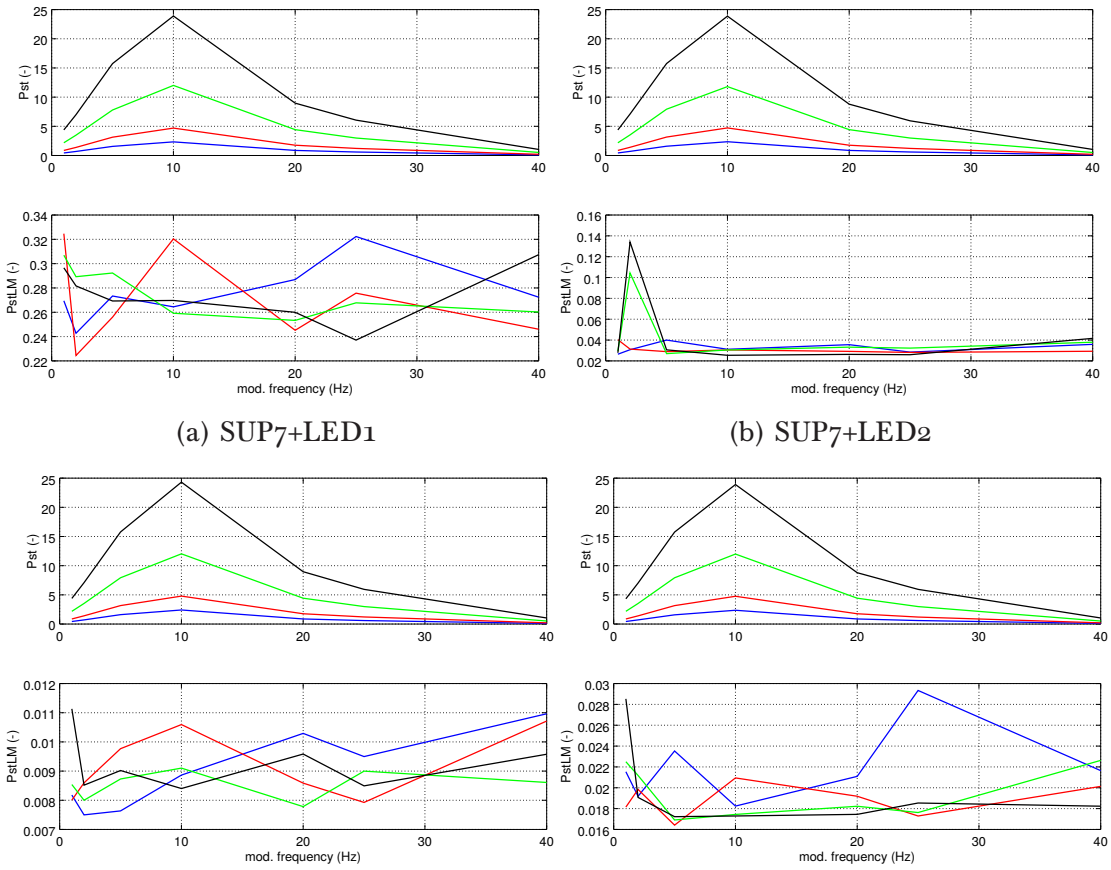

(a) SUP7+LED1

(b) SUP7+LED2

(c) SUP7+LED3

(d) SUP7+LED4

Figure 6.9: Supply SUP7, four LED lamps: comparison of P_{st} evaluated from the AC voltage and $P_{\mathrm{st}}^{\mathrm{LM}}$, evaluated from flux. The subharmonic SAM, various f_{m}; line colour blue, red, green and black: $m_{\mathrm{SM}} = 1\,\%$, $2\,\%$, $5\,\%$ and $10\,\%$, respectively

Thirdly, in some cases an interaction of an unresolved origin between the lamp and the supply causes $50\,\mathrm{Hz}$ fluctuations of the DC voltage (see Fig. 6.10). Further investigation of this phenomenon is necessary and strongly recommended. These fluctuations represent a possibly serious PQ issue and may affect the function of other connected devices. Also, the flicker level (see Tabs. 6.4a, 6.4c, 6.4b and 6.4d, combination SUP7+LED1) is worsened.

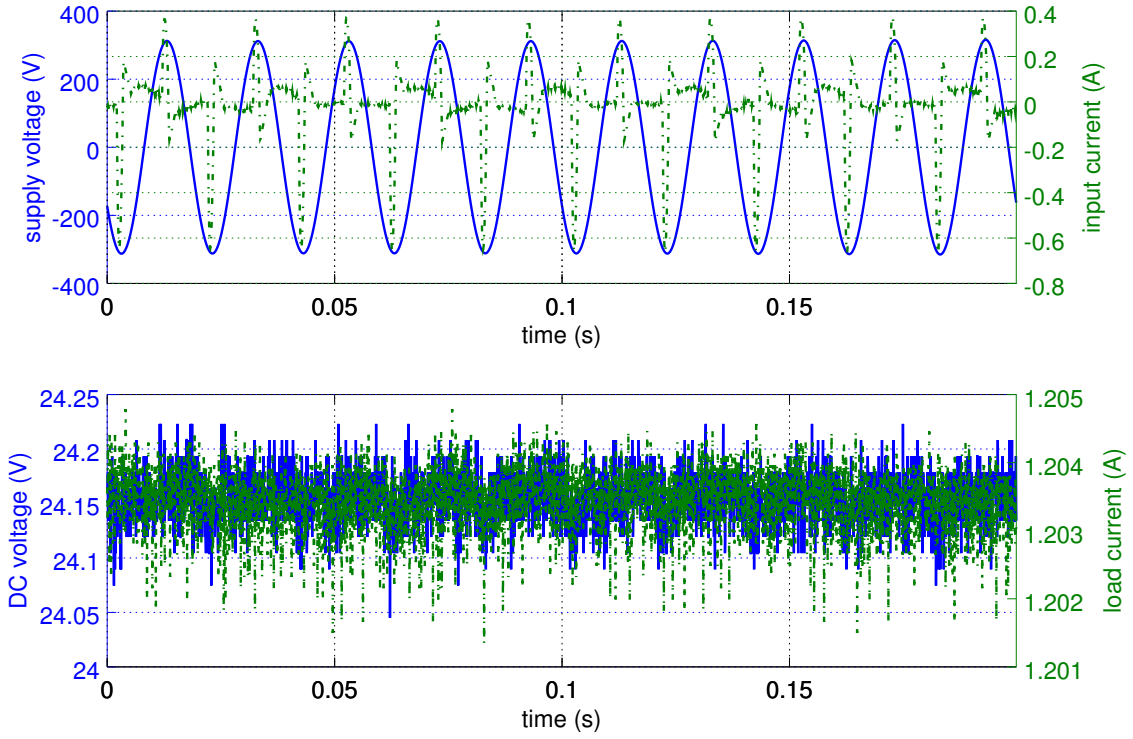

(a) SUP_5 + resistive load (MeaTest), $m_{DC} = (0.43 \pm 0.23)\,\%$

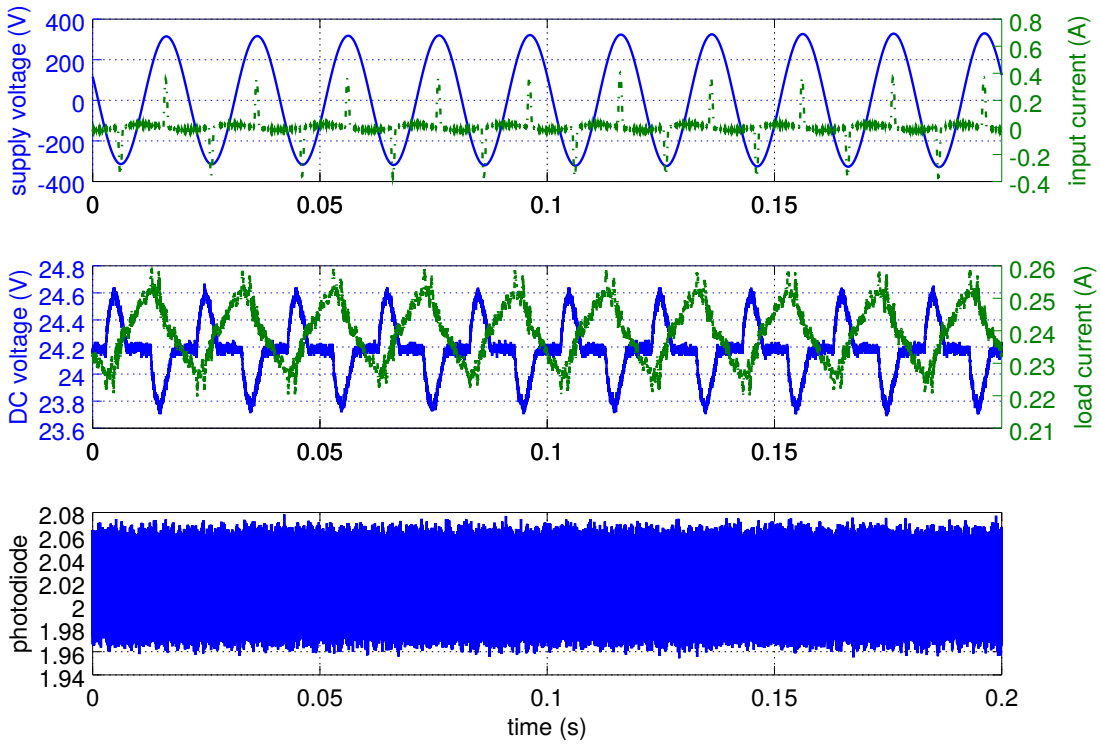

(b) SUP_5 + LED_4, $m_{DC} = (1.99 \pm 0.23)\,\%$

Figure 6.10: Temporal view of the supply voltage, DC voltage, currents and photodiode output, SAM $f_m = 1\,\text{Hz}$, $m_{SM} = 10\,\%$. Comparison with the resistive load and with the LED

6.3 AC Supply Induced Fluctuations of 230 V Lamp Luminous Flux

This experiment was designed to show how retrofit (designed to replace incandescent bulbs, i.e., equipped with an E27 socket) 230 V LED lamps react to AC supply voltage in terms of the produced flicker.

The experiment setup was designed to supply the lamps with clean AC voltage (free of distortion and with small impedance, mimicking an ideal grid supply) produced by a Kikusui PCR500M power supply. The lamps were placed in an Ulbricht sphere (diam. 1.73 m) and the produced luminous flux was measured by a photodiode. The photodiode output was amplified using a logarithmic amplifier (Sec. 6.1). The amplifier output was acquired by a Tektronix oscilloscope. The *FI* and *FP* were evaluated. The setup is sketched in Fig. 6.11.

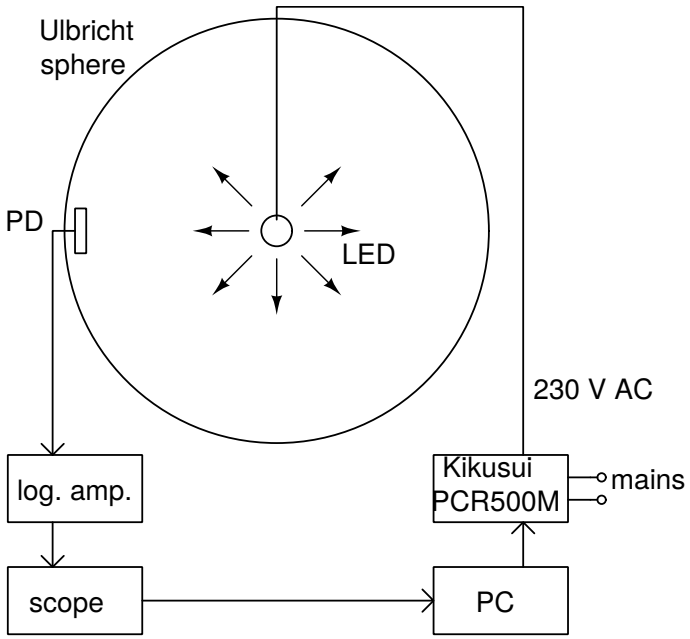

Figure 6.11: Laboratory setup for measuring *FI* and *FP* of retrofit lamps

The results of this experiment (Tab. 6.5) show that there are large differences among the available LED lamps. Most notably, flicker (at 100 Hz if 50 Hz supply voltage is used) can be easily caused even if there is no harmonic distortion in the supply voltage. The 50 Hz supply voltage is enough to cause significant flux fluctuations if a low quality driver is used. Comparison with flux fluctuation limits at 100 Hz given by [STD1] ($FP \leq 8\,\%$) shows that eight of the lamps do not satisfy this requirement (indicated by the red colour in the table). The results were published in [LK1].

Table 6.5: Flicker values per each lamp, measurement at thermal equilibrium; a 100 W incandescent lamp is included for comparison. The red colour indicates non-compliance with the IEEE std. 1789-2015 (also see Fig. 3.2).

Lamp	Power (W)	Flux (lm)	*FP* (%)	*FI* (—)
LED1	6	340	3.12	$3.31 \cdot 10^{-3}$
LED2	10	806	19.13	$4.95 \cdot 10^{-2}$
LED3	10	700	4.03	$5.56 \cdot 10^{-3}$
LED4	12	1 055	16.80	$3.31 \cdot 10^{-2}$
LED5	10	810	45.79	$1.25 \cdot 10^{-1}$
LED6	4	450	100	$3.72 \cdot 10^{-1}$
LED7	4	260	67.24	$2.06 \cdot 10^{-1}$
LED8	7	470	29.16	$7.38 \cdot 10^{-2}$
LED9	6	450	0.8	$1.05 \cdot 10^{-3}$
LED10	6	450	0.51	$3.11 \cdot 10^{-4}$
LED11	4.5	598	32.68	$8.01 \cdot 10^{-2}$
LED12	4.5	585	55.86	$1.62 \cdot 10^{-1}$
LED13	6	600	1.14	$1.74 \cdot 10^{-3}$
incandescent	100	ca. 1 100	9.05	$2.65 \cdot 10^{-2}$

6.4 Flicker Immunity of 12 V LED Lamps

This section consists of two sets of experiments which were performed upon identical EUT but in separate laboratories. A set of 12 V LED lamps (see the details in Tab. 6.6) was deeply analysed in terms of immunity against supply voltage fluctuations. The lamps (for hardware details see Tab. 6.6) were supplied by DC voltage contaminated with sinusoidal fluctuations of variable magnitude. The lamps were placed in an Ulbricht sphere.

Table 6.6: The declared properties of the analysed lamps

Label	Rated voltage	Power (W)	Socket	Flux (lm)	CCT (K)
LED1	12 VAC/50 Hz	1.4	GU5.3,MR16	45	4 300
LED2	12 VAC/DC	5	GU5.3	340	3 000
LED3	10–18 VAC/DC	5	GU5.3	260	3 700
LED4	12 VAC/DC	5	GU5.3,MR16	—	warm white
LED5	12 VAC/DC	4	GU5.3,MR16	200	3 000
LED6	12 VAC/DC	7	GU5.3,MR16	390	2 700

6.4.1 12 V LED Lamp Drivers—Reverse Engineering

Reverse engineering methods were applied on the lamps in order to link the lamp flicker properties and hardware implementation. This is important to understand

Table 6.7: LED lamps reverse engineering

(a) LED drivers—components summary

Lamp label	Scheme	R_I (Ω)	C_B (μF)	C_B/P (μF W^{-1})	μController	R_{Sens} (Ω)	LED matrix (ser x par)
LED1	fig. 6.12a	3.4	10	6.67	N.A.	N.A.	3(2)x7
LED2	fig. 6.12b	0	330	66	PT4205 [100]	0.43	3x5
LED3	fig. 6.12b	0.15	430	86	PT4115 [101]	0.24	1x1
LED4	fig. 6.12b	0	470	94	SD42527 [102]	0.1	1x1
LED5	fig. 6.12b	0	250	66	—	—	3x1
LED6	fig. 6.12b	0.5	330	47	—	—	1x1

(b) LED drivers—diode bridge summary; the V_{fw} is given per diode

Lamp	DB type	forward voltage V_{fw} (V)
LED1	MB6S [103]	0.5
LED2	SK24A [104]	0.5
LED3	SS14 [105]	0.5
LED4	SS14 [105]	0.5
LED5	MD24S	N.A.
LED6	B340A [106]	0.5

what is going on in the drivers during regular operation or during experiments. Information from this section is also used for creating models used in Chapter 7. The information is summarised in this section. The disassembled lamps are shown in Appendix F.

Table 6.7a shows all key parts of the disassembled lamps. The diagrams are shown in Fig. 6.12. Table 6.7b contains the forward voltage drops of the diode bridges (or individual diodes in bridge connection) used in the LED design. The forward voltage is shown per diode; because in the DB connection, two diodes are always operating in series, the total forward voltage will be twice as high.

Most notably, in the LED1, the driver is passive (see Fig. 6.12a). Any kind of control mechanism is lacking; this allows for an interesting comparison of the LED1 properties with other lamps. Other tested lamps (LED2–6) contain active electronics to supply the LED matrix (see Fig. 6.12b). A step–down (buck) converter is used in all cases. There are differences among the lamps in the LED matrix topology and in the part properties. For details see Tab. 6.7a.

In the buck topology, the LED current is sensed by measuring the voltage drop over the sensing resistor R_{sens}. The sensed voltage is proportional to the inductor current:

$$V_{sens} = R_{sens} I_L \,, \tag{6.6}$$

which is also equal to the LED current.

The driver datasheets [100, 101] explain that the v_{sens} voltage is kept within range from 170 mV to 230 mV. This means that the converter is operated by hysteretic con-

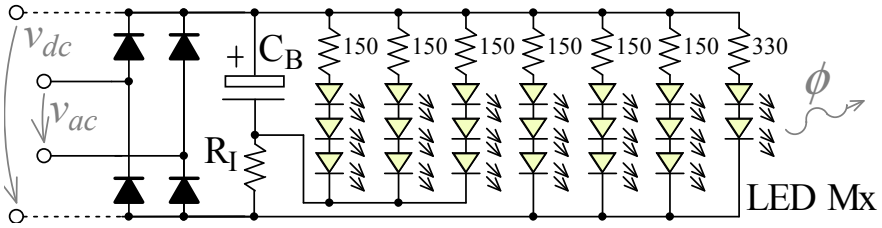

(a) LED1 connection diagram; the converter part is missing, the LED matrix is connected directly to the rectifier output

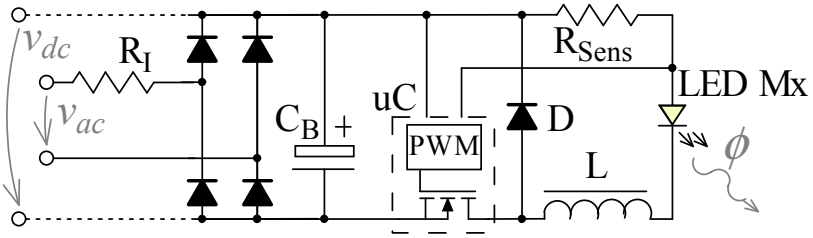

(b) LED2–6 simplified connection diagram—a step–down DC-DC converter is employed to supply the LED matrix

Figure 6.12: LED1–6 connection diagrams

trol in continuous conduction mode. Regarding the relative complexity of synchronous switching implementation, it can be expected that the switching is asynchronous.

The sensing resistor is placed on the high side of the LED branch. This requires that the voltage is sensed by a differential amplifier. The situation is sketched in a simplified manner in Fig. 6.13. In an ideal case, the feedback voltage would be equal to

$$V_{\text{fb}} = G(V_1 - V_2) = GV_{\text{sens}} = GR_{\text{sens}}I_{\text{L}}\,, \tag{6.7}$$

with G being the amplifier gain, I_{L} the sensed inductor current, R_{sens} the sensing resistor value, V_1 and V_2 the voltages as shown in Fig. 6.13. This way, the V_{fb} will always be proportional to the inductor current and voltage perturbations can only enter the feedback loop if they affect the I_{L} first.

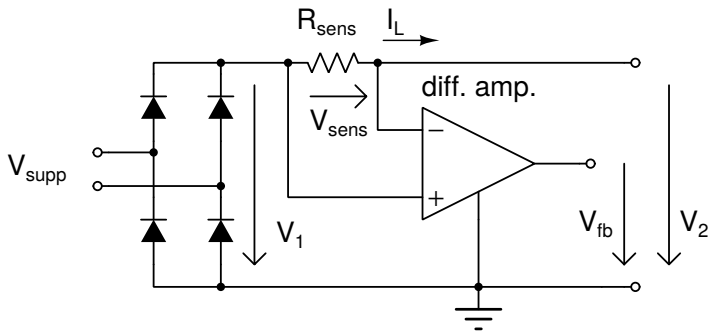

Figure 6.13: High side inductor current sensing

However, differential amplifiers are known to amplify a common mode signal

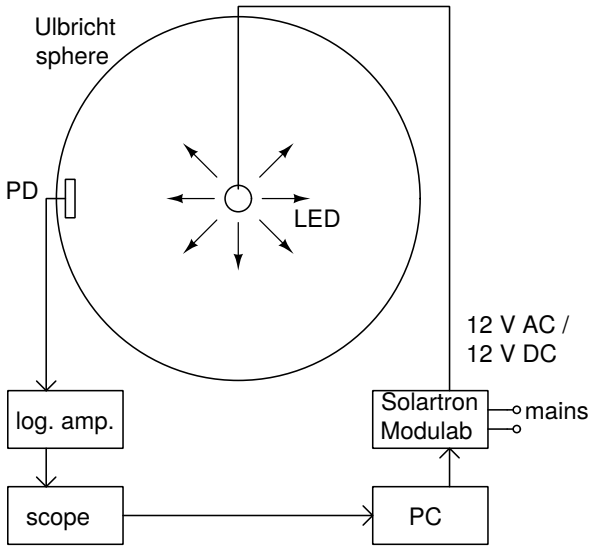

Figure 6.14: Laboratory setup for measuring the *FI* and *FP* of 12 V lamps

along with the differential signal. This property is usually quantified as *common mode rejection ratio* (*CMRR*) or *common mode rejection* (*CMR*). With *CMRR* assumed, the feedback voltage will be equal to

$$V_{\mathrm{fb}} = G(V_1 - V_2) + G_{\mathrm{cm}}\frac{1}{2}(V_1 + V_2)\,, \tag{6.8}$$

where G_{cm} is the common mode gain. The *CMR* is then equal to ([107]):

$$\mathit{CMR} = 20\log_{10}\mathit{CMRR} = 20\log_{10}\left(\frac{G}{G_{\mathrm{cm}}}\right)\,. \tag{6.9}$$

This way, the perturbations may enter the feedback loop directly and, thus, have a larger affect on flicker than in the ideal case. This hypothesis is tested in the simulations in Sec. 7.4. This problem may be removed completely if low side sensing is used. With low side current sensing, there is no need for a differential amplifier.

6.4.2 *FI* And *FP* Measurements

In this part of the measurement analysis, the lamps were placed in an Ulbricht sphere (1.73 m in diameter). The light output was observed using an SLD-70BG2 photodiode together with a logarithmic amplifier. The signal was acquired by a Tektronix oscilloscope. The laboratory setup was similar as in the previous experiment; a different voltage supply was used (Solartron Modulab XM, see Fig. 6.14). The *FI*, *FP* and (where applicable) the *GF* were evaluated from light output observations. The oscilloscope accuracy does not allow for accurate signal acquisition and, thus, *FP* values around 1 % may be considered as zero flicker.

Clean AC

For comparison, the LED lamps were first supplied by clean 12 V AC. The results are shown in Tab. 6.8. The first value in Tab. 6.8 shows the values measured directly after switch-on. The second value shows the results after reaching thermal equilibrium (approx. 20 mins).

Table 6.8: Pure AC supply—flicker measurements; the red colour indicates non-compliance with IEEE std. 1789-2015

Lamp	*FP* 1 (%)	*FP* 2 (%)	*FI* 1	*FI* 2
LED1	100	100	$4.61 \cdot 10^{-1}$	$5.04 \cdot 10^{-1}$
LED2	14.50	3.12	$1.01 \cdot 10^{-2}$	$5.54 \cdot 10^{-3}$
LED3	2.48	2.05	$4.84 \cdot 10^{-3}$	$4.71 \cdot 10^{-3}$
LED4	1.43	0.72	$1.58 \cdot 10^{-3}$	$1.18 \cdot 10^{-3}$
LED5	0.61	0.68	$8.79 \cdot 10^{-4}$	$9.13 \cdot 10^{-4}$
LED6	7.76	1.12	$2.25 \cdot 10^{-3}$	$1.37 \cdot 10^{-3}$

The results show that there are large differences among the lamps. It is notable that for lamp LED1, the $FP = 100\,\%$, i.e. the light output goes completely off during the cycle. On the contrary, LED5 exhibits practically no flicker at all under ideal AC supply conditions.

Distorted DC

In the following experiment, the lamps were supplied by 12 V DC with sinusoidal voltage modulation provided by Solartron Modulab XM:

$$v(t) = V_{\mathrm{DC}} + \frac{\Delta V}{2} \sin(2\pi f_{\mathrm{m}} t)\,. \tag{6.10}$$

The modulation frequency f_{m} was chosen from 25 Hz to 2 000 Hz. For the chosen modulation magnitudes ΔV, see Tab. 6.9. The largest ΔV is considered an extreme value seldom to be found in real conditions.

With the AC supply, the voltage reached peak value $V_{\mathrm{peak}} = 12\sqrt{2} = 17\,\mathrm{V}$ and dropped back to zero every 10 ms, which implies a very large modulation depth. Yet the *FP* was very low (practically zero, see Tab. 6.8). It would naturally be expected that a DC supply, even with a large ripple, can be used without causing flicker. Measurements show otherwise.

The results for the largest modulation $\Delta V = 5\,657\,\mathrm{mV}$ are shown in Tab. 6.10. Compliance with the standard [STD1] was determined for *FP*. The red colour indicates non-compliance. The yellow colour indicates that the acquisition inaccuracy does not allow to reliably determine compliance. This happened for the modulation frequency $f_{\mathrm{m}} = 25\,\mathrm{Hz}$ where the allowed limit is $FP < 0.625\,\%$.

Figure 6.15 shows the light output of LED5 during the experiment. The waveforms show that for a large modulation magnitude ($\Delta V > 2.8\,\mathrm{V} \simeq m_{\mathrm{DC}} = 11.79\,\%$), the control loop fails to compensate the perturbations. In these cases, the flicker response worsens considerably. This phenomenon is also observable from Fig. 6.16b.

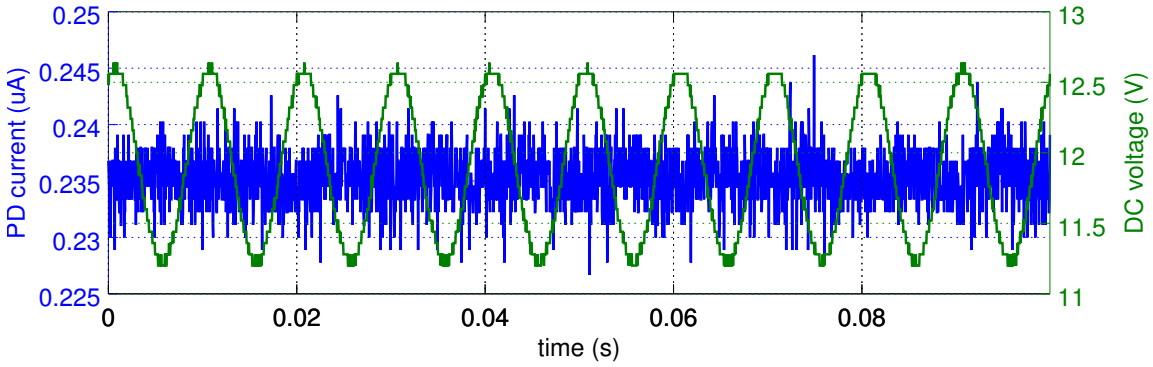

(a) Voltage supply: 12 V DC + 0.5 V_{RMS} AC, 100 Hz; *FP* = 1.5 %

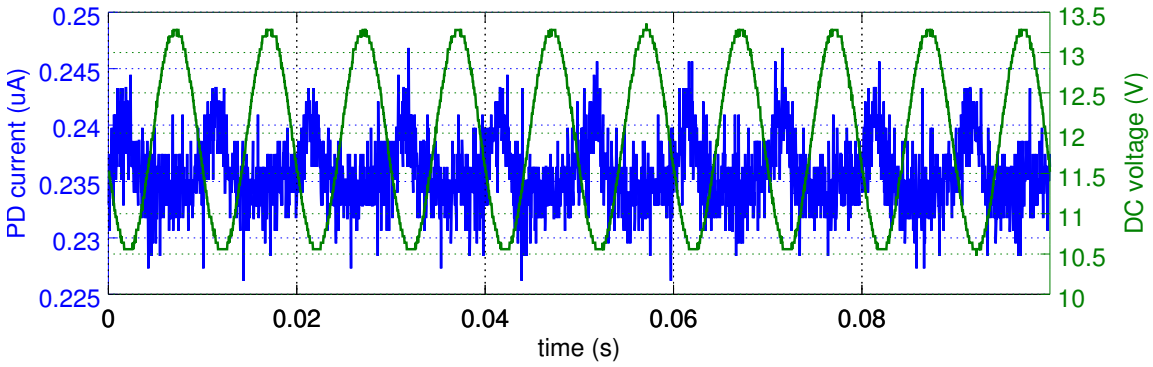

(b) Voltage supply: 12 V DC + 1 V_{RMS} AC, 100 Hz; *FP* = 2.6 %

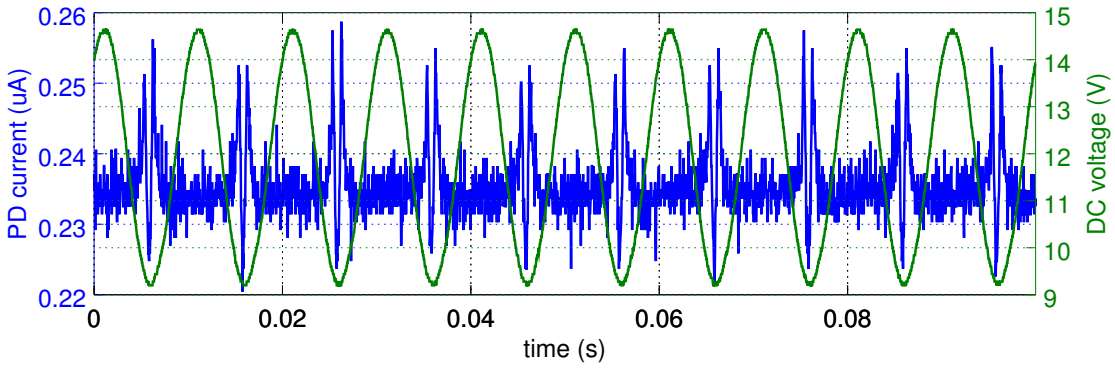

(c) Voltage supply: 12 V DC + 2 V_{RMS} AC, 100 Hz; *FP* = 6.5 %

Figure 6.15: Active driver (LED 5): Recoverable compensation failure due to large DC voltage modulation; three levels of distortion. The green curves show modulated supply voltage, the blue curves represent the light output (light sensor photodiode current).

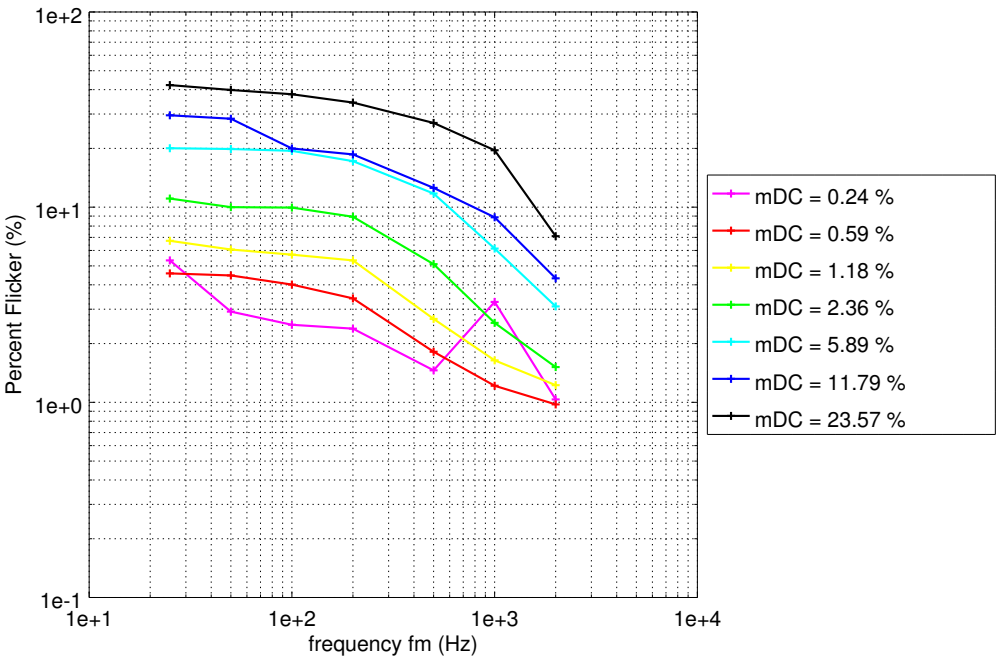

(a) LED1; for this lamp, the *FP* is linearly dependent on the m_{DC}.

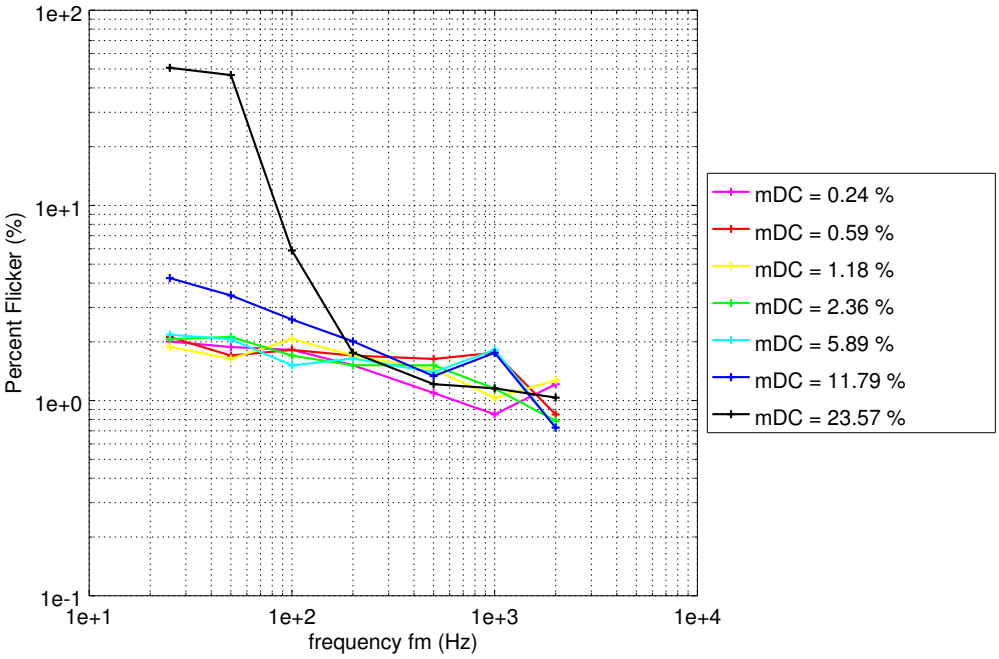

(b) LED5; for $m_{\mathrm{DC}} = 11.79$ and $23.57\,\%$, the compensation failure is apparent for lower frequencies

Figure 6.16: *FP* for LED1 and LED5, variable frequency and modulation magnitude

Table 6.9: Modulation magnitude values used in this experiment, expressed by several means

AC RMS (mV)	AC peak (mV)	ΔV (mV)	m_{DC} (%)	d_{DC} (%)
20	28.3	56.6	0.24	0.47
50	70.7	141.4	0.59	1.18
100	141.4	282.8	1.18	2.36
200	282.8	565.7	2.36	4.71
500	707.1	1 414.2	5.89	11.79
1 000	1 414.2	2 828.4	11.79	23.57
2 000	2 828.4	5 656.9	23.57	47.14

For smaller frequencies the flicker is even worse (see Tab. 6.10; the *FP* for LED5 is 47 % for 50 Hz distortion and 51 % for 25 Hz distortion).

The voltage supply was 12 V DC plus a sinusoidal component of variable magnitude at 100 Hz. In the lowest subfigure of the Fig. 6.15 the supply voltage oscillates between 9 and 15 V, which is equal to the modulation depth $d_{\mathrm{DC}} = 47.14\,\%$. In this case, the percent flicker rose to 6.5 %. Figure 6.16b reveals that the percent flicker rises at relatively high supply voltage modulation and low frequencies (100 Hz and below).

Surely, the modulation depth $d_{\mathrm{DC}} = 47\,\%$ is an extreme value hardly to be met in real conditions. The aim of this experiment is to point out that AC supply cannot be assumed as the worst-case scenario for flicker evaluation where distorted DC supply is expected.

Conclusion

In the results, there are vast differences between LED1 (passive driver) and LED2–6 (active drivers). LED1 exhibits very low immunity to voltage variations and, thus, flickers a lot. With a distorted DC supply, the light output copies the voltage variation.

The AC measurements in this part show that all the lamps equipped with an active driver comply with IEEE Standard 1789-2015 [STD1] and exhibit very low flicker after reaching thermal equilibrium. The results show that for large modulations, the flicker worsens with the distorted DC, even though the modulation is smaller than with the AC supply. The results of these measurements were published in [LK8].

6.4.3 Measurements with a Light Flicker Meter

In this part of the experiments the $P_{\mathrm{st}}^{\mathrm{LM}}$ was evaluated from the produced light. The lamps under test were placed in an Ulbricht sphere (diam. 2.5 m) and supplied from the power amplifier APS 125, controlled by the controller PXI-8106 and the arbitrary wave generator NI PXI-5412. The laboratory setup is depicted in Fig. 6.17. The lamps were supplied by both distorted AC and DC. The $P_{\mathrm{st}}^{\mathrm{LM}}$ is measured by an

Table 6.10: *FI*, *FP* and *GF* for various lamps and frequencies for $\Delta V = 5\,657\,\text{mV}$ SAM (*FP* in %); the red colour indicates non-compliance with the IEEE 1789-2015, the yellow colour indicates inability to determine compliance

Lamp	quantity	25 Hz	50 Hz	100 Hz	200 Hz	500 Hz	1 000 Hz	2 000 Hz
LED1	*FP*	41.90	39.49	38.10	34.72	30.82	19.68	7.28
	$FI \times 10^{-1}$	1.47	1.54	1.55	1.34	0.96	0.64	0.28
	GF	1.96	1.90	1.83	1.74	1.38	0.93	0.47
LED2	*FP*	0.72	0.56	0.64	0.62	0.64	0.73	0.97
	$FI \times 10^{-4}$	9.23	9.6	11.3	12.1	15.9	16.8	21.4
	GF	0.03	0.04	0.03	0.06	0.05	0.05	0.08
LED3	*FP*	53.80	50.94	9.69	2.31	1.15	1.28	1.46
	$FI \times 10^{-1}$	1.15	1.17	0.11	0.04	0.02	0.03	0.03
	GF	2.19	1.88	0.40	0.14	0.14	0.14	0.28
LED4	*FP*	58.49	52.81	20.26	1.18	1.34	1.40	1.68
	$FI \times 10^{-2}$	14.4	13.6	3.56	0.19	0.03	0.03	0.04
	GF	2.56	2.10	0.85	0.14	0.12	0.14	0.27
LED5	*FP*	51.03	46.98	6.54	1.03	0.82	0.41	0.47
	$FI \times 10^{-3}$	93.4	90.8	7.20	1.88	1.56	1.45	1.51
	GF	2.02	1.71	0.19	0.06	0.07	0.07	0.10
LED6	*FP*	0.81	0.71	0.64	0.77	0.50	0.86	0.59
	$FI \times 10^{-3}$	1.22	1.04	1.27	1.50	1.14	2.62	1.57
	GF	0.06	0.04	0.04	0.07	0.08	0.08	0.13

LFM [51, 52]. Modulation magnitudes were chosen from Tab. 6.11. The modulation frequency resolution was 1 Hz.

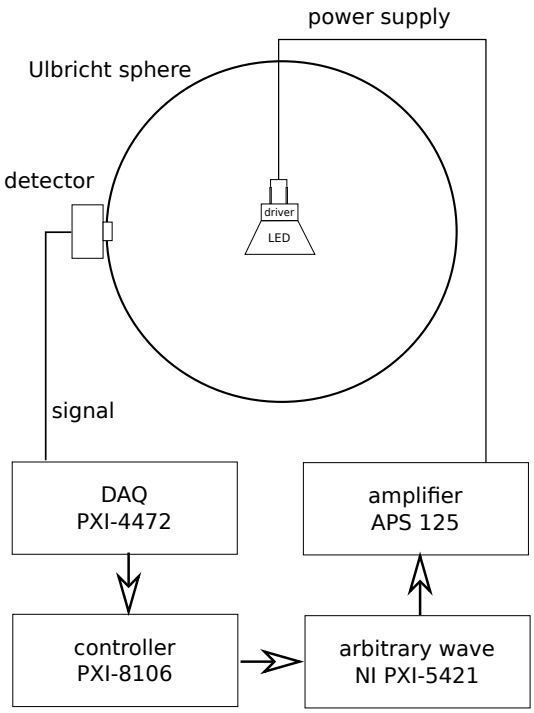

Figure 6.17: Laboratory setup for measuring $P_{\mathrm{st}}^{\mathrm{LM}}$ produced by the EUT

Figure 6.18 shows examples of the $P_{\mathrm{st}}^{\mathrm{LM}}$ response to the AC supply in the frequency domain. It compares the response of a passive driver (LED1) and an active driver (LED5). Above the CFF (let us assume that $CFF = 50$ Hz for simplicity, as it is the fundamental supply frequency), the flicker is not caused by the injected interharmonic itself, but with its intermodulation with the fundamental frequency. This is the reason why flicker in AC is caused by much higher frequencies than in DC. This phenomenon is described in more detail in Sections 3.4.5 and 7.2.

Table 6.11: Modulation magnitudes used in this experiment, both for AC and DC tests

AC RMS (mV)	AC peak (mV)	ΔV (mV)	$m_{\mathrm{SM/DC}}$ (%)	$d_{\mathrm{SM/DC}}$ (%)
60	84.9	169.7	0.71	1.41
120	169.7	339.4	1.41	2.83
240	339.4	678.8	2.83	5.66
600	848.5	1 697.1	7.07	14.14

Figure 6.19 shows the $P_{\mathrm{st}}^{\mathrm{LM}}$ measurements with a DC supply, where the intermodulation does not take effect. The figure compares measurements of all the lamps with sinusoidal and rectangular modulation (SM and RM, respectively). The curves for SM roughly follow the eye sensitivity curve used in LFM (see App. A). The nature of the $P_{\mathrm{st}}^{\mathrm{LM}}$ quantity does not allow one to distinguish between lamp properties and the effect of the eye response model.

The situation is very similar with RM. The most notable difference is in the area around 5 Hz where the response to RM is higher. This is caused by the rich harmonic spectrum of the RM. For $f_{\mathrm{m}} = 5\,\mathrm{Hz}$, the second harmonic component is 10 Hz which is the point of largest sensitivity in the eye model used in the flickermeter.

6.4.4 The Impact of a Diode Bridge on Flicker Properties of DC Supplied LED Lamps

In AC applications, the topology of LED drivers necessarily contains a diode bridge in order to rectify the voltage and convert it to DC. The diode bridge does not pose a problem under DC supply, on the contrary it protects the driver from the wrong voltage polarisation. Even though, so far it is not clear how the future DC-only lamp drivers can look like. The reduction of power losses and financial cost might result in excluding the DB in DC-only applications. This experiment was designed to analyse the impact of the DB presence on the flicker ($P_{\mathrm{st}}^{\mathrm{LM}}$) response.

Firstly, the lamps $P_{\mathrm{st}}^{\mathrm{LM}}$ response to DC supply with SM was measured. Afterwards the connection was changed to bypass the DB and the measurements were repeated. It is expected that the results will depend upon the driver topology. In one of the lamps (LED4), the DB could not have been bypassed; it is excluded from the analysis. The results are summarised in Tab. 6.12. The relative $P_{\mathrm{st}}^{\mathrm{LM}}$ change was evaluated as

$$\Delta P_{\mathrm{st}}^{\mathrm{LM}} = \frac{P_{\mathrm{st2}}^{\mathrm{LM}} - P_{\mathrm{st1}}^{\mathrm{LM}}}{P_{\mathrm{st1}}^{\mathrm{LM}}} \cdot 100\,, \tag{6.11}$$

where $P_{\mathrm{st1}}^{\mathrm{LM}}$ denotes the $P_{\mathrm{st}}^{\mathrm{LM}}$ measured with the diode bridge and $f_{\mathrm{m}} = 10\,\mathrm{Hz}$ and $P_{\mathrm{st2}}^{\mathrm{LM}}$ denotes the $P_{\mathrm{st}}^{\mathrm{LM}}$ evaluated with the diode bridge bypassed. This way, positive values of $\Delta P_{\mathrm{st}}^{\mathrm{LM}}$ indicate that the DB has a positive impact on flicker immunity (flicker is lower with the DB), negative $\Delta P_{\mathrm{st}}^{\mathrm{LM}}$ values indicate the opposite (flicker is higher with the DB).

Figure 6.20 shows the $P_{\mathrm{st}}^{\mathrm{LM}}$ response in the frequency domain both in connection with the DB and without. The figure only shows examples—LED1 (passive driver) and LED5 (active driver).

Table 6.12 shows the $P_{\mathrm{st}}^{\mathrm{LM}}$ results for both topologies as well as the $\Delta P_{\mathrm{st}}^{\mathrm{LM}}$ evaluated at four distinct modulation magnitude levels. In the table, the red colour (negative $\Delta P_{\mathrm{st}}^{\mathrm{LM}}$ values) indicates that the DB *worsens* the $P_{\mathrm{st}}^{\mathrm{LM}}$ response; the green colour (positive $\Delta P_{\mathrm{st}}^{\mathrm{LM}}$ values) indicates the opposite. In LED4, the DB bypass was not possible due to protective cast around the driver; therefore, it was excluded from these comparisons.

Table 6.12 shows that, for some lamps, the DB helps to minimise the $P_{\mathrm{st}}^{\mathrm{LM}}$ while,

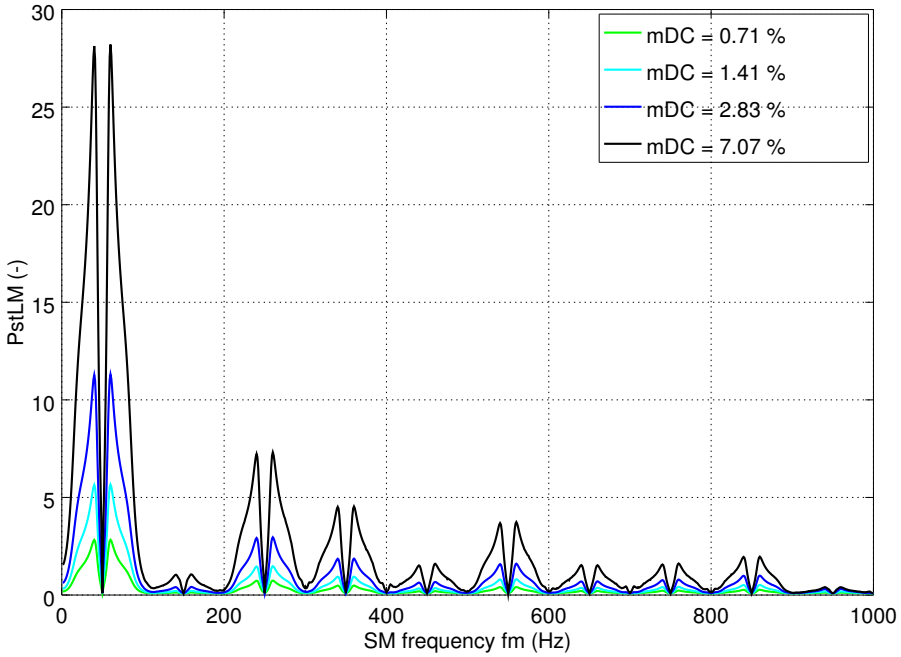

(a) LED 1—passive driver

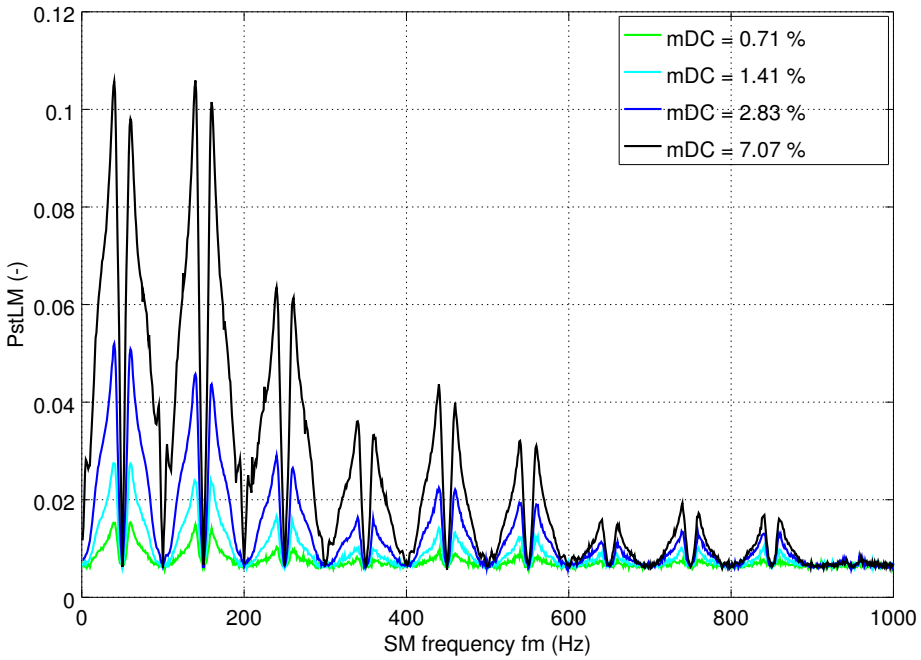

(b) LED 5—active driver

Figure 6.18: $P_{\mathrm{st}}^{\mathrm{LM}}$ produced by LED 1 and LED 5 under AC supply; the higher frequencies intermodulate with the fundamental and, thus, frequencies up to 1 000 Hz are relevant.

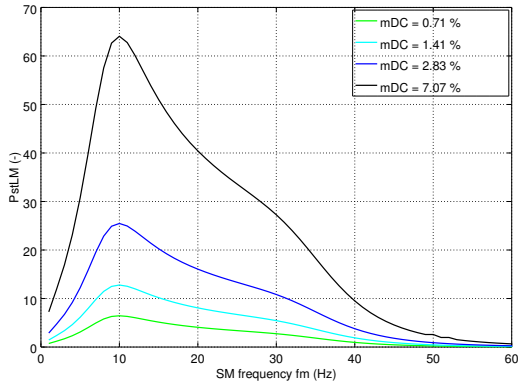

(a) LED 1—sinusoidal modulation

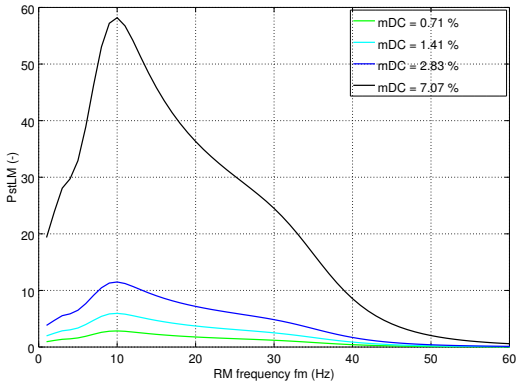

(b) LED 1—rectangular modulation

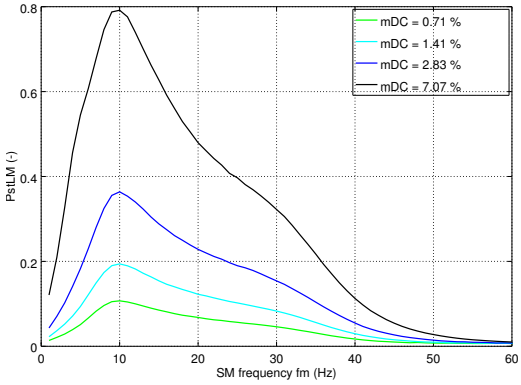

(c) LED 2—sinusoidal modulation

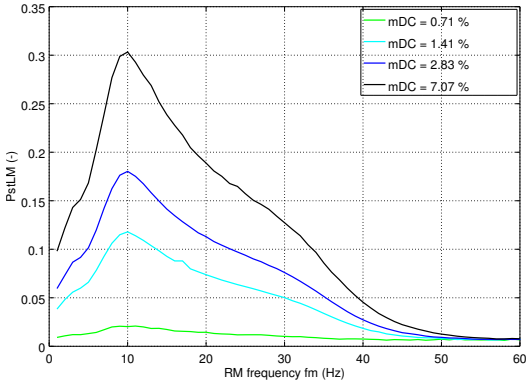

(d) LED 2—rectangular modulation

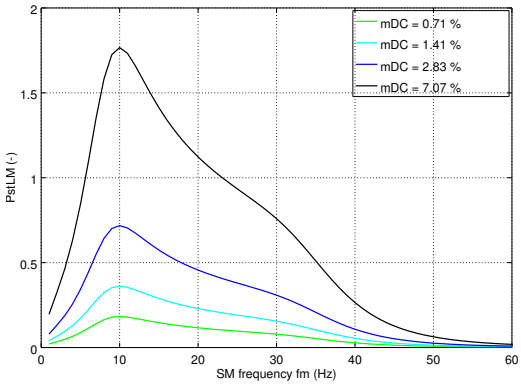

(e) LED 3—sinusoidal modulation

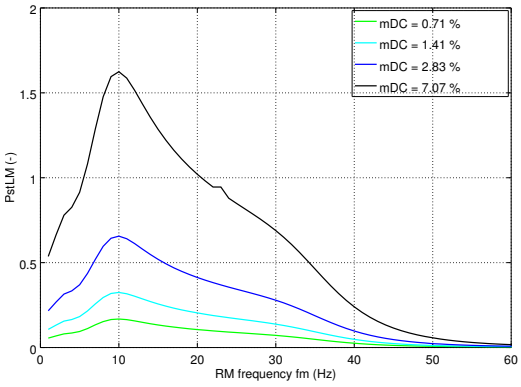

(f) LED 3—rectangular modulation

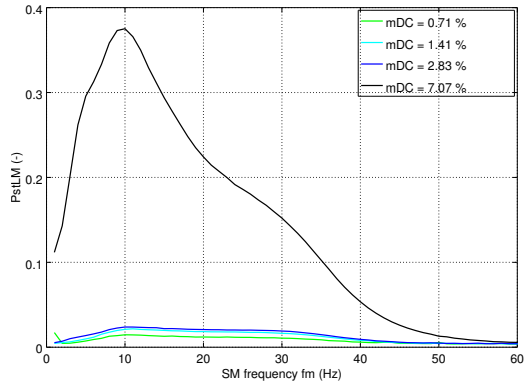

(g) LED 4—sinusoidal modulation

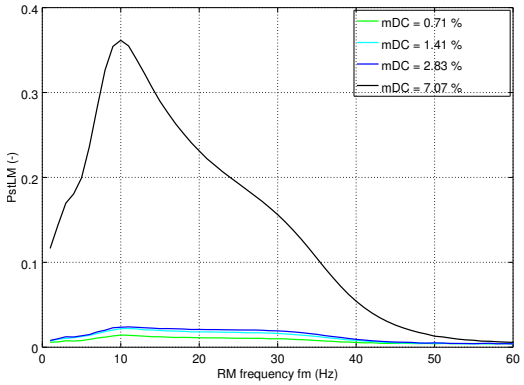

(h) LED 4—rectangular modulation

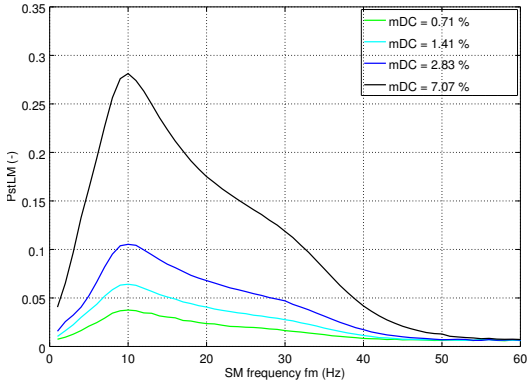

(i) LED 5—sinusoidal modulation

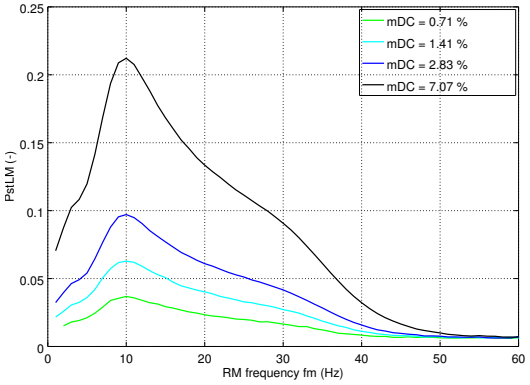

(j) LED 5—rectangular modulation

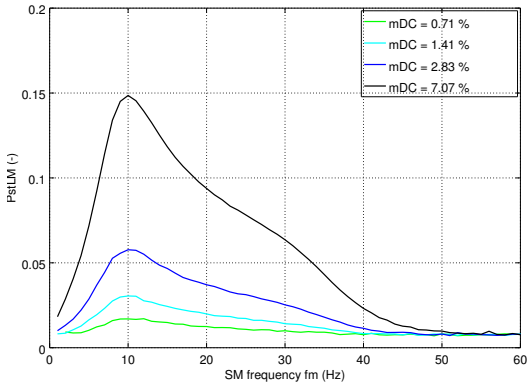

(k) LED 6—sinusoidal modulation

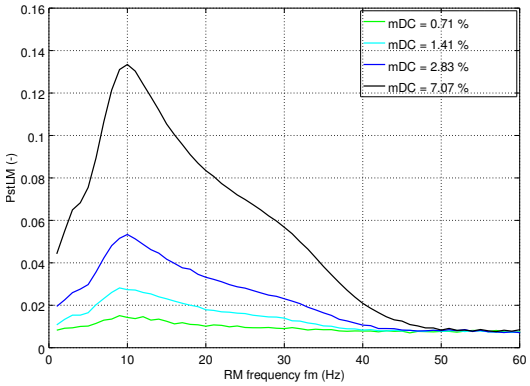

(l) LED 6—rectangular modulation

Figure 6.19: LED 1–6: comparison of the sinusoidal and rectangular DC supply modulation; for DC, the relevant frequencies are up to 60 Hz

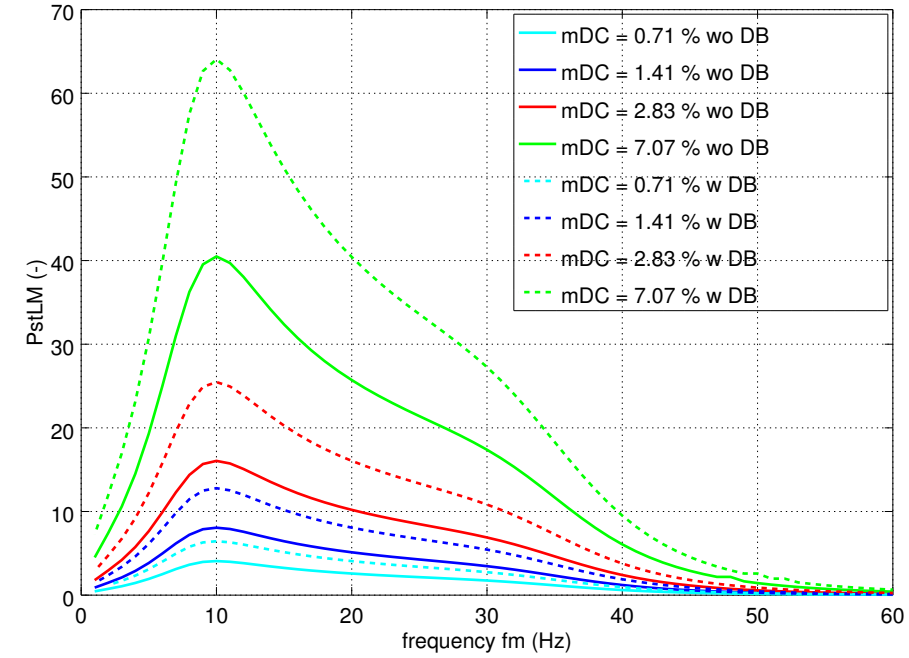

(a) LED1: $P_{\mathrm{st}}^{\mathrm{LM}}$ caused by the SM in the DC supply—comparison in connection with the DB and without the DB.

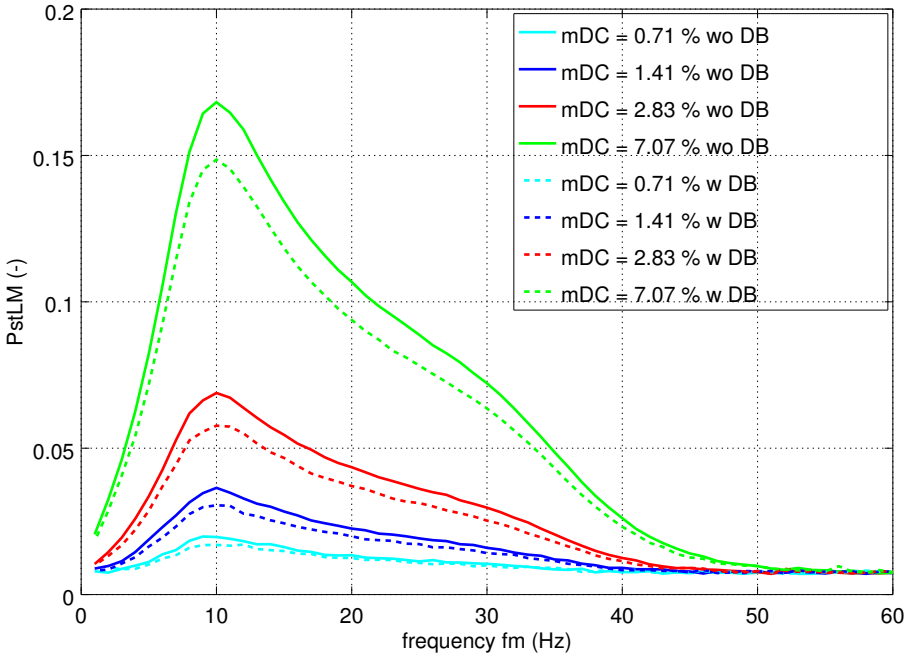

(b) LED6: $P_{\mathrm{st}}^{\mathrm{LM}}$ caused by the SM in the DC supply—comparison in connection with the DB and without the DB.

Figure 6.20: Comparison: $P_{\mathrm{st}}^{\mathrm{LM}}$ with and without the DB; Subfigure a: DB worsens the flicker response, Subfigure b: DB attenuates the flicker response.

Table 6.12: The P_{st}^{LM} and ΔP_{st}^{LM} measured for SM, $f_m = 10\,\text{Hz}$, varying m_{DC}; comparison of the lamps performance with (P_{st1}^{LM}) or without the DB (P_{st2}^{LM})

	m_{DC} (%)	0.71	1.41	2.83	7.07
LED1	P_{st1}^{LM}	6.45	12.78	25.47	64.06
	P_{st2}^{LM}	4.07	8.06	16.05	40.49
	ΔP_{st}^{LM} (%)	−36.82	−36.94	−36.99	−36.79
LED2	P_{st1}^{LM}	0.11	0.19	0.36	0.79
	P_{st2}^{LM}	0.14	0.28	0.55	1.28
	ΔP_{st}^{LM} (%)	+34.89	+41.78	+49.84	+61.54
LED3	P_{st1}^{LM}	0.18	0.36	0.72	1.77
	P_{st2}^{LM}	0.17	0.34	0.67	1.69
	ΔP_{st}^{LM} (%)	−6.30	−6.60	−6.45	−4.53
LED5	P_{st1}^{LM}	0.04	0.06	0.11	0.28
	P_{st2}^{LM}	0.02	0.03	0.02	0.08
	ΔP_{st}^{LM} (%)	−52.04	−60.04	−77.83	−71.62
LED6	P_{st1}^{LM}	0.02	0.03	0.06	0.15
	P_{st2}^{LM}	0.02	0.04	0.07	0.17
	ΔP_{st}^{LM} (%)	+15.91	+19.55	+19.36	+13.21

for other lamps it worsens the response. This experiment is accompanied by a simulation also, see Sec. 7.4. The results from this section were published in [LK9].

6.4.5 Measurement Results in the Magnitude Domain

Measurements of P_{st}^{LM} were also performed in the magnitude domain. The P_{st}^{LM} produced by individual lamps was observed at a constant modulation frequency in dependence on the modulation magnitude m_{DC}. Only four out of six lamps were measured this way, LED1, LED2, LED3 and LED5. The results are shown in Fig. 6.21 both in connection with the DB and without.

The figure shows that the m-P_{st}^{LM} response is linear only in some cases. Namely for LED1 it is linear under all conditions; for LED3 it is linear below $m_{DC} = 10\,\%$; above this value, only with the DB removed.

Linear Flicker Response in Magnitude Domain

Linearity in terms of the m-P_{st}^{LM} response is defined by the linear relationship between supply voltage modulation depth and induced P_{st}^{LM}:

$$P_{st}^{LM}\big(a\,W(t)\big) = a\,P_{st}^{LM}\big(W(t)\big)\,, \tag{6.12}$$

where a is a non-negative modulation depth multiplier and $W(t)$ is an arbitrary modulation waveform of a DC supply. Assuming the $W(t)$ is periodic with fundamental

frequency f_1, it can be expanded using sine transformation:

$$W(t) = \int_0^{\inf} k(f) \sin\left[2\pi f t + \varphi(f)\right] \mathrm{d}f \,. \tag{6.13}$$

From the LFM specifications, one can obtain

$$P_{\mathrm{st}}^{\mathrm{LM}}(W_1 + W_2) = \sqrt{\left[P_{\mathrm{st}}^{\mathrm{LM}}(W_1)\right]^2 + \left[P_{\mathrm{st}}^{\mathrm{LM}}(W_2)\right]^2} \,. \tag{6.14}$$

This way one can deduce that the $P_{\mathrm{st}}^{\mathrm{LM}}$ caused by $W(t)$ (with the fundamental frequency f_1) can be approximated using the $P_{\mathrm{st}}^{\mathrm{LM}}$ caused by SM at specified frequencies (multiples of f_{m}):

$$P_{\mathrm{st}}^{\mathrm{LM}}(W) = a \sqrt{\int_0^{60} k^2(f) \left[P_{\mathrm{st}}^{\mathrm{LM}}(\mathrm{SM}, f)\right]^2 \mathrm{d}f} \,. \tag{6.15}$$

In the equation above, the modulation depth multiplier a is equal to $a = \frac{m_W}{m_{\mathrm{SM}}}$, where m_W and m_{SM} denotes the modulation magnitude of $W(t)$ and SM, respectively. Upper limit of the integral is given by the definition of $P_{\mathrm{st}}^{\mathrm{LM}}$ —it is effectively zero for frequencies above $60\,\mathrm{Hz}$ and, thus, including more components at higher frequencies would only introduce noise. Using the sampled signal and DFT, the Eq. (6.15) becomes

$$P_{\mathrm{st}}^{\mathrm{LM}}(W) = \frac{m_W}{m_{\mathrm{SM}}} \sqrt{\sum_{i=1}^{if_{\mathrm{m}} \leq 60} k_i \left[P_{\mathrm{st}}^{\mathrm{LM}}(\mathrm{SM}, i f_1)\right]^2} \,. \tag{6.16}$$

Equation (6.14) is a property of the $P_{\mathrm{st}}^{\mathrm{LM}}$, Eq. (6.13) is a property of the waveform $W(t)$ and the Eq. (6.12) must be a property of the lamp driver. Therefore, the relationship (6.16) holds if Eq. (6.12) is fulfilled.

Figure 6.21 shows the m-$P_{\mathrm{st}}^{\mathrm{LM}}$ characteristics of LED1,2,3,5 for SM. It is clear that for LED1 Eq. (6.12) holds in connection with the DB as well as without the DB. For LED3, the equation holds only without the DB. For LED2 and LED5, the equation never holds.

The approximation theorem (6.16) was experimentally verified for the available lamps using measurements of $P_{\mathrm{st}}^{\mathrm{LM}}$ (SM) and $P_{\mathrm{st}}^{\mathrm{LM}}$ (RM)—rectangular modulation with known k_i coefficients. First, these coefficients of $W(t) = \mathrm{square}(2\pi f_1 t)$ were determined from Fourier decomposition. Then, the $P_{\mathrm{st}}^{\mathrm{LM}}$ was measured with sinusoidal supply voltage modulation at frequency f_1 and its multiples up to $60\,\mathrm{Hz}$, m_{DC} being constant. From the acquired values, the $P_{\mathrm{st}}^{\mathrm{LM}}$ (RM) was estimated using Eq. (6.16). These estimated values were then compared with the measurements. This procedure was repeated for $f_1 = 5\,\mathrm{Hz}$, $10\,\mathrm{Hz}$ and $15\,\mathrm{Hz}$ and evaluated with several m_W.

The comparison is documented for LED1 and LED5 in Fig. 6.22. The upper left subplots show $P_{\mathrm{st}}^{\mathrm{LM}}$ (SM) measurement at $m_{\mathrm{SM}} = 7.07\,\%$; the measured values at multiples of $f_1 = 5\,\mathrm{Hz}$ are indicated. The lower subplots of 6.22a and 6.22b show

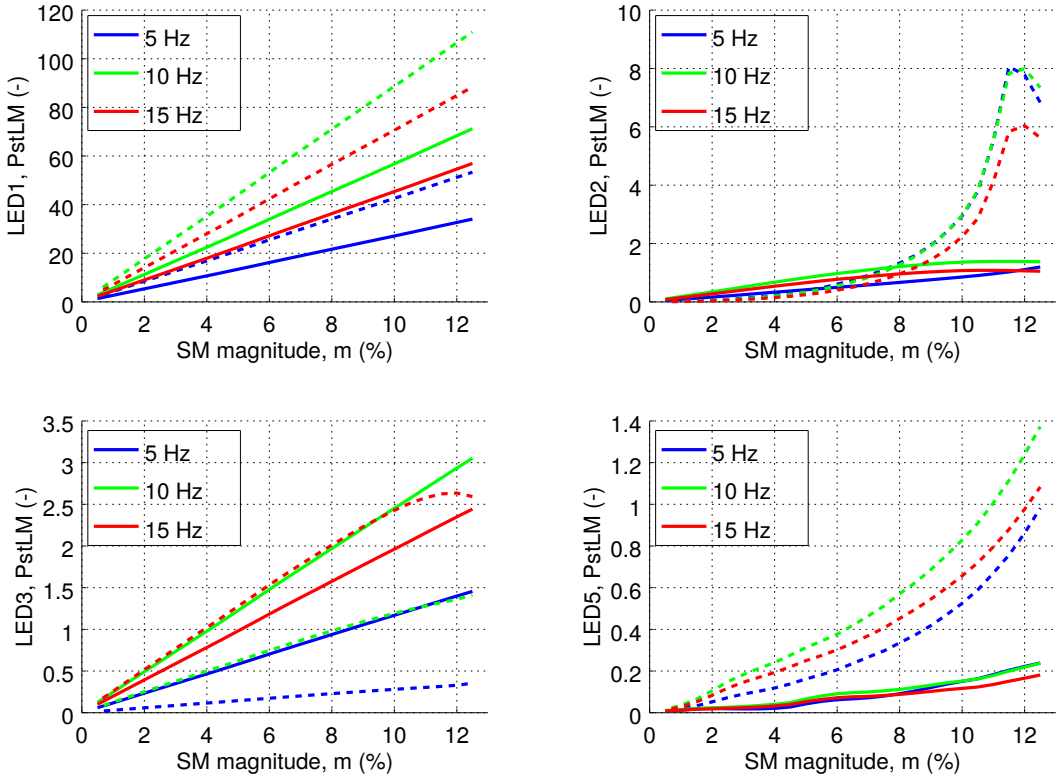

Figure 6.21: m-$P_{\mathrm{st}}^{\mathrm{LM}}$ characteristics of the analysed lamps; dotted lines—with DB, solid lines—without DB

$P_{\mathrm{st}}^{\mathrm{LM}}$ (RM) measured with several f_1 and various $m_W = m_{\mathrm{RM}}$. The estimated values of $P_{\mathrm{st}}^{\mathrm{LM}}$ (RM) are shown too. Measurements in this section were performed with the DB.

From the graphical comparison (Fig. 6.22), it is clear that the theorem (6.16) may indeed be used to estimate the $P_{\mathrm{st}}^{\mathrm{LM}}$ caused by an arbitrary waveform, provided that the $P_{\mathrm{st}}^{\mathrm{LM}}$ caused by the SM is known and that the m-$P_{\mathrm{st}}^{\mathrm{LM}}$ response is linear.

6.4.6 Experiment Summary

This section described a thorough analysis of six ELV LED lamps. Several important observations can be noted.

Firstly, when comparing the flicker response between a clean AC supply and distorted DC one, the flicker level may be significantly higher for the distorted DC than for the clean AC one, even though the modulation depth is much smaller and the downslope is also less steep. This situation is demonstrated in Fig. 6.23, where perturbed DC is compared to rectified AC supply.

Secondly, the measurements suggest that the size of the smoothing capacitor does not affect flicker when DC supply is applied. Lamp LED6 shows a very small flicker level even though its smoothing capacitor is small relatively to the other lamps.

Thirdly, the active drivers are based upon hysteretic control. Except for LED5

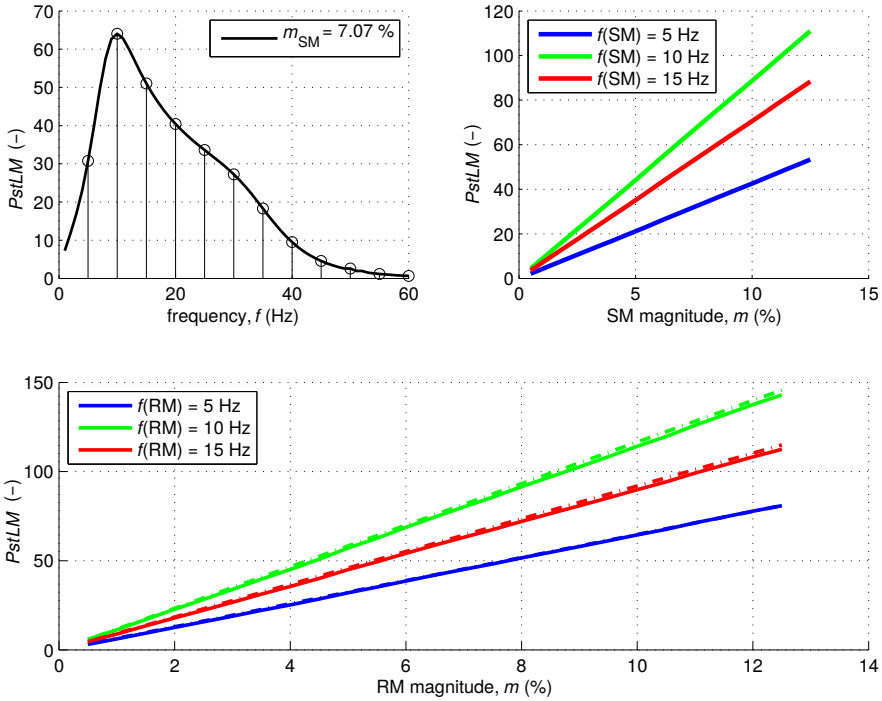

(a) LED1 (passive driver); approximation is successful because the m-$P_{\mathrm{st}}^{\mathrm{LM}}$ response is linear, the error is less than 5 %

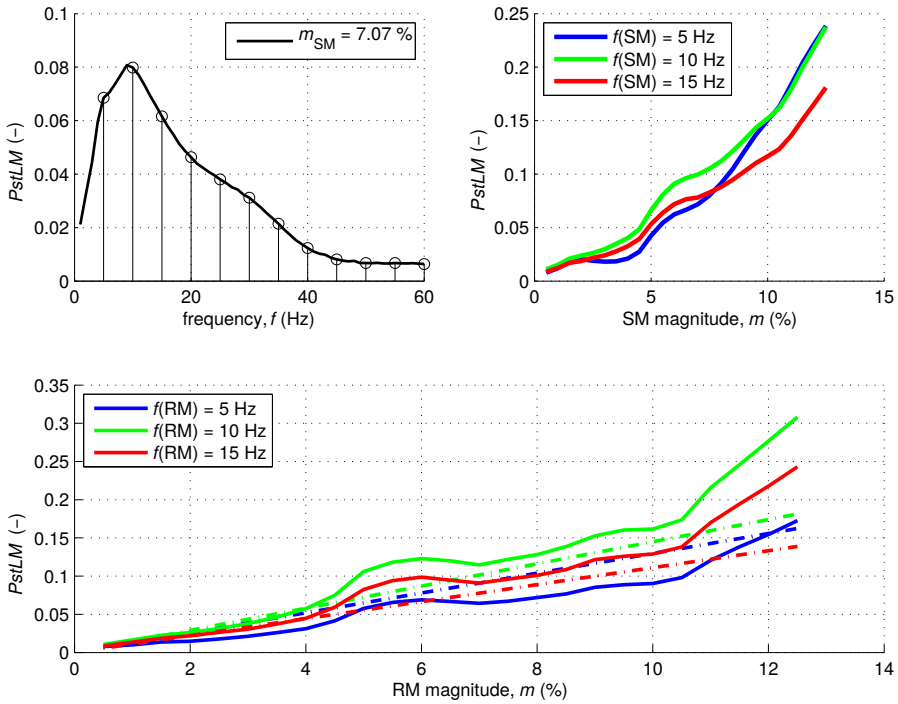

(b) LED5 (active driver); approximation is unsuccessful because the m-$P_{\mathrm{st}}^{\mathrm{LM}}$ response is not linear

Figure 6.22: $P_{\mathrm{st}}^{\mathrm{LM}}$ (RM) estimation from $P_{\mathrm{st}}^{\mathrm{LM}}$ (SM) at three distinct frequencies; upper left: $P_{\mathrm{st}}^{\mathrm{LM}}$ (SM) values used for the estimation, upper right: $P_{\mathrm{st}}^{\mathrm{LM}}$ (SM) measurements, lower subfigure: $P_{\mathrm{st}}^{\mathrm{LM}}$ (RM) measurements (solid) and estimation (dashed) from $P_{\mathrm{st}}^{\mathrm{LM}}$ (SM)

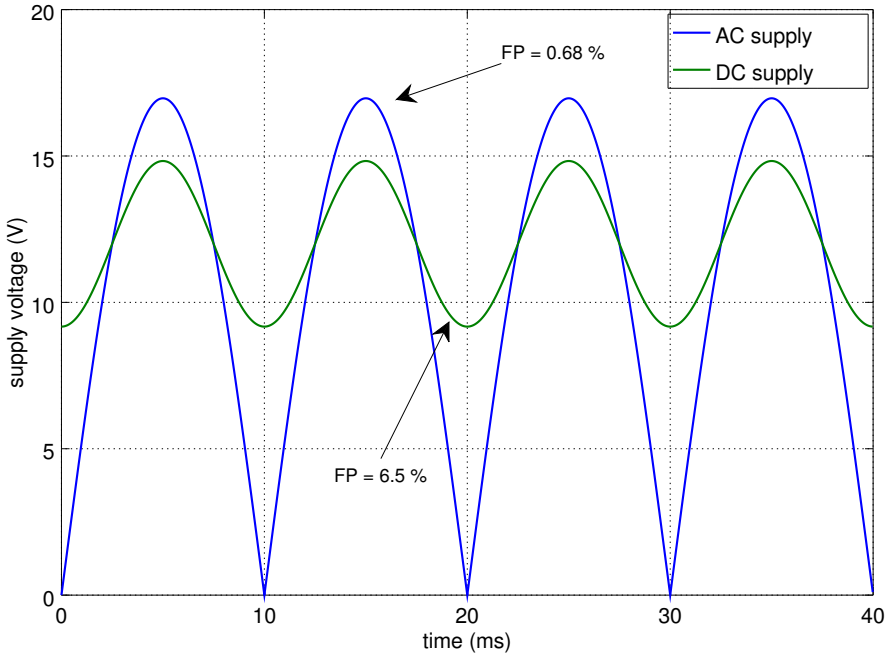

Figure 6.23: Clean AC supply and perturbed DC supply; *FP* level of lamp LED5 noted

and LED6 where a detailed analysis was complicated, the lamps have the current sensing resistor placed on the high side. This means that a differential amplifier is necessary for acquiring the resistor voltage. These findings were published in [LK8].

Fourthly, for some of the lamps (LED1, LED3 and LED5) the diode bridge has a negative impact on the flicker sensitivity. Removing the DB helped to decrease the flicker level. For LED2 and LED6, the effect was the opposite. For these lamps, removing the DB increased the flicker level. These differences among the lamps may be caused by:

1. perturbations affecting the voltage reference inside the driver ICs at different levels,
2. various *CMRR* among the driver ICs,
3. various series resistance of the DB or a series resistor placed at the input,
4. various dimensioning of the circuit elements (inductor, smoothing capacitor) relative to the LED load.

The next chapter tests these hypotheses using a model.

Lastly, the m-$P_{\mathrm{st}}^{\mathrm{LM}}$ responses of the individual lamps were measured. It was experimentally verified that the $P_{\mathrm{st}}^{\mathrm{LM}}$ caused by an arbitrary DC modulation may be estimated from the $P_{\mathrm{st}}^{\mathrm{LM}}$ caused by SM if the m-$P_{\mathrm{st}}^{\mathrm{LM}}$ response is linear. These findings were published in [LK9].

7 Simulations

This chapter contains a detailed description of the performed simulations. Some of the simulations will demonstrate specific phenomena, others are intended to explain the specific behaviour of LED drivers.

Simulation 1 Section 7.2 is dedicated to simple simulations of a loaded diode rectifier. This section is intended to demonstrate the intermodulation effect in the AC supply, which does not occur in DC grids.

Simulation 2 The following section (Sec. 7.4) is dedicated to simulations which are intended to explain the significance of diode bridge in a DC supplied LED driver. Section 6.4 presents measurement results from experiments where lamp flicker immunity was compared with and without the diode bridge. The results show that for some lamps the diode bridge has a positive impact on the flicker immunity and for some lamps the impact is negative. The purpose of the simulations described in this section is to try to model these results, explain the difference and thus to provide some particular conclusions and instructions for driver manufacturers.

Simulation 3 Section 7.5 compares several regulation approaches in terms of flux fluctuations caused by the driver itself. Then their ability to suppress supply voltage perturbation is compared. The purpose of this simulation is to compare the hysteretic regulation against other possibilities.

7.1 Simulation Techniques Involved

7.1.1 Generalized Lamp Model

In purely electric simulations, LEDs can be modelled as regular diodes. In simulations involving LED light output, the link to the produced light is required. A CFL lamp model linking consumed power and produced luminous flux was published in [96]. This model can be used for LEDs with some customizations.

The model origins from an incandescent lamp model used in the IEC FM (see Appendices A and B). It allows to model the flicker sensitivity and the frequency response of a phosphor layer used in the modelled LED.

In the electric circuit, at given operating point, the LED is replaced by an equivalent resistor R_{eq}. Instantaneous power consumed by the resistor can be obtained:

$$p(t) = \frac{v^2(t)}{R_{\mathrm{eq}}} \,. \tag{7.1}$$

The instantaneous consumed power is filtered with a transfer function simulating the time response of the lamp:

$$F_{\mathrm{L}}(s) = \frac{1}{\frac{\tau_{\mathrm{L}}}{2000} s^2 + \tau_{\mathrm{L}} s + 1} \,. \tag{7.2}$$

The time constant τ_{L} models the phosphor properties either in CFL or in LED. Finally, a mapping between the power and luminous flux is applied:

$$\Phi(t) = L_{\mathrm{L}}\, p^{K_{\mathrm{L}}}(t) \,. \tag{7.3}$$

The parameter K_{L} represents the lamp sensitivity and L_{L} is a conversion efficiency constant (gain). When analysing flicker, we are only interested in relative flux changes and, thus, L_{L} can be constantly set to $1\,\mathrm{lm\,W^{-1}}$. The lamp sensitivity K_{L} affects the resulting flicker in such a way as if it were scaled by a constant. Thus, higher K_{L} will result in higher flicker uniformly at all frequencies, while lower K_{L} will result in lower flicker response.

7.1.2 LED Model

When a more detailed model of LEDs is necessary, the equivalent resistor cannot be used. A model of a diode is used instead for the electrical circuit. The diode model can be

- ideal,
- piecewise linear,
- a Shockley model, or
- a modified Shockley model.

The ideal model substitutes the V-I characteristic of a diode by two idealised regions. In reverse bias, it would be ideally isolating, while in forward bias, it would be ideally conducting. The piecewise linear model differs in the forward voltage region. When the voltage is forward biased, the diode is modelled as a resistor. The Shockley model is a relationship between the voltage and current following Shockley's Equation (Eq. (4.1)). A modification is possible by adding a series resistance, which is important especially at higher currents.

The reverse Shockley's Equation can be written as

$$V_{\mathrm{d}} = n V_{\mathrm{T}} \ln\left(\frac{I_{\mathrm{d}}}{I_0} + 1\right) \,. \tag{7.4}$$

As the ratio $\frac{I_\mathrm{d}}{I_0}$ will be usually very high, the $+1$ in the logarithm may be neglected, which allows us to arrive to

$$V_\mathrm{d} = nV_\mathrm{T} \left(\ln I_\mathrm{d} - \ln I_0\right) \,. \tag{7.5}$$

For an LED chain of three LEDs in series, a model from [108] was adjusted and used. The original model was a relationship between the voltage and current of five LEDs connected in series. The model comprised an exponential term, a constant term and a linear term describing the series resistance:

$$V_\mathrm{d} = V_\mathrm{const} + k_1 \ln(I_\mathrm{d} + k_2) + R_\mathrm{s} I_\mathrm{d} \,, \tag{7.6}$$

which is in fact rearranged (7.5) with an additional series resistance.

For the purpose of this thesis, a model of three series connected LEDs was required. Assuming the diodes are identical, the voltage drop will be distributed evenly among the five LEDs and, thus, the behaviour of three LEDs can be obtained by scaling the voltage down by a factor of $\frac{3}{5}$. This way, the following model parameters were obtained:

$$\begin{aligned} V_\mathrm{const} &= 8.051\,\mathrm{V} \,, \\ k_1 &= 0.120\,734\,\mathrm{V} \,, \\ k_2 &= 10.95 \cdot 10^{-30}\,\mathrm{A} \,, \\ R_\mathrm{s} &= 0.414\,33\,\Omega \,. \end{aligned}$$

The constant k_2 emerged from the regression process. It ensures a smooth model calculation when $I_\mathrm{d} \to 0\,\mathrm{A}$; its impact is negligible in other situations (in fact when $I_\mathrm{d} = 1\,\mathrm{A}$, k_2 is neglected automatically as it is many orders of magnitude smaller than the machine ε, which is $\varepsilon \doteq 2 \cdot 10^{-16}$ on the computer where the simulations are run). Because $k_1 = nV_\mathrm{T}$, we can identify the ideality factor as approx. $n = 4.67$. The final LED model as implemented in MATLAB Simulink is shown in Fig. 7.1. The model allows one to add a parallel capacitance if desired. During the simulations described in this thesis, the capacitance was set to $C_\mathrm{led} = 0\,\mathrm{F}$.

For the successful modelling of the LEDs, it is necessary to estimate the diode light output from the electrical quantities. The lamp model used in the IEC FM is specific for an incandescent lamp. According to the physical nature of the incandescent lamp operating principle, the current (or voltage) is used to calculate the normalised instantaneous power over an equivalent resistor, and then a second order filter is applied to approximate the thermal inertia of the lamp filament. This approach might not be suitable for LEDs.

For the purpose of this thesis (estimating the flux fluctuation in a close proximity to a given operating point), the LED's luminous flux can be modelled using Eq. (4.10). Assuming isothermal conditions and neglecting current dependencies of *EQE*, λ and κ (these are weak relative to the thermal dependencies) the equation will become

$$\Phi = \alpha I_\mathrm{d} \,, \tag{7.7}$$

where $\alpha = \kappa V_\mathrm{g} \mathit{EQE}$ is a linear coefficient.

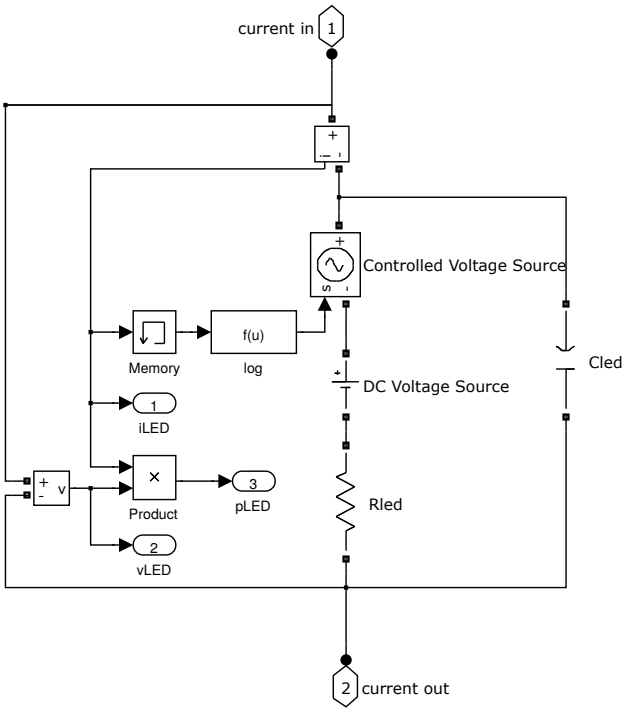

Figure 7.1: LED lamp model—LED head, 3 LEDs in series

Further, looking at definitions of the flicker quantities (3.42), (3.43), (4.12), or App. B, it is clear that only relative changes of flux are relevant for flicker. Thus, for example, *FP* will be calculated using (7.7):

$$\frac{FP}{100\,\%} = \frac{\max\Phi - \min\Phi}{\max\Phi + \min\Phi} = \frac{\max\alpha I_\mathrm{d} - \min\alpha I_\mathrm{d}}{\max\alpha I_\mathrm{d} + \min\alpha I_\mathrm{d}} = \frac{\max I_\mathrm{d} - \min I_\mathrm{d}}{\max I_\mathrm{d} + \min I_\mathrm{d}}\,. \tag{7.8}$$

This way, the coefficient α becomes irrelevant for flicker and the flicker quantities may be estimated directly from the diode current.

7.1.3 Averaged Switch Modelling

DC-DC converters can be modelled via a classical approach used for instance in SPICE programs. In this approach, nodal analysis is used to construct differential circuit equations and the resulting equation system is solved. However, with transistors switched at high frequency (usually tens or hundreds of kHz), this approach is extremely computationally demanding.

Averaged switch modelling (ASM) [109] is an approach used to model low frequency converter circuit properties without the need to simulate transistor high frequency switching. Over the hypothetical switching period, an average value of all variables is solved instead. This greatly reduces the computational complexity. Low frequency phenomena (lower than the switching frequency) can only be modelled, however.

The key principle is in representing the switched transistor and diode by a controlled voltage source and a controlled current source, respectively. Such a model

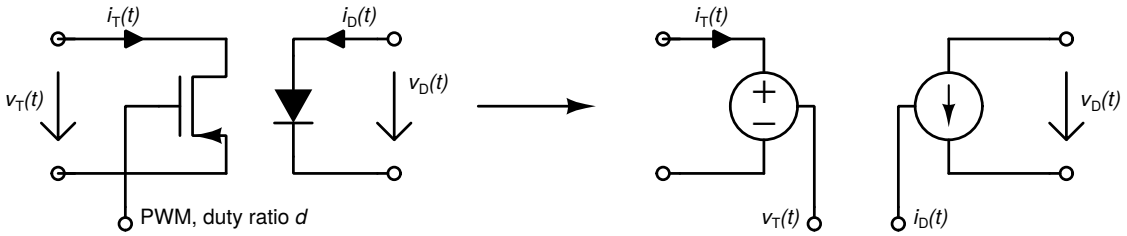

Figure 7.2: Averaged switch modelling approach; the switching transistor and diode are replaced by a controlled voltage source and controlled current source, respectively.

is capable of modelling a converter both in CCM and DCM mode. The input variable of an averaged switch model is the duty ratio of the hypothetical PWM control signal. Output variables are the values of the controlled voltage and current source. First, an equivalent duty ratio $\widetilde{D}$ is calculated:

$$\widetilde{D} = \max\left(D\,,\ \frac{D^2}{D^2 + 2L_\mathrm{b} f_\mathrm{sw} \frac{i_\mathrm{T}(t)}{v_\mathrm{D}(t)}}\right)\,, \tag{7.9}$$

where f_sw is the switching (PWM) frequency, L_b is the inductor size, d is the input duty ratio and $i_\mathrm{T}(t)$ and $v_\mathrm{D}(t)$ is the (known) transistor current and diode voltage, respectively. The choice of the first or latter option in Eq. (7.9) relates to CCM or DCM operation, respectively. Afterwards, the resulting transistor voltage and diode current are determined:

$$v_\mathrm{T}(t) = \frac{1-\widetilde{D}}{\widetilde{D}}\, v_\mathrm{D}(t)\,, \tag{7.10}$$

$$i_\mathrm{D}(t) = \frac{1-\widetilde{D}}{\widetilde{D}}\, i_\mathrm{T}(t)\,. \tag{7.11}$$

This way any switched converter topology can be simulated as long as the simulated phenomena are slower than the hypothetical switching frequency.

7.2 Diode Bridge—AC Supply and DC Supply Intermodulation

This simple simulation demonstrates how interharmonic distortion translates to subharmonic oscillations with the AC supply. Firstly, a simple SPICE model is created (see Fig. 7.3) containing an AC voltage source (230 V, 50 Hz) with an interharmonic component (5 %, 140 Hz). A diode rectifier is included along with a smoothing capacitor and a load resistor. The capacitor and resistor values are taken from [LK7]. The SPICE source code used for the simulation is part of App. C.

Without the capacitor, the rectified voltage would be equal to the absolute value of the sine voltage (half-cycle pulses). The capacitor is necessary for smoothing and

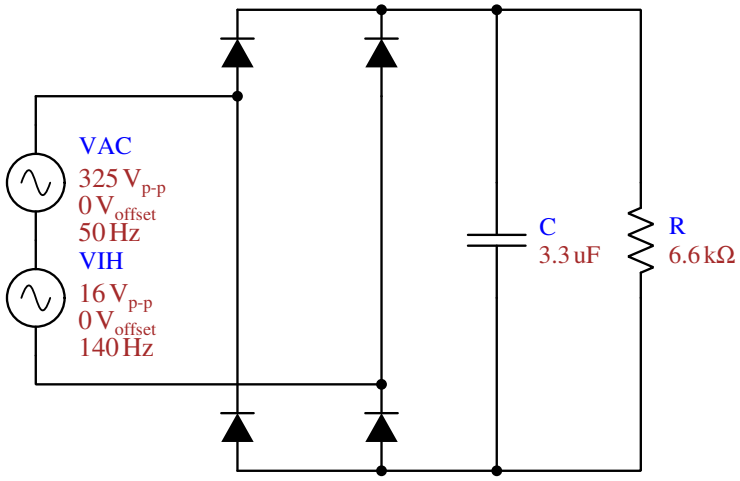

Figure 7.3: A simple SPICE model used for demonstrating intermodulation and the DB effect

maintaining a DC offset of the voltage. The size of the capacitor plays a significant role in this. The larger the capacitor, the larger DC offset of the rectified voltage (peak value will always be equal to the supply voltage peak value. In this case, the ratio of the capacitor value and the load power consumption C/P_{LED} ($\mathrm{F\,W^{-1}}$) plays a role. From the frequency point of view, the time constant $\tau_C = R_{\mathrm{eq}}C$ (s) is important [96]. These two parameters are linked, because $P_{\mathrm{LED}} = V_{\mathrm{DC}}^2/R_{\mathrm{eq}}$ and, thus, $C/P_{\mathrm{LED}} = CR_{\mathrm{eq}}/V_{\mathrm{DC}}^2 = \tau_C/V_{\mathrm{DC}}^2$.

The (normalised) AC supply voltage can be written as

$$v(t) = \sin(2\pi 50t) + 0.05\sin(2\pi 140t)\,. \tag{7.12}$$

The harmonic order closest to $f_{\mathrm{ih}} = 140\,\mathrm{Hz}$ is $j = 3$ ($jf_1 = 150\,\mathrm{Hz}$). Thus, $\Delta f = jf_1 - f_{\mathrm{ih}} = 10\,\mathrm{Hz}$. The voltage waveform can be rewritten according to (3.46) to obtain:

$$\begin{aligned} v(t) = {} & [\sin(2\pi 50t) + 0.05\cos(2\pi 10t)]\sin(2\pi 150t) + \\ & + 0.05\sin(2\pi 10t)\cos(2\pi 150t)\,. \end{aligned} \tag{7.13}$$

So far, the 10 Hz frequency component is only virtual (although clearly visible on the upper Subfigure of 7.4), as the spectrum still contains only two components (see the upper Subfigure of 7.5). When the voltage is rectified, the low frequency intermodulation results (not only the original 10 Hz component, but also higher multiples of this frequency) become real (compare with the lower Subfigures of 7.4 and 7.5.) This mechanism is responsible for transferring high frequency interharmonics to the visible-flicker range.

The simulation was repeated for several capacitor values. The overview of the capacitor values is shown in Tab. 7.1. From Fig. 7.4, it is clear that small capacitors help significantly with high order harmonics, but very large capacitor values are necessary to filter out subharmonic oscillations caused by interharmonics.

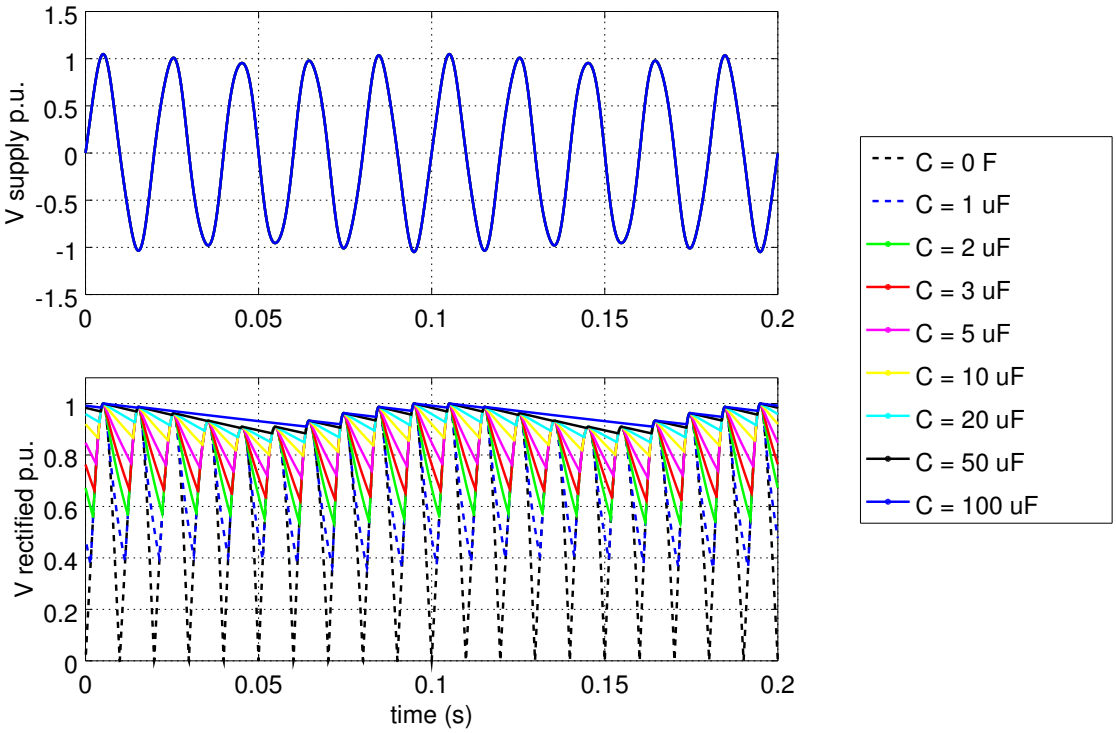

Figure 7.4: The diode bridge simulation results in a time domain—distorted AC supply voltage (50 Hz + 5 % 140 Hz component) and rectified voltage—both normalised

For comparison, the simulation was repeated with DC supply voltage contaminated with the same amount of ripple at 140 Hz. As shown in Fig. 7.6, no intermodulation occurs and no low frequency components are created.

Displaying the voltage over one of the rectifier diodes (Fig. 7.7) with the circuit under a distorted DC supply reveals that, for smaller capacitor values, the voltage does not leave the conduction region. This means that the diode does not enter the blocking mode and the load voltage copies the shape of the supply voltage waveform.

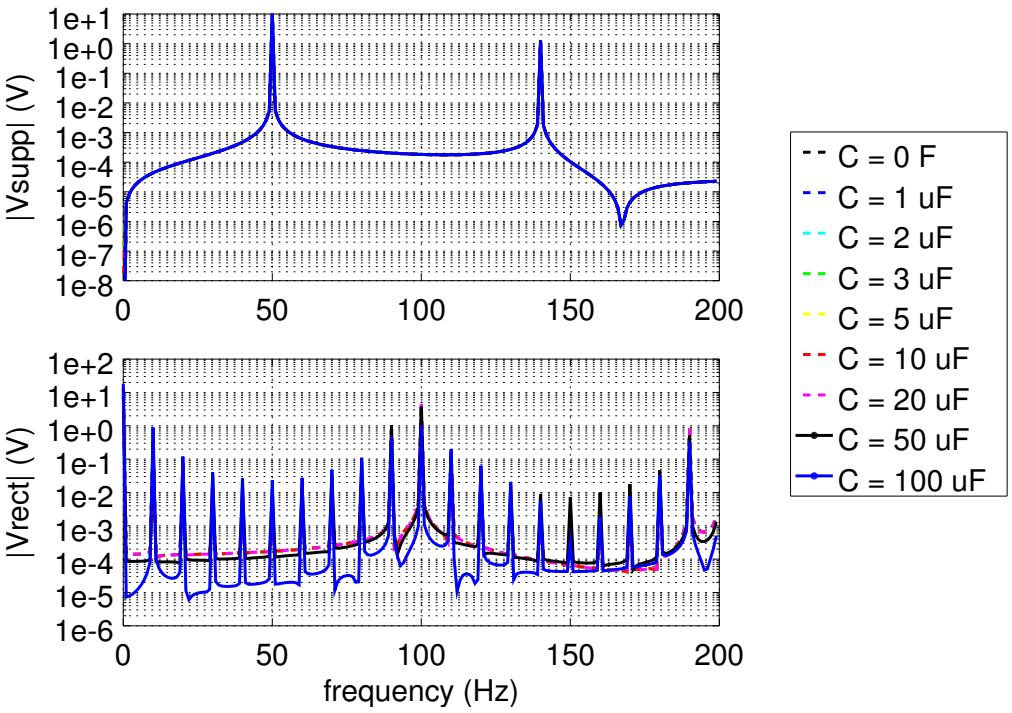

Figure 7.5: Diode bridge simulation results in the frequency domain—distorted AC supply voltage (50 Hz + 5 % 140 Hz component) and rectified voltage—both normalised

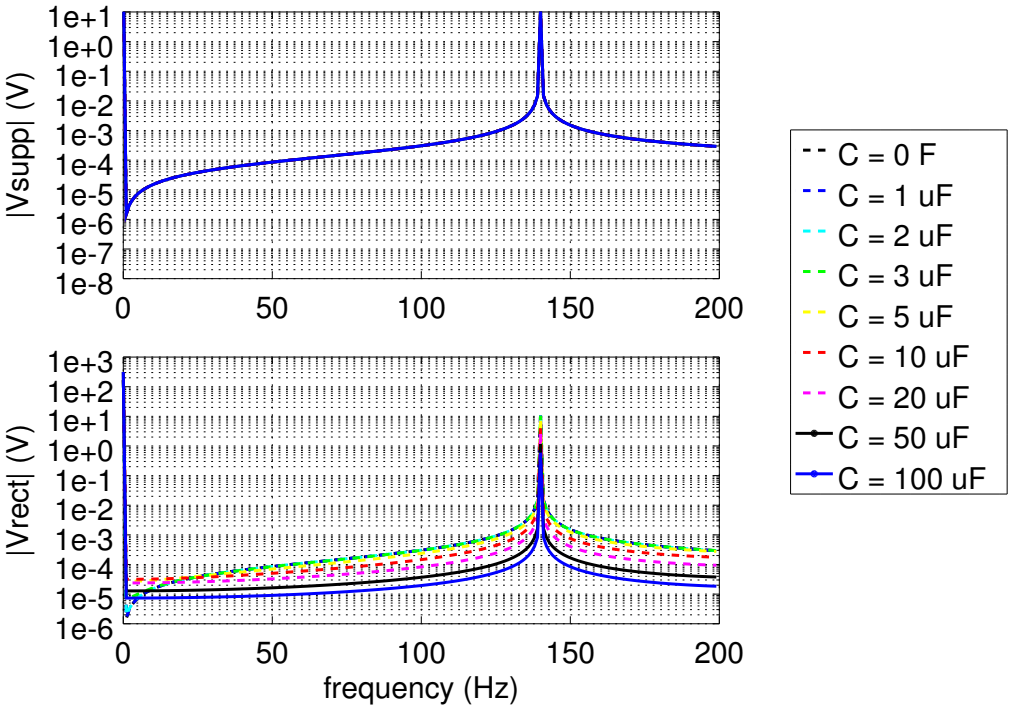

Figure 7.6: Diode bridge simulation results in the frequency domain—DC supply voltage contaminated with a 5 % 140 Hz component and voltage at the load resistor—both normalised

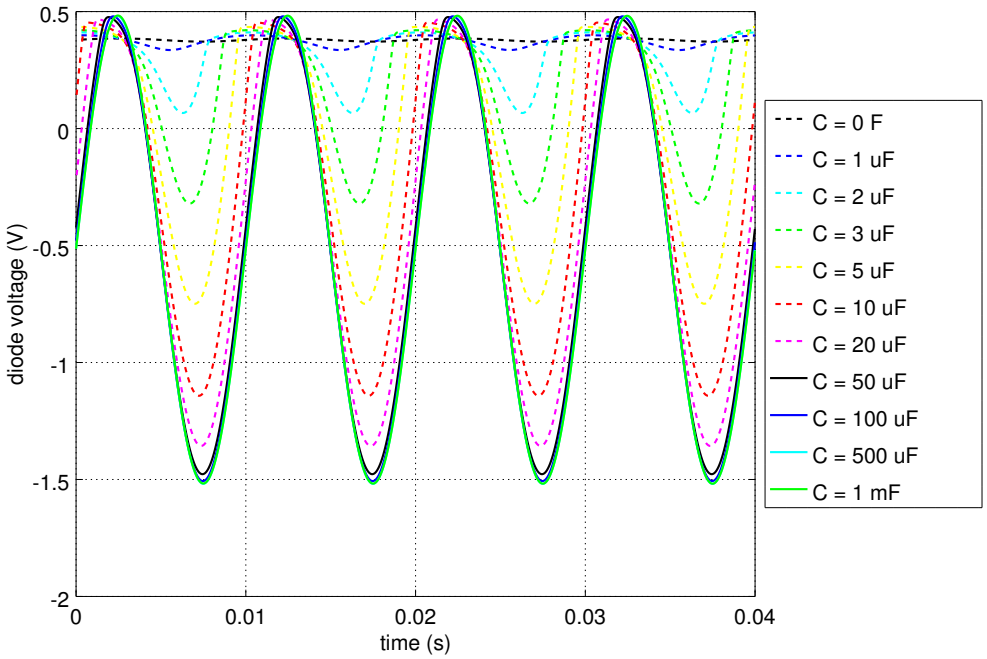

Figure 7.7: Rectifier under DC supply—diode voltage

Table 7.1: Capacitor values used in the simulation; $R_{\text{eq}} = 6\,600\,\Omega$

cap. value (µF)	time const. τ_C (ms)	C/P_{LED} (µF W^{-1})
0	0	0
1	6.6	0.13
2	13.2	0.25
3	19.8	0.38
5	33	0.61
10	66	1.2
20	132	2.3
50	330	5.6
100	660	11
500	3 300	56
1 000	6 600	110

7.3 LED Driver—Switch Averaging Model

This set of simulations is meant to explain the results obtained experimentally in Sec. 6.4.4. The research question in this section is: is it possible, by varying the driver parameters, to affect the relative difference between $P_{\mathrm{st}}^{\mathrm{LM}}$ caused by a driver with DB and a driver without DB, given that otherwise the drivers are identical? The aim of the simulations is not to predict a particular level of flicker. Instead, the aim is to compare the lamp and driver behaviour when the DB is removed from the system in terms of the relative quantity $\Delta P_{\mathrm{st}}^{\mathrm{LM}}$.

7.3.1 Model Description

For the above stated purpose, a lamp model was created in MATLAB Simulink [110]. The driver is composed from a diode bridge, a buck converter implemented using the averaged switch approach (see Sec. 7.1.3) and a generalized lamp model (see Sec. 7.1.1). The model schematic is shown in Fig. 7.8. The buck converter model includes an output voltage feedback control, employing a simple PI controller.

Thus, this model is very general and versatile. It can be, with a slight modification, used to model $P_{\mathrm{st}}^{\mathrm{LM}}$ of any kind of DC-DC converter (buck and boost were tested by the author) in the driver, and, more generally, any kind of lamp (incandescent, CFL, LED). In this part of work, it will be tested whether this kind of model is also suitable for modelling the $\Delta P_{\mathrm{st}}^{\mathrm{LM}}$.

In order to allow to analyse frequencies with 1 Hz resolution, the analysed signal length needs to be $T_{\mathrm{sim}} = 1\,\mathrm{s}$ long. In the simulation, the signal length needs to be even longer than that because of the initial transient. The transient is caused by an imperfect setting of initial conditions (the initial capacitor voltages and inductor currents, initial controller output value). In reality, the simulation time was $T_{\mathrm{sim}} = 2\,\mathrm{s}$ with the first half of the signal discarded prior to calculating the flicker.

From the simulated flux waveform, the flicker quantities were evaluated—*FI*, *FP*, *GF*. The $P_{\mathrm{st}}^{\mathrm{LM}}$ was evaluated from 1 s long interval using a software implementation of LFM described in App. B.

Absolute and Relative Parameter Model Description

For the active driver models, the parameters were set close to values read from real lamps (where possible; see Tab. 6.7a) or from the driver IC datasheets [100, 101, 102]. The parameter values are listed in the table 7.2.

The lamp model parameters are only used for calculating the luminous flux. Except for the equivalent resistor R_{eq}, they do not affect the electric circuit in any way. Vice versa, they should not be affected by the presence of DB. Therefore, they are kept constant during the work.

From all the converter parameters, the low frequency behaviour of the driver is determined most importantly by the parameters $\{C_{\mathrm{O}}, C_{\mathrm{DC}}, L_{\mathrm{b}}, f_{\mathrm{sw}}, K, \tau_{\mathrm{PI}}, R_{\mathrm{eq}}\}$. The sensing resistor was placed in the model, but it may be also merged with R_{b}. Its value was important for determining the output current and voltage and the equivalent

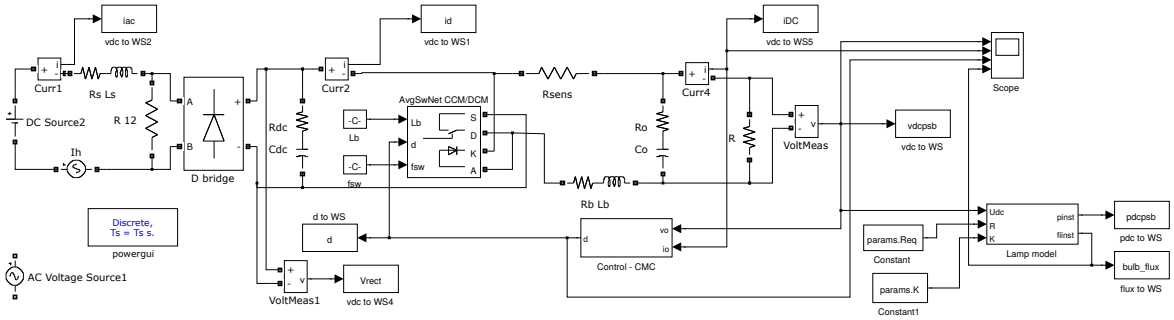

(a) Complete schematic of the model

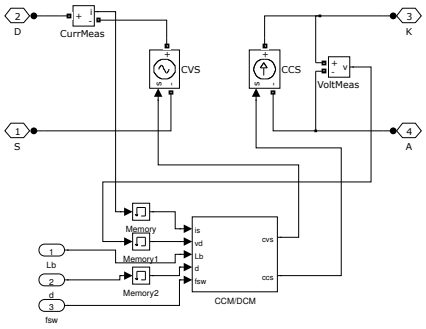

(b) The averaged switch model—the controlled voltage and current sources replace the diode and switching transistor

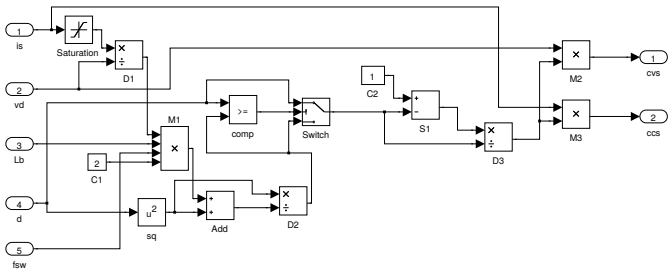

(c) The averaged switch model—calculation of the equivalent duty ratio $\widetilde{D}$ according to Eq. (7.9)

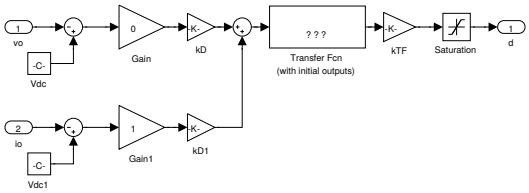

(d) The feedback controller; model allows both the CMC and VMC regulation mode; the resulting duty ratio D is subject to limits (0.1 and 0.95)

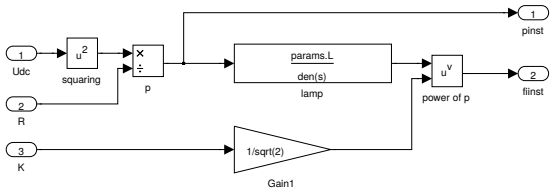

(e) Lamp model for estimating the luminous flux, see Sec. 7.1.1

Figure 7.8: The averaged switch model of a buck LED driver used for the simulations

Table 7.2: Averaged switch model of a buck driver—reference parameter values

voltage supply			
supply DC voltage	V_{supp}	12	V
supply voltage mod. magnitude	m_{DC}	2.83	%
supply voltage mod. frequency	f_{m}	1–60	Hz
DC-DC converter			
sensing resistor	R_{sens}	0.43	Ω
output voltage	V_{out}	9.675	V
buck inductor size	L_{b}	47	µH
buck inductor ESR	R_{b}	0.128	Ω
smoothing capacitor size	C_{DC}	330	µF
smoothing capacitor ESR	R_{DC}	0.1	Ω
output capacitor size	C_{O}	0	µF
output capacitor ESR	R_{O}	0	Ω
switching frequency	f_{sw}	100	kHz
PI controller gain	K	0.3	—
PI controller integral time const.	τ_{PI}	5	ms
generalized lamp model			
equivalent resistor	R_{eq}	20.8	Ω
lamp model time const.	τ_{L}	3.5	ms
lamp model gain	L_{L}	1	—
lamp model sensitivity	K_{L}	0.02	—

resistor:

$$I_{\text{out}} = \frac{0.2}{R_{\text{sens}}}\,, \tag{7.14}$$

$$R_{\text{eq}} = \frac{P}{I_{\text{out}}^2}\,, \tag{7.15}$$

$$V_{\text{out}} = R_{\text{eq}} I_{\text{out}}\,. \tag{7.16}$$

Because for the desired consumed power $P = 5\,\text{W}$ the duty ratio was very close to 0.95 and, thus, the simulation was not running correctly, the desired consumed power was decreased to $P = 4.5\,\text{W}$, which led to the voltage and resistor values shown in the table 7.2.

Using an equivalent resistor as a load for the circuit allows one to relate the above mentioned absolute parameter set to the equivalent resistor value. This way a set of relative model parameters may be created:

$$\tau_{Cdc} = R_{\text{eq}} C_{\text{DC}}\,, \tag{7.17}$$

$$\tau_{Co} = R_{\text{eq}} C_{\text{O}}\,, \tag{7.18}$$

$$\tau_{Lb} = \frac{R_{\text{eq}}}{L_{\text{b}}}\,. \tag{7.19}$$

These parameters are de facto time constants in seconds.

Further during the work, it was experimentally verified that the effect of changing the inductor size L_{b} has an identical impact on the simulation as changing the switching frequency f_{sw} and the opposite impact as changing the square of K. This implies that the behaviour of the model is dependant on the parameter

$$X_{Lb} = 2\pi f_{\text{sw}} L_{\text{b}}\,, \tag{7.20}$$

whose physical dimension is in Ohms. Replacing L_{b} by τ_{Lb} will yield

$$F_{\text{A}} = 2\pi f_{\text{sw}} \tau_{Lb} = \frac{2\pi f_{\text{sw}} L_{\text{b}}}{R_{\text{eq}}} = \frac{X_{Lb}}{R_{\text{eq}}}\,, \tag{7.21}$$

which is a dimensionless parameter. Incorporating K will result in a more general parameter:

$$F_{\text{B}} = \frac{2\pi f_{\text{sw}} \tau_{Lb}}{K^2} = \frac{2\pi f_{\text{sw}} L_{\text{b}}}{R_{\text{eq}} K^2}\,, \tag{7.22}$$

which is a dimensionless parameter too.

The output voltage setpoint may be related to the supply voltage using the duty ratio D, which is also a relative parameter. The relation between the supply voltage, output voltage setpoint, and D should be given by Eq. (2.1) or (2.4), depending on the type of converter modelled and if the converter is operated in CCM. The parameter D expresses an ideal duty ratio. The actual duty ratio will be close to this value, but not equal, due to parasitic element properties and supply voltage perturbations.

Alternatively to $\{K, \tau_{\mathrm{PI}}\}$, the PI controller can be expressed as a proportional and integral component separately (see Eq. (2.10)). In this case, the parameters will be $\{P_{\mathrm{PI}}, I_{\mathrm{PI}}\}$.

This way, the set of absolute parameters may be expressed via a set of relative parameters $\{\tau_{Co}, \tau_{Cdc}, \tau_{Lb}, F_{\mathrm{A}}, F_{\mathrm{B}}, \tau_{\mathrm{PI}}, D\}$, whose physical dimensions are either none or in seconds. A model expressed in this fashion is indifferent with respect to the absolute value of R_{eq} and, thus, may be scaled independently on the voltage level and power consumption of the modelled device.

For the purpose of running a simulation, the absolute values of circuit elements must be calculated from the relative parameter set:

Source Code 7.1: The averaged switch driver model: Element value evaluation from relative model parameters

```
Vsupp = 12;      % V
Req = 1000;      % Ohm

% relative parameters:
tauCdc = 0;      % s
tauCo = 0.02;    % s
tauLb = 1e-6;    % s
FA = 0.1257;     % -
FB = 1.3963;     % -
D = 0.4612;      % -
tauPI = 5e-3;    % s

% absolute element values
Cdc = tauCdc / Req;
Co = tauCo / Req;
Lb = tauLb * Req;
fsw = FA / 2 / pi / tauLb;
K = sqrt( 2 * pi * fsw * tauLb / FB );
Vout = D * Vsupp * sqrt(2);

% in case of PI controller expressed in
% proportional-integral component form:
Ppi = K;         % -
Ipi = K / tauPI;         % 1/s
```

It is apparent now that the simulation is not dependant on parameters τ_{Lb} and F_{A}, because any change in τ_{Lb} will be compensated for by adjusting the value of f_{sw} and, similarly, any change in F_{A} will be compensated for by adjusting the K_{reg}. Thus, the parameter set which truly matters may be reduced to $\{\tau_{Co}, \tau_{Cdc}, F_{\mathrm{B}}, \tau_{\mathrm{PI}}, D\}$, resp. $\{\tau_{Co}, \tau_{Cdc}, F_{\mathrm{B}}, I_{\mathrm{PI}}, D\}$.

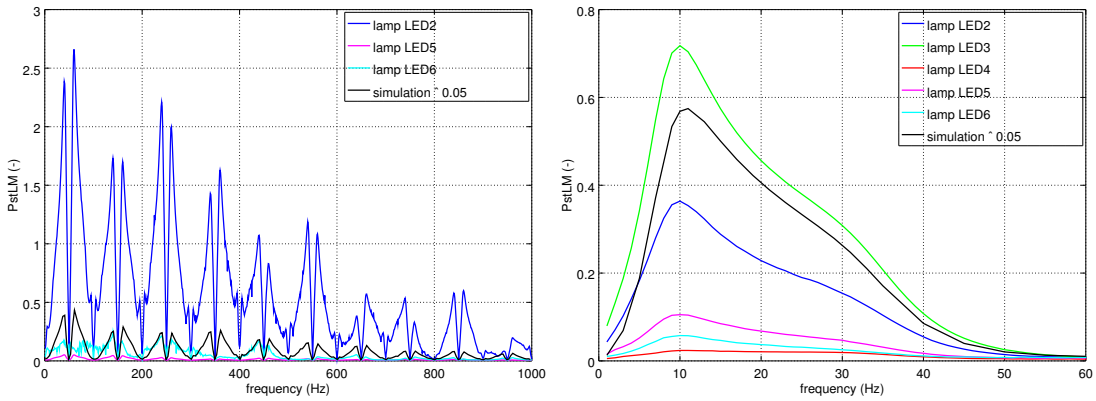

(a) AC supply—frequencies up to 1 kHz (b) DC supply—frequencies up to 60 Hz

Figure 7.9: The averaged switch driver—verification, frequency domain.

7.3.2 Model Verification

The value of the lamp sensitivity constant has a very straightforward impact on the frequency domain results of the calculated flicker. Changing the value of K_{L} is equivalent to multiplying the resulting $P_{\mathrm{st}}^{\mathrm{LM}}$ by a constant. This is also shown in [96]. The value $K_{\mathrm{L}} = 0.02$ was identified to fit roughly with the measurements (see Tab. 7.3).

However, smaller values of K_{L} tend to more expose the effect of the initial transient and, thus, cause numerical instability of the simulation. In order to mitigate this effect, the simulation time needs to be longer and the minimum step size needs to be decreased. This leads to more demanding and numerically more problematic calculations. Because of this, the value $K_{\mathrm{L}} = 0.02$ was not used. During the simulations, the K_{L} was set to 1, and, for verifying the model frequency response (see Fig. 7.9a), the results were scaled by 0.05 to fit roughly with the measurement. This approach is deemed acceptable because the value of K_{L} does not affect the resulting $\Delta P_{\mathrm{st}}^{\mathrm{LM}}$.

The simulation results with reference parameter values were verified in frequency domain against the real measurements both with AC and DC supply. The comparison is shown in Fig. 7.9. The figure shows that the model is most sensitive at $f_{\mathrm{m}} = 10\,\mathrm{Hz}$ which conforms with the measurements.

Figure. 7.9a shows that in the frequency band from 1 Hz to 50 Hz the $P_{\mathrm{st}}^{\mathrm{LM}}$ values are mirrored around the midpoint (25 Hz). This is due to the intermodulation effect

Table 7.3: $P_{\mathrm{st}}^{\mathrm{LM}}$ comparison of active driver with DB—simulation vs. measurements, SM, $f_{\mathrm{m}} = 10\,\mathrm{Hz}$, $m = 2.83\,\%$, the measured values were taken from Tab. 6.12

	simulation		LED2	LED3	LED5	LED6
	$K_{\mathrm{L}} = 0.02$	$K_{\mathrm{L}} = 1$				
$P_{\mathrm{st}}^{\mathrm{LM}}$	0.51	15.66	0.36	0.72	0.11	0.06

described in previous section (Sec. 7.2). For higher frequencies, the intermodulation phenomenon results in repeating the pattern, alternating between mirrored and straight mapping.

During the verification, it was concluded that the model is capable of modelling the $P_{\mathrm{st}}^{\mathrm{LM}}$ of the analysed lamps.

7.3.3 Time Domain Analysis

Figure 7.10 shows some key quantities during the simulation in the time domain ($f_{\mathrm{m}} = 10\,\mathrm{Hz}$, $m = 2.83\,\%$). The diode current is the current flowing through the DB in the first case; in the latter case, it is the current drawn from the grid into the circuit. The current never reaches zero; this means that when the DB is present, the diodes are in the conducting mode at all times, and the rectified voltage is identical to the supply voltage. The difference between the model with and without the DB can be clearly seen in the current flow, in the duty ratio, instantaneous power dissipated by the equivalent resistor R_{eq} and in the luminous flux produced by the lamp also. Most importantly, the diode bridge significantly decreases the duty ratio oscillations.

7.3.4 Simulations of $P_{\mathrm{st}}^{\mathrm{LM}}$ and $\Delta P_{\mathrm{st}}^{\mathrm{LM}}$

In order to be close to real experiments, the power supply was 12 V DC with a sinusoidal modulation. For frequency-dependant simulations the frequency was between 1 and 60 Hz, the modulation magnitude was kept constant at $m_{\mathrm{DC}} = 2.83\,\%$. The simulation step size was set to $T_{\mathrm{s}} = 0.5\,\mu\mathrm{s}$.

The simulating procedure was as follows: firstly, the simulation was run with the reference values shown in Tab. 7.2. Then, each parameter was separately varied around its original value and the impact on the simulation results was observed.

Only some model parameters were chosen for varying during the simulations. For majority of parameters, the variation was achieved by multiplying its value by a multiplier $b \in \{0.1,\ 0.2,\ 0.5,\ 1.5,\ 2,\ 5,\ 10\}$. For the feedback regulator, parameters the range of meaningful values was different.

The results of this set of simulations are relative changes of $P_{\mathrm{st}}^{\mathrm{LM}}$ when the DB is removed, and effect of driver parameters upon these changes. The relative change $\Delta P_{\mathrm{st}}^{\mathrm{LM}}$ was evaluated according to Eq. (6.11). The results are summarised in Tab. 7.4. With the reference parameter values, the $\Delta P_{\mathrm{st}}^{\mathrm{LM}}$ was equal to $\Delta P_{\mathrm{st}}^{\mathrm{LM}} = -37.6\,\%$.

With some parameter values, the simulation result differed from measurements in such a way that the peak was shifted towards frequencies higher than 10 Hz. These simulations were discarded as they fail to approximate the behaviour of the real lamp properly. In Tab. 7.4 these results are not shown. Sometimes, the parameter variation causes the duty ratio D to saturate at $D = 95\,\%$, in which case the simulation is invalid also.

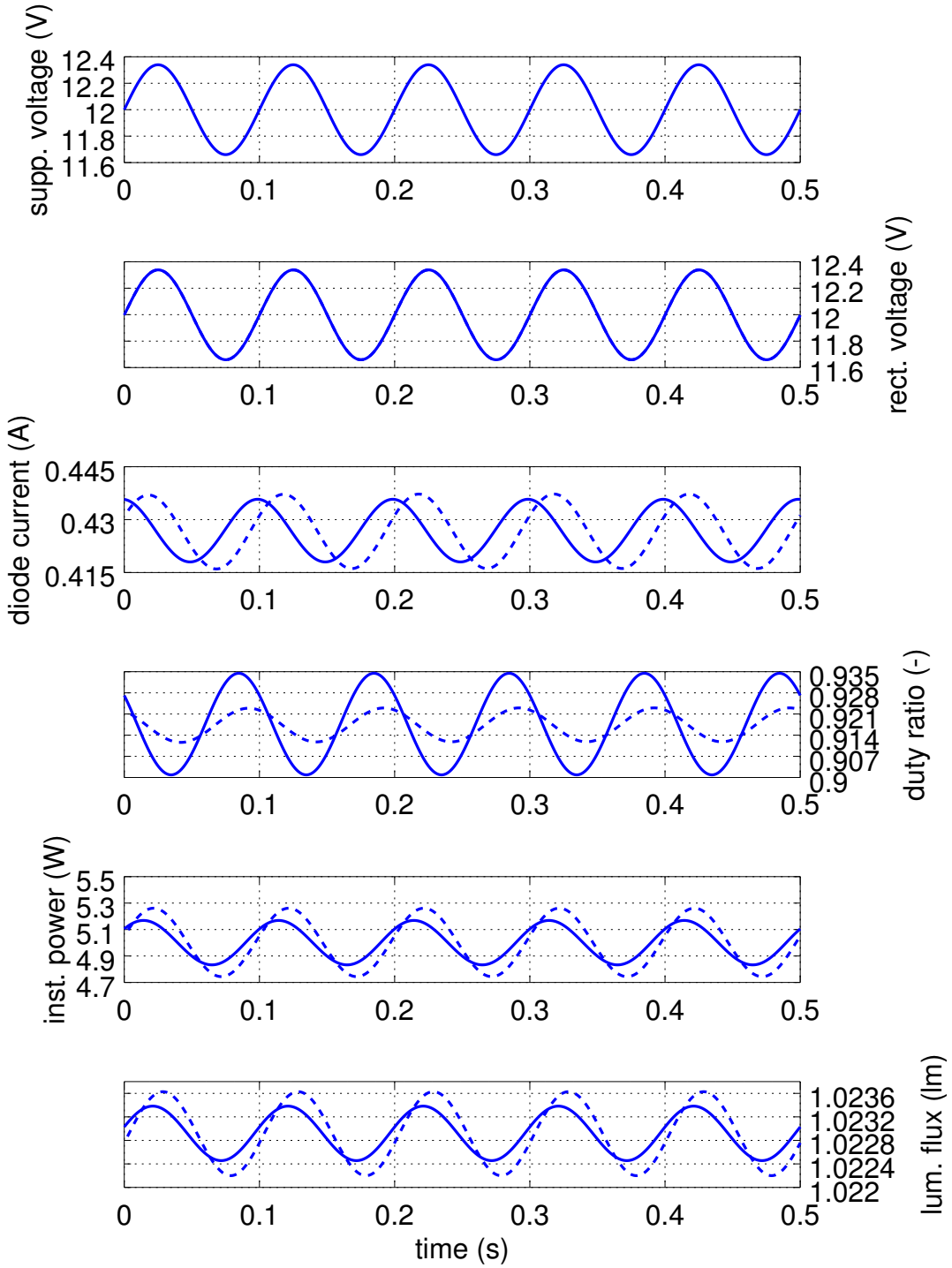

Figure 7.10: The active driver model under DC supply—key quantities; simulation without the DB (the solid line) and with the DB (the dashed line), modulation frequency $f_{\mathrm{m}} = 10\,\mathrm{Hz}$, $m = 2.83\,\%$. Because the lamp gain is set to $L = 1$, the luminous flux might not be up to scale corresponding to a real lamp; this is not an issue when flicker is analysed. Only $0.5\,\mathrm{s}$ of the signals is shown.

Table 7.4: The ΔP_{st}^{LM} (in %) for the averaged switch driver model, model parameter variations

parameter	parameter multiplier b							
	0.1	0.2	0.5	1	1.5	2	5	10
f_{sw}	−12.8	−8.5	−37.4	−37.6	−37.6	−37.6	−37.6	−37.6
L_b	−12.8	−8.5	−37.4	−37.6	−37.6	−37.6	−37.6	−37.6
R_b	−37.8	−37.8	−37.7	−37.6	−37.6	−37.5	−29.3	—
R_{sens}	−38.1	−38.1	−37.9	−37.6	−37.4	−35.3	—	—
C_{dc}	−37.6	−37.6	−37.6	−37.6	−37.6	−37.6	−37.6	−37.6

parameter	parameter multiplier b							
	0.005	0.01	0.02	0.05	0.1	0.2	0.5	1
K	−0.3	−0.4	−0.6	−1.1	−2.8	−6.8	−19.8	−37.6

parameter	parameter multiplier b							
	1	1.5	2	5	10	20	50	100
τ_{PI}	−37.6	−29.5	−25.6	−20.3	−19.3	−19.2	−19.3	−19.4

7.3.5 Simulation Results Summary

The results in Tab. 7.4 show that changing the parameters C_{dc} has no impact on the ΔP_{st}^{LM}. The effect of varying f_{sw} and L_b is identical.

As seen from the Tab. 7.4, the ΔP_{st}^{LM} is always non-positive. The used model allows one to manipulate the ΔP_{st}^{LM} by varying the properties of the feedback regulator, but the result never exceeds zero. The inability of the model to achieve positive ΔP_{st}^{LM} suggests that the model is unsuitable for the intended purpose.

Another argument against usage of this model is that while with the AC supply the absolute level of flicker may be controlled with both K_L and C_{DC}, with the DC supply it can only be controlled with K_L. This leads to unusually low value of $K_L = 0.02$. For these reasons, it was concluded that a more detailed model is necessary.

7.4 LED Driver Model—Hysteretic Regulation

For this section, a more detailed model of the LED drivers described in Sec. 6.4.1 was created in MATLAB Simulink [110]. The drivers all follow a very similar design, differing only in the smoothing capacitor sizes and the number of employed LEDs. The drivers may also differ in inductor and sensing resistor sizes that could not have been read from the disassembled circuits, but are prescribed in the datasheets.

Compared to the switch averaged model described in the previous section, this model fully implements the switching mechanism of the hysteretic control. A more detailed electrical model of the LED head was used (Sec. 7.1.2) instead of the generalised lamp model. The model schematic is shown in Fig. 7.11. The model parameters are listed in Tab. 7.5. As has already been mentioned in Sec. 6.4.1, placing the sensing resistor on a high side of the LED branch requires using a differential

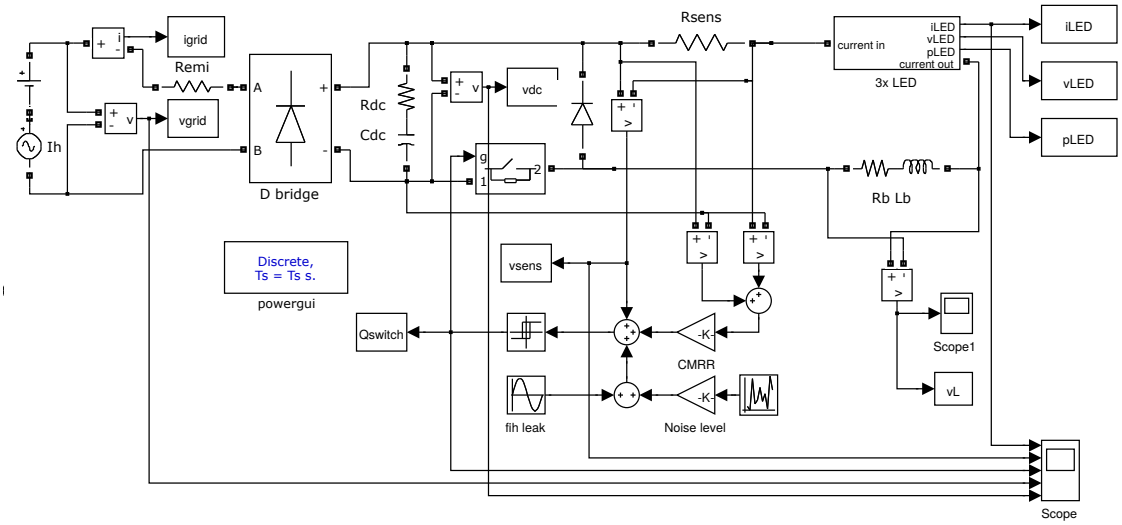

Figure 7.11: LED lamp model—driver, hysteretic control

Table 7.5: LED lamp model—parameter values

parameter name	symbol	value	unit
supply DC voltage	V_{supp}	12	V
sensing resistor	R_{sens}	0.43	Ω
buck inductor size	L_{b}	47	µH
buck inductor ESR	R_{b}	0.128	Ω
smoothing capacitor size	C_{DC}	330	µF
smoothing capacitor ESR	R_{DC}	0.1	Ω
DB forward voltage	V_{DBfw}	0.5	V
DB on resistance	R_{DBon}	40	mΩ
DB snubber resistance	R_{DBoff}	100	kΩ
Schottky diode forward voltage	V_{Sfw}	0.2	V
switch transistor on resistance	R_{trans}	560	µΩ

amplifier. A common undesired property of differential amplifiers is the common mode voltage leakage. This property has been included in the model.

Following the approach shown in Sec. 7.1.2, $P_{\text{st}}^{\text{LM}}$ was evaluated from the LED current. For this purpose, the LFM implementation described in App. B was used. The simulation was run with the simulation step size of $T_{\text{s}} = 0.1\,\mu\text{s}$.

7.4.1 Model Verification

The model was verified comparing $P_{\text{st}}^{\text{LM}}$ from the simulation and measurements of lamps LED2–6 in the frequency domain. The comparison is shown in Fig. 7.12. The simulated $P_{\text{st}}^{\text{LM}}$ corresponds with the measured values. Importantly, the curve shape in 7.12a is identical with the measurements. The largest notable difference is at the modulation frequency $f_{\text{m}} = 1\,\text{Hz}$, where the simulated $P_{\text{st}}^{\text{LM}}$ unexpectedly rises.

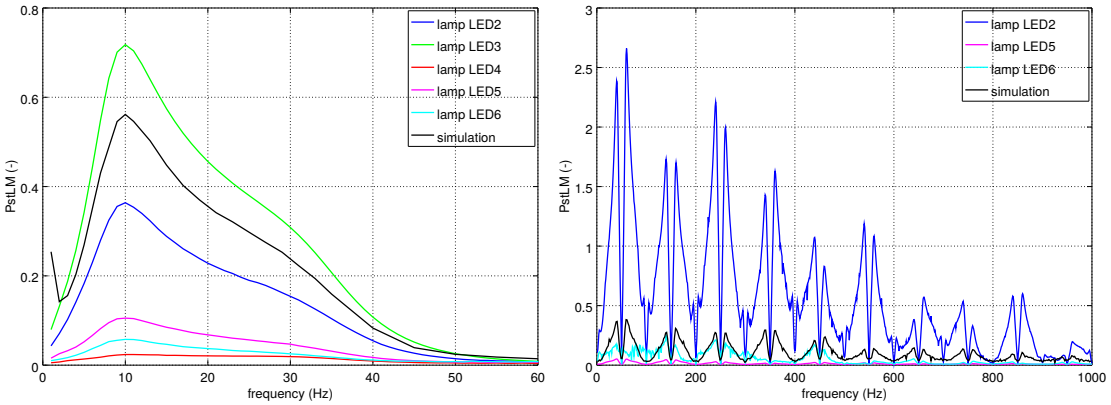

(a) DC supply—frequencies up to 60 Hz (b) AC supply—frequencies up to 1 kHz

Figure 7.12: Active driver—model verification, frequency domain

With the AC supply, the simulation results correspond roughly to the real behaviour. It is concluded that the model is suitable for simulating the $P_{\mathrm{st}}^{\mathrm{LM}}$ response of lamps LED2–6.

7.4.2 Time Domain Analysis, Power Losses

According to [111], up to 63 % of converter losses are caused by the freewheeling diode. This is why, for the freewheeling diode, a Schottky diode with low forward voltage is usually recommended in order to minimise losses. However, for the DB, regular diodes with forward voltage ranging from 0.5 V to 0.7 V are usually used. For the switching transistor, usually, a low gate charge and low on resistance are required to minimise the conducting and switching losses [112].

Figure 7.13 shows some key quantities of the hysteresis model in microsecond temporal zoom. The figure shows how a hysteretic control works: when the sensed voltage reaches the lower boundary (170 mV) the switch turns on, the inductor is charging and the voltage (proportional to the inductor current and LED current) rises. When the sensed voltage reaches the upper boundary (230 mV) the switch turns off and the inductor discharges into the LED. The switching frequency is given by the inductor size and the LED load which both affect the on-slope and the off-slope of the v_{sens} voltage. In this case, the switching frequency is approx. $f_{\mathrm{sw}} = 263\,\mathrm{kHz}$. The *FP* caused by the LED current ripple is $FP = 17.4\,\%$.

The simulation allows one to calculate the DB losses. The losses were calculated from one switching period. The total active power consumption of the lamp was $P_{\mathrm{total}} = 4.26\,\mathrm{W}$, which is comparable to the nominal power consumption of the real tested LED lamps (5 W for LED2, LED3 and LED4). The LED head active power consumption was $P_{\mathrm{LED}} = 3.72\,\mathrm{W}$. This makes up the total driver efficiency $\eta = 87\,\%$.

The DB losses can be calculated as follows: in DC operation, the DB is represented by two diodes in series with the rest of the circuit. Thus, the grid voltage can be expressed as:

$$v_{\mathrm{grid}} = v_{\mathrm{d1}} + v_{\mathrm{d2}} + v_{\mathrm{DC}}\,, \tag{7.23}$$

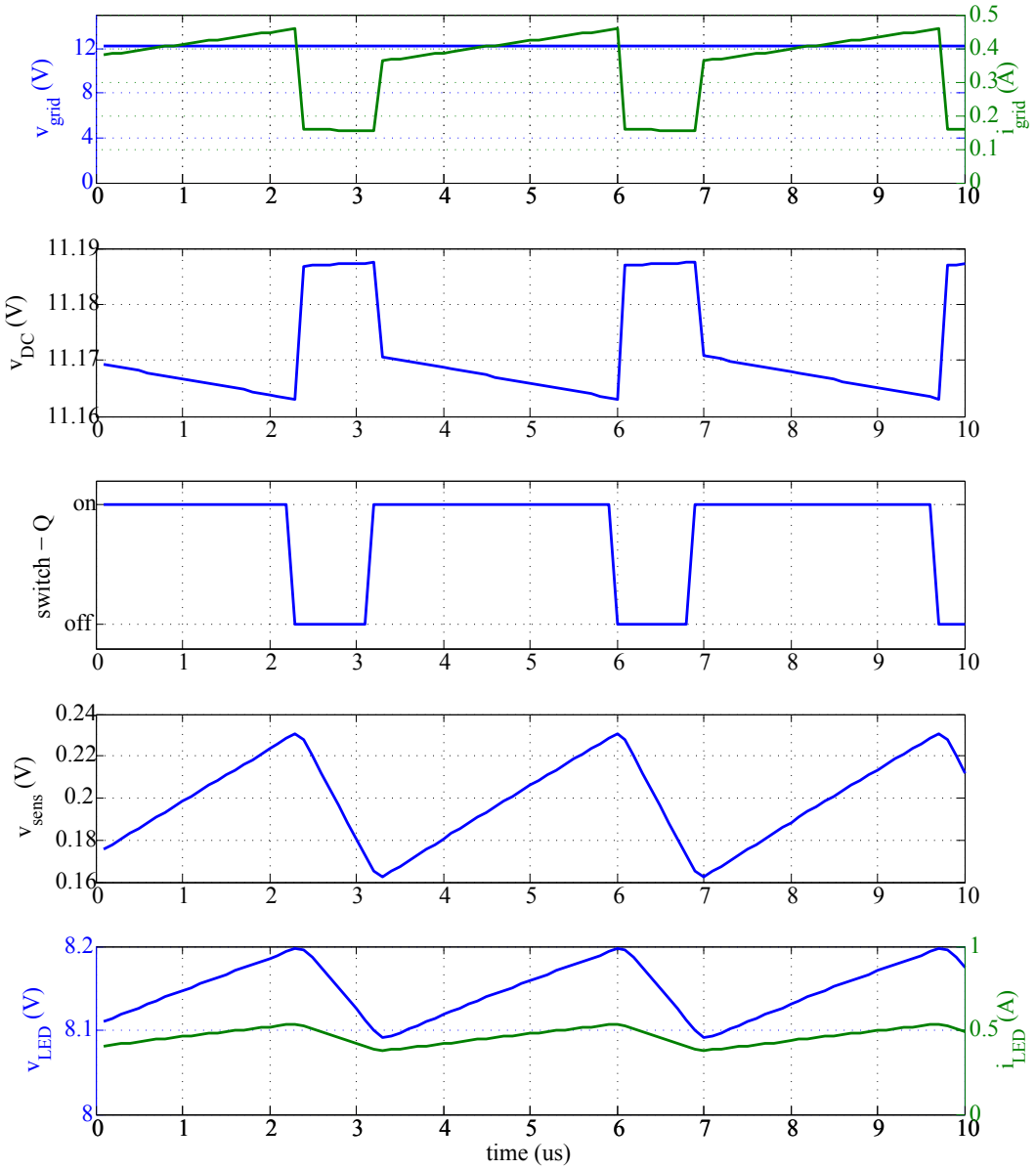

Figure 7.13: Temporal domain view of the key quantities in the hysteretic model; from top to bottom: grid voltage and current; voltage at the DB output; switch signal; sense resistor voltage; LED voltage and current.

where v_{grid} is the grid voltage, v_{d} is the diode voltage (for diodes 1 and 2) and v_{DC} is the voltage at the output of the DB. Then the DB voltage is equal to $v_{\text{grid}} - v_{\text{DC}}$ and, assuming constant switching frequency, the DB losses are expressed as

$$P_{\text{DB}} = \frac{1}{T_{\text{sw}}} \int_0^{T_{\text{sw}}} i_{\text{grid}}(v_{\text{grid}} - v_{\text{DC}})\,\mathrm{d}t\,, \tag{7.24}$$

with T_{sw} being the switch period. The simulation revealed the DB losses are $P_{\text{DB}} = 0.36\,\text{W}$, which is $8.5\,\%$ of the total active power consumption of the lamp. The DB losses can be expected to be smaller for higher supply voltage levels; the average grid current will then be smaller and, thus, the DB losses will be smaller and possibly negligible for $230\,\text{V}$ lamps. However, the power loss in ELV lamps is not negligible and *the urge to remove the DB in ELV DC lamps design may be justified.*

The power balance after removing the DB will be as follows:

$$\begin{aligned} P_{\text{total}} &= 3.92\,\text{W}\,, \\ P_{\text{LED}} &= 3.77\,\text{W}\,, \\ P_{\text{DB}} &= 0\,\text{W}\,, \\ \eta &= 96\,\%\,. \end{aligned}$$

The change in efficacy is significant. With the DB removed, the switching frequency rises to approx. $344\,\text{kHz}$. This happens because the voltage applied to the inductor during the charging phase is slightly higher and, thus, the on slope is steeper.

7.4.3 Flicker Simulations

After verifying and examining the model in a temporal and frequency domain, the simulation was run with sinusoidal modulation of the DC supply. The sinusoidal modulation simulates the ripple of the DC grid supplying the lamp. The simulation time was chosen to be one second in order to provide $1\,\text{Hz}$ resolution for the choice of modulation frequency and for the frequency domain analysis. For the frequency domain simulations, the frequencies were chosen from the range $1\,\text{Hz}$ to $60\,\text{Hz}$ and the modulation magnitude was $m_{\text{DC}} = 2.83\,\%$. Flicker quantities were evaluated from the LED current; most importantly, the $P_{\text{st}}^{\text{LM}}$, which is shown in the figures and tables of this section. A second model with identical parameters, but without the DB was used; its results were used to acquire and evaluate $\Delta P_{\text{st}}^{\text{LM}}$.

The minimum time for the $P_{\text{st}}^{\text{LM}}$ evaluation is $10\,\text{s}$ plus approx. $5\,\text{s}$ for the step response of the inner LFM filters. The simulation would be extremely demanding to generate such a long signal. Therefore the signal was downsampled to $5\,\text{kHz}$ and repeated in order to generate a $15\,\text{s}$ long signal.

Section 6.4.6 discussed several hypotheses about the cause of $\Delta P_{\text{st}}^{\text{LM}}$. Let us remind that these were:

1. perturbations affecting the voltage reference inside the driver ICs,
2. various *CMRR* among the driver ICs,

3. various series resistance of the DB or a series resistor placed at the input,
4. various dimensioning of circuit elements (inductor, smoothing capacitor) relative to the LED load.

At this point we will try to address each of these and test them by introducing a proper variation in the simulated model.

Reference voltage sensitivity In the default setup, the flicker is caused by the supply voltage ripple, which results in the DC link voltage ripple being transferred to the LED head. In an ideal case, the ripple is eliminated as the LED current is kept within the predefined boundaries. These boundaries are defined by a reference voltage within the driver IC. If the supply voltage is perturbed, it is possible that the reference voltage is also subject to certain level of perturbation. In order to simulate this leakage, a copy of the ripple signal was injected into the current sensing signal (see the model schematic in Fig. 7.11). The simulations were repeated with the perturbation leakage magnitude being 0.1 and $0.2\,\%$ of m_{DC}.

Common mode The next possible way of ripple amplification is the *CMRR* of the differential amplifier sensing the inductor current. This is why the simulations were run with a common mode signal added to the sensed voltage at several values of the *CMRR*.

Series resistance Series resistance may represent a parasitic property of the DB, or, as we can see in one of the analysed lamps (Tab. 6.7a), there may be a series resistor included in the design intended as a simple EMI filter (this is why this parameter is denoted as R_{EMI}). During the measurements, such a resistor was necessarily bypassed along with the DB and, thus, might affect the measurement results. In order to be able to differentiate the effect of series resistance from other parameters, simulations were run with several values of extra series resistance connected at the supply port.

Circuit elements variations The datasheets for driver ICs [100, 101, 102] only give us recommendations about the size of circuit elements like smoothing capacitor, inductor and its series resistance or the current sensing resistor. The particular choice depends on the designer and will probably depend on the load (the size of the LED matrix) and supply voltage level. Engineers will also look for a way to minimise the cost and volume of the driver. This is why the values of key elements affecting the driver behaviour were varied. R_{b} represents the inductor series resistance and is not an element on its own. Various inductors may have different series resistance, this is why this property was included in this analysis.

7.4.4 Results

Fig. 7.14 shows the flicker simulations of the active driver model without any variations. The same data was used for the model verification in Sec. 7.4.1. The *GF*

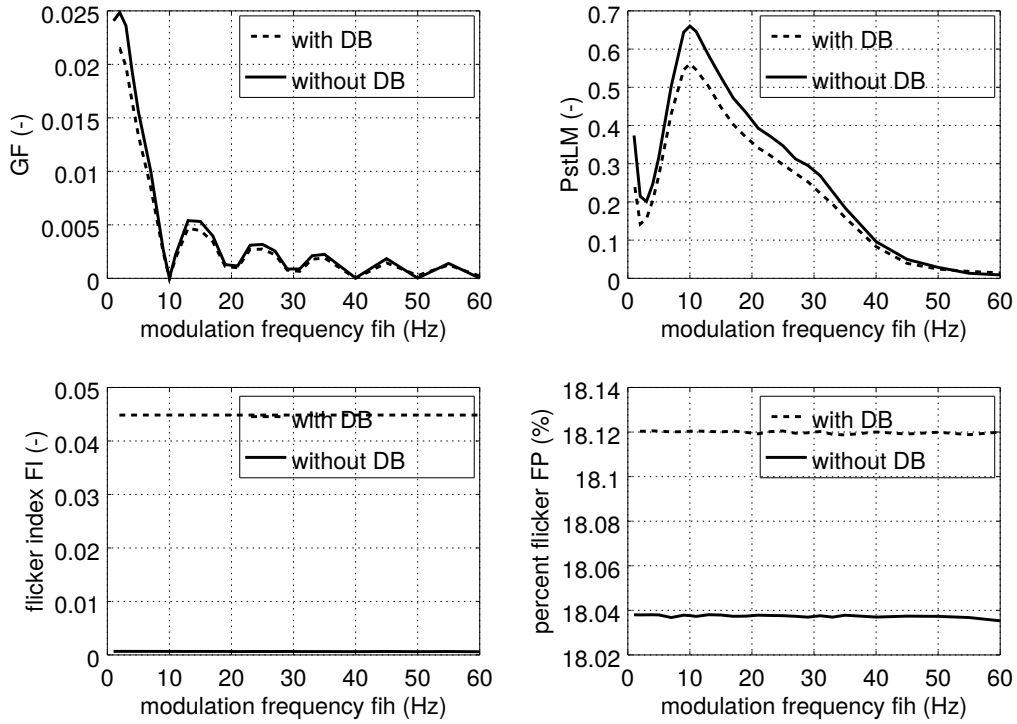

Figure 7.14: Flicker quantities with an active driver: *GF*, $P_{\mathrm{st}}^{\mathrm{LM}}$, *FI* and *FP*; comparison with and without DB

shows the frequency response of the driver at a given operating point. *FP* changes very little with the DB removal. As for the *FI*, the figure shows that it is almost 0 when the DB is removed. Here, the change is significant; this means that the shape of the luminous flux waveform changes. Both *FI* and *FP* are constant with the perturbation frequency.

Table 7.6 shows the numerical results of the simulation with varying modulation depth m_{DC}. The $\Delta P_{\mathrm{st}}^{\mathrm{LM}}$ is calculated and compared to measurements. Let us recall that $P_{\mathrm{st1}}^{\mathrm{LM}}$ is the flicker level achieved by the original driver and $P_{\mathrm{st2}}^{\mathrm{LM}}$ is the flicker level after bypassing the DB. The quantity $\Delta P_{\mathrm{st}}^{\mathrm{LM}}$ is defined in such a way (see Eq. (6.11)) that positive values indicate the DB helps minimise the flicker response and negative values indicate that DB worsens the flicker response.

Figure 7.15a shows the simulation results with varied reference voltage sensitivity to the supply voltage perturbations. This sensitivity is noted as *leak* and is given in % of m_{DC}.

From the figure, it can be seen that the perturbation injection causes flicker at higher frequencies. This means that a perturbation at f_{ih} causes flicker at frequencies below f_{ih}. This phenomenon was never observed in the measurements and, thus, it can be concluded that it does not occur in real situations.

The *CMRR* is usually between 70 and 120 dB [107]. For poor quality amplifiers embedded in ICs, it may be lower. The simulations were run for several levels of *CMRR*. The results are summarised in Tab. 7.7 and a graphical comparison of these results is shown in Fig. 7.15b. The results show that *CMRR* has large impact on

the produced flicker. Interestingly, for a certain value of *CMRR* (60 dB) the flicker level decreases; this is because the perturbing signal enters the system at two different points, each time with an opposite phase. This causes a cancellation at a certain level. The numerical results in Tab. 7.7 show that the *CMRR* of the differential amplifier affects not only absolute flicker level, but also the $\Delta P_{\mathrm{st}}^{\mathrm{LM}}$.

Figure 7.15c shows the results for various values of R_{EMI}. Numerical results for $f_{\mathrm{ih}} = 10\,\mathrm{Hz}$ are in Tab. 7.7. It can be observed that the series resistance decreases the flicker response. Thus with higher values of R_{EMI} the $\Delta P_{\mathrm{st}}^{\mathrm{LM}}$ rises also.

Fig. 7.15d shows the flicker response when extra LED branches were added to provide more load. In order to feed sufficient level of current, the R_{sens} was changed accordingly also (half the original value for two parallel LED branches, etc.). The numerical results are shown in Tab. 7.7d.

Figure 7.16 and Tab. 7.8 show the results for circuit element variations. It is apparent (Subfig. 7.16a, Tab. 7.8a) that the size of the smoothing capacitor relative to the rest of the circuit has absolutely no impact on the flicker level. Removing the capacitor completely will result in a voltage drop of the DC link and the lamp will not operate.

Changing the value of R_{sens} will result in changing the LED current. This increases the power consumption and the luminous flux output also. Subfigure 7.16b and Tab. 7.8b show how flicker sensitivity is changed. For larger values, the circuit is more loaded and, thus, without a proper change of the inductor, more prone to flicker.

Generally, larger L_{b} values will decrease the flicker. However, it is difficult to observe a clear trend in the effect on $\Delta P_{\mathrm{st}}^{\mathrm{LM}}$.

7.4.5 Simulation Summary

Section 7.4: LED Driver Model—Hysteretic Regulation was concerned with simulating the $P_{\mathrm{st}}^{\mathrm{LM}}$ and $\Delta P_{\mathrm{st}}^{\mathrm{LM}}$ of 12 V LED lamps analysed in Sec. 6.4. In the same section, several hypotheses were proposed, aiming to explain the results. In this section, a model was created and verified. The purpose of the simulations was to determine the conditions under which removing the DB from the circuit will not raise the flicker response of the circuit. This means that the $\Delta P_{\mathrm{st}}^{\mathrm{LM}}$ must be non-positive. The shown

Table 7.6: Simulated $P_{\mathrm{st}}^{\mathrm{LM}}$ with the DB ($P_{\mathrm{st1}}^{\mathrm{LM}}$) and without ($P_{\mathrm{st2}}^{\mathrm{LM}}$); $\Delta P_{\mathrm{st}}^{\mathrm{LM}}$ for LED2,3,5,6 and simulation; various m_{DC}, constant $f_{\mathrm{ih}} = 10\,\mathrm{Hz}$

m_{DC} (%)		0.71	1.41	2.83	7.07
$P_{\mathrm{st1}}^{\mathrm{LM}}$	sim.	0.21	0.31	0.55	1.40
$P_{\mathrm{st2}}^{\mathrm{LM}}$		0.37	0.36	0.65	1.60
$\Delta P_{\mathrm{st}}^{\mathrm{LM}}$	sim.	+77.45	+17.36	+17.93	+14.69
	LED2	+34.89	+41.78	+49.84	+61.54
	LED3	−6.30	−6.60	−6.45	−4.53
	LED5	−52.04	−60.04	−77.83	−71.62
	LED6	+15.91	+19.55	+19.36	+13.21

Table 7.7: Simulated $P_{\mathrm{st}}^{\mathrm{LM}}$ results with various changes to the simulation, $m_{\mathrm{DC}} = 2.83\,\%$, $f_{\mathrm{ih}} = 10\,\mathrm{Hz}$

(a) Reference voltage contamination

leak (%)	$P_{\mathrm{st1}}^{\mathrm{LM}}$	$P_{\mathrm{st2}}^{\mathrm{LM}}$	$\Delta P_{\mathrm{st}}^{\mathrm{LM}}$
0	0.56	0.66	+17.93
0.1	0.58	0.66	+13.44
0.2	0.64	0.70	+8.99

(b) Series resistance at the input

R_{EMI} (Ω)	$P_{\mathrm{st1}}^{\mathrm{LM}}$	$P_{\mathrm{st2}}^{\mathrm{LM}}$	$\Delta P_{\mathrm{st}}^{\mathrm{LM}}$
0	0.56	0.66	+17.93
0.5	0.49	0.66	+34.97
1	0.45	0.66	+47.94

(c) Sensing amplifier *CMR*

CMR (dB)	$P_{\mathrm{st1}}^{\mathrm{LM}}$	$P_{\mathrm{st2}}^{\mathrm{LM}}$	$\Delta P_{\mathrm{st}}^{\mathrm{LM}}$
∞	0.56	0.66	+17.93
140	0.56	0.66	+17.75
100	0.57	0.65	+14.30
80	0.52	0.57	+9.42
60	0.22	0.13	−40.56
53.98	1.03	0.97	−5.77
46.02	4.48	4.39	−2.03
40	17.35	20.06	+15.63

(d) Extra parallel branches of LEDs

branches	$P_{\mathrm{st1}}^{\mathrm{LM}}$	$P_{\mathrm{st2}}^{\mathrm{LM}}$	$\Delta P_{\mathrm{st}}^{\mathrm{LM}}$
0	0.56	0.66	+17.93
1	0.52	0.11	−79.39
2	0.35	0.14	−58.91
3	0.16	0.06	−60.01

Table 7.8: Simulated $P_{\mathrm{st}}^{\mathrm{LM}}$ and $\Delta P_{\mathrm{st}}^{\mathrm{LM}}$ results with various changes to the circuit elements, $m_{\mathrm{DC}} = 2.83\,\%$, $f_{\mathrm{ih}} = 10\,\mathrm{Hz}$

(a) Smoothing capacitor, C_{DC}

C_{DC} (µF)	$P_{\mathrm{st1}}^{\mathrm{LM}}$	$P_{\mathrm{st2}}^{\mathrm{LM}}$	$\Delta P_{\mathrm{st}}^{\mathrm{LM}}$
2	0.55	0.66	+19.38
25	0.56	0.66	+18.70
100	0.56	0.66	+18.67
200	0.56	0.66	+17.64
330	0.56	0.66	+17.93
500	0.56	0.66	+17.84

(b) Sensing resistor, R_{sens}

R_{sens} (Ω)	$P_{\mathrm{st1}}^{\mathrm{LM}}$	$P_{\mathrm{st2}}^{\mathrm{LM}}$	$\Delta P_{\mathrm{st}}^{\mathrm{LM}}$
0.1	1.13	0.40	−64.94
0.2	0.07	0.18	+144.06
0.3	0.34	0.42	+23.08
0.34	0.56	0.66	+17.93
0.75	1.09	1.21	+10.54
1	1.50	1.77	+17.81

(c) Inductor, L_{b}

L_{b} (µH)	$P_{\mathrm{st1}}^{\mathrm{LM}}$	$P_{\mathrm{st2}}^{\mathrm{LM}}$	$\Delta P_{\mathrm{st}}^{\mathrm{LM}}$
10	3.72	2.38	−35.93
20	0.53	1.54	+192.43
47	0.56	0.66	+17.93
100	0.36	0.16	−55.44
500	0.05	0.08	+67.21

(d) Inductor resistance, R_{b}

R_{b} (mΩ)	$P_{\mathrm{st1}}^{\mathrm{LM}}$	$P_{\mathrm{st2}}^{\mathrm{LM}}$	$\Delta P_{\mathrm{st}}^{\mathrm{LM}}$
32	0.48	0.70	+45.20
64	0.61	0.63	+2.44
128	0.56	0.66	+17.93
256	0.44	0.59	+34.41

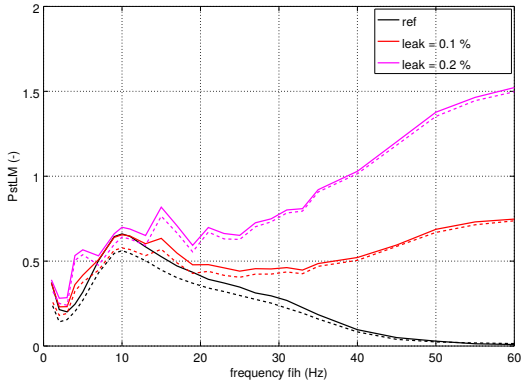

(a) Various level of reference voltage contamination

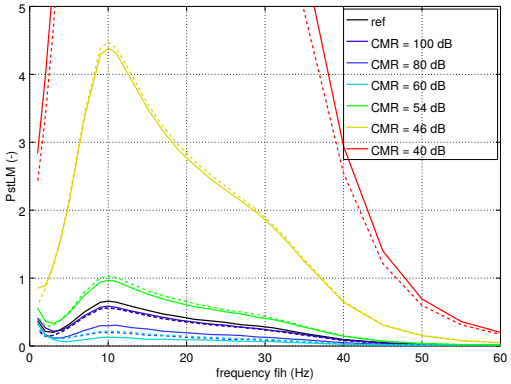

(b) Several values of *CMRR*; first three lines almost overlap

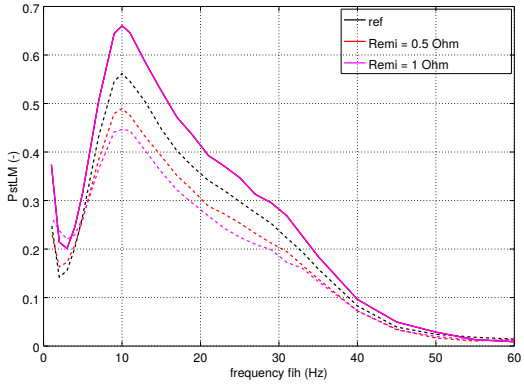

(c) Several values of R_{EMI}

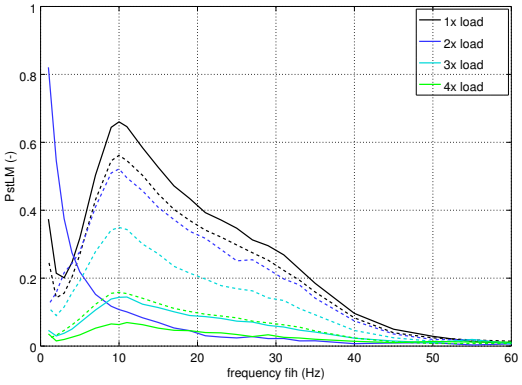

(d) Adding extra LED branches as additional load

Figure 7.15: Simulated $P_{\mathrm{st}}^{\mathrm{LM}}$ with various changes to the model; dotted line with DB, solid line without DB

figures depict the flicker levels for the modulation frequencies $f_{\mathrm{m}} = 1$ to $60\,\mathrm{Hz}$; in the tables, only the values for $f_{\mathrm{m}} = 10\,\mathrm{Hz}$ are shown and used to determine the $\Delta P_{\mathrm{st}}^{\mathrm{LM}}$. Throughout this section, the modulation magnitude was kept constant at $m_{\mathrm{DC}} = 2.83\,\%$. It is to be noted that the flicker level is always below $P_{\mathrm{st}}^{\mathrm{LM}} = 1$, except for special cases (e.g., too small a *CMRR*).

Hypothesis 1: Voltage Reference From the simulation results several conclusions may be drawn. Firstly, hypothesis no. 1 (perturbations affecting the voltage reference inside the driver IC) may be rejected, as the simulation results do not correspond to any performed measurements. This means that, in the studied lamps, the voltage reference is not compromised by voltage perturbations.

Hypothesis 2: *CMR* Secondly, hypothesis no. 2 (*CMR* of the current sensing subsystem) may be accepted. It was shown that the *CMR* directly affects the absolute

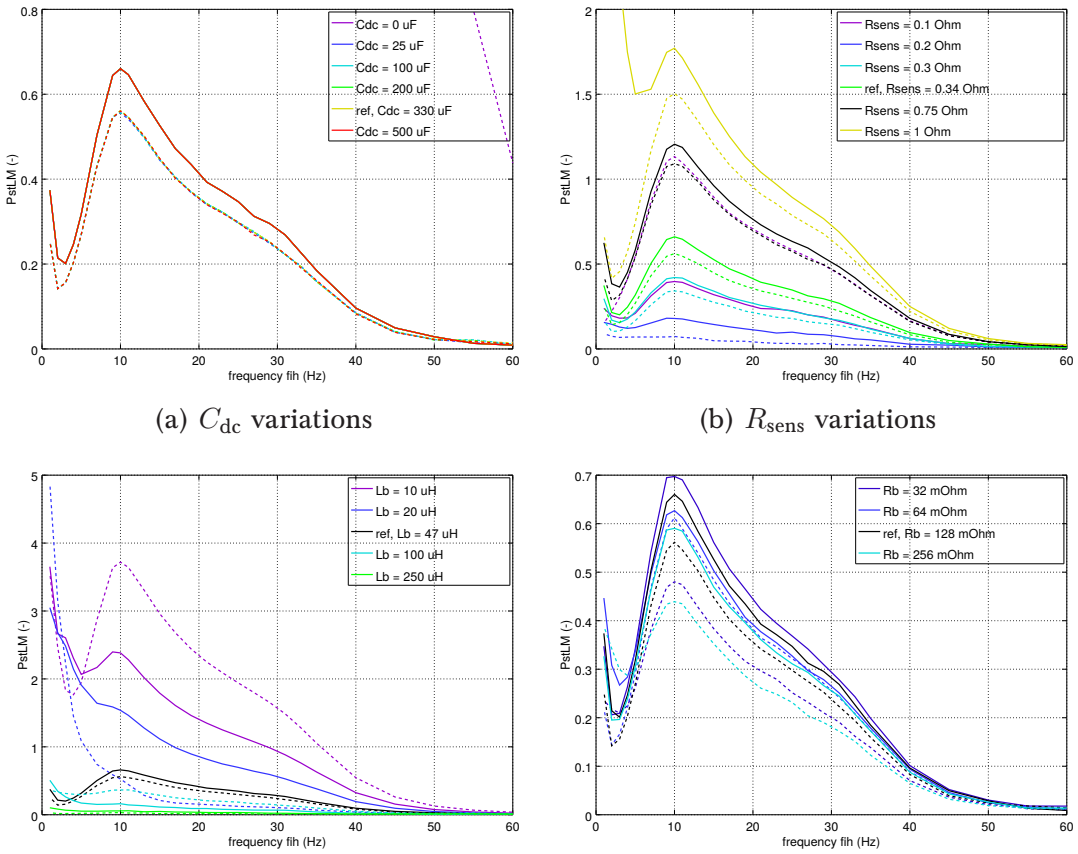

(a) C_{dc} variations

(b) R_{sens} variations

(c) L_{b} variations

(d) R_{b} variations

Figure 7.16: Simulation results with varied circuit elements, dotted line with DB, solid line without DB; $m_{\mathrm{DC}} = 2.83\,\%$

level of $P_{\mathrm{st}}^{\mathrm{LM}}$ both with the DB and without. The simulations revealed that with an increasing *CMR*, the $P_{\mathrm{st}}^{\mathrm{LM}}$ drops until it reaches a minimum at $\mathit{CMR} = 60\,\mathrm{dB}$, only to start rising for higher values of a *CMR*. A similar pattern can be observed with $\Delta P_{\mathrm{st}}^{\mathrm{LM}}$.

Hypothesis 3: Input Port Series Resistance Hypothesis no. 3 (series resistance at the supply port) may be accepted too. The simulations show that the series resistance decreases the $P_{\mathrm{st}}^{\mathrm{LM}}$ of the lamp, which in turn leads to higher values of $\Delta P_{\mathrm{st}}^{\mathrm{LM}}$. In this sense the effect of the DB is positive. The same flicker attenuation effect may be achieved by placing a series resistor at the supply port even when the DB is not used; this is a lossy approach though and, thus, the bonus of increasing the power efficiency is lost.

Hypothesis 4: Circuit Elements Dimensioning The answer to hypothesis no. 4 (other circuit elements dimensioning) must be given in several parts. Firstly, the smoothing capacitor size was shown to have no impact on the flicker when a DC supply is used. With an AC supply, the smoothing capacitor is an important factor

affecting the flicker response.

When more LED branches are connected in parallel, flicker is decreased, as is shown in Tab. 7.7d. Additionally, the $\Delta P_{\mathrm{st}}^{\mathrm{LM}}$ drops significantly to negative values. Adding more LED branches to the circuit means more load for the converter.

The sensing resistor itself is used to set the desired LED current; thus, too small or too large values may lead to instability if the load is not changed appropriately. From the results, one can see that small increase in its value causes larger flicker, while decreasing the sensing resistor (increasing the LED current) decreases the flicker response. This might be the same effect as when more parallel LED branches were added to the circuit.

The inductor effect on flicker is very simple—larger inductor values help decrease flicker significantly. Its effect upon $\Delta P_{\mathrm{st}}^{\mathrm{LM}}$ is ambiguous though. The same can be said about its series resistance. In these cases, the simulation results are inconclusive.

7.5 LED Driver Models—Other Regulation Techniques

In this section, other regulation techniques were modelled and simulated. The models are intended to compare the fluctuations of the flux output of each regulation technique. These tested regulation techniques include:

- hysteretic control with synchronised switching,
- voltage mode control,
- current mode control.

For each technique, a new MATLAB Simulink model was created with the same parameters, load and circuit elements as the original model with hysteresis control. The models are shown in Fig. 7.17.

The hysteretic regulation with synchronised switching (Fig. 7.17a) is very similar to the original model (Fig. 7.11). As an extra, it comprises a D latch which allows switching at clock pulses only. Advantage of this approach is a constant switching frequency.

The VMC model (Fig. 7.17b) represents a classical feedback control example. The control variable is the LED voltage. The error is calculated and fed to a controller. In this case, the controller was a simple PI structure with the following parameters:

$$K = 0.3\,, \tag{7.25}$$

$$\tau_{\mathrm{PI}} = 5\,\mathrm{ms}\,. \tag{7.26}$$

The PWM signal is created by comparing the PI output with a ramp signal. The magnitude of the ramp signal was $V_{\mathrm{ramp}} = 1\,\mathrm{V}$. The stability of the simulation required adding a small output capacitor; its value was $C_{\mathrm{o}} = 10\,\mathrm{pF}$. The rest of the circuit parameters were kept intact so that the simulation is comparable with the previous results.

Table 7.9: Various regulation techniques, flicker comparison

(a) Clean DC supply

regulation	*FP*	*FI*	$P_{\mathrm{st}}^{\mathrm{LM}}$
hysteresis	18	$4.4 \cdot 10^{-2}$	0
sync. hyst.	26	$6.1 \cdot 10^{-2}$	0
VMC	24	$3.3 \cdot 10^{-2}$	0.04
CMC	10	$2.1 \cdot 10^{-2}$	0

(b) Modulated DC supply, $f_{\mathrm{m}} = 9.54\,\mathrm{Hz}$, $m_{\mathrm{DC}} = 2.83\,\%$

regulation	*FP*	*FI*	$P_{\mathrm{st}}^{\mathrm{LM}}$
hysteresis	18	$4.4 \cdot 10^{-2}$	0.55
sync. hyst.	27	$6.0 \cdot 10^{-2}$	2.64
VMC	22	$2.4 \cdot 10^{-2}$	0.05
CMC	12	$2.1 \cdot 10^{-2}$	0.03

The CMC model (Fig. 7.17c) is very similar to the VMC, but with a small difference. Instead of an artificial ramp signal, an inductor current is used. The current is sensed via a sensing resistor.

7.5.1 Results

From the models, the LED current was saved. Assuming isothermal conditions in the p-n junction (similarly to the previous section), the flux will be linearly dependant on the LED current. The normalised frequency spectrum of the LED current will, thus, be identical to the flux spectrum. The frequency spectra are shown in Fig. 7.18.

Subfigure 7.18a shows the spectra under clean DC supply conditions. Above 100 Hz, only maximum values within 100 Hz bands are shown (dotted lines), for the sake of a clear depiction. It can be seen that the VMC causes small low frequency fluctuations together with high frequency noise. Other techniques only cause high frequency noise. The least noise is produced by the hysteretic control, practically only a single frequency is present. The evaluated flicker quantities are shown in Tab. 7.9a.

Subfigure 7.18b shows a perturbed DC supply case. In this case, the supply was contaminated by sinusoidal modulation, $f_{\mathrm{m}} = 9.54\,\mathrm{Hz}$ (in order to prevent spectral leakage), $m_{\mathrm{DC}} = 2.83\,\mathrm{Hz}$. The figure clearly shows the frequency components present in LED light output. For a better depiction clarity, these components are marked by a cross in the figure. The evaluated flicker quantities are shown in Tab. 7.9b.

7.5.2 Simulation Summary

The results in Tab. 7.9a show that the flux ripple is relatively high for all techniques, but the ripple frequency is very high and so ripple is irrelevant for flicker (the $P_{\mathrm{st}}^{\mathrm{LM}}$ is practically zero for all techniques except VMC).

The flicker level notably rises with low frequency modulation added to the supply voltage. Fig. 7.18b shows that many harmonics are present in the resulting spectra. The results also show that VMC is very effective at eliminating the perturbation; the flux is almost intact by the perturbation.

The worst result is from the synchronised hysteresis regulation, where the $P_{\mathrm{st}}^{\mathrm{LM}}$ reaches above the acceptable values. This is because there is always a small

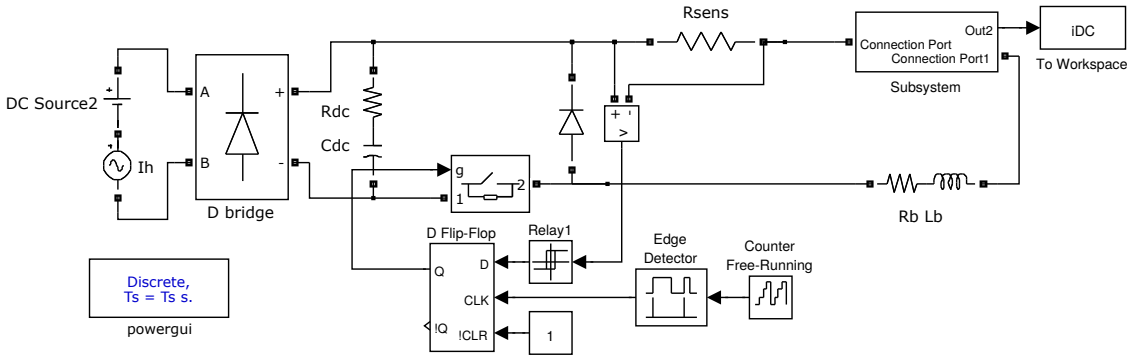

(a) Hysteretic regulation—synchronised switching

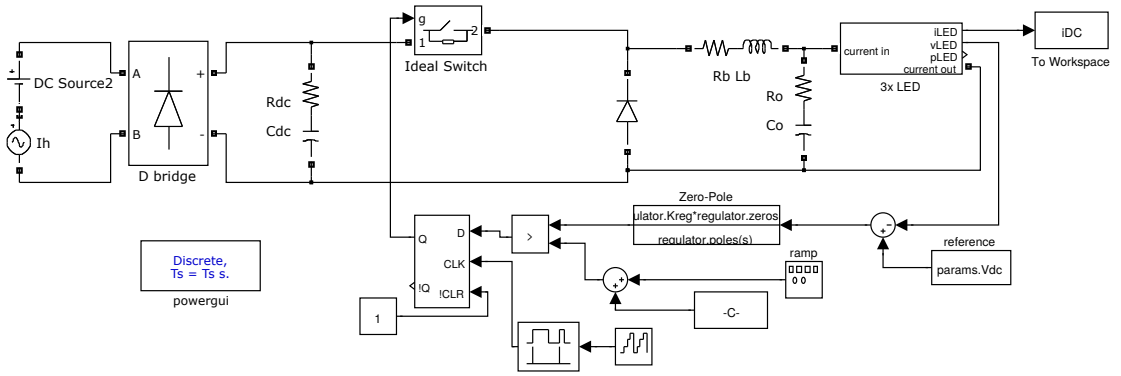

(b) VMC regulation

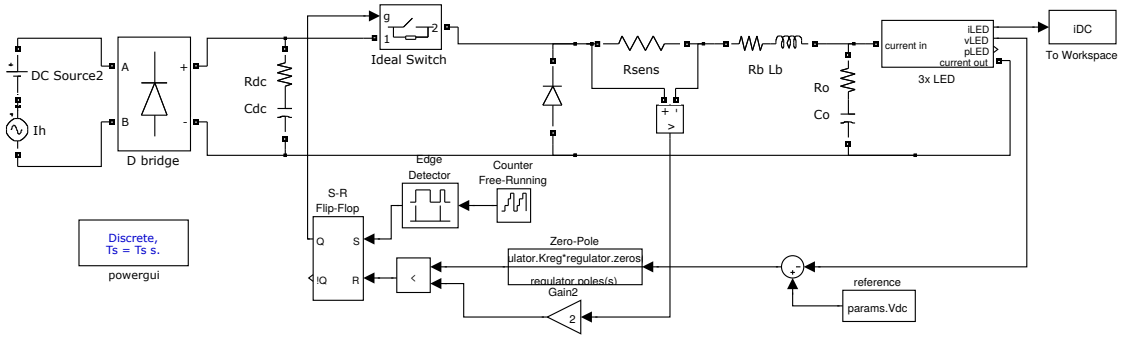

(c) CMC regulation

Figure 7.17: Active driver models—other regulation techniques

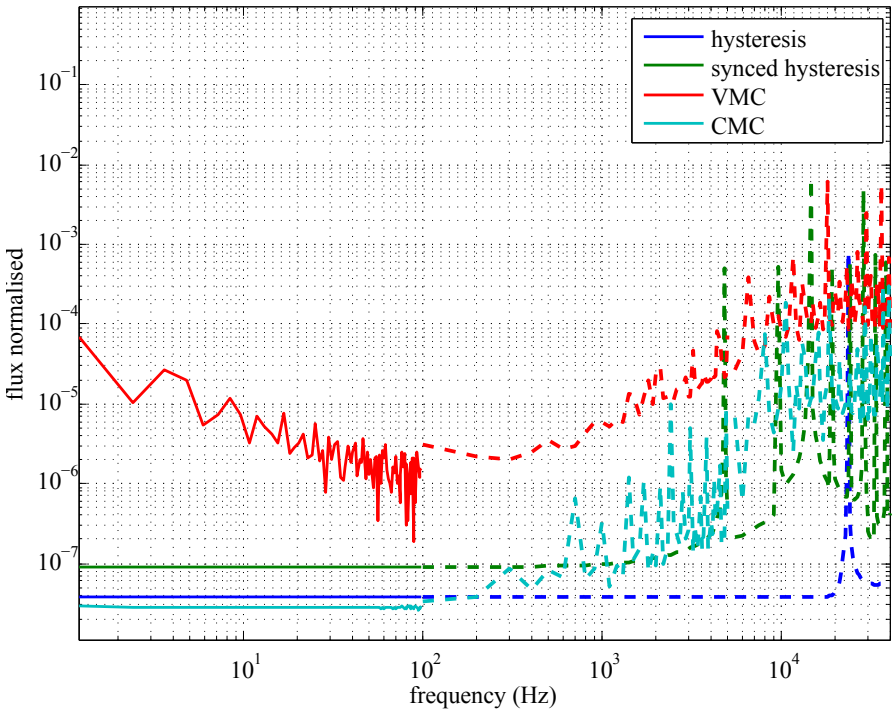

(a) Clean DC supply

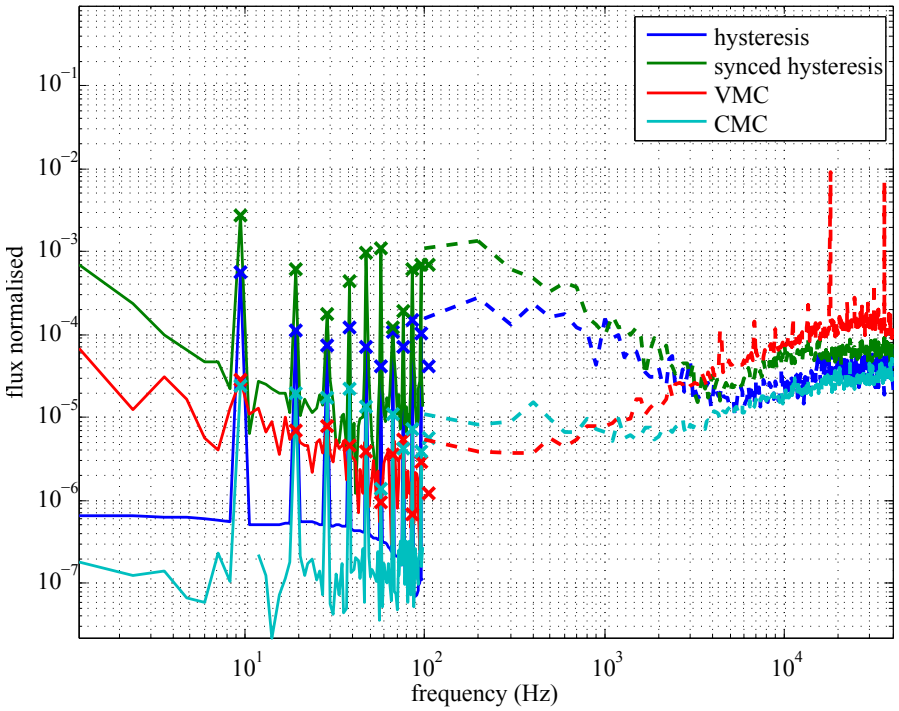

(b) Perturbed DC supply, $f_{\mathrm{m}} = 9.54\,\mathrm{Hz}$, $m_{\mathrm{DC}} = 2.83\,\%$

Figure 7.18: Various regulation techniques: Luminous flux spectrum comparison

delay between the moment when the current reaches beyond the allowed limit and the switch. These small delays accumulate into an error in the mean current value which gets corrected periodically after several switch periods. When combined with supply voltage perturbation, this behaviour worsens considerably, thus, producing serious flicker. It is to be concluded that the synchronised hysteretic regulation is unacceptable for LED drivers. The classical hysteretic approach and CMC behave in a similar manner and are suitable for controlling LED drivers.

8 Conclusion

LEDs are a relatively young technology compared to other technologies. This is why most of the standards were not updated yet to cover all specificities linked with LEDs. It has already been recognised that, with LEDs, the responsibility for flicker has moved towards the lamp manufacturer and their driver design. This further means that the lamps' reaction to perturbations may vary significantly from lamp to lamp. The ways to measure flicker need to reflect this fact, which is already happening [STD1, STD17].

This thesis is concerned with analysing flicker properties of LED lamps under DC supply. The core experiment was designed to determine the role of a diode bridge in flicker immunity of ELV LED lamps equipped with a hysteretically controlled buck converter. The measurement results are ambiguous; some of the tested lamps show better flicker response with the DB bypassed while other lamps show the opposite (see Sec. 6.4). This is why simulations were necessary to provide a more detailed explanation.

8.1 Results Summary

Some parts of the work were intended merely for demonstrative purposes (Experiment 2, Simulation 1). These are not discussed further in this section. The following paragraph describes the results obtained from the core work; other experiments and simulations are discussed afterwards.

The Core Work: Experiment 3 and Simulation 2 During the work on the simulations, an averaged switch model of a generic buck converter with a generalised lamp model was created and tested (Simulation 2a). It was concluded that such a model can reproduce the measured results of $P_{\mathrm{st}}^{\mathrm{LM}}$, but it fails to model all the measured results of $\Delta P_{\mathrm{st}}^{\mathrm{LM}}$ and, thus, to give an explanation about the origin of its various values.

This is why a more detailed, "full switch" model, together with a more detailed LED head model was used further on (Simulation 2b). Such a model can simulate the $P_{\mathrm{st}}^{\mathrm{LM}}$ response of the lamps as well as the various $\Delta P_{\mathrm{st}}^{\mathrm{LM}}$ values observed at the lamps under test.

Simulation Results In Sec. 6.4 several hypotheses were proposed to explain a lamps' behaviour. As for the flicker response, generally, the simulations show that:

- removing the DB results in applying a higher voltage to the DC-DC converter input port, which may affect its operating point and switching frequency;
- the reference voltage in the lamps' driver IC is not compromised by supply voltage perturbations;
- flicker immunity is not affected by the size of the smoothing capacitor placed at the DC-DC converter input ports, regardless of the DB presence; this is in accordance with the measurements and conclusions presented in [LK8];
- the *CMR* of the current sensing subsystem plays a role; it is possible to decrease the flicker response by introducing a certain level of *CMR*;
- a larger L_{b}, R_{b} and a larger load (more parallel LEDs and / or smaller current sensing resistor) help decrease the flicker response.

The main aim of the simulations was to reveal under which conditions the $\Delta P_{\mathrm{st}}^{\mathrm{LM}}$ metric becomes negative (i.e., removing the diode bridge will not increase the flicker response). It was concluded that:

- in most simulations, the $\Delta P_{\mathrm{st}}^{\mathrm{LM}}$ was positive;
- DB series resistance may play a role in decreasing the flicker level and, thus, relatively increasing the flicker response when the DB is removed (increase the $\Delta P_{\mathrm{st}}^{\mathrm{LM}}$);
- for certain levels of introduced *CMR* in the current sensing subsystem of the driver (in particular the value $\mathit{CMR} = 60\,\mathrm{dB}$), apart from flicker response decrease, negative $\Delta P_{\mathrm{st}}^{\mathrm{LM}}$ was achieved also, which means that a given level of *CMR* positively affects the driver flicker properties and the DB may be removed for further decreasing the flicker response also;
- using more LED branches in the LED head (more load for the DC-DC converter) results in better flicker response, but also helps decrease the $\Delta P_{\mathrm{st}}^{\mathrm{LM}}$.

Recommendations for DB–less Driver Design Considering the above described findings, it may be recommended that if the DB is to be removed from the driver design, the following conditions should be met:

- the driver should be loaded properly;
- in the case when high side current sensing is used, the *CMR* of the current sensing subsystem should be known and, in the particular case of buck converter with hysteretic control, it should be ideally around $\mathit{CMR} = 60\,\mathrm{dB}$.

Regardless of the DB removal, it is advisable that the inductor is sufficiently large in order to decrease the flicker response of the driver.

In the lamps analysed experimentally, all the simulated effects may have combined and counteracted each other. Because not all details about the driver circuitries were available, there are some uncertainties about the particular values of

some circuit elements. For this reason, a direct comparison of the simulation results with real measurements is impossible.

Other Experiments and Simulations

Experiment 1 The experiment 1 revealed that the combination of AC-DC converter and an LED equipped with a driver is robust enough with respect to AC voltage disturbances. Their presence does not affect the flicker significantly. This conclusion corresponds with the expectation, as the setup represents a cascade of two regulated controllers. On the other hand, the author noticed appearance of significant DC voltage ripple caused by an interaction between the tested pieces of equipment during the experiments. This phenomenon may pose a significant problem for DC power quality. Its further investigation is inevitably necessary.

Simulation 3 Simulation 3 was designed to compare four various means of feedback control for LED drivers. It was shown that their properties differ in two aspects; a) switching noise, and b) perturbation immunity. The VMC produces by far the largest switching noise even at low frequencies, but is absolutely immune to DC supply fluctuations. The worst response was from the synchronised hysteretic control. Asynchronous hysteretic control is comparable to the CMC and both are deemed suitable for driver control.

8.2 Flicker in DC Grids—Assessment

Due to the fundamental nature of DC voltage, it might be expected that the risk of flicker is much lower with DC than with AC. The reality is not so trivial. AC voltage itself is only one of the possible causes of flicker and it is not difficult to compensate. The other possible causes of flicker (see Sec. 4.3—distorted supply voltage and driver switching frequency) still pose a risk in the DC environment.

It is true that in the AC scenario, flicker may be caused by interharmonic components at up to units of kHz due to their intermodulation with the fundamental frequency. This phenomenon was identified in literature already [54, 56] and also demonstrated in this thesis in Simulation 1 (Sec. 7.2). With DC supply, the intermodulation does not take place and, thus, the set of flicker relevant frequencies is smaller. Visible flicker may be caused by frequencies below 60 Hz only, invisible flicker below 200 Hz etc. Driver immunity is then given purely by the transfer function of the driver expressed by the gain factor.

Table 8.1 summarises the individual possible causes of flicker of LED lamps (as listed in Sec. 4.3) and their risk under AC and DC supply. It can be seen that adopting DC to supply the LED lamps will mitigate some of the typical causes of flicker.

Table 8.1: Causes of flicker with LED lamps—comparison of the AC and DC supply

flicker cause	char. property	AC	DC
clean AC supply	invisible	yes	no
supply perturbations	visible, invisible	yes	lower risk
switching noise	very high frequency	yes, irrelevant	yes, irrelevant
PWM dimming	only with PWM	yes, avoidable	yes, avoidable

8.3 Discussion

Standard IEC 61000-3-3 [STD6] lays the requirements upon electrical appliances concerning P_{st} emissions in AC grids. A question is appropriate, whether a similar standard should be issued concerning DC grids. If LED lighting is expected to be a major lighting technology in DC grids, the P_{st} metric—even if the standard flickermeter were adapted to DC—would become obsolete. Thus, issuing such standard seems unnecessary.

P_{st} and P_{st}^{LM} Metrics In the context of LED technology, it is obvious that the metric P_{st} is losing its importance as a flicker index since it may not be related to actual level of flicker any more. It still may be used as one of the VQ indices for evaluating the severity of low frequency phenomena, although other indices may be more appropriate for that purpose.

The P_{st}^{LM} metric is a more proper way of evaluating flicker severity with LED technology. The transition from voltage evaluation to luminous flux evaluation means that flicker is not purely a voltage quality phenomenon any more. Such an approach still does not respect all aspects of LED flicker though. The P_{st}^{LM} metric only evaluates visible flicker; this is the heritage of P_{st} and its incandescent lamp model where invisible and high frequency flicker was irrelevant. Because invisible and high frequency flicker may pose a risk to human health and safety and is relevant with LEDs, these phenomena should be also covered by P_{st}^{LM} (or a similar metric).

Immunity Requirements The theoretical research revealed that there is a lack of standardised immunity requirements for LED lamps with respect to flicker. For future work on immunity requirements for LEDs in DC grids there is a key observation that zero flicker level with clean AC voltage does not imply good flicker immunity with perturbed DC supply, as is shown in Sec. 6.4.6. This means that *AC may not be assumed as a worst–case scenario when laying requirements on flicker immunity in DC environment.* Extra considerations need to be taken.

8.4 Recommendations About a Future Research

During the work on this thesis the following points were found worthy of attention for future directions of research in the discussed field:

- Interaction between equipment in DC grids need to be analysed deeper. This phenomenon need to be examined and its cause identified and described properly.
- Experiment 1 should be repeated with the diode bridge removed from the tested LED lamps. Comparison of the results would be an appropriate expansion of the work presented in this thesis.
- Simulations testing the *CMRR*'s effect on flicker response should be tested experimentally in order to validate the results.
- $P_{\mathrm{st}}^{\mathrm{LM}}$ should be adapted to account for invisible flicker and high frequency flicker also. Alternatively, a similar index should be defined which would account for these phenomena and which would be used in parallel with the contemporary $P_{\mathrm{st}}^{\mathrm{LM}}$ metric.
- Heterochromatic flicker is a phenomenon never deeply studied with LEDs and, as such, it represents an appealing field of research.

8.5 Closing Statements

There is still surely a long way to go before DC grids will enter people's everyday life. Many practical aspects need to be settled and appropriate standards issued. Together with other positive aspects they can offer, they also represent a way to mitigate flicker, which is shown in this thesis.

LED lamps entered the lighting applications field even before appropriate standards could have been issued to reflect their specific behaviour. This means that some products available on the market may be a source of flicker at a hazardous level. Fortunately, this aspect has been recognised and appropriate standards are being issued to address this topic.

But even so, it is the author's personal experience that the wide public is not familiar with the flicker phenomenon and does not recognise it as a problem. Some people may report headaches or dizziness when using LEDs for lighting, unaware that these symptoms may be caused by invisible flicker. The end user has absolutely no means of telling whether the product he intends to buy will flicker or not. For the lamp manufacturers, there is no obligation to quantify the flicker response of given product and to state it on the package label.

Bibliography

[1] A. Plepys and J. L. Richter, "Public Procurement Barriers in Promoting Market Uptake of Innovative LED Lighting," in *2016 Electronics Goes Green 2016+ (EGG)*, Sep. 2016, pp. 1–8.

[2] S. Nakamura, T. Mukai, and M. Senoh, "Candela-class high-brightness InGaN/AlGaN double-heterostructure blue-light-emitting diodes," *Applied Physics Letters*, vol. 64, no. 13, pp. 1687–1689, 1994.

[3] Statista, The Statistical Portal, "Estimated LED penetration of the global lighting market from 2010 to 2020," 2017. [Online]. Available: https://www.statista.com/statistics/246030/estimated-led-penetration-of-the-global-lighting-market/

[4] M. Yabada and K. Stober, "Adoption of Light-Emitting Diodes in Common Lighting Applications," Jul. 2015. [Online]. Available: https://energy.gov/sites/prod/files/2015/07/f24/led-adoption-report_2015.pdf

[5] A. Sannino, G. Postiglione, and M. Bollen, "Feasibility of a DC network for commercial facilities," *IEEE Transactions on Industry Applications*, vol. 39, no. 5, pp. 1499–1507, Sep. 2003.

[6] M. Celidonio, D. Di Zenobio, E. Fionda, L. Pulcini, and E. Sergio, "The EDISON project: Enhanced energy saving solution for lighting using DC power supply," in *2013 IEEE Online Conference on Green Communications (GreenCom)*, Oct. 2013, pp. 143–149.

[7] M. Celidonio, E. Fionda, L. Pulcini, E. Sergio, and D. Di Zenobio, "A centralised DC power supply solution for LED lighting networks," in *ENERGYCON 2014 - IEEE International Energy Conference*, 2014, pp. 1137–1143.

[8] "ABCDE: Appropriation sociale d'un Bus Continu pour la Distribution de L'Éclairage du Bâtiment - une approche sociotechnique," 2014.

[9] B. Lehman and A. Wilkins, "Designing to Mitigate Effects of Flicker in LED Lighting: Reducing risks to health and safety," *IEEE Power Electronics Magazine*, vol. 1, no. 3, pp. 18–26, Sep. 2014.

[10] C. Martinsons and G. Zissis, "Solid State Lighting Annex: Potential Health Issues of SSL, Final Report," Sep. 2014.

[11] IET Standards Limited, Ed., *IET code of practice for the application of LED lighting systems.* Stevenage, Hertfordshire: IET Standards, 2014.

[12] K. Engelen, E. L. Shun, P. Vermeyen, I. Pardon, R. D'hulst, J. Driesen, and R. Belmans, "The Feasibility of Small-Scale Residential DC Distribution Systems," in *IECON 2006 - 32nd Annual Conference on IEEE Industrial Electronics*, Nov. 2006, pp. 2618–2623.

[13] H. Lotfi and A. Khodaei, "AC Versus DC Microgrid Planning," *IEEE Transactions on Smart Grid*, vol. 8, no. 1, pp. 296–304, Jan. 2017.

[14] L. Che and M. Shahidehpour, "DC Microgrids: Economic Operation and Enhancement of Resilience by Hierarchical Control," *IEEE Transactions on Smart Grid*, vol. 5, no. 5, pp. 2517–2526, Sep. 2014.

[15] T. Dragičević, X. Lu, J. C. Vasquez, and J. M. Guerrero, "DC Microgrids - Part II: A Review of Power Architectures, Applications, and Standardization Issues," *IEEE Transactions on Power Electronics*, vol. 31, no. 5, pp. 3528–3549, May 2016.

[16] T. Kaipia, P. Nuutinen, A. Pinomaa, A. Lana, J. Partanen, J. Lohjala, and M. Matikainen, "Field test environment for LVDC distribution - Implementation experiences," in *Integration of Renewables into the Distribution Grid, CIRED 2012 Workshop*, May 2012, pp. 1–4.

[17] D. Kumar, F. Zare, and A. Ghosh, "DC Microgrid Technology: System Architectures, AC Grid Interfaces, Grounding Schemes, Power Quality, Communication Networks, Applications and Standardizations Aspects," *IEEE Access*, vol. PP, no. 99, pp. 12 230 – 12 256, 2017.

[18] D. Ricchiuto, R. Mastromauro, M. Liserre, I. Trintis, and S. Munk-Nielsen, "Overview of multi-DC-bus solutions for DC microgrids," in *2013 4th IEEE International Symposium on Power Electronics for Distributed Generation Systems (PEDG)*, Jul. 2013, pp. 1–8.

[19] S. Whaite, B. Grainger, and A. Kwasinski, "Power Quality in DC Power Distribution Systems and Microgrids," *Energies*, vol. 8, no. 5, pp. 4378–4399, May 2015. [Online]. Available: http://www.mdpi.com/1996-1073/8/5/4378/

[20] D. Becker and B. Sonnenberg, "DC microgrids in buildings and data centers," in *Telecommunications Energy Conference (IN□EC), 2011 IEEE 33rd International*, Oct. 2011, pp. 1–7.

[21] J. D. I. Cottingham, W. Bassett, and G. Melendez, "SAE/TP - 2008-01-2890 Aircraft DC Power Quality Characteristics of a PCTRU," in *Power Systems Conference.* Bellevue, Washington, USA: SAE International - Technical Papers, Nov. 2008, p. 7.

[22] W. Li, X. Mou, Y. Zhou, and C. Marnay, "On voltage standards for DC home microgrids energized by distributed sources," in *Proceedings of The 7th International Power Electronics and Motion Control Conference*, vol. 3, Jun. 2012, pp. 2282–2286.

[23] B. Singh, B. Singh, A. Chandra, K. Al-Haddad, A. Pandey, and D. Kothari, "A review of single-phase improved power quality AC-DC converters," *IEEE Transactions on Industrial Electronics*, vol. 50, no. 5, pp. 962–981, Oct. 2003.

[24] T. D. Mai, G. V. d. Broeck, A. Pevere, and J. Driesen, "Power electronics for potential distribution dc power evolution: A review," in *2016 IEEE International Energy Conference (ENERGYCON)*, Apr. 2016, pp. 1–6.

[25] E. Rogers, "Understanding Boost Power Stages in Switchmode Power Supplies - Application Report," Mar. 1999. [Online]. Available: http://www.ti.com/lit/an/slva061/slva061.pdf

[26] S. Maniktala, "Voltage-Mode, Current-Mode (and Hysteretic Control), Technical Note," Nov. 2012. [Online]. Available: https://www.microsemi.com/document-portal/doc_view/124786-voltage-mode-current-mode-and-hysteretic-control

[27] E. Rogers, "Understanding Buck Power Stages in Switchmode Power Supplies - Application Report," Mar. 1999. [Online]. Available: http://www.ti.com/lit/an/slva057/slva057.pdf

[28] S. Lee, "Demystifying Type II and Type III Compensators Using Op-Amp and OTA for DC/DC Converters, Application Report," Jul. 2014. [Online]. Available: http://www.ti.com/lit/an/slva662/slva662.pdf

[29] J. Meyer, M. H. J. Bollen, H. Amaris, A. Blanco, A. Gil De Castro, J. Desmet, M. Klatt, L. Kocewiak, S. K. Ronnberg, and K. Yang, "Future work on harmonics - Some expert opinions Part II - Supraharmonics, standards and measurements," in *Proceedings of International Conference on Harmonics and Quality of Power, ICHQP*, 2014, pp. 909–913.

[30] M. Castro-Nunez and R. Castro-Puche, "The IEEE Standard 1459, the CPC Power Theory, and Geometric Algebra in Circuits With Nonsinusoidal Sources and Linear Loads," *IEEE Transactions on Circuits and Systems I: Regular Papers*, vol. 59, no. 12, pp. 2980–2990, Dec. 2012. [Online]. Available: http://ieeexplore.ieee.org/lpdocs/epic03/wrapper.htm?arnumber=6265343

[31] J. Almeida, P. Silveira, H. Arango, M. Parentoni, and J. Abreu, "Wye Apparent Power - An alternative proposal," in *2010 14th International Conference on Harmonics and Quality of Power (ICHQP)*, Sep. 2010, pp. 1–8.

[32] L. Czarnecki and P. Haley, "Unbalanced Power in Four-Wire Systems and its Reactive Compensation," *IEEE Transactions on Power Delivery*, vol. 30, no. 1,

pp. 53–63, Feb. 2015. [Online]. Available: http://www.lsczar.info/wp-content/uploads/2014/07/130-Power-and-Comp-in-4-wire-Syst.pdf

[33] M. Caserza, A. Mariscotti, and P. Pinceti, "Definition of Power Quality Indices for DC Low Voltage Distribution Networks," in *Proceedings of the IEEE Instrumentation and Measurement Technology Conference, 2006. IMTC 2006*, Apr. 2006, pp. 1885–1888.

[34] J. Drápela and L. Kukačka, "DC metrics," Brno University of Technology, FEEC, DEPE, Brno, Czech Republic, Tech. Rep. TAČR TA185S01001, 2016.

[35] R. Faktor, "Voltage Quality in DC Grids," Master Thesis, Brno University of Technology, Brno, 2017.

[36] S. Berman, D. Greenhouse, I. Bailey, R. Clear, and T. Raasch, "Human Electroretinogram Responses to Video Displays, Fluorescent Lighting, and Other High-Frequency Sources," *Optometry and Vision Science*, vol. 68, no. 8, pp. 645–662, Aug. 1991, wOS:A1991GB12300012.

[37] B. Lehman, A. Wilkins, S. Berman, M. Poplawski, and N. Miller, "Proposing measures of flicker in the low frequencies for lighting applications," in *2011 IEEE Energy Conversion Congress and Exposition (ECCE)*, Sep. 2011, pp. 2865–2872.

[38] C.-S. Lee, J.-H. Lee, H. Pak, S. Park, and D.-W. Song, "Phantom array and stroboscopic effects of a time-modulated moving light source during saccadic eye movement," *Lighting Research & Technology*, p. 147715351769346, Jan. 2017. [Online]. Available: http://journals.sagepub.com/doi/10.1177/1477153517693468

[39] S. Shady, D. I. A. MacLeod, and H. S. Fisher, "Adaptation from Invisible Flicker," *Proceedings of the National Academy of Sciences*, vol. 101, no. 14, pp. 5170–5173, Apr. 2004. [Online]. Available: http://www.pnas.org/cgi/doi/10.1073/pnas.0303452101

[40] A. C. Silk, "Flicker and electroclinical syndromes: the effects of migraine variants in control room situations and on drivers," in *2001 People in Control. The Second International Conference on Human Interfaces in Control Rooms, Cockpits and Command Centres*, 2001, pp. 316–320.

[41] J. T. Walker, "Brightness enhancement and the Talbot level in stationary gratings," *Perception & Psychophysics*, vol. 23, no. 4, pp. 356–359, Jul. 1978. [Online]. Available: http://www.springerlink.com/index/10.3758/BF03199722

[42] A. Hooshyar and E. El-Saadany, "Development of a Flickermeter to Measure Non-Incandescent Lamps Flicker," *IEEE Transactions on Power Delivery*, vol. 28, no. 4, pp. 2103–2115, Oct. 2013.

[43] J. Drápela and J. Šlezingr, "A Flickermeter Based on Voltage Peak Detection Method - Part I: LabView Implementation," in *Proceedings of the 13th International*

Scientific Conference Electric Power Engineering 2012, EPE 2012, vol. 1, 2012, pp. 437–442.

[44] J. Drápela, "A Time Domain Based Flickermeter with Response to High Frequency Interharmonics," in *13th International Conference on Harmonics and Quality of Power, 2008. ICHQP 2008*, Sep. 2008, pp. 1–7.

[45] J. Drápela, R. Langella, J. Šlezingr, and A. Testa, "A Tunable Flickermeter to Account for Different Lamp Technologies," *IEEE Transactions on Power Delivery*, vol. 32, no. 2, pp. 872 – 880, 2016.

[46] L. Feola, R. Langella, and A. Testa, "A new frequency approach for light flicker evaluation in electric power systems," *EURASIP Journal on Advances in Signal Processing*, vol. 2015, no. 1, Dec. 2015. [Online]. Available: https://asp-eurasipjournals.springeropen.com/articles/10.1186/s13634-015-0207-0

[47] N. Kose and O. Salor, "A new frequency domain approach for light flicker evaluation of power systems," in *2009 IEEE Instrumentation and Measurement Technology Conference*, May 2009, pp. 618–623.

[48] P. Teikari, "Flicker Metrology," May 2006. [Online]. Available: http://www.petteri-teikari.com/pdf/Teikari_FlickerMetrology.pdf

[49] Y. Y. Hong and L. H. Lee, "Analysis of equivalent 10 Hz voltage flicker in power systems," *Transmission and Distribution IEE Proceedings - Generation*, vol. 146, no. 5, pp. 447–452, Sep. 1999.

[50] A. Novitskiy and H. Schau, "Analysis of a Ratio between Delta V10 and Pst Flicker Criteria," in *Universities' Power Engineering Conference (UPEC), Proceedings of 2011 46th International*, Sep. 2011, pp. 1–4.

[51] J. Drápela and J. Šlezingr, "A Light Flickermeter - Part I: Design," in *Proccedings of the 11th International Scientific Conference Electric Power Engineering 2010.* Brno, Czech Republic: Brno University of Technology, FEEC, DEPE, 2010, pp. 453–458.

[52] J. Drápela and J. Šlezingr, "A Light Flickermeter - Part II: Realization and Verification," in *Proccedings of the 11th International Scientific Conference Electric Power Engineering 2010*, vol. 459-464. Brno, Czech Republic: Brno University of Technology, FEEC, DEPE, 2010.

[53] D. Gallo, C. Landi, and N. Pasquino, "Design and Calibration of an Objective Flickermeter," *IEEE Transactions on Instrumentation and Measurement*, vol. 55, no. 6, pp. 2118–2125, Dec. 2006.

[54] J. Drápela, "Blikání světelných zdrojů způsobené meziharmonickými složkami napětí," Habilitation thesis, Brno University of Technology, Brno, Czech Republic, 2008.

[55] T. Tayjasanant, W. Wang, C. Li, and W. Xu, "Interharmonic-flicker curves," *IEEE Transactions on Power Delivery*, vol. 20, no. 2, pp. 1017–1024, Apr. 2005.

[56] J. Drápela, M. Krátký, L. Weidinger, and M. Zavodny, "Light Flicker of Fluorescent Lamps with Different Types of Ballasts Caused by Interharmonics," in *Power Tech, 2005 IEEE Russia*, Jun. 2005, pp. 1–7.

[57] J. A. F. Plateau, "Betrachtungen über ein von Hrn Talbot vorgeschlagenes photometrisches Princip," *Bulletin de l'acad. roy. des sciences et belles-lettres de Bruxelles*, no. 2, 1835.

[58] A. Broca and D. Sulzer, "La Sensation Lumineuse en Function du Temps," *Comptes Rendus de l'Académie des Sciences (Paris)*, 1902. [Online]. Available: http://bibliothequedesphares.fr/bibliothequeD/bib_D046

[59] S. Bartley, "Subjective brightness in relation to flash rate and the light-dark ratio," *Journal of Experimental Psychology*, vol. 23, no. 3, pp. 313–319, 1938.

[60] S. Bartley, G. Paczewitz, and E. Valsi, "Brightness Enhancement and the Stimulus Cycle," *Journal of Psychology: Interdisciplinary and Applied*, vol. 43, no. 2, pp. 187–192, 1957.

[61] A. Sato, "Brightness enhancement of flicker and response variability," *The Japanese journal of psychology*, vol. 40, no. 5, pp. 267–272, 1969.

[62] M. Jinno, K. Morita, Y. Tomita, Y. Toda, and H. Motomura, "Beyond the physical limit: Energy saving lighting and illumination by using repetitive intense and fast pulsed light sources and the effect on human eyes," *Journal of Light and Visual Environment*, vol. 32, no. 2, pp. 170–176, 2008.

[63] M. Jinno, K. Morita, Y. Tomita, Y. Toda, and H. Motomura, "Effective illuminance improvement of a light source by using pulse modulation and its psychophysical effect on the human eye," *Journal of Light and Visual Environment*, vol. 32, no. 2, pp. 161–169, 2008.

[64] G. Xin, "Pulse modulation effect of light-emitting diodes on human perception enhancement," *Optical Engineering*, vol. 51, no. 7, p. 073608, Jul. 2012. [Online]. Available: http://opticalengineering.spiedigitallibrary.org/article.aspx?doi=10.1117/1.OE.51.7.073608

[65] I. Fryc, W. Davis, and Y. Ohno, "Experiment on Visual Perception of Pulsed LED Lighting - Can it Save Energy for Lighting?" in *CIE 2010 "Lighting Quality and Energy Efficiency"*, 2010.

[66] H. Motomura, Y. Ikeda, and M. Jinno, "Evaluation of Visual Perception Enhancement Effect by Pulsed Operation of LEDs," in *14th International Symposium on the Science and Technology of Lighting*, vol. 14, Italy, 2014.

[67] S. Fan, X. Gu, X. Zhang, and M. Liu, "Human Perception on Pulsed Red and Green Lights," *Optical Engineering*, vol. 53, no. 6, p. 065105, Jun. 2014.

[68] S. Fan, X. Zhang, X. Gu, H. Shen, and M. Liu, "Influence of pulse width on luminous efficiency for a two-degree field," *Lighting Research and Technology*, Jan. 2016. [Online]. Available: http://lrt.sagepub.com/cgi/doi/10.1177/1477153515626772

[69] C. Branas, F. J. Azcondo, and J. M. Alonso, "Solid-State Lighting: A System Review," *IEEE Industrial Electronics Magazine*, vol. 7, no. 4, pp. 6–14, Dec. 2013.

[70] V. C. Bender, T. B. Marchesan, and J. M. Alonso, "Solid-State Lighting: A Concise Review of the State of the Art on LED and OLED Modeling," *IEEE Industrial Electronics Magazine*, vol. 9, no. 2, pp. 6–16, Jun. 2015.

[71] L. Sandahl, K. Cort, and K. Gordon, "Solid State Lighting: Early Lessons Learned on the Way to Market," Dec. 2013. [Online]. Available: https://www1.eere.energy.gov/buildings/publications/pdfs/ssl/ssl_lessons-learned_2014.pdf

[72] S. M. Sze, *Physics of semiconductor devices*, 3rd ed. United States of America: Wiley-Interscience, 1969.

[73] A. Poppe, "Multi-domain compact modeling of LEDs: An overview of models and experimental data," *Microelectronics Journal*, vol. 46, no. 12, pp. 1138–1151, Dec. 2015. [Online]. Available: http://www.sciencedirect.com/science/article/pii/S002626921500227X

[74] S. Lin, T. m. Shih, W. Yan, Y. Lu, Y. Lin, R. R. G. Chang, and Z. Chen, "Maximum Limits on External Quantum Efficiencies in Bare LEDs," *IEEE Transactions on Electron Devices*, vol. 64, no. 4, pp. 1597–1601, Apr. 2017.

[75] C. Biber, "LED Light Emission as a Function of Thermal Conditions," in *2008 Twenty-fourth Annual IEEE Semiconductor Thermal Measurement and Management Symposium*, Mar. 2008, pp. 180–184.

[76] I. Fryc, S. W. Brown, G. Eppeldauer, and Y. Ohno, "LED-based spectrally tunable source for radiometric, photometric, and colorimetric applications," *Optical Engineering*, vol. 44, no. 11, p. 111309, Nov. 2005. [Online]. Available: http://opticalengineering.spiedigitallibrary.org/article.aspx?doi=10.1117/1.2127952

[77] S. Y. R. Hui, H. Chen, and X. Tao, "An Extended Photoelectrothermal Theory for LED Systems: A Tutorial From Device Characteristic to System Design for General Lighting," *IEEE Transactions on Power Electronics*, vol. 27, no. 11, pp. 4571–4583, Nov. 2012.

[78] K. Górecki and P. Ptak, "Modelling LED lamps with thermal phenomena taken into account," in *2016 22nd International Workshop on Thermal Investigations of ICs and Systems (THERMINIC)*, Sep. 2016, pp. 202–207.

[79] Lumileds Holding B.V., "DS061 LUXEON Rebel ES Product Datasheet," Jun. 2016. [Online]. Available: http://www.lumileds.com/uploads/17/DS61-pdf

[80] Lumileds Holding B.V., "LUXEON Emitter, Technical Datasheet DS25," 2007. [Online]. Available: http://www.luxeonstar.com/assets/downloads/ds25.pdf

[81] M. Brooks, "High Powered White LED Technology," Jan. 2009. [Online]. Available: http://s03e04c9f5e0a73fe.jimcontent.com/download/version/1318769206/module/5530830113/name/rrlIntroduction%20to%20LED%20Lighting.docx

[82] Z. Silalahi, P. Dupuis, L. Massol, G. Zissis, and N. Sinisuka, "Color Shift Study on the Practical LED Lamps During the Ageing Process," in *Light Sources 2016*, vol. 15, Kyoto, Japan, May 2016, pp. 315–320.

[83] L. Canale, P. Dupuis, S. Leng, and G. Zissis, "Study of high brightness LED samples aged under stress temperature conditions: Electrical characterizations and signature evolution analysis," *IEEE Transactions on Industry Applications*, vol. 2015, pp. 1–11, 2015.

[84] M. Arias, A. Vazquez, and J. Sebastián, "An Overview of the AC-DC and DC-DC Converters for LED Lighting Applications," *Automatika – Journal for Control, Measurement, Electronics, Computing and Communications*, vol. 53, no. 2, May 2012. [Online]. Available: https://automatika.korema.hr/index.php/automatika/article/view/154

[85] Infineon, "RGB LED Lighting Shield with XMC1202 for Arduino, Board Manual," 2014. [Online]. Available: https://www.infineon.com/dgdl/Infineon-Board_Manual_-_XMC1202_-_RGB_LED_Lighting_Shield_with_XMC1202_for_Arduino_-_v1_0-UM-v01_00-EN.pdf?fileId=5546d46249be182c0149ccca3860734d

[86] E. M. Sa, C. S. Postiglione, R. S. Santiago, F. L. M. Antunes, and A. J. Perin, "Self-oscillating flyback driver for power LEDs," in *2009 IEEE Energy Conversion Congress and Exposition*, Sep. 2009, pp. 2827–2832.

[87] T. Liu, S. Wang, S. Song, and Y. Ai, "Research on High-Efficiency Driving Technology for High Power LED Lighting," in *Power and Energy Engineering Conference (APPEEC), 2010 Asia-Pacific*, Mar. 2010, pp. 1–4.

[88] S. Wang, X. Ruan, K. Yao, S.-C. Tan, Y. Yang, and Z. Ye, "A Flicker-Free Electrolytic Capacitor-Less AC-DC LED Driver," *IEEE Transactions on Power Electronics*, vol. 27, no. 11, pp. 4540–4548, Nov. 2012.

[89] J. Cardesin, D. Garcia-Llera, E. Lopez-Corominas, A. Calleja, J. Ribas, and D. Gacio, "Low cost intelligent LED driver for public Lighting Smart Grids," in *2013 International Conference on New Concepts in Smart Cities: Fostering Public and Private Alliances (SmartMILE)*, Dec. 2013, pp. 1–6.

[90] Z. Mao, L. Ge, and G. Hua, "Removing the LED light strobe flicker by proper driver designs," in *2013 10th China International Forum on Solid State Lighting (ChinaSSL)*, Nov. 2013, pp. 210–213.

[91] A. Leon-Masich, H. Valderrama-Blavi, J. Bosque-Moncusi, and L. Martinez-Salamero, "A high voltage SiC-based boost PFC for LED applications," in *2014 9th International Conference on Ecological Vehicles and Renewable Energies, EVER 2014*, 2014.

[92] S. Ma and C. Wang, "The design of the high-power LED constant current drive circuit and research," *Advanced Materials Research*, vol. 1021, pp. 196–199, 2014.

[93] Z. Tang, D. Zhao, X. Huang, and X. Zhang, "LED constant current drive power supply based on flyback with active ripple compensation," *Journal of Computational Information Systems*, vol. 10, no. 3, pp. 1065–1075, 2014.

[94] J. M. Alonso, M. Perdig£o, M. A. D. Costa, G. Martínez, and R. Osorio, "Analysis and design of a novel variable-inductor-based LED driver for DC lighting grids," in *2016 IEEE Industry Applications Society Annual Meeting*, Oct. 2016, pp. 1–8.

[95] W. A. Rodrigues, L. M. F. Morais, P. F. Donoso-Garcia, P. C. Cortizo, and S. I. Seleme, "Comparative analysis of power LEDs dimming methods," in *IECON 2011 - 37th Annual Conference of the IEEE Industrial Electronics Society*, Nov. 2011, pp. 2907–2912.

[96] J. Šlezingr, J. Drápela, R. Langella, and A. Testa, "A new simplified model of compact fluorescent lamps in the scenario of smart grids," in *2012 IEEE 15th International Conference on Harmonics and Quality of Power (ICHQP)*, Jun. 2012, pp. 835–841.

[97] Hamamatsu, "Opto-semiconductor Handbook," 2014. [Online]. Available: https://www.hamamatsu-news.de/hamamatsu_optosemiconductor_handbook/files/assets/basic-html/index.html#1

[98] Hamamatsu, "Photodiode with sensitivity close to spectral luminous efficiency," Apr. 2016. [Online]. Available: www.hamamatsu.com

[99] Silonex, "SLD-70bg2 - Infrared Rejection Filter Planar Photodiode." [Online]. Available: http://www.alldatasheet.com/datasheet-pdf/pdf/193307/SILONEX/SLD-70BG2.html

[100] PowTech, "PT4205 - 30v, 1.2a Step-down HB LED Driver." [Online]. Available: www.crpowtech.com

[101] PowTech, "PT4115 - 30v, 1.2a Step-down High Brightness LED Driver with 5000:1 Dimming." [Online]. Available: www.crpowtech.com

[102] Silan Microelectronics, "SD42527 - 1a HIGH POWER LED DRIVER WITH 6~60v INPUT," 2011. [Online]. Available: www.silan.com.cn

[103] Fairchild Semiconductor Corporation, "MB1s - MB8s: 0.5 A Bridge Rectifiers," 2007. [Online]. Available: http://www.mouser.com/ds/2/149/MB1S-195678.pdf

[104] Taiwan Semiconductor Company, "SK22a Trhough SK210a 2.0 Amps Surface Mount Shottky Barrier Rectifiers." [Online]. Available: http://www.htmldatasheet.com/tsc/sk210a[1].htm

[105] Vishay General Semiconductor, "Surface Mount Shottky Barrier Rectifier," Apr. 2017. [Online]. Available: www.vishay.com

[106] Diodes Incorporated, "B320 - B360 3.0 A Surface Mount Shottky Barrier Rectifier," Feb. 2016. [Online]. Available: https://www.diodes.com/assets/Datasheets/ds30923.pdf

[107] Analog Devices, "Op Amp Common-Mode Rejection Ratio (CMRR)," 2009. [Online]. Available: http://www.analog.com/media/en/training-seminars/tutorials/MT-042.pdf

[108] A. Barroso, "Optimisation des systèmes d'éclairage des bâtiments de l'Université Paul Sabatier basé sur un résau novateur de type bus continu/basse tension," dissertation thesis, Université Toulouse III - Paul Sabatier, Toulouse, France, Jan. 2017.

[109] D. Maksimovic and R. Erickson, "Advances in Averaged Switch Modeling an Simulation," in *1999 Power Electronics Specialists Conference*, 1999.

[110] Mathworks, "Mathworks MATLAB." [Online]. Available: https://www.mathworks.com/products/matlab.html

[111] D. Schelle and J. Castorena, "Buck-Converter Design Demystified," *Power Electronics Technology*, pp. 46–52, Jun. 2006. [Online]. Available: http://read.pudn.com/downloads157/ebook/697438/Buck_Converter_Design_Demystified.pdf

[112] N. Safari, "Design of a DC/DC Buck Converter for Ultra Low Power Applications in 65nm CMOS Process," diploma thesis, Linköping Institute of Technology, Linköping, Mar. 2012. [Online]. Available: http://liu.diva-portal.org/smash/get/diva2:546843/FULLTEXT01.pdf

[113] "NGSPICE - mixed-mode, mixed-level circuit simulator," Jan. 2014. [Online]. Available: http://ngspice.sourceforge.net/#

[114] Joint Committee for Guides in Metrology, "Evaluation of measurement data - Guide to the expression of uncertainty in measurement," 2008. [Online]. Available: www.bipm.org/utils/common/documents/jcgm/JCGM_100_2008_E.pdf

[115] National Instruments, "NI USB 6212 Device Specifications." [Online]. Available: http://www.ni.com/pdf/manuals/375196c.pdf

[116] Joint Committee for Guides in Metrology, "Evaluation of measurement data - Supplement 1 to the 'Guide to the expression of uncertainty in measurement' - Propagation of distributions using a Monte Carlo method," 2008. [Online]. Available: http://www.bipm.org/utils/common/documents/jcgm/JCGM_101_2008_E.pdf

Referenced Standards

[STD1] *IEEE 1789-2015 IEEE Recommended Practices for Modulating Current in High-Brightness LEDs for Mitigating Health Risks to Viewers*, IEEE Std. 1789, Jun. 2015.

[STD2] *IEC 60038 ed.7:2009 IEC standard voltages*, IEC Std. 60 038, Rev. 7, 2009.

[STD3] *IEC 61000-2-2:2002 Electromagnetic compatibility (EMC) - Part 2-2: Environment - Compatibility levels for low-frequency conducted disturbances and signalling in public low-voltage power supply systems*, IEC Std. 61 000-2-2, 2002.

[STD4] *IEEE 519:2014 IEEE Recommended Practice and Requirements for Harmonic Control in Electric Power Systems*, IEEE Std. 519, 2014.

[STD5] *IEC 61000-3-2 ed.4:2015 Electromagnetic compatibility (EMC) - Part 3-2: Limits - Limits for harmonic current emissions (equipment input current ≤ 16 A per phase)*, IEC Std. 61 000-3-2, Rev. 4, 2015.

[STD6] *IEC 61000-3-3 ed. 3:2014 Electromagnetic compatibility (EMC) - Part 3-3: Limits - Limitation of voltage changes, voltage fluctuations and flicker in public low-voltage supply systems, for equipment with rated current ≤16 A per phase and not subject to conditional connection*, IEC Std. 61 000-3-3, Rev. 3, 2014.

[STD7] *IEC 61000-4-11 ed.2:2004 Electromagnetic compatibility (EMC) - Part 4-11: Testing and measurement techniques - Voltage dips, short interruptions and voltage variations immunity tests*, IEC Std. 61 000-4-11, 2004.

[STD8] *IEC 61000-4-13:2003 Electromagnetic compatibility (EMC) - Part 4-13: Testing and measurement techniques - Harmonics and interharmonics including mains signalling at a.c. power port, low frequency immunity tests*, IEC Std. 61 000-4-13, 2003.

[STD9] *IEC 61000-4-14:2000 Electromagnetic compatibility (EMC) - Part 4-14: Testing and measurement techniques - Voltage fluctuation immunity test for equipment with input current not exceeding 16 A per phase*, IEC Std. 61 000-4-14, 2000.

[STD10] *IEC 61000-4-15:2010 Electromagnetic compatibility (EMC) – Testing and measurement techniques – Flickermeter – Functional and design specifications*, IEC Std. 61 000-4-15, 2010.

[STD11] *IEEE 1453-2015 Recommended Practice for the Analysis of Fluctuating Installations on Power Systems*, IEEE Std. 1453, Oct. 2015.

[STD12] *IEC 61000-4-17:1999 Electromagnetic compatibility (EMC) - Part 4-17: Testing and measurement techniques - Ripple on d.c. input power port immunity test*, IEC Std. 61 000-4-17, 1999.

[STD13] *IEC 61000-4-19:2014 Electromagnetic compatibility (EMC) - Part 4-19: Testing and measurement techniques - Test for immunity to conducted, differential mode disturbances and signalling in the frequency range 2 kHz to 150 kHz at a.c. power ports*, IEC Std. 61 000-4-19, 2014.

[STD14] *IEC 61000-4-29:2000 Electromagnetic compatibility (EMC) - Part 4-29: Testing and measurement techniques - Voltage dips, short interruptions and voltage variations on DC input power port immunity test*, IEC Std. 61 000-4-29, 2000.

[STD15] *IEC 61000-6-1:2005 Electromagnetic compatibility (EMC) - Part 6-1: Generic standards - Immunity for residential, commercial and light-industrial environments*, IEC Std. 61 000-6-1, 2005.

[STD16] *IEC 61547 ed.2:2009 Equipment for general lighting purposes - EMC immunity requirements*, IEC Std. 61 547, Rev. 2, 2009.

[STD17] *IEC TR 61547-1:2015 Equipment for general lighting purposes - EMC immunity requirements - Part 1: An objective voltage fluctuation immunity test method*, IEC Technical Report 61 547-1, 2015.

[STD18] *EN 50160 Voltage Characteristics of Electricity Supplied by Public Distribution Systems*, EN Std. 50 160, 2000.

[STD19] *IEEE 1159-2009 Recommended Practice for Monitoring Electric Power Quality*, IEEE Std. 1159, Jun. 2009.

[STD20] *IEC 61000-4-30:2003 Electromagnetic Compatibility - Testing and Measurement Techniques - Power Quality Measurements Methods*, IEC Std. 61 000-4-30, 2003.

[STD21] *IEC 61000-4-7:2002 Electromagnetic compatibility (EMC) - Part 4-5: Testing and measurement techniques - General Guide on Harmonics and Interharmonics Measurements and Instrumentation, for Power Supply Systems and Equipment Connected Thereto*, IEC Std. 61 000-4-7, 2002.

[STD22] *IEEE 1459-2010 IEEE Standard Definitions for the Measurement of Electric Power Quantities Under Sinusoidal, Nonsinusoidal, Balanced, or Unbalanced Conditions*, IEEE Std. 1459, 2010.

[STD23] IESNA Testing Procedures Committee, Subcommittee on Solid-State Lighting, and Illuminating Engineering Society of North America, *IES LM-79-08 IES approved method for the electrical and photometric measurements of solid-state lighting products.* New York, N.Y.: Illuminating Engineering Society, 2008.

Author's Publications

[LK1] L. Kukačka, P. Dupuis, G. Zissis, and M. Kolář, "Retrofit LED Lamps: Photometric Flicker Analysis," in *2015 IEEE Industry Applications Society Annual Meeting*, Dallas, Texas, 2015.

[LK2] T. Bedrník, J. Kraus, and L. Kukačka, "Magnitude Oriented Intelligent Grouping Scheme for Harmonics Above 2 kHz," in *2014 16th European Conference on Power Electronics and Applications (EPE'14-ECCE Europe)*, Aug. 2014, pp. 1–7.

[LK3] L. Kukačka, J. Kraus, M. Kolář, P. Dupuis, and G. Zissis, "Review of AC Power Theories under Stationary and Non-stationary, Clean and Distorted Conditions," *IET Generation, Transmission & Distribution*, Oct. 2015. [Online]. Available: http://digital-library.theiet.org/content/journals/10.1049/iet-gtd.2015.0713

[LK4] L. Kukačka, C. Lassfolk, H. Motomura, Y. Ikeda, and M. Jinno, "Broca-Sulzer Effect Detection over Critical Fusion Frequency for Pulse Operated White LEDs with Varied Pulse Shape," in *15th International Symposium on the Science and Technology of Lighting*, vol. 15, Kyoto, Japan, 2016.

[LK5] C. Lassfolk, L. Kukačka, H. Motomura, Y. Ikeda, and M. Jinno, "Brightness Enhancement by Pulsed Operation of LEDs," in *15th International Symposium on the Science and Technology of Lighting*, vol. 15, Kyoto, Japan, 2016.

[LK6] L. Kukačka, P. Dupuis, H. Motomura, J. Rozkovec, G. Zissis, M. Kolář, and M. Jinno, "On Correct Evaluation Techniques of Pulsing Light Brightness Enhancement Effect Measurement Data," *Optical Engineering*, p. in review process.

[LK7] L. Kukačka, P. Dupuis, R. Simanjuntak, and G. Zissis, "Simplified Models of LED Ballasts for SPICE," in *2014 IEEE Industry Applications Society Annual Meeting*, Oct. 2014, pp. 1–5.

[LK8] L. Kukačka, P. Dupuis, G. Zissis, J. Kraus, and M. Kolář, "Extra Low Voltage DC Grid Lighting Systems: Photometric Flicker Analysis," in *2015 IEEE International Workshop of Electronics, Control, Measurement, Signals and their application to Mechatronics*, vol. 12th. Liberec, Czech Republic: TU of Liberec, FMIIS - ITE, Jun. 2015, pp. 173–178.

[LK9] L. Kukačka and J. Drápela, "Flicker and Driver Topology Assessment of Extra Low Voltage LED Lamps Under DC Supply," in *Proceedings of International Conference on Harmonics and Quality of Power, ICHQP*, vol. 2016-December, 2016, pp. 605–610.

[LK10] J. Kraus, V. Bubla, and L. Kukačka, "Data Modeling for Reduction of Volume in Large Archives of Power Quality Data," in *21st International Conference on Electricity Distribution, CIRED Frankfurt*, Frankfurt, Germany, Jun. 2011.

[LK11] J. Kraus, T. Bedmík, and L. Kukačka, "Common Three Phase Active Power Definition and its Questionable Suitability for the Smart Grid Meters," in *2016 17th International Scientific Conference on Electric Power Engineering (EPE)*, May 2016, pp. 1–5.

[LK12] L. Kukačka and J. Kraus, "CPC teorie - praktická analýza běžných jevů v síti," in *Conference on Electric Engineering, Czech Technical University, Prague*, 2012.

[LK13] J. Kraus, P. Štěpán, and L. Kukačka, "Optimal Data Compression Techniques for Smart Grid and Power Quality Trend Data," in *2012 IEEE 15th International Conference on Harmonics and Quality of Power (ICHQP)*, Jun. 2012, pp. 707–712.

[LK14] P. Štěpán, L. Kukačka, and J. Kraus, "Detailed Analysis of Class F1/F3 Flickermeter Implementations According to the Recent IEC Standards," in *The 23rd International Conference and Exhibition on Electricity Distribution*, vol. 23, Lyon, France, Jun. 2015.

[LK15] P. Štěpán, V. Bubla, L. Kukačka, and J. Kraus, "Implementation of Flicker Meter in Power Quality Analyzers," in *PCIM Europe 2015*, Nürnberg, Germany, May 2015, pp. 1763–1770.

[LK16] T. Bedrník, L. Kukačka, P. Štěpán, and J. Kraus, "Dynamic Intelligent Compression for Power Quality Analysers," in *The 23rd International Conference and Exhibition on Electricity Distribution*, vol. 23rd, Lyon, France, Jun. 2015.

[LK17] L. Kukačka, J. Kraus, V. Bubla, and P. Štěpán, "CPC and IEEE Power Theory - Application for Offline Waveform Data Analysis," in *IET Conference Publications*, vol. 2013, Stockholm, 2013.

[LK18] J. Kraus, T. Bedrník, and L. Kukačka, "Ambiguous Definitions of the Polyphase Active Energy Evaluation in Quadrants," *IEEE Transactions on Power Electronics*, p. in review process.

The author has seven publications indexed in the *Web of Science* database where one of them has been cited once. Ten publications are indexed in the *Scopus* database with eleven citations in total. Autocitations are not counted. One paper ([LK3]) was published in a journal with impact factor 1.35, another paper ([LK6]) was conditionally accepted for publication in a journal with impact factor 0.97.

The author participates in the research project TAČR TA185S01001 "Modular system for complex monitoring and management of DC and AC/DC hybrid smart grids", Technology Agency of the Czech Republic. A co-authored patent application was submitted to the Industrial Property Office of the Czech Republic.

The author supervised three successfully defended bachelor projects and two successfully defended bachelor theses. One master thesis is being supervised in the year 2017/2018.

Part III

Appendices

A IEC Flickermeter Details

The IEC flickermeter [STD10] is a device capable of estimating the visible flicker of an incandescent lamp from voltage measurements. It consists of five blocks. This appendix describes its simplified implementation for offline data analysis. All parameters are given for a 230 V supply at 50 Hz. For 60 Hz systems, the parameters will be slightly different.

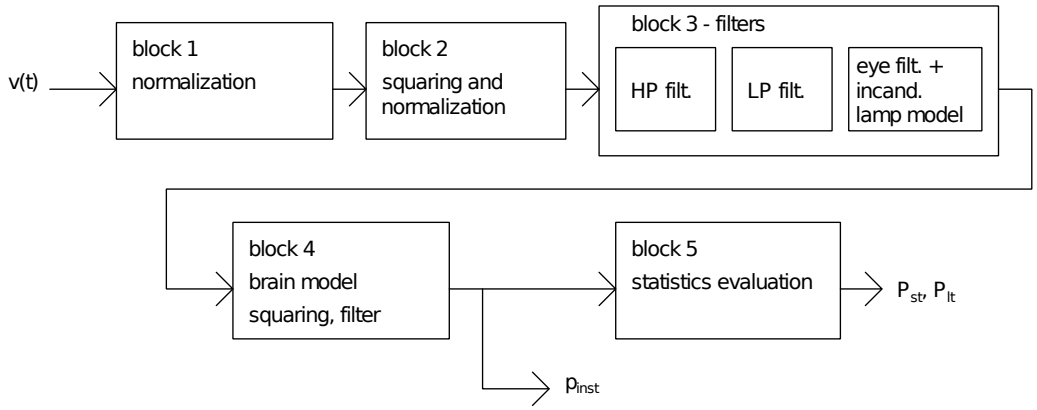

Figure A.1: The diagram of the IEC flickermeter

1. Block 1 normalises the input signal by its RMS value.
2. Block 2 squares the signal in order to obtain a signal representing instantaneous power, consumed by a resistive load. A new normalisation is made after the squaring.
3. Block 3 contains three filters. The first filter is a high pass filter with cutoff frequency of 0.5 Hz. This filter is included for removing the DC offset from the signal; for offline applications it can be replaced by the simple removal of the DC component. The second filter is a low pass 6th order Butterworth filter with a cutoff frequency of 35 Hz. The third filter mimics both the response of a 60 W two–filament incandescent lamp and the eye response. The transfer function of this filter is given:

$$F(s) = \frac{p\omega_1 s}{s^2 + 2\lambda_{\mathrm{FM}} s + \omega_1^2} \cdot \frac{1 + \dfrac{s}{\omega_2}}{\left(1 + \dfrac{s}{\omega_3}\right)\left(1 + \dfrac{s}{\omega_4}\right)}, \tag{A.1}$$

where

$$\begin{aligned} p &= 1.748\,02\,, \\ \lambda_{\text{FM}} &= 2\pi\,4.059\,81\,, \\ \omega_1 &= 2\pi\,9.154\,94\,\text{rad}\,\text{s}^{-1}\,, \\ \omega_2 &= 2\pi\,2.279\,79\,\text{rad}\,\text{s}^{-1}\,, \\ \omega_3 &= 2\pi\,1.225\,35\,\text{rad}\,\text{s}^{-1}\,, \\ \text{and}\quad \omega_4 &= 2\pi\,21.9\,\text{rad}\,\text{s}^{-1}\,. \end{aligned}$$

4. Block 4 mimics the brain response to the flickering light. It comprises the squaring and a low pass filter with a time constant of $0.3\,\text{s}$. From the resulting signal, the absolute value is acquired. The output of block 4 is scaled in order to give the instantaneous flicker $p_{\text{inst}}(t)$. It is a dimensionless number with the value 1 indicating that in average $50\,\%$ of the population would report a flickering sensation.

5. Block 5 provides a statistical evaluation of the instantaneous flicker within the given interval. Within the interval, individual samples of $p_{\text{inst}}(t)$ are sorted into classes. The following percentiles are calculated: 0.1, 0.7, 1, 1.5, 2.2, 3, 4, 6, 8, 10, 13, 17, 30, 50 and $80\,\%$. From these percentiles the P_{st} is calculated:

$$P_{\text{st}} = \sqrt{0.0314P_{0.1} + 0.052P_{1\text{s}} + 0.0657P_{3\text{s}} + 0.28P_{10\text{s}} + 0.08P_{50\text{s}}}\,, \tag{A.2}$$

where

$$P_{1\text{s}} = \frac{1}{3}(P_{0.7} + P_1 + P_{1.5})\,, \tag{A.3}$$

$$P_{3\text{s}} = \frac{1}{3}(P_{2.2} + P_3 + P_4)\,, \tag{A.4}$$

$$P_{10\text{s}} = \frac{1}{5}(P_6 + P_8 + P_{10} + P_{13} + P_{17})\,, \tag{A.5}$$

$$P_{50\text{s}} = \frac{1}{3}(P_{30} + P_{50} + P_{80})\,. \tag{A.6}$$

The quantity P_{lt} is calculated from P_{st} values per given time interval (several hours):

$$P_{\text{lt}} = \sqrt[3]{\frac{1}{N}\sum_{i=1}^{N} P_{\text{st},i}^3} \tag{A.7}$$

P_{st} is a dimensionless number with the value 1 being a recognised flicker limit ([STD18, STD6]). P_{st} should be evaluated from a time interval between 1 and 15 minutes. If a different time interval is used, it should be given in the subscript index. Thus, if evaluated from the $10\,\text{s}$ interval, the quantity should be noted as $P_{10\text{s}}$ (not to be confused with the percentile in the equations above). However, for simplicity, in this thesis, it is always noted as P_{st} and the evaluation interval is noted along with its use (usually $10\,\text{s}$).

The standard defines a set of testing signals which are meant for calibrating the FM and to provide some feedback about the accuracy of a particular implementation.

A.1 Implementation

The following is the implementation in MATLAB / Octave code used in this thesis.

In block 1, the RMS value is computed directly from the signal instead of using a filter. This reduces the response time of the flickermeter, but a stationary signal can only be used for the analysis.

In block 3, the high pass filter is replaced by simply removing the DC component (mean value of the signal). This further reduces the impulse response and, thus, the response time of the flickermeter.

The response of this implementation was tested using prescribed tests from [STD10]. The LFM implementation successfully passed all tests except for test no. 7 (Chapter 6.8, Tab. 11 in the referenced standard) where the tested values were slightly out of the required limits. The reason for this behaviour was not identified. Thus, the implementation passes the requirements for class C flickermeters.

Source Code A.1: IEC flickermeter implementation

```
function [Pst pinst] = iec_fm(Uin, Fs, Tst)
%
% [Pst pinst] = iec_fm(Uin, Fs, Tst)
% leos.kukacka@tul.cz
%
% calculates Pst according to IEC 61000-4-15
%
% This implementation is simplified as it ignores the
% normalization filters
% Presampled periodic signal is assumed for normalizing,
% see block 1
%
% input:
% Uin - sampled voltage, should be minimum Tst+5 s long
%       5 s is necessary to wait for filter impulse response;
% Fs - sampling rate, should not be too low, approx. 5 kSmpl
% Tst - length of signal analysed (s)
%       for standard Pst the Tst should be between 60 and 900 s
%       for measurements and testing purposes the Tst can be 10 s
%
% output:
% Pst - short time flicker severity index estimated from the last
%       Tst seconds of the input signal
% pinst - last Tst seconds of instantaneous flicker
%         (output of block 4)
%
```

```
% b1 = block1(Uin, Fs);
% b2 = block2(b1, Fs);
% b3 = block3(b2, Fs);
% [pinst S] = block4(b3, Fs);
% pinst = pinst(end-Tst*Fs:end);
% Pst = block5(pinst, S);
%

s = tf('s');
N = length(Uin);
T = N/Fs;
t = (0:N-1)/Fs;

if Tst>T
  Tst = T;
end

%% block 1
% normalise input

%tau = 27.3;
%sys = c2d(filt(1, [tau 1]), 0.01);
% normalise the input relative to its RMS value filtered
% with filter 'sys'

% for pre-sampled constant signal just normalise to the RMS value
rms = sqrt(sum(Uin.^2)/N);
b1 = Uin ./ rms;

%% block 2
% squaring and new normalisation

% for pre-sampled constant signal just normalise to the RMS value
b2 = b1.^2;
rms = sqrt(sum(b2.^2)/N);
b2 = b2 ./ rms;

%% block 3
% filters

% high pass filter (remove DC)
%fhp = 0.05;
%HP = s/2/pi/fhp / (s/2/pi/fhp + 1);

% low pass filter
flp = 35;
LP = 1 / ( (s/2/pi/flp)^2 + 0.2587*s/pi/flp + 1 ) ...
       / ( (s/2/pi/flp)^2 + 0.7073*s/pi/flp + 1 ) ...
```

```
       / ( (s/2/pi/flp)^2 + 0.9659*s/pi/flp + 1 );

% eye sens function
k=1.74802;
lambda=2*pi*4.05981;
omega1=2*pi*9.15494;
omega2=2*pi*2.27979;
omega3=2*pi*1.22535;
omega4=2*pi*21.9;
F = k*omega1*s / (s^2+2*lambda*s+omega1^2) ...
    * (1+s/omega2) / (1+s/omega3) / (1+s/omega4);

% remove DC and HF
%f1 = lsim(HP, b2, t);
f1 = b2 - mean(b2);
f2 = lsim(LP, f1, t);
% brain filter
b3 = lsim(F, f2, t);

%% block 4
% brain

tau = 0.3;
sys = 1 / (tau*s+1);

% scaling factor S determined from test "0"
S = 4.642319407046525e+05;
pinst = S*abs(lsim(sys, b3.^2, t));
% take only Tst seconds of pinst for block 5 eval
pinst = pinst(end-Tst*Fs:end);

%% block 5
% statistics evaluation

NC = 1e5;
M = S;
X=[0.1, 0.7, 1, 1.5, 2.2, 3, 4, 6, 8, 10, 13, 17, 30, 50, 80];

Cl = floor(NC/2*(1+log10(pinst)/log10(M)));
Cl(Cl<0) = 0;
Cl(Cl>NC) = NC;

ClX = prctile(Cl, 100.-X);

PX = power(10, log10(M)*(ClX*2/NC-1));

P1S = mean(PX(2:4));
P3S = mean(PX(5:7));
```

```
123 P10S = mean(PX(8:12));
124 P50S = mean(PX(13:15));
125 Pst = sqrt( 0.0314*PX(1) + 0.0525*P1S + ...
126              0.0657*P3S + 0.28*P10S + 0.08*P50S );
```

B Objective Flickermeter Details

An *objective flickermeter* [STD17], [51, 52] (or *light flickermeter*, LFM) is a device capable of calculating the P_{st} quantity from luminous flux measurements. The quantity obtained in this way is denoted as $P_{\mathrm{st}}^{\mathrm{LM}}$. The LFM is comprised of similar blocks to the IEC flickermeter with the incandescent lamp model removed.

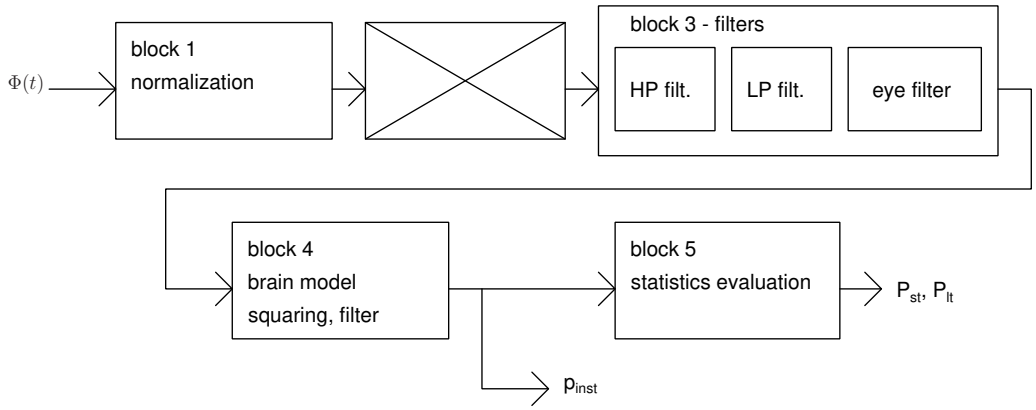

Figure B.1: A diagram of an objective flickermeter

1. Block 1 normalises the signal to the RMS value.

2. Block 2 in IEC FM converts the voltage signal to the instantaneous power by squaring; this feature is omitted in the LFM because the input signal is the luminous flux.

3. Block 3 contains the same HP and LP filters as the IEC FM. The eye filter is obtained from Eq. (A.1) by removing the incandescent lamp part. The filter transfer function will then be

$$F(s) = \frac{p\omega_1 s}{s^2 + 2\lambda_{\mathrm{FM}} s + \omega_1^2} \cdot \frac{1 + \dfrac{s}{\omega_2}}{\left(1 + \dfrac{s}{\omega_3}\right)\left(1 + \dfrac{s}{\omega_4}\right)} \cdot \frac{s^2 \dfrac{\tau_{\mathrm{L}}}{2000} + s\tau_{\mathrm{L}} + 1}{\dfrac{K_{\mathrm{L}}}{2}}, \tag{B.1}$$

where the last fraction is the inverse incandescent lamp model [51] and the constants are

$$\tau_{\mathrm{L}} = 21.2\,\mathrm{ms}\,,$$
$$\text{and} \quad K_{\mathrm{L}} = 3.64\,.$$

4. Blocks 4 and 5 are identical with the IEC FM.

For testing the objective FM, the same tests can be used as were for IEC FM, provided that an incandescent lamp (or its model) is used between the voltage source and the flickermeter.

B.1 Implementation

The following is the implementation in MATLAB / Octave code used in this thesis.

Similarly to the IEC FM, in block 1, the mean value is computed directly from the signal instead of using a filter. This reduces the response time of the flickermeter, but a stationary signal can only be analysed this way.

In block 3, the high pass filter is replaced by simply removing the DC component (mean value of the signal). This further reduces the impulse response and, thus, the response time of the flickermeter.

The response of this implementation was tested using the prescribed tests from [STD10]. The test signals were applied upon an incandescent lamp model whose output was fed into the LFM. The LFM implementation successfully passed all tests except for test no. 7 (Chapter 6.8, Tab. 11 in the referenced standard) where the tested values were slightly out of the required limits. The reason for this behaviour was not identified; the author believes this does not disqualify LFM from usage in this thesis. The response to the constant signal is $P_{\mathrm{st}}^{\mathrm{LM}} = 4.979\,1 \cdot 10^{-4}$. When this value is encountered it is interpreted as $P_{\mathrm{st}}^{\mathrm{LM}} = 0$.

Source Code B.1: Light flickermeter implementation

```
function [Pst pinst] = obj_fm(Phi, Fs, Tst)
%
% [Pst pinst] = obj_fm(Phi, Fs, Tst)
% leos.kukacka@tul.cz
%
% Calculates objective Pst
% implementation mainly based on:
% [1] J. Drapela and J. Slezingr, "A Light Flickermeter -
%     Part I: Design," in Proccedings of the 11th International
%     Scientific Conference Electric Power Engineering 2010,
%     Brno, Czech Republic, 2010, pp. 453-458.
% [2] J. Drapela and J. Slezingr, "A Light Flickermeter -
%     Part II: Realization and Verification," in Proccedings
%     of the 11th International Scientific Conference Electric
%     Power Engineering 2010, Brno, Czech Republic, 2010,
```

```
%     vol. 459-464.
% please cite when you use
%
% This implementation is simplified as it ignores
% the normalisation filters; presampled periodic signal is
% assumed for normalising, see block 1
%
% input:
% Phi - sampled luminous flux, should be minimum Tst+5 s long
%       5 s is necessary to wait for filter impulse response;
%       Phi needs not to be normalised, block 1 normalises to RMS
% Fs - sampling rate, should not be too low, approx. 5 kSmpl
% Tst - length of pinst analysed for block 5 (s)
%       for standard Pst the Tst should be between 60 and 900 s
%       for measurements and testing purposes the Tst can be 10 s
%
% output:
% Pst - short time flicker severity index estimated from the last
%       Tst seconds of the input signal
% pinst - last Tst seconds of instantaneous flicker
%         (output of block 4)
%
% obj_fm() function is organised as follows:
% b1 = block1(Phi, Fs); % normalisation
% b2 = block2(b1, Fs); % ! no block 2 in objective flickermeter!
% b3 = block3(b1, Fs);  % filters
% [pinst S] = block4(b3, Fs); % brain memory
% pinst = pinst(end-Tst*Fs:end);
% Pst = block5(pinst, S); % statistics
%

s = tf('s');
N = length(Phi);
t = (0:N-1)/Fs;
T = N/Fs;

if Tst>T
    Tst = T;
end

%% block 1
% normalise input

% original filter proposed by IEC std.:
%tau = 27.3;
%sys = c2d(filt(1, [tau 1]), 0.01);

b1 = Phi ./ mean(Phi);
```

```
64
65  %% block 2
66  % in objective FM there is no block 2
67  b2 = b1;
68
69  %% block 3
70  % filters
71
72  % high pass filter (remove DC)
73  % very slow impulse response
74  % for presampled signal: simply remove mean (see below)
75  %fhp = 0.05;
76  %HP = s/2/pi/fhp / (s/2/pi/fhp + 1);
77
78  % low pass 6th order BW filter to remove freqs above 35 Hz
79  flp = 35;
80  LP = 1 / ( (s/2/pi/flp)^2 + 0.2587*s/pi/flp + 1 ) ...
81         / ( (s/2/pi/flp)^2 + 0.7073*s/pi/flp + 1 ) ...
82         / ( (s/2/pi/flp)^2 + 0.9659*s/pi/flp + 1 );
83
84  % eye sens function parameters
85  k=1.74802;
86  lambda=2*pi*4.05981;
87  omega1=2*pi*9.15494;
88  omega2=2*pi*2.27979;
89  omega3=2*pi*1.22535;
90  omega4=2*pi*21.9;
91
92  % incand. lamp model parameters
93  K = 3.64/sqrt(2);
94  tauL = 21.2e-3;
95
96  % eye sensitivity filter divided by incand lamp. model
97  F = k/K*omega1*s / (s^2+2*lambda*s+omega1^2) ...
98      * (1+s/omega2) / (1+s/omega3) / (1+s/omega4) ...
99      * ( s^2*tauL/2000 + s*tauL + 1 );
100
101 % remove DC
102 % instead of filter simply remove mean
103 %f1 = lsim(HP, b2, t);
104 f1 = b2 - mean(b2);
105 % remove HF
106 f2 = lsim(LP, f1, t);
107 % brain filter
108 b3 = lsim(F, f2, t);
109
110
111 %% block 4
```

```
% brain memory filter, squaring, absolute value, scaling

% low pass
tau = 0.3;
sys = 1 / (tau*s+1);

% scaling factor S determined from test "0"
S = 2047840.02229395;
pinst = S*abs(lsim(sys, b3.^2, t));
% take only Tst seconds of pinst for block 5 eval
pinst = pinst(end-Tst*Fs:end);

%% block 5
% statistics evaluation

NC = 1e5;
M = S;
X=[0.1, 0.7, 1, 1.5, 2.2, 3, 4, 6, 8, 10, 13, 17, 30, 50, 80];

Cl = floor(NC/2*(1+log10(pinst)/log10(M)));
Cl(Cl<0) = 0;
Cl(Cl>NC) = NC;

ClX = prctile(Cl, 100.-X);

PX = power(10, log10(M)*(ClX*2/NC-1));

P1S = mean(PX(2:4));
P3S = mean(PX(5:7));
P10S = mean(PX(8:12));
P50S = mean(PX(13:15));

Pst = sqrt( 0.0314*PX(1) + 0.0525*P1S ...
          + 0.0657*P3S + 0.28*P10S + 0.08*P50S );
```

C Other Source Codes

This appendix contains the MATLAB / Octave scripts used to evaluate key parts of performed experiments or to calculate key quantities. SPICE source codes are also included.

C.1 Logarithmic Amplifier—Reverse Transfer Function

The following is the function used for calculating the photodiode current from the amplifier output voltage. Because the amplifier transfer function is transcendental (Eq. (6.3)), its reverse is calculated iteratively using Newton's method. Empirical amplifier parameters (Eq. (6.3)) can either be passed as a parameter, or will be estimated from nominal values of the circuit components (Eq. (6.2)).

Source Code C.1: Logarithmic amplifier inverse transfer function

```
function [Iin, fNewton, dNewton] = LM10_LightSens(Vo, p)
%# function [Id] = LM10_LightSens(Vo)
%# Given the LM10 Light-to-Voltage converter output voltage,
%# convert back to current.

if (nargin < 2)
  p = [];
end

if (isempty (p))
  % use analytical formula
  p.R1 = 1650;  % 1k65 default
  p.R2 = 499; % 499 default
  p.R3 = 120e3; % 120k default
  p.R4 = 10.2e3;
  p.R5 = 2e3;
  p.R6 = 84;  % 84 default
  p.Rout = 100;
  p.PVoutVD1=[-.022865 .058277 .596918];

  q=1.602176565e-19;
  k=1.3806488e-23;
  T0 = -273.15; T = 27-T0;
  p.I3 = 6.3534e-6;
```

```
  p.VT = k*T/q;
  p.Idark = 36e-9;

  xVoutLin_theor = p.Rout* [(p.R2+p.R6)/(p.R1*p.R6)*1.22
                            p.VT*(p.R1+p.R2+p.R6)/(p.R1*p.R6);
                            (1+p.R6/p.R2)/p.Rout;
                            -(p.R2+p.R6)/(p.R1*p.R6)];
  xVoutLin = xVoutLin_theor;
else
  if (~isfield (p, 'I3'))
    p.I3 = 1;  %# was p.I3 = 6.3534e-6;
  end
  xVoutLin = p.xVoutLin(:);
  p.PVoutVD1=[-.022865 .058277 .596918];
  if (~isfield (p, 'Idark'))
    p.Idark = 0;  %# was p.Idark = 36e-9;
  end
  p.Rout=100;
end

%# inverse formula
VD1 = polyval(p.PVoutVD1, Vo);
Iin = p.I3*exp((Vo-xVoutLin(4)*VD1-xVoutLin(1))/xVoutLin(2)) ...
      - p.Idark;

Iin =  Iin(:);
A = [ones(size(Iin))
     log((Iin+p.Idark)/p.I3)
     zeros(size(Iin))
     VD1];
for indi = (2:8)
  fNewton(:,indi) = (A*xVoutLin-Vo)./(xVoutLin(2));
  dNewton(:,indi) = xVoutLin(2) ./ ...
                    (Iin(:, indi-1)+p.Idark)+xVoutLin(3);
  Iin(:,indi) = Iin(:,indi-1) - ...
                (A*xVoutLin-Vo)./(xVoutLin(2)./(Iin(:,indi-1) ...
                + p.Idark) + xVoutLin(3));
  A(:, 2:3) = [log((Iin(:,indi)+p.Idark)/p.I3) Iin(:,indi)];
end

Iin = Iin(:,end);
end
```

C.2 Frequency Intermodulation—SPICE Simulation

The following is the code used for simulating the frequency intermodulation in the diode bridge, Sec. 7.2. The simulation was run using *ngspice* [113].

Source Code C.2: Frequency intermodulation

```
* diode bridge frequency effect
* dependance on C

* voltage source
VAC 1 0 sin(0 16.97 50 0 0)
*VDC 1 0 12
Vih 1 2 sin(0 2 140 0 0)

* diode bridge
D1 2 11 D1N4007
D2 0 11 D1N4007
D3 10 0 D1N4007
D4 10 2 D1N4007
.MODEL D1N4007 D  ( IS=76.9n RS=42.0m BV=1.00k IBV=5.00u
+ CJO=26.5p M=0.333 N=1.45 TT=4.32u )

* smooth cap
C 10 11 3.3uF
* load res
*R 10 11 6k6
Iload 11 10 0.3

.options reltol=.01
.options abstol=1N vntol=1M

.CONTROL
  set filetype=ascii
  foreach cval 1e-6 2e-6 3e-6 5e-6 1e-5 2e-5 5e-5 1e-4 5e-4 1e-3
    alter C $cval
    tran 10us 1.1s
    linearize
    reset
  end
  write diode_bridge_AC.raw tran2.V(2) tran2.V(10) tran2.V(11)
  + tran4.V(2) tran4.V(10) tran4.V(11)
  + tran6.V(2) tran6.V(10) tran6.V(11)
  + tran8.V(2) tran8.V(10) tran8.V(11)
  + tran10.V(2) tran10.V(10) tran10.V(11)
  + tran12.V(2) tran12.V(10) tran12.V(11)
  + tran14.V(2) tran14.V(10) tran14.V(11)
  + tran16.V(2) tran16.V(10) tran16.V(11)
  + tran18.V(2) tran18.V(10) tran18.V(11)
```

```
43    + tran20.V(2) tran20.V(10) tran20.V(11)
44  *  + tran22.V(2) tran22.V(10) tran22.V(11)
45  .ENDC
```

D Uncertainties Evaluation

This appendix describes the approach to estimate the measurement of the uncertainties used, particularly in Sec. 6.2. The approach is largely based on [114]. An example is given—uncertainty evaluation for *percent flicker*.

Uncertainty expresses the lack of knowledge of a true value of a measurand. In a closer sense it is a "*parameter, associated with the result of a measurement, that characterises the dispersion of the values that could reasonably be attributed to the measurand*" [114]. Thus, the uncertainty represents an interval within which the true value lies with given probability, usually under the assumption of normal distribution.

The *FP* is defined as

$$FP = \frac{mx_\Phi - mn_\Phi}{mx_\Phi + mn_\Phi} \cdot 100\,, \tag{D.1}$$

where $mx_\Phi = \max(\Phi(t))$ and $mn_\Phi = \min(\Phi(t))$, $\Phi(t)$ is the luminous flux waveform. Because this definition is insensitive to multiplication of $\Phi(t)$ by a constant, it can be evaluated directly from the acquired waveform in volts.

The cited document defines two types of uncertainty according to their origin. *Type A* uncertainty expresses the empirically acquired repeatability of the measured value. Thus, for the measured quantity X, it is defined as an estimated standard deviation of the mean of the observations:

$$u_\mathrm{A}(X) = \sqrt{\frac{1}{N(N-1)} \sum_{i=1}^{N} (X_i - \bar{X})^2}\,, \tag{D.2}$$

where X_i is i-th measured value, $\bar{X}$ is the mean value and N is the number of measurements performed; usually $N = 10$.

When performing the experiments in Sec. 6.2, one simple short experiment (SUP8+LED$_4$) was run ten times in a row in order to provide a set of ten measured signals per each channel (AC voltage, AC current, DC voltage, DC current, photodiode amplifier output). For example: when evaluating type A uncertainty of a maximum of the photodiode signal, the maximum was evaluated ten times from ten acquired signals and then

$$u_\mathrm{A}(mx_\Phi) = \sqrt{\frac{1}{90} \sum_{i=1}^{10} (mx_{\Phi\,i} - \bar{mx}_\Phi)^2}\,. \tag{D.3}$$

It is assumed that type A uncertainty will be approximately constant and thus the u_A was calculated once for the maximum mx_Φ and once for the minimum mn_Φ; these

values were then used for all the other following measurements without the need to repeat them ten times. It was found out that $u_{\mathrm{A}}(\boldsymbol{mx}_{\Phi}) = 8.247\,3 \cdot 10^{-4}\,\mathrm{V}$ and $u_{\mathrm{A}}(\boldsymbol{mn}_{\Phi}) = 1.207\,6 \cdot 10^{-3}\,\mathrm{V}$.

Type B uncertainty expresses any known property of the measurement process. In the case of our measurement, type B uncertainty can be obtained by analysing the data acquisition error in the sampling device NI 6212. According to [115], the absolute measurement accuracy can be evaluated as

$$\mathit{Acc} = \mathit{Reading} \cdot \mathit{GainErr} + \mathit{Range} \cdot \mathit{OffsetErr} + \mathit{NoiseUnc}\,, \tag{D.4}$$

where *Reading* is the acquired value, *GainErr* is the gain error, *Range* is the chosen range for the given channel, *OffsetErr* is the offset error and *NoiseUnc* is the noise uncertainty. [115] gives for $\mathit{Range} = \pm 5\,\mathrm{V}$:

$$\begin{aligned} \mathit{NoiseUnc} &= \frac{3 \cdot \mathit{RndNoise}}{\sqrt{100}}\,, \\ \mathit{RndNoise} &= 149\,\mu\mathrm{V}\,. \end{aligned}$$

The gain error can be obtained as

$$\mathit{GainErr} = \mathit{ResGainErr} + \mathit{GainTempCo} \cdot \Delta\tau_{\mathrm{int}} + \mathit{RefTempCo} \cdot \Delta\tau_{\mathrm{ext}}\,, \tag{D.5}$$

where

$$\begin{aligned} \mathit{ResGainErr} &= 85\,\mathrm{ppm}_{\mathrm{reading}}\,, \\ \mathit{GainTempCo} &= 7.3\,\mathrm{ppm}/^{\circ}\mathrm{C}\,, \\ \mathit{RefTempCo} &= 5\,\mathrm{ppm}/^{\circ}\mathrm{C}\,, \end{aligned}$$

$\Delta\tau_{\mathrm{int}}$ is the temperature change from the last internal calibration (assumed $1\,^{\circ}\mathrm{C}$) and $\Delta\tau_{\mathrm{ext}}$ is the temperature change from the last external calibration (estimated as $5\,^{\circ}\mathrm{C}$). The offset error can be obtained as

$$\mathit{OffsetErr} = \mathit{ResOffsetErr} + \mathit{OffsetTempCo} \cdot \Delta\tau_{\mathrm{int}} + \mathit{INL}\,, \tag{D.6}$$

where

$$\begin{aligned} \mathit{ResOffsetErr} &= 20\,\mathrm{ppm}_{\mathrm{range}}\,, \\ \mathit{OffsetTempCo} &= 36\,\mathrm{ppm}_{\mathrm{range}}/^{\circ}\mathrm{C}\,, \\ \mathit{INL} &= 76\,\mathrm{ppm}_{\mathrm{range}}\,. \end{aligned}$$

The absolute accuracy represents an interval within which the true value lies with $100\,\%$ probability; uniform distribution is assumed within the interval. This value needs to be converted to type B uncertainty using a conversion [114, Sec. 4.3.7]

$$u_{\mathrm{B}}(X) = \frac{\mathit{Acc}}{\sqrt{3}}\,. \tag{D.7}$$

From (D.4), it is clear that the accuracy (and also type B uncertainty) is dependant on the reading.

When both type A and type B uncertainties are known, it is a common practice to evaluate a *combined uncertainty*:

$$u_{\mathrm{AB}}(X) = \sqrt{u_{\mathrm{A}}^2(X) + u_{\mathrm{B}}^2(X)}\,. \tag{D.8}$$

The combined uncertainty expresses both the empirically obtained spread of the results and the known acquisition accuracy.

The *combined standard uncertainty* evaluates the uncertainty of the quantity calculated using the other measured quantities. In our example the measured quantities are $\boldsymbol{mx}_\Phi$ and $\boldsymbol{mn}_\Phi$, the calculated quantity is the *FP* (D.4). Because $\boldsymbol{FP} = \boldsymbol{FP}(\boldsymbol{mx}_\Phi, \boldsymbol{mn}_\Phi)$, the combined standard uncertainty can be calculated as

$$u_{\mathrm{C}}(\boldsymbol{FP}) = \sqrt{\left(\frac{\partial \boldsymbol{FP}}{\partial \boldsymbol{mx}_\Phi} u_{\mathrm{AB}}(\boldsymbol{mx}_\Phi)\right)^2 + \left(\frac{\partial \boldsymbol{FP}}{\partial \boldsymbol{mn}_\Phi} u_{\mathrm{AB}}(\boldsymbol{mn}_\Phi)\right)^2}\,, \tag{D.9}$$

where the partial derivatives of *FP* are

$$\frac{\partial \boldsymbol{FP}}{\partial \boldsymbol{mx}_\Phi} = -100 \cdot 2 \cdot \frac{\boldsymbol{mn}_\Phi}{(\boldsymbol{mx}_\Phi + \boldsymbol{mn}_\Phi)^2}\,,$$
$$\frac{\partial \boldsymbol{FP}}{\partial \boldsymbol{mn}_\Phi} = 100 \cdot 2 \cdot \frac{\boldsymbol{mx}_\Phi}{(\boldsymbol{mx}_\Phi + \boldsymbol{mn}_\Phi)^2}\,.$$

The combined standard uncertainty expresses an interval within which the true value lies with approx. $66\,\%$ under the assumption of the normal distribution of the readings ($\mu \pm \sigma$). In order to cover larger probability, a *coverage factor* ρ is used to calculate the *expanded uncertainty*

$$U(X) = \rho u_{\mathrm{C}}(X)\,. \tag{D.10}$$

The coverage factor is usually chosen as $\rho = 2$ so that the expanded uncertainty expresses an interval within which the true value lies with $95\,\%$ probability ($\mu \pm 2\sigma$) [116, Sec. 6.3.3].

When expressing the final measurement result, the value is given as $\boldsymbol{FP} \pm U$. The uncertainty U is rounded upwards to one significant digit (if the first significant digit is 1 or 2, then it is rounded to two significant digits). Then the *FP* value is rounded in the usual way so that the last significant digit is the same position as the last significant digit of the uncertainty.

E Contents of the Attached DVD-ROM

The attached DVD-ROM contains all the data relevant to this thesis organised in folders. The following is an overview of the folder system and a list of the files to be found therein.

- `Kukacka_PhD.pdf` is a PDF/A-1b file containing this thesis.
- Experiment data and scripts
  - The folder **Experiment 1a** contains all the measurement data from experiment 1a in .mat v7.3 files. The folder also contains evaluation scripts coded in MATLAB / Octave. To save disk space, the current measurements were excluded.
  - The folder **Experiment 1b** contains all the measurement data from experiment 1b in .mat v7.3 files. The folder also contains evaluation scripts coded in MATLAB / Octave. To save disk space, the current measurements were excluded.
  - The folder **Experiment 2** contains all the measurement data from experiment 2 in CSV compressed by xz.
  - The folder **Experiment 3a** contains all the measurement data from experiment 3a in CSV compressed by xz.
  - The folder **Experiment 3b** contains all the measurement data from experiment 3b in CSV. The folder also contains evaluation scripts coded in MATLAB / Octave.
- Simulation data and scripts
  - The folder **Simulation 1** contains the SPICE code as well as the Octave evaluation script.
  - The folder **Simulation 2a** contains the MATLAB Simulink files housing the used models as well as an m-file which should be used to control, run and evaluate the simulation.
  - The folder **Simulation 2b** contains the MATLAB Simulink files housing the used models as well as an m-file which should be used to control, run and evaluate the simulation.

  - The folder **Simulation 3** contains three subfolders, each containing the MATLAB Simulink files housing the used models as well as an m-file which should be used to control, run and evaluate the simulations.

- The folder **Thesis XeLaTeXSource Codes** contains all the files necessary to compile this thesis using XeLaTeX. A bash script issuing all the necessary commands is provided in the file `compile.sh`.

- The folder **Author's Publications** contains all papers authored or coauthored by the author of this thesis.

- The folder **Miscellaneous** contains these source codes:

  - `obj_fm.m` is the LFM used in this thesis, see also App. B;
  - `test_obj_fm.m` is a script which allows one to run all the FM tests described by std. IEC 61000-4-15:2010 [STD10];
  - `iec_fm.m` and `text_iec_fm.m` are, similarly, a regular voltage-based IEC FM and the standard tests, see also App. A;
  - `LM10_Light_Sens.m` contains the reverse transfer function of the logarithmic transimpedance amplifier used in some of the evaluation scripts, see also Sec. 6.1 and App. C;
  - `FlickerIndex.m` is a simple function to calculate the *FI* used in some of the evaluation scripts.

F Disassembled LED Lamps - Photographs

Photographs of disassembled 12 V LED lamps analysed in Experiment 3 are shown. Details about the drivers design are described in Sec. 6.4.1.

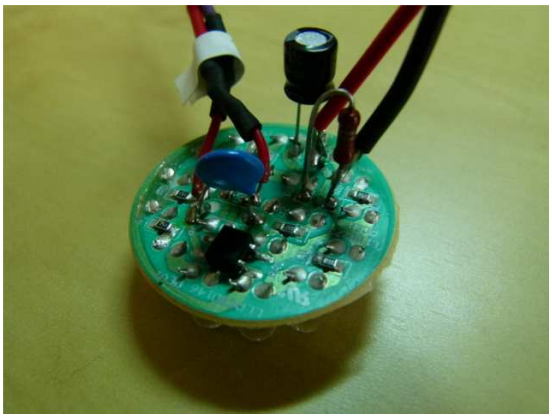

(a) LED1 driver

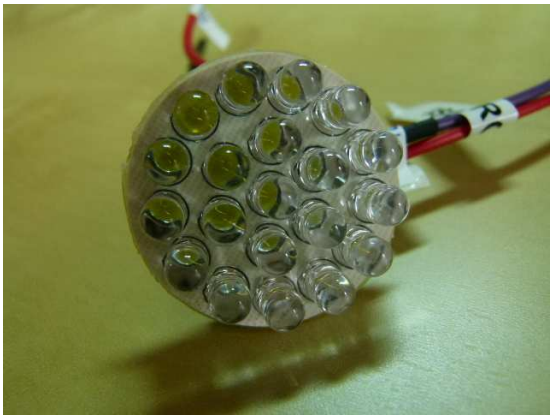

(b) LED1 head

Figure F.1: LED1 disassembled

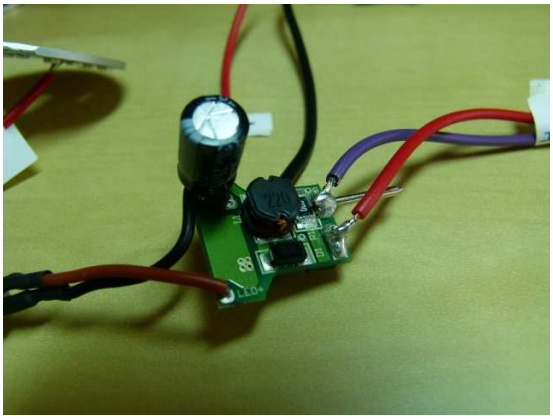

(a) LED2 driver

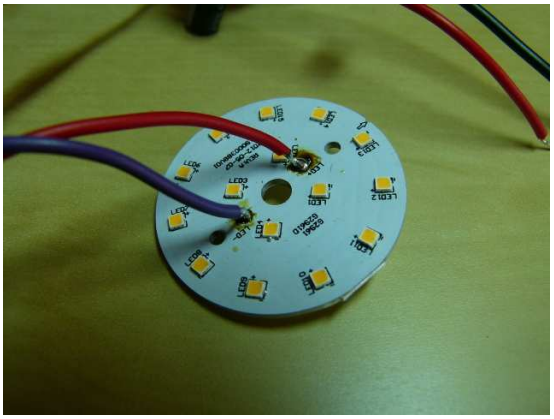

(b) LED2 head

Figure F.2: LED2 disassembled

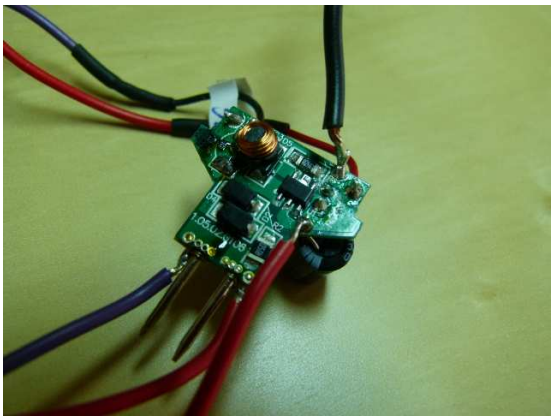

(a) LED3 driver

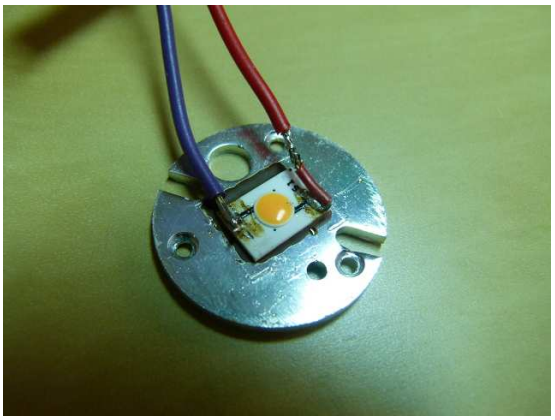

(b) LED3 head

Figure F.3: LED3 disassembled

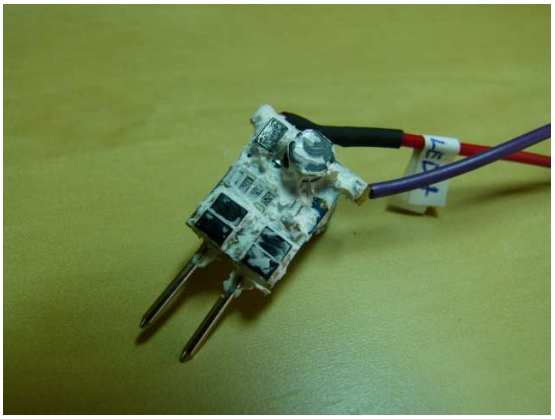

(a) LED4 driver

(b) LED4 head

Figure F.4: LED4 disassembled

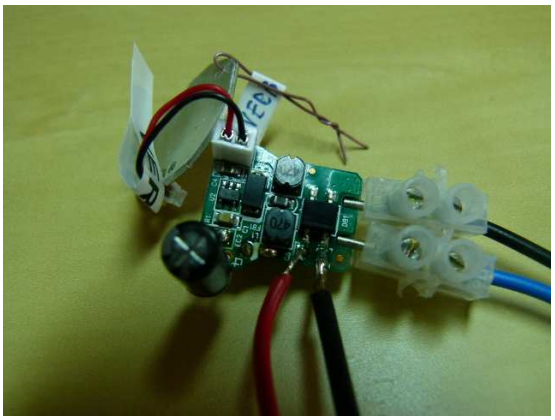

(a) LED5 driver

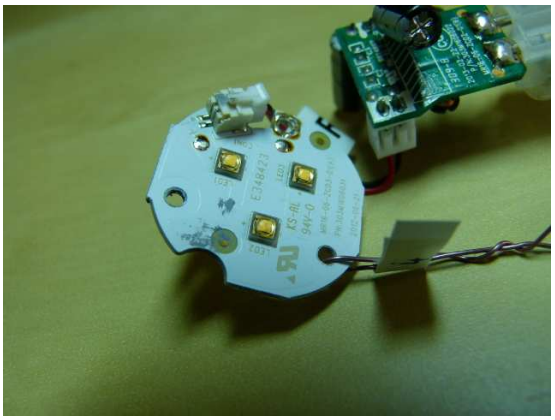

(b) LED5 head

Figure F.5: LED5 disassembled

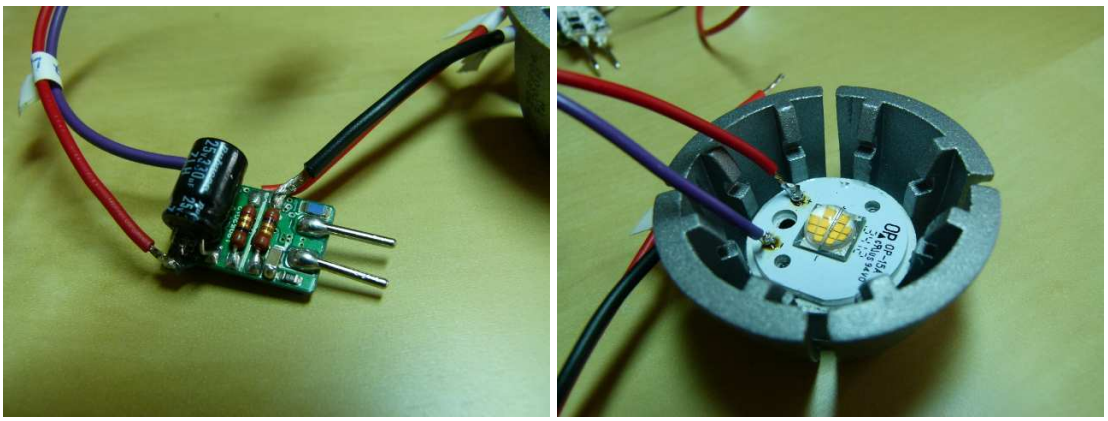

(a) LED6 driver (b) LED6 head

Figure F.6: LED6 disassembled